This is to certify that the

thesis entitled

" MECHANISM OF FRICTION AND

COHESION IN CLAYS "

presented by

Abraham K. Loh

has been accepted towards fulfillment
of the requirements for

Ph. D. degree in Civil Engineering

Major professor

Date Dec 10, 1964

O-169

ABSTRACT

MECHANISM OF FRICTION AND COHESION IN CLAYS

by Abraham K. Loh

A particle model is proposed for the behavior of friction and cohesion in clays. In this model, the resistance at the contacts of the particles is assumed to consist of a mineral friction and an adhesion. It varies with the orientation of the particle relative to the direction of shear.

The angle of internal friction is the result of the resistance due to mineral friction at the contacts. The cohesion consists of a non-viscous part and a viscous part. The non-viscous part of cohesion is the result of the resistance due to adhesion at the contacts. The behavior of the viscous part of cohesion follows the flow phenomenon of the clay particle structure as a rate process.

The experimental behaviors of friction and cohesion were investigated by means of the triaxial test. Creep, Creep-CFS and CFS tests were carried out on five different clays that include laboratory-prepared and undisturbed clays.

It is found that the experimental behavior of friction and cohesion under constant strain rate and creep can be satisfactorily correlated with the predicted behavior according to the proposed model.

MECHANISM OF FRICTION AND COHESION

IN CLAYS

By

Abraham K. Loh

A THESIS

submitted to
Michigan State University
in partial fulfillment of the requirements
for the degree of

DOCTOR OF PHILOSOPHY

Department of Civil Engineering

1964

ACKNOWLEDGEMENTS

The author wishes to express his sincere gratitude to his major professor, Dr. T. H. Wu for his guidance and encouragement in the preparation of this thesis as well as throughout the author's doctoral study. He is also indebted to his guidance Committee members, Dr. O. B. Andersland, Department of Civil Engineering, Dr. L. E. Malvern, Department of Metallurgy, Mechanics and Materials Science, Dr. D. J. Montgomery, Department of Physics and Astronomy and Dr. J. L. Dye, Department of Chemistry for their guidance throughout his doctoral study. F. J. Holliday and W. L. Warder are thanked for their assistance in the laboratory.

The financial support of the National Science Foundation is gratefully acknowledged.

TABLE OF CONTENTS

LIST OF TABLES

LIST OF FIGURES

Figure | Page

Figure		Page

LIST OF APPENDICES

Appendix Page

Appendix | Page

NOTATION

a	$= \dfrac{n_\theta A_c}{A_\alpha}$
A_c	area of a contact along θ
A_θ	total soil area parallel to θ along section A-A (Fig. 1b)
A_α	$= \sum_{\theta=0}^{\theta=\pi} A_\theta \cos(\theta-\alpha)$, gross soil area along the α-plane
A	$= \tanh^{-1} \exp\left(- \dfrac{\alpha k_1 \tau}{k_1 + k_2}\right)$ in Equation (27)
α	rate parameter assoc. with the geometry and number of flow units $= \dfrac{\lambda}{2 kT}$
α	angle of inclination of a potential failure plane
β	rate parameter assoc. with the activation energy $= \dfrac{2\lambda}{\lambda_1} \dfrac{kT}{h} \exp\left(- \dfrac{\Delta F}{RT}\right)$
β'	$= \dot{\gamma}/\beta$, ratio of shear strain rate to β
c'	cohesion at any strain ϵ
c'_{oct}	c' along octahedral plane
c'_f	c' @ peak $(\sigma_1 - \sigma_3)$
c'_u	c' @ $\bar{\sigma}_1/\bar{\sigma}_3$ = constant
c'_c	cohesion @ any elapsed time of creep
c'_o	c'_c at zero time
c'_∞	c'_c at infinite time
c^*	dimensionless cohesion function $= \dfrac{c'_c - c'_\infty}{c'_o - c'_\infty}$
c'_d	c'_c obtained from c'-$\dot{\epsilon}$ curve at $\dot{\epsilon} = \dot{\epsilon}_c$
c_a	adhesion in force per unit gross soil area
C_a	adhesion force
D	deviator stress $= (\sigma_1 - \sigma_3)$

	axial strain
$_o$	initial axial strain in creep
$_\infty$	final axial strain in creep
$_c$	@ any elapsed time of creep
$_f$	@ peak $(_1 - _3)$
$_u$	@ $\bar{}_1/\bar{}_3$ = constant
$_{um}$	minimal of $_u$ required to attain $\dagger'_{um}$
$\dot{\varepsilon}$	rate of axial strain
$\dot{\varepsilon}_c$	strain rate @ or near end of creep in Creep-CFS test
e	displacement along due to one contact failure
f_1	shear stress that causes flow in viscous element of rheologic model for clay particle structure = predicted viscous cohesion
f_o	f_1 @ zero time
f*	predicted cohesion function = f_1/f_o
ΔF	Activation Energy
	total shear strain
$_1$	shear strain of the viscous element in rheologic model
$\dot{}$	rate of total shear strain
$\dot{}_1$	rate of shear strain of viscous element in rheologic model
$\dot{}_{oct}$	rate of octahedral shear strain
h	Plank's constant
k	Boltzmann's constant

k	effective principal stress ratio = $\bar{\sigma}_1/\bar{\sigma}_3$
k_1, k_2	Hookean springs in rheologic model
λ	vertical distance between successive interparticle equilibrium positions
λ_1	distance between flow units in direction of flow
tanφ	coefficient of mineral friction
λ	number of bonds per unit area over the plane of shear
m	number of slipping contacts associated with the displacement of particle 2
M	range in θ (degrees) in which contact failure occurs under k
n	number of contacts within a gross soil area A_α along the α-plane
n_θ	number of contacts with the angle θ
n_m	number of contact failure in M
N	= $n_m \cdot e$, contact displacement at any strain
N_u	$\dot{N} \cdot t_u$, contact displacement at $\bar{\sigma}_1/\bar{\sigma}_3$ = constant
N_c	contact displacement at any elapsed time of creep
$\dot{N}$	= N/t, rate of contact displacement
$\dot{N}_c$	= N_c/t_c, rate of displacement under creep
$\dot{N}_k$	N_c/t_k, rate of displacement under creep required to attain ϕ_k'

$\dot{N}_m$	$= N/t_m$, rate of contact displacement required to attain Φ'_m
d_p	probability of particle orientation
P_θ	normal force to the θ-plane of a particle
P_F	displacement resistance due to friction
P_A	displacement resistance due to adhesion
Φ'	angle of internal friction at any strain ϵ
Φ'_f	Φ' at peak $(\sigma_1 - \sigma_3)$
Φ'_u	Φ' at $\bar{\sigma}_1/\bar{\sigma}_3$ = constant
Φ'_m	maximum value of Φ' at any strain ϵ
Φ'_c	Φ' at any elapsed time of creep
Φ'_k	maximum value of Φ'_c attainable at the stress level k in creep
Φ'_{um}	maximum value of Φ' attainable under $\dot{N}_m$ (@ $\bar{\sigma}_1/\bar{\sigma}_3$ = constant)
R	universal gas constant
R_θ	sliding resistance due to friction
ρ	a coefficient in Frictional Resistance against Displacement
ρ_m	a coefficient in Adhesional Resistance against Displacement
$\bar{\sigma}_\theta$	Effective normal stress to the plane θ

σ_s	normal stress at a contact with an angle θ (force per unit contact area)
σ_c	consolidation pressure
σ_1, σ_3	total major and minor principal stresses
$\bar{\sigma}_1, \bar{\sigma}_2, \bar{\sigma}_3$	effective major, intermediate and minor principal stresses
σ_{1s}, σ_{3s}	major and minor principal stresses at a contact
t	time; also time required to reach N
t_c	elapsed time of creep
t_m	minimal of time required to attain $'_m$
t_k	time required to attain $'_k$
t_u	time required to reach N_u
t_{um}	Minimal of time required to attain $'_{um}$
t_1	frictional resistance against sliding contributed by a contact with an angle (shear force per unit contact area)
t_2	frictional resistance against displacement contributed by a contact with an angle (shear force per unit contact area)
t_3	adhesional resistance against sliding contributed by a contact with an angle (shear force per unit contact area)
t_4	adhesional resistance against displacement contributed by a contact with an angle (shear force per unit contact area)
T	absolute temperature

T	tangential force on the α-plane of a particle
τ	applied shear stress
τ_{oct}	octahedral shear stress
τ_α	applied shear stress along the α-plane
τ'_α	shearing resistance on the α-plane due to the frictional resistance against sliding at the n contacts within a soil area A_α (force per unit soil area)
τ''_α	shearing resistance on the α-plane due to the frictional resistance against displacement at the n contacts within a soil area A_α (force per unit soil area)
τ'''_α	shearing resistance on the α-plane due to the adhesional resistance against sliding at the n contacts within a soil area A_α (force per unit soil area)
τ''''_α	shearing resistance on the α-plane due to the adhesional resistance against displacement at the n contacts within a soil area A_α (force per unit soil area)
τ_θ	shear stress along a plane θ
τ_s	shear stress at a contact with an angle θ (force per unit contact area)
τ'_{θ}	that portion of τ'_α due to n_θ contacts with angle θ (force per unit soil area).

$\tau'''_{\alpha\theta}$	that portion of τ'''_{α} due to n_{θ} contacts with angle θ (force per unit soil area)
$\dot{\tau}$	rate of applied shear stress
stress-factor	magnification factor on τ_{α} due to redistribution of contacts
θ	angle of orientation of a particle with the horizontal
u	axial deformation in creep = $\Delta(\text{length})$
u_o	initial deformation in creep = $\Delta(\text{length})_o$
u_f	ultimate deformation in creep = $\Delta(\text{length})_f$
U^*	creep function = $\dfrac{u - u_o}{u_f - u_o}$
w_i	initial water content
w_f	final water content
$Z(t)$	$= 1/2\ \alpha\xi \dfrac{k_1 k_2}{k_1 + k_2}\ t$ in Equation (27)

CHAPTER I

INTRODUCTION

The shearing resistance of clays is not well understood. The lack of understanding arises from the complexity of the physical properties of clays.

The conventional concept of expressing the shearing resistance of clays in terms of a cohesion and a friction is attributed to Coulomb. While this concept is relatively simple, it does not explain the mechanism of shearing resistance in clays.

Hvorslev (1936, 1960) expressed the Coulomb criterion in terms of a true cohesion (c_e) and a true angle of friction (Φ_e). Experimental studies have shown, however, that the parameters c_e and Φ_e are not unique for a given soil but depend upon the structure and stress history of the soil. Conceivably, other factors may also affect c_e and Φ_e.

The Coulomb-Hvorslev criterion is a failure theory and is not concerned with the deformation phenomena at stresses below failure. Schmertmann and Osterberg (1960) studied the variation of the cohesion and friction components of the shearing resistance with strain prior to failure. Their results show that the cohesion is mobilized at small strains while considerable deformation is needed to mobilize the full frictional resistance. Similar observations are also reported by Wu, Douglas and Goughnour (1962).

For an understanding of the shearing resistance of cohesive soils, an examination of the clay structure appears to be a logical starting point. Tan (1957) presented a schematic picture of clay mineral network with edge-to-face contacts of clay particles. Tan's concept of the structure of clay as a solid skeleton of plate-like particles in a "card-house" structure was verified by Rosenqvist (1959) by means of the electron microscope. Mitchell (1956) and Lambe (1960) have demonstrated that deformations tend to cause particle orientation in clays. By means of the petrographic micrograph, Wu, Douglas and Goughnour (1962) illustrated the tendency of the particles to align themselves parallel to a slip plane.

The movement of the clay particles under load is considered as a rate process (Glasstone, Laidler and Eyring, 1941) by Murayama and Shibata (1961), Christensen (1964) and Mitchell (1964). These studies have shown that the shearing resistance can be related to the bonds at the contacts between the clay particles.

In this study, friction and cohesion are defined respectively as the components of shearing resistance dependent and independent of the effective stress as proposed by Schmertmann and Osterberg (1960). The general objective is to correlate the behavior of friction and cohesion with the movement and resistance of the clay particles. A particle model is proposed. In this model, the angle of internal friction and the non-viscous part of cohesion are assumed to be the result of the resistance at the particle contacts. The viscous part of cohesion is treated as the result of the flow characteristics of the contacts and is assumed to obey the rate process theory.

The region within which two adjacent particles come closest together is termed a "contact." Actual mineral-to-mineral contact of the surfaces is not required.

CHAPTER 2

THEORETICAL CONSIDERATIONS

In this chapter, friction and cohesion are considered from the viewpoint of the clay particle structure. A particle model is developed. In this model, the resistance at the contacts of the particles is assumed to consist of a mineral friction and an adhesion. The angle of internal friction is assumed to be derived from mineral friction at the contacts. The resistance due to adhesion at the contacts is considered to be a non-viscous cohesion. The behavior of the viscous cohesion is assumed to be governed by the flow characteristics of the contacts as a rate process. A rheologic model is used to represent the combined action of the contact resistance and the viscous flow.

2.1 Particle Model

The deformation and thereby the deformational resistance of clays involve, in essence, the interaction of the clay particles. The arrangement and contact geometry of the particles in the clay mineral network, therefore, play an important role in the strength and deformation behavior of clays. In the following, the shearing resistance is treated as the result of the contact resistance of the particles in the clay matrix. Following the derivation by Skempton (1960), the contact resistance is assumed to consist of a mineral friction and an adhesion. It is further assumed that the mineral friction and adhesion at the contacts constitute the resistance to sliding and to displacement of the contacts.

2.1.2 Particle Movement and Resistance

The mechanism assumes that the strength of the clay matrix is derived from consolidation, during which the clay particles arrange themselves in some manner such that they form a network. Due to different contact geometry, the strength of the contacts may vary widely. When the matrix is under stress, some contacts fail while others remain intact.

In order to make an analysis of the mechanism, a model is proposed in the following sections based on several simplifying assumptions. It is not intended to imply that these assumptions truly represent the local conditions in an actual clay structure. However, it is believed that the analysis based on the model nevertheless contributes to the understanding of the phenomenon and provides a systematic basis for correlating experimental observations.

The simplifying assumptions of the model are: 1) deformations are the result of particle movements and may be represented by the displacements at the contacts; 2) stresses on the contact may be calculated by the equations for the stresses in a continuum; 3) the major and minor principal stresses at the contact, σ_{1s} and σ_{3s} act in the same directions as the effective major and minor principal stresses on a specimen, $\bar{\sigma}_1$ and $\bar{\sigma}_3$ respectively; 4) all contacts have the same area A_c; 5) normal and tangential forces are the same at all contacts with the same angle θ; 6) all contacts with the same angle θ have equal strengths;

7) applied stresses are uniformly distributed over the soil area under consideration; 8) applied loads are equally distributed among the contacts; 9) the model is two-dimensional only.

In an assembly of particles, various types of particle movement can be expected. For example, a particle can rotate, translate or slide over another. One may even envision a particle to slide over another while causing the other to rotate or translate. The movements therefore are combinations of sliding, rotation, translation and others. Since the particles are interconnected through the contacts, the particle movements must necessarily follow the movements at the contacts. Therefore, it may be assumed that the particle movements can be represented by the movements at the contacts.

In Fig. 1a is shown a section A-A at an inclination of α with the horizontal cut through the particles in a specimen under the effective major and minor principal stresses $\bar{\sigma}_1$ and $\bar{\sigma}_3$. Along the α-direction, the shear stresses τ whose magnitudes are equal but of opposite direction are also shown in Fig. 1a.

If we consider relative displacement between the two halves along A-A, we can distinguish two kinds of contact displacement. At a, the upper half may slip over the lower half by simple sliding of particle 2 over particle 1. At b, the upper half can slip over the lower half only if particle 2 is displaced. This would involve the displacement of particles 3 and 4.

The two types of movement and the corresponding resistance are as follows.

a. Sliding Type of Movement and Resistance

The simplest type of contact displacement is that produced by one particle sliding over another. Consider the contact between particles 1 and 2 at a in Fig. 1a; the forces acting on it are shown in Fig. 2.

With reference to Fig. 2,

P_θ is the normal force to the face of particle 1 on which slip occurs

T_θ is the tangential force along the face of particle 1

C_a is the resisting force due to adhesion

$P_\theta \tan\mu$ is the resisting force due to mineral friction along θ

$\tan\mu$ is the coefficient of mineral friction

R is the total resisting force along θ at the contact

The sliding movement of the contact is analogous to the sliding phenomenon of solid bodies (Bowden and Tabor, 1954). When the contact is acted upon by the forces P_θ and T_θ, $P_\theta \tan\mu$ and C_a are brought into action. The force R is given by

$$R = C_a + P_\theta \tan\mu \tag{1}$$

Sliding occurs when

$$T_\theta = R = C_a + P_\theta \tan\mu \tag{2}$$

Equation (1) defines the resistance to sliding of the contact along θ. In 2.1.2, $P_\theta \tan\mu$ and C_a are considered separately. $P_\theta \tan\mu$ is considered under "Frictional Resistance against Sliding" in 2.1.2.a. C_a is considered under "Adhesional Resistance against Sliding" in 2.1.2.c.

b. Displacement Type of Movement and Resistance

Consider the contact between particles 2 and 5 at b in Fig. 1a. Sliding is unlikely since the contact is required to undergo an "uphill" displacement along the face of particle 2. However, even if this contact at b remains intact, it may still undergo displacement--if particle 2 is unable to resist the forces transmitted to it by the contact. Particle 2 is in contact with particles 1 and 4; particle 4 is in turn in contact with particle 3. Thus, to displace particle 2 (and thereby the contact at b), the resisting forces due to the contacts with particles 1 and 4 have to be overcome. Accordingly, we define the displacement resistance of particle 2 (and thereby the contact at b) as the force perpendicular to the particle that the contacts with particles 1 and 4 are able to withstand.

In Fig. 3, P is the displacement resistance of particle 2. It is the total resistance against the displacement of particle 2. It acts at an angle of $(\theta - 90^{\circ})$ with the horizontal. P consists of two parts: one part due to mineral friction, denoted by P_F and the other part due to adhesion, denoted by P_A. P_F is considered under "Frictional Resistance against Displacement" in 2.1.2.b. P_A is considered under "Adhesional Resistance against Displacement" in 2.1.2.d.

2.1.2 Contact Resistance

The contact resistance consists of: a) Frictional Resistance against Sliding; b) Frictional Resistance against

Displacement; c) Adhesional Resistance against Sliding; d) Adhesional Resistance against Displacement.

a. Frictional Resistance against Sliding

Fig. 4(a) shows the forces acting on the contact at a; it differs from Fig. 2 in that only the sliding resistance due to friction is shown. P_θ and T_θ are, as before, the normal and tangential forces on the face of particle 1. $t_{1\theta}$ is that part of the contact resistance against sliding which is due to friction. It acts at an angle α, the inclincation of the failure plane, with the horizontal.

The sliding resistance due to friction is $P_\theta \tan\mu$. Sliding occurs when

$$\tan\mu = T_\theta / P_\theta \tag{3}$$

Assuming that each contact is treated as a continuum, the stress condition at incipient sliding as defined by (3) can be represented by a Mohr circle. Such a representation is shown in Fig. 4(b).

Let

n_θ = the number of contacts with an angle θ along section A-A in Fig. 1a

n = $\sum_{\theta=0}^{\theta=\pi} n_\theta$

A_θ = the total soil area parallel to θ along section A-A (Fig. 1b)

A_α = the gross soil area along the α-plane (Fig. 1b)

Hence

$$A_\alpha = \sum_{\theta=0}^{\theta=\pi} A_\theta \cos(\theta - \alpha)$$

In Fig. 4(b), σ_{1s} and σ_{3s} (in force per unit contact area) are the major and minor principal stresses at the contact. According to assumptions (2) to (5) on p. 5,

$$n_\theta\ A_c \cos\theta\ \sigma_{1s} = A_\theta \cos\theta\ \bar{\sigma}_1$$

$$n_\theta\ A_c \cos\theta\ \sigma_{3s} = A_\theta \sin\theta\ \bar{\sigma}_3$$

or

$$\left.\begin{aligned} \sigma_{1s} &= \bar{\sigma}_1 \frac{A_\theta}{n_\theta\ A_c} \\ \sigma_{3s} &= \bar{\sigma}_3 \frac{A_\theta}{n_\theta\ A_c} \end{aligned}\right\} \qquad (4)$$

where A_c is the area of a contact along θ

$A_\theta \cos\theta$ and $A_c \cos\theta$ are respectively the projections of A_θ and A_c on the horizontal plane

$A_\theta \sin\theta$ and $A_c \sin\theta$ are respectively the projections of A_θ and A_c on the vertical plane

$\bar{\sigma}_1$ and $\bar{\sigma}_3$ are assumed uniformly distributed

$A_c \cos\theta\ \sigma_{1s}$ and $A_c \sin\theta\ \sigma_{3s}$ are assumed to be the same at all contacts with angle θ

For forces normal and parallel to θ,

$$A_\theta\ \bar{\sigma}_\theta = n_\theta\ A_c\ \sigma_{s\theta}$$

$$A_\theta\ \tau_\theta = n_\theta\ A_c\ \tau_{s\theta}$$

where

$\bar{\sigma}_\theta$ is the effective normal stress to the plane θ (force per unit soil area)

$\sigma_{s\theta}$ is the normal stress at the contacts with angle θ (force per unit contact area)

τ_{θ} is the shear stress along the plane θ (force per unit soil area)

$\tau_{s\theta}$ is the shear stress at the contacts with angle θ (force per unit contact area)

$A_c\ \sigma_{s\theta}$ and $A_c\ \tau_{s\theta}$ are assumed to be the same at all contacts with angle θ

For a contact with an angle θ:

$$T_{\theta} = A_c\ \tau_{s\theta} = \frac{A_{\theta}\ \tau_{\theta}}{n_{\theta}}$$

$$P_{\theta} = A_c\ \sigma_{s\theta} = \frac{A_{\theta}\ \sigma_{\theta}}{n_{\theta}}$$

Equation (3) becomes

$$\tan\mu = \frac{T_{\theta}}{P_{\theta}} = \frac{\tau_{\theta}}{\sigma_{\theta}} = \frac{\tau_{s\theta}}{\sigma_{s\theta}}$$

Hence sliding at the n_{θ} contacts occurs at the contact stress $\sigma_{s\theta}$ and $\tau_{s\theta}$ in Fig. 4(b).

Along the α-plane,

$$\left.\begin{aligned} A_\alpha \tau'_{\alpha\theta} &= n_\theta\, A_c\, t_{1\theta} \\ \text{and} \quad A_\alpha \sum_{\theta=0}^{\theta=\pi} \tau'_{\alpha\theta} = A_\alpha \tau'_\alpha &= \sum_{\theta=0}^{\theta=\pi} n_\theta\, A_c\, t_{1\theta} \end{aligned}\right\} \qquad (5)$$

where

$t_{1\theta}$ is the frictional resistance against sliding contributed by a contact with an angle θ (force per unit contact area)

τ'_α is the shearing resistance on the α-plane due to the frictional resistance against sliding at the n contacts; it is assumed uniformly distributed over A_α (force per unit soil area)

$\tau'_{\alpha\theta}$ is that portion of τ'_α due to n_θ contacts with angle θ (force per unit soil area)

In Fig. 4(b), the vector OB has components $\tau_{s\theta}$ and $\sigma_{s\theta}$. It is inclined at an angle μ to the σ_s-axis. From the Mohr diagram in Fig. 4(b), the radius of the circle is $(\sigma_{s\theta} - \frac{\sigma_{1s} + \sigma_{3s}}{2}) \frac{1}{\cos 2\theta}$.

Hence

$$t_{1\theta} = (\sigma_{s\theta} - \frac{\sigma_{1s} + \sigma_{3s}}{2}) \frac{\sin (\pi - 2\theta)}{\cos 2\theta}) \qquad (6a)$$

Also

$$\sigma_{s\theta} \tan\mu = (\sigma_{s\theta} - \frac{\sigma_{1s} + \sigma_{3s}}{2}) \tan 2\theta$$

Whence

$$\sigma_{s\theta} = (\frac{\sigma_{1s} + \sigma_{3s}}{2}) \frac{\sin 2\theta}{\sin 2\theta - \tan\mu \cos 2\theta}$$

Substituting this value for $\sigma_{s\theta}$ in (6a),

$$t_{1\theta} = 1/2(1+k)\ \sigma_{3s}\ \sin 2\alpha\ \left(\frac{\tan\mu}{\sin 2\theta - \tan\mu \cos 2\theta}\right) \quad (6b)$$

where

$$k = \frac{\bar{\sigma}_1}{\bar{\sigma}_3} = \frac{\sigma_{1s}}{\sigma_{3s}}$$

Substituting for σ_{3s} from (4) in (6b),

$$t_{1\theta} = 1/2(1+k)\ \bar{\sigma}_3\ \sin 2\alpha\ \left(\frac{\tan\mu}{\sin 2\theta - \tan\mu \cos 2\theta}\right) \cdot \frac{A_\theta}{n_\theta A_c} \quad (6)$$

The applied shear stress along α is given by

$$\tau_\alpha = 1/2\ (\bar{\sigma}_1 - \bar{\sigma}_3)\ \sin 2\alpha$$

$$= 1/2\ (k-1)\ \bar{\sigma}_3\ \sin 2\alpha$$

When τ_α is imposed on a soil area A_α within which there are n contacts of area A_c each and

$$n = \sum_{\theta=0}^{\theta=\pi} n_\theta ,$$

$$\left.\begin{aligned} n\ A_c\ t_\alpha &= A_\alpha \tau_\alpha \\ n_\theta A_c\ t_\alpha &= A_\alpha \tau_{\alpha\theta} \end{aligned}\right\} \quad (7)$$

where

τ_α is the applied shear stress assumed uniformly distributed over A_α

$\tau_{\alpha\theta}$ is that portion of τ_α to be carried by n_θ contacts with angle θ (force per unit soil area)

t_α is the shear stress along α at a contact with an angle θ. It is assumed to be the same at all contacts (force per unit contact area).

From Fig. 4(b),

$$t_\alpha = 1/2\ (\sigma_{1s} - \sigma_{3s})\ \sin 2\alpha$$

$$= 1/2\ (k-1)\ \sigma_{3s}\ \sin 2\alpha$$

Substituting for σ_{3s} from (4),

$$t_\alpha = 1/2(k-1)\ \bar{\sigma}_3\ \sin 2\alpha\ \frac{A_\theta}{n_\theta\ A_c} \qquad (7a)$$

It can be seen that the ratio $\frac{A_\theta}{n_\theta\ A_c}$ appears

both in equation (7a) for t_α and equation (6) for $t_{1\theta}$.

Let this ratio be $a_\theta = \frac{n_\theta\ A_c}{A_\theta}$. We write (6) as

$$t_{1\theta} = 1/2\ (1+k)\ \bar{\sigma}_3\ \sin 2\alpha\ \left(\frac{\tan\mu}{\sin 2\theta - \tan\mu\ \cos 2\theta}\right)\ \frac{1}{a_\theta}$$

It is to be noted that unless the particle distribution is uniform with respect to θ, A_θ and n_θ vary with θ. The absolute magnitude of $t_{1\theta}$ in equation (6) therefore also varies with A_θ and n_θ.

b. Frictional Resistance against Displacement

Fig. 5(a) shows the displacement resistance of particle 2 due to friction. It is assumed that the displacement of the particle is perpendicular to the direction θ. The resistance offered by friction is denoted by P_F; it is assumed to act in a direction perpendicular to the particle. $A_c t_{2\theta}$ is the shear force along the α-plane that is required to overcome P_F. α is the angle of the inclination of the failure plane with the horizontal.

The particles in the network are interconnected. Hence, to displace particle 2, a number of particles must be displaced. Let m be the number of slipping contacts associated with the displacement of particle 2.

For the displacement of particle 2 to take place, the frictional resistance at each of the m contacts must be exceeded. P_F is defined as a resistance contributed by the m slipping contacts. It is assumed to be the same for all contacts. For simplicity, we assume,

$$P_F = \frac{A_\theta}{n_\theta}\, p_F = \frac{A_\theta}{n_\theta}\, \bar{\sigma}_n\, m \tan\mu \qquad (8)$$

where

p_F = $\bar{\sigma}_n$ m $\tan\mu$. It is assumed to act in the same direction as P_F and uniformly distributed (force per unit soil area).

$\bar{\sigma}_n$ is the mean effective normal stress (force per unit soil area)

m is the number of slipping contacts associated with the displacement of particle 2.

In this study, only the experimental behaviors under triaxial compression with $\bar{\sigma}_2 = \bar{\sigma}_3$ are investigated. Hence

$$\bar{\sigma}_n = \left(\frac{2 + k}{3}\right) \bar{\sigma}_3$$

Substituting this value for $\bar{\sigma}_n$ in (8),

$$P_F = \left(\frac{2 + k}{3}\right) \bar{\sigma}_3 \frac{A_\theta}{n_\theta} \cdot m \tan\mu \qquad (8')$$

Let there be n contacts of area A_c each within A_α

and

$$n = \sum_{\theta=0}^{\theta=\pi} n_\theta$$

Along the α-plane,

$$P_F \sin(\theta-\alpha) = A_c \, t_{2\theta}$$

or

$$t_{2\theta} = \frac{P_F \sin(\theta - \alpha)}{A_c} \qquad (9)$$

and

$$\sum_{\theta=0}^{\theta=\pi} n_\theta \, P_F \sin(\theta - \alpha) = \sum_{\theta=0}^{\theta=\pi} n_\theta \, A_c \, t_2 = A_\alpha \tau''_\alpha$$

where

$t_{2\theta}$ is the frictional resistance against displacement contributed by a contact with an angle θ (force per unit contact area).

τ''_α is the shearing resistance on the α-plane due to the frictional resistance against displacement at the n contacts. It is assumed uniformly distributed over A_α. (force pre unit soil area)

Substituting for P_F from (8') in (9a),

$$t_2 = m \tan\mu \left(\frac{2+k}{3}\right)\bar{\sigma}_3 \sin(\theta-\alpha) \frac{A_\theta}{n_\theta A_c} \qquad (9)$$

Alternatively, we assume p_F to be the average normal stress, or $p_F = \bar{\sigma}_n$. Assuming that P_F is the same for all contacts, we write

$$P_F = \frac{A_\theta}{n_\theta} \quad p_F = \left(\frac{2 + k}{3}\right) \bar{\sigma}_3 \frac{A_\theta}{n_\theta} \tag{10a}$$

Substituting for $\bar{\sigma}_3$ from (4) in (10a),

$$P_F = \left(\frac{2 + k}{3}\right) \sigma_{3s} A_c$$

or

$$p_s = p_F \frac{1}{a_\theta} = \left(\frac{2 + k}{3}\right) \sigma_{3s} \tag{10b}$$

The stress condition at the contact b as defined by (10b) is represented by the Mohr circle shown in Fig. 5(b).

In Fig. 5(b), σ_{1s} and σ_{3s} are the major and minor principal stresses at the contact. The major principal plane is in the horizontal direction. According to assumptions (2) to (5) on p. 5, p_s and τ_s (in force per unit contact area) are respectively the normal and shear stresses at the contact. α is the angle of the inclination of the failure plane. The objective is to calculate $t_{2\theta}$.

From the Mohr diagram in Fig. 5(b),

$$t_{2\theta} = (p_s - \sigma_{3s})\tan(\pi-\theta) \frac{1}{\sin (2\theta-\pi)} \sin(\pi-2\alpha)$$

or

$$t_{2\theta} = (p_s - \sigma_{3s}) \frac{\sin 2\alpha}{1 + \cos 2\theta}$$

Substituting for p_s from (10b) and $\bar{\sigma}_{3s}$ from (4),

$$t_{2\theta} = \left(\frac{k-1}{3}\right) \bar{\sigma}_3 \frac{\sin 2\alpha}{1 + \cos 2\theta} \cdot \frac{A_\theta}{n_\theta A_c}$$

Using $a_\theta = \dfrac{n_\theta A_c}{A_\theta}$,

$$t_{2\theta} = \left(\frac{k-1}{3}\right) \bar{\sigma}_3 \frac{\sin 2\alpha}{1 + \cos 2\theta} \cdot \frac{1}{a_\theta} \qquad (10)$$

Using equation (9), $t_{2\theta}$ can be obtained with given values of m, k, α and μ for a range in θ. As an approximation, we assume m = 6. This means that the displacement of particle 2 involves the slip of 6 contacts. The variation of $t_{2\theta}$ with respect to θ for m = 6, k = 1.3, $\alpha = 50^\circ$ and $\tan\mu = 0.1$ is shown in Fig. 6. Results of the computations are tabulated in Table A-1 in Appendix I.

Using equation (10), the variation of $t_{2\theta}$ with respect to θ for k = 1.3, $\alpha = 50^\circ$ and $\tan\mu = 0.1$ is shown in Fig. 6. Results of the computations are tabulated in Table A-1 in Appendix I.

Since the assumptions used in the derivation of equations (9) and (10) are rather severe, the variation of $t_{2\theta}$ with θ can only be considered as estimates of the range of P_F. If we take an average of the 2 equations, we may represent this average by

$$t_{2\theta} = \rho \left(\frac{2+k}{3}\right) \bar{\sigma}_3 \frac{1}{\sin(\theta - \alpha)} \cdot \frac{1}{a_\theta} \qquad (11)$$

where ρ is a coefficient.

Using equation (11), the variation of $t_{2\theta}$ with respect to θ is shown for ρ = 0.3 and 0.5 in Fig. 6. For comparison, the values of k = 1.3, α = 50° and tanμ = 0.1 are used. Results of the computations are tabulated in Table A-1 in Appendix I.

It can be seen from Fig. 6 that equation (11) is a reasonable average of equations (9) and (10). Throughout this study, (11) is used for $t_{2\theta}$ for convenience.

Using equations (6) and (11), the contact resistance can be obtained with given values of k, α, μ and ρ for a range in θ, which represents the direction of contact movement.

According to Horn and Deere (1962), for most clay minerals, tanμ is of the order of 0.1 and appears to vary only within limited ranges. In this study, tanμ is assumed to be a constant equal to 0.1.

For most clays, the angle of internal friction Φ ranges between 10 - 30 degrees. Since $\alpha = 45^\circ + \Phi/2$, α ranges between 50 - 60 degrees.

An examination of equations (6) and (11) indicates that for the above values of tanμ, α and ρ

$t_{1\theta} > t_{2\theta}$ when $0^\circ < \theta \leqslant 6^\circ$,

$t_{1\theta} \doteq t_{2\theta}$ when $6^\circ < \theta < 10^\circ$,

$t_{1\theta} < t_{2\theta}$ when $10^\circ \leqslant \theta \leqslant 85^\circ$,

and

$$t_{1\theta} \doteq t_{2\theta} \quad \text{when } 85^\circ < \theta < 90^\circ.$$

For $90^\circ < \theta < 180^\circ$, sliding is unlikely to take place since the contact has to undergo an "uphill" displacement (see e.g. the contact at b in Fig. 1a). Since contact displacement would occur by whichever means possible, for particles oriented at $10^\circ \leqslant \theta \leqslant 85^\circ$, the contact resistance is governed by equation (6). And, for particles oriented at $0^\circ < \theta < 10^\circ$ and $85^\circ < \theta$ 180°, the contact resistance is governed by equation (11).

The contact resistance due to friction is, therefore, given by

$$t_{1\theta} = 1/2(1+k)\ \bar{\sigma}_3 \sin 2 \ \left(\frac{\tan\mu}{\sin 2\theta - \tan\mu \cos 2\theta}\right) \frac{1}{a_\theta} \qquad (6)$$

$$\text{for } 10^\circ \leqslant \theta \leqslant 85^\circ$$

and

$$\left.\begin{aligned} t_{2\theta} &= \rho\left(\frac{2+k}{3}\right) \bar{\sigma}_3 \frac{1}{\sin(\theta - \alpha)} \frac{1}{a_\theta} \\ &\qquad \text{for } 85^\circ < \theta < 180^\circ \\ t_{2\theta} &= \rho\left(\frac{2+k}{3}\right) \bar{\sigma}_3 \frac{1}{\sin(\alpha - \theta)} \frac{1}{a_\theta} \end{aligned}\right\} \qquad (11)$$

$$\text{for } 0^\circ < \theta < 10^\circ$$

By using various values of k in (6) and (11), $\alpha = 50^{\circ}$ and $\tan\mu = 0.1$, the variation of contact resistance with respect to θ is computed for $\rho = 0.2$, 0.3, 0.4 and 0.5. Results of the computations are tabulated in Tables A-2, A-3, A-4, A-5 and A-6 in Appendix I. Figs. 7 and 8 show the calculated spectrum for $\rho = 0.3$ and 0.5 respectively.

Fig. 9 shows the comparison of contact resistance due to friction for the same value of $\tan\mu = 0.1$ and $\rho = 0.3$ but different values of $\alpha = 50^{\circ}$ and 60°. It can be seen from Fig. 9 that for k between 1.5 and 2.9, the difference is rather small. Hence, throughout this study, the value of $\alpha = 50^{\circ}$ is used.

c. Adhesional Resistance against Sliding

Fig. 10(a) shows the forces acting on the contact at a; it differs from Fig. 2 in that only the sliding resistance due to adhesion is shown. P_{θ} and T_{θ} are, as before, the normal and tangential forces on the face of particle 1. $t_{3\theta}$ is that part of the contact resistance atainst sliding which is due to adhesion. It acts at an angle α, the inclination of the failure plane, with the horizontal.

The sliding resistance due to adhesion is C_a. Sliding occurs when

$$T_{\theta} = C_a \qquad (12)$$

The stress condition at incipient sliding as defined by (12) is represented by the Mohr circle shown in Fig. 10(b).

In Fig. 10(b), σ_{1s} and σ_{3s} are the major and minor principal stresses at the contact. The major principal plane is in the horizontal direction. OB is the resistance due to adhesion at the contact. It is a constant equal to c_s. c_s is defined by

$$n_\theta \; A_c \; c_s = A_\theta \; c_a \text{ or } c_s = c_a \; \frac{1}{a_\theta},$$

and

$$\sum_{\theta=0}^{\theta=\pi} n_\theta \; A_c \; c_s = A_\alpha \; c_a$$

where

c_s is the adhesion at a contact with angle θ; it is assumed to be the same for all contacts (force per unit contact area)

c_a is the adhesion along θ; it is assumed to be a constant along any θ and independent of stress (force per unit soil area)

For a contact with an angle θ:

$$T_\theta = A_c \; \tau_{s\theta} \text{ and } C_a = A_c \; c_s$$

Equation (12) becomes $\tau_{s\theta} = c_s$

Hence sliding at the n_θ contacts occurs at the stress $\sigma_{s\theta}$ and $\tau_{s\theta}$ in Fig. 10(b).

Along the α-plane,

$$
\left.\begin{aligned}
&A_\alpha \tau'''_{\alpha\theta} = n_\theta A_c t_{3\theta} \\
\text{and} \\
&A_\alpha \sum_{\theta=0}^{\theta=\pi} \tau'''_{\alpha\theta} = A_\alpha \tau'''_\alpha = \sum_{\theta=0}^{\theta=\pi} n_\theta A_c t_{3\theta}
\end{aligned}\right\} \tag{13}
$$

where

$t_{3\theta}$ is the adhesional resistance against sliding contributed by a contact with an angle θ (force per unit contact area)

τ'''_α is the shearing resistance on the α-plane due to the adhesional resistance against sliding at the n contacts. It is assumed uniformly distributed over A_α . (force per unit soil area)

$\tau'''_{\alpha\theta}$ is that portion of τ'''_α due to n_θ contacts with angle θ (force per unit soil area)

From the Mohr diagram in Fig. 10(b),

$$t_{3\theta} = (\sigma_{1s} - \sigma_{3s})1/2 \sin(\pi - 2\alpha) = 1/2\ (\sigma_{1s} - \sigma_{3s})\sin 2\alpha$$

Also

$$c_s = 1/2\ (\sigma_{1s} - \sigma_{3s})\ \sin 2\theta$$

Whence

$$t_{3\theta} = \frac{\sin 2\alpha}{\sin 2\theta}\, c_s \tag{14a}$$

Substituting for $c_s = c_a \dfrac{1}{a_\theta}$ in (14a),

$$t_{3\theta} = \frac{\sin 2\alpha}{\sin 2\theta}\, c_a \cdot \frac{1}{a_\theta} \tag{14}$$

d. Adhesional Resistance against Displacement

Fig. 11 shows the displacement resistance of particle 2 due to adhesion. This resistance is denoted by P_A and is assumed to act in a direction perpendicular to the particle. $A_c t_{4\theta}$ is the shear force along the α-plane that is required to overcome P_A. α is the angle of the inclination of the failure plane with the horizontal.

In accordance with the assumptions in 2.1.2.b, we write

$$P_A = m\, c_s\, A_c$$

$$P_A \sin(\theta - \alpha) = A_c\, t_{4\theta}$$

or

$$t_{4\theta} = m\, c_s \sin(\theta - \alpha) \qquad (15)$$

and

$$\sum_{\theta=0}^{\theta=\pi} n_\theta P_A \sin(\theta - \alpha) = \sum_{\theta=0}^{\theta=\pi} n_\theta A_c\, t_{4\theta} = A_\alpha\, \tau_\alpha''''$$

where

$t_{4\theta}$ is the adhesional resistance against displacement contributed by a contact with an angle θ (force per unit contact area)

τ_α'''' is the shearing resistance on the α-plane due to the adhesional resistance against displacement at the n contacts. It is assumed uniformly distributed over A_α.

As before, we represent (15) by

$$t_{4\theta} = \rho_m \frac{c_s}{\sin(\theta - \alpha)}$$

where ρ_m is a coefficient ranging approximately between 2 - 5.

Substituting for $c_s = c_a \frac{1}{a_\theta}$,

$$t_{4\theta} = \rho_m \frac{c_a}{\sin(\theta - \alpha)} \cdot \frac{1}{a_\theta} \tag{16}$$

Since contact displacement would occur by whichever means possible, equations (14) and (16) are subject to the same restrictions on θ as equations (6) and (11). Accordingly, the contact resistance due to adhesion is given by

$$t_{3\theta} = c_a \frac{\sin 2\alpha}{\sin 2\theta} \cdot \frac{1}{a_\theta} \qquad \text{for } 10^\circ < \theta < 85^\circ \tag{14}$$

and

$$\left.\begin{aligned} t_{4\theta} &= \rho_m \frac{c_a}{\sin(\theta - \alpha)} \cdot \frac{1}{a_\theta} \\ &\quad \text{for } 85^\circ < \theta < 180^\circ \\ t_{4\theta} &= \rho_m \frac{c_a}{\sin(\alpha - \theta)} \cdot \frac{1}{a_\theta} \\ &\quad \text{for } 0^\circ < \theta < 10^\circ \end{aligned}\right\} \tag{16}$$

Using $\alpha = 50^\circ$ in (14) and (16), the variation of the contact resistance with respect to θ is computed for $\rho_m = 2,3,4$ and 5. Results of the computations are tabulated in Tables A-7(a) and A-7(b) in Appendix I.

Fig. 12 shows the calculated spectrum for $\rho_m = 2,3,4$ and 5.

To estimate the values of t_3 and t_4, we find from Fig. 12:

$$t_3 \quad \begin{cases} \text{minimum} = 1\ c_a \frac{1}{a} \\[2ex] \text{maximum} = 5.7\ c_a \frac{1}{a} \\[2ex] \text{average} = 3.35\ c_a \frac{1}{a} \end{cases}$$

$$\begin{matrix} t_4 \\ (\rho_{m=3}) \end{matrix} \quad \begin{cases} \text{minimum} = 3\ c_a \frac{1}{a} \\[2ex] \text{maximum} = 5.5\ c_a \frac{1}{a} \\[2ex] \text{average} = 4.25\ c_a \frac{1}{a} \end{cases}$$

Consider t_3 and t_4 as contributing directly to the non-viscous cohesion c'. As an approximation, take

$$\text{average} \quad \left.\begin{matrix} t_3 \\[2ex] t_4 \end{matrix}\right\} = c' \frac{1}{a}$$

For $\bar{\sigma}_3 = 2.0$ kg/cm^2, the average value of non-viscous c' is at most 0.15 kg/cm^2 for the slow CFS tests (Table 2). Thus

$$\text{average} \quad \left.\begin{matrix} t_3 \\[2ex] t_4 \end{matrix}\right\} = 0.15 \frac{1}{a} \text{ kg/cm}^2$$

$$\text{Average } t_3 = 3.35\ c_a \frac{1}{a} = 0.15 \frac{1}{a}, \quad c_a = 0.0448 \text{ kg/cm}^2$$

$$\therefore \text{ max. } t_3 = 5.7\ c_a \frac{1}{n} = 5.7 \times 0.0448 \frac{1}{a} = 0.255 \frac{1}{a} \text{ kg/cm}^2$$

$$\text{Average } t_4 = 4.25\, c_a \frac{1}{a} = 0.15 \frac{1}{a}, \quad c_a = 0.0353 \text{ kg/cm}^2$$

$$\therefore \text{ max. } t_4 = 5.5\, c_a \frac{1}{a} = 5.5 \times 0.0353 \frac{1}{a} = 0.194 \frac{1}{a} \text{ kg/cm}^2$$

For comparison, we take $k = 1.3$ and $\bar{\sigma}_3 = 2.0$ kg/cm^2.

From Fig. 7 ($\rho = 0.3$):

$$t_1 \begin{cases} \text{minimum} = 0.1 \dfrac{1}{a} \times \bar{\sigma}_3 = 0.2 \dfrac{1}{a} & \text{kg/cm}^2 \\ \text{maximum} = 0.4 \dfrac{1}{a} \times \bar{\sigma}_3 = 0.8 \dfrac{1}{a} & \text{kg/cm}^2 \end{cases}$$

$$t_2 \begin{cases} \text{minimum} = 0.35 \dfrac{1}{a} \times \bar{\sigma}_3 = 0.7 \dfrac{1}{a} & \text{kg/cm}^2 \\ \text{maximum} = 0.5 \dfrac{1}{a} \times \bar{\sigma}_3 = 1.0 \dfrac{1}{a} & \text{kg/cm}^2 \end{cases}$$

Comparing the average value of t_3 and t_4 (0.255 and $0.194 \times \frac{1}{a}$ kg/cm^2) with the range of values for t_1 and t_2, we find that t_3 and t_4 will attain their maximum value long before t_1 and t_2 become fully developed.

2.1.3 Redistribution of Contacts

The contact resistance expressed by equations (6), (11), (14), and (16) is inadequate to describe the shear behavior of a matrix of clay particles in that the re-distribution of the displaced particles resulting from failure of the contacts has not been considered. Taking up new positions in the network, the displaced particles may or may not give rise to the reforming of contacts. If no contacts are reformed, a reduction in overall strength results. Even if contacts are reformed, the overall strength can increase, decrease or remain the same. For example, if a contact is reformed as a result of the displacement of a contact that has failed, the strength of this reformed contact depends on the new position taken up by the displaced particle. The strength of this reformed contact, therefore, can be equal to, greater or smaller than that of the displaced contact. It follows that various new states of particle arrangements are possible as a result of the various modes of redistribution of the displaced particles. In the following, four possible modes of redistribution are presented.

As shown in 2.1.2 on p. 27, when the matrix is under stress, the adhesion resistance is overcome before the friction resistance becomes fully developed. Since the range in adhesion resistance is much smaller than that in friction resistance, the various modes of redistribution would have only a small effect on the adhesion resistance. For simplicity, only the friction resistance is considered in the analysis of contact redistribution.

The four modes of redistribution are defined as follows: a) Partial Remolding; b) Complete Remolding; c) Partial Re-orientation; d) Complete Re-orientation.

a. Partial Remolding

Partial Remolding is a mode of redistribution in which when the resistance of a contact is exceeded, the movement of this displaced contact is such that the contact maintains the same resistance. This contact, therefore, can carry no additional shear stress.

b. Complete Remolding

Complete Remolding is a mode of redistribution in which when the resistance of a contact is exceeded, the movement of this displaced contact is such that no contact is reformed. Once its resistance is exceeded, this displaced contact, therefore, transfers all of its share of shear stress to the other contacts.

c. Partial Re-orientation

Partial Re-orientation is a mode of redistribution in which when the resistance of a contact is exceeded, the movement of this displaced contact is such that a contact having a greater strength than that of the displaced contact is reformed. Since the reformed contacts can carry additional shear stress, the overall strength of the matrix increases. All particle contacts whose resistance are governed by equation (6) belong to the sliding group; all particle contacts whose resistance are governed by equation (11) belong to the displacement group.

If a contact is reformed as a result of the movement of a displaced contact in the sliding group, the position taken up by the reformed contact is assumed to be restricted to the range of the sliding group. Likewise, if a contact is reformed as a result of the movement of a displaced contact in the displacement group, the position taken up by the reformed contact is assumed to be restricted to the range of the displacement group. Uniform distribution of the displaced contacts is assumed within the two groups.

Since the sliding group has a lower maximum resistance than the displacement group, contacts in the sliding group will be exhausted first. Once the sliding group is exhausted, all displaced contacts redistribute themselves into the displacement group.

d. Complete Re-orientation

Complete Re-orientation is a mode of redistribution in which when the resistance of a contact is exceeded, the movement of this displaced contact is such that a contact having a greater strength than that of the displaced contact is reformed. It is assumed that this reformed contact can take all possible position of orientations. While both groups are in existence, the position taken up by the reformed contact is not restricted to be within the range of either group. Uniform distribution of the displaced contacts is assumed. Becuase of the smaller maximum strength of the sliding group, this group is exhausted first. After this, all contacts are in the displacement group. Since the reformed contacts can carry additional shear stress, the overall strength of the matrix increases.

The behavior of the real material most probably is a combination of the four modes presented.

2.1.4 Behavior of the Particle Model

In this section, the stress-displacement characteristics of the contacts according to the various modes of redistribution are calculated. The spectrum of contact strengths due to friction are given graphically in Figs. 7 and 8. The modes of redistribution are defined in 2.1.3.

For convenience, the following definitions and symbols have been introduced:

<u>Stress</u> — All stresses applied to the matrix are expressed in terms of k, the effective principal stress ratio.

<u>Matrix Failure</u> — That state of stress at which every point on the failure plane satisfies the condition of maximum obliquity.

<u>n</u> — Number of contacts within a soil area A_α along an α-plane.

<u>M</u> — Range in θ (degrees) in which contact failure occurs under k.

<u>n_m</u> — Number of contact failure in M.

<u>τ_α</u> — Applied shear stress along α-plane (failure plane) in force per gross area of soil.

<u>stress-factor</u> — A magnification factor on τ_α resulting from redistribution of displaced contacts.

Assuming a random arrangement of particles and using $\tan_{\mu} = 0.1$, $\alpha = 50^{\circ}$ and $\rho = 0.3$, the variation of n_m with respect to k is computed for the four modes of redistribution. The detailed procedure of computations for each mode of redistribution is presented in Appendix II.

Figs. A-1, A-2, A-3 and A-4 in Appendix II serve as illustrations to the procedure of computations. Results of the computations for the various modes are summarized in Tables A-8(a), A-8(b), A-8(c) and A-8(d) in Appendix II.

In the same manner, computations for the k-n_m characteristics are also carried out for $\rho = 0.5$. They are summarized in Tables A-9(a), A-9(b), A-9(c) and A-9(d) in Appendix II.

Assuming that each contact failure contributes a displacement of e along the θ-plane, the total displacement due to n_m contacts is given by $N = n_m e$. The results obtained in Tables A-8(a), A-8(b), A-8(c), A-8(d), A-9(a), A-9(b), A-9(c) and A-9(d) are used to plot the stress-displacement (k-N) curves for the various modes of redistribution. Figs. 13 and 15 show the stress-displacement curves for $\rho = 0.3$ and 0.5 respectively.

In Figs. 13 and 15, curve (a) shows the k-N characteristics for partial remolding. The characteristic of this curve is such that when a stress is applied to the matrix, contacts with the smallest resistance along a failure plane slip first. Upon failure of these contacts, displacements take place. As displacements are taking place, these contacts maintain the same strengths. Therefore these contacts can carry no additional stress. When the next load increment is applied, the remaining contacts are required to carry a bigger share of the increment than that in the first increment. Thus as displacements proceed under additional applied stresses, more contacts fail and more contacts with the same strengths as those displaced are reformed. The remaining intact contacts are required to carry a progressively bigger share of the stress. A point is reached at which there are no longer any intact contacts left along the failure planes of the matrix. At this point, the matrix has reached failure. Thus when failure is reached, the matrix deforms indefinitely under the failure stress. The behavior described by curve (a) is similar to that of a remolded clay whose overall strength may be explained in terms of the "exhaustions" of intact contacts as stresses are applied to the matrix.

In Figs. 13, and 15, curve (b) shows the k-N characteristic for complete remolding. The characteristic of this curve is such that when a stress is applied to the matrix, contacts with the smallest resistance along a failure plane slip first. Upon failure of these contacts, displacements take place. As displacements are taking place, contacts are <u>not</u> reformed. As displacements proceed, the contacts that have failed transfer all of their share of stress to the other intact contacts thus causing more contacts to fail. When all the stresses carried by the failed contacts are transferred to the stronger contacts, displacements cease. Thus the intact contacts are required to carry a bigger share of the load as displacements proceed under the same load. Under additional stresses, more contacts fail and the remaining contacts are required to carry a progressively bigger share. A point is reached at which there are no longer any intact contacts left along the failure planes of the matrix. At this point, the matrix has reached failure. Thus when the failure stress is reached, the failure of all the contacts along the failure planes results in a reduction in strength of the matrix to zero. The behavior of curve (b) is therefore similar to that of a quick clay, which is known to have a sudden reduction in strength at failure.

In Figs. 13 and 15, curves (c) and (d) show the k-N characteristics for partial re-orientation and complete re-orientation respectively. The characteristics of these curves are such that when a stress is applied to the matrix, contacts with the smallest resistance along a failure plane slip first. Upon failure of these contacts, displacements take place. As displacements are taking place, contacts with greater strengths are reformed. After these contacts are reformed, displacements cease. As displacements proceed under additional applied stresses, more contacts fail and more contacts with greater strengths are reformed. A point is reached at which the load on the contacts reaches the maximum value attainable. At this point, the matrix has reached failure. Thus when failure is reached, the matrix deforms indefinitely. The behavior described by curves (c) and (d) is thus similar to that of a consolidated clay whose overall strength requires a considerable amount of deformation to be fully mobilized.

Each of the four stress-displacement curves is admittedly a gross simplification of the behavior of a real material. To approximate the behavior of a real material in which all four processes take place, an average is taken of the four cases. Figs. 14 and 16 show the average k-N curves for μ = 0.3 and 0.5 respectively. In Figs. 14 and 16, curve A is obtained by averaging all the four curves (a), (b), (c) and (d) at N = 0 to n_e and by averaging only curves (a), (c) and (d) at $N > n_e$. Curve B is obtained by averaging all the four curves at all values of N. Since complete remolding is probably only valid for a quick clay, curve A may be a more realistic representation. Results of the computations for Curves A and B for μ = 0.3 and 0.5 are tabulated in Table A-10 in Appendix II.

2.1.5 The Mechanism of Friction in Clays

The behavior of the particle model represented by the stress-displacement characteristics of curve A in Figs. 14 and 16 may be summarized in the following hypothesis for the mechanism of friction.

The resistance at the contact consists of an adhesion and a mineral friction; the adhesion and mineral friction constitute the resistance against sliding and that against displacement. The contact resistance is dependent on the geometric orientations and contact geometry of the particles. Along the direction of shear, the variation of the contact resistance with respect to the particle orientation is expressed by a spectrum. The contact resistance due to adhesion is estimated to be small in comparison with that due to friction and is considered to have little effect on the stress-strain properties.

When a shear stress is imposed on a specimen, contacts with the smallest resistance along the direction of shear slip first. Since the resistance due to adhesion is small in comparison with that due to friction, it is fully mobilized at all the contacts instantaneously. This quantity is independent of the normal stress and is considered to be a non-viscous cohesion. The part due to mineral friction is directly proportional to the normal stress and contributes to the angle of internal friction Φ'. Following these contact failures, particles are displaced from one position to another and new contacts may be reformed. Even if the position taken up by a displaced particle is favorable to the reforming of contacts, this process requires a certain time interval. However, even if this requirement of time is met, for a reformed contact to develop its maximum resistance to shear, a certain minimal of time may be required. Furthermore, due to the different orientations and contact geometry of the displaced particles in their new positions, the strengths of the reformed contacts vary. Thus, the resistance of a reformed contact depends on the orientation and contact geometry of the displaced particle as well as the time available or elapsed time between displacements.

Consider the behavior of the angle of internal friction Φ' when a specimen is subjected to a constant strain rate test. When shear stresses are applied to the specimen, contacts fail and displacements take place. As displacements are taking place, contacts with greater strengths are being developed. The overall strength of the matrix therefore increases gradually with the deformation. Accordingly, Φ' increases gradually with the deformation. As deformation proceeds further, all the contacts are loaded to the maximum contact strength attainable. Then the reformed contacts have the same strengths as those displaced. Thus, when failure is reached, Φ' reaches a maximum and remains at this value with further deformation.

For simplicity, we may assume that the rate of contact displacement is proportional to the strain rate. If the strain rate that corresponds to a rate of contact displacement $\dot{N}_m$ is such that sufficient time is available for the reformed contacts to develop their maximum resistance, the maximum value of Φ' at any given strain is attained. This is denoted by Φ'_m. If a faster strain rate that corresponds to a rate of contact displacement $\dot{N}_1$ is used, then there is insufficient time for the reformed contacts to develop their maximum resistance. The value of Φ' at any given strain would then be smaller than Φ'_m. Accordingly, the value of Φ' at failure (Φ'_u) is also smaller. If the strain rate is less than that required to create the rate of contact displacement $\dot{N}_m$, the same Φ'-strain characteristic as for that of $\dot{N}_m$ is obtained.

Thus, according to the hypothesis, the behavior of the angle of internal friction under constant strain rate is as follows:

$$\left.\begin{array}{lll} \text{At any strain } \epsilon, & \text{if} & \dot{N} > \dot{N}_m,\ \Phi' < \Phi'_m \\ & & \dot{N} \leqslant \dot{N}_m,\ \Phi' = \Phi'_m \\ \text{At failure } (\overline{\sigma}_1/\overline{\sigma}_3 = \text{const.}), & & \\ & \text{if} & \dot{N} > \dot{N}_m,\ \Phi'_u < \Phi'_{um} \\ & & \dot{N} \leqslant \dot{N}_m,\ \Phi'_u = \Phi'_{um} \end{array}\right\} \quad (17)$$

where $\dot{N}$ = N/t, is the rate of contact displacement

N is the contact displacement at any strain ϵ

t is the time required to reach N

$\dot{N}_m$ = N/t_m, is the rate of contact displacement required to attain Φ'_m

t_m is the minimal of time required to attain Φ'_m

Φ' is the angle of internal friction at any strain ϵ

Φ'_m is the maximum value of Φ' at any strain ϵ

N_u = $\dot{N} \times t_u$, is the contact displacement at failure

t_u is the time required to reach N_u

Φ'_u is the value of Φ' at N_u (at failure)

t_{um} is the minimal of time required to attain Φ'_{um} $= N/\dot{N}_m$

and Φ'_{um} is the maximum value of Φ' attainable under $\dot{N}_m$ (at failure)

The variation of Φ' with respect to strain ϵ at various rates of contact displacement $\dot{N}$ is illustrated in Fig. 17(a). It can be seen from Fig. 17(a) that

at any strain ϵ,

$$\text{since } \dot{N}_2 > \dot{N}_1 > \dot{N}_m , \quad \Phi'_2 < \Phi'_1 < \Phi'_m$$

and at failure,

$$\text{since } \dot{N}_2 > \dot{N}_1 > \dot{N}_m , \quad \Phi'_{u2} < \Phi'_{u1} < \Phi'_{um}$$

Fig. 17(b) shows qualitatively the variation of Φ' with the rate of contact displacement $\dot{N}$ at various strains ϵ.

The variation of Φ' under creep with respect to the displacement rate under creep is assumed to be similar to that of Φ' with respect to $\dot{N}$. When a creep load k is applied, the weaker contacts along a failure plane slip first. Following these contact failures, displacements take place and contacts with greater strengths are reformed. After these contacts are reformed, displacements cease. At any creep strain ϵ_c, in order to attain a value of Φ' denoted by Φ'_c, a certain number of contacts must be displaced. This gives rise to a displacement N_c which requires a time t_c to reach. Thus, Φ'_c increases with t_c and approaches a maximum value Φ'_k at a time t_k beyond which it remains virtually constant. Alternatively, Φ'_c increases with decreasing displacement rate under creep $\dot{N}_c$ and approaches a maximum value Φ'_k at a rate $\dot{N}_k$ below which it remains virtually constant. According to the hypothesis, however, only the value of Φ'_k at t_k is known. Values of Φ'_c at any creep time t_c may be obtained as follows.

The Φ'_c-$\dot{N}_c$ curve as shown in Fig. 17(c) is similar to the Φ'_u-$\dot{N}$ characteristics under constant strain rate in Fig. 17(b). We may obtain values of Φ'_c at any creep time t_c by comparing $\dot{N}_c = N_c/t_c$ and $\dot{N} = N_u/t_u$ in the following manner:

$$\left.\begin{array}{llll} \text{If} & \dot{N}_c \leqslant \dot{N}_m , & \Phi'_c = \Phi'_k \\ & \dot{N}_c > \dot{N}_m , & \Phi'_c = \dfrac{\Phi'_k}{\Phi'_{um}} \times \Phi'_u \end{array}\right\} \quad . \qquad (18)$$

where the value of Φ'_u corresponds to $\dot{N} = \dot{N}_c$.

2.2. The Mechanism of Cohesion in Clays

To fully describe the shearing resistance, the mechanism of friction advanced in 2.1.5 must necessarily be supplemented by the hypothesis proposed for the mechanism of cohesion.

In the development of the mechanism of friction in 2.1.5, the resistance encountered by a particle when it is displaced from one position to another has not been taken into consideration. The clay particle is known to be surrounded by a layer of adsorbed water of high viscosity. When a particle is displaced from one position to another, it would encounter viscous resistance. It is the hypothesis that this viscous resistance constitutes a large part of the cohesion in clays. Accordingly, the flow phenomenon is treated by a viscous flow model, after the initial yield value given by the contact resistance due to friction and adhesion has been exceeded. If the applied stress on the contact is less than this yield value, no flow occurs.

As shown by Christensen (1964), the deformational properties of the clay particle structure can be represented schematically by a rheologic model shown in Fig. 18. In Fig. 18,

k_1 represents the initial elastic response of the flowing contacts,

k_2 corresponds to the resistance due to Φ' and non-viscous cohesion as calculated by the particle model,

α and β correspond to viscous cohesion.

According to the rate theory (Glasstone, Laidler and Eyring, 1941), the flow equation of the contacts is given by

$$\dot{\gamma}_1 = \beta \sinh \alpha f_1 \qquad (19$$

where

$\dot{\gamma}_1$ = rate of shear strain in the viscous element

β = $\frac{2}{\lambda_1} \frac{kT}{h} \exp\left(- \frac{\Delta F}{RT}\right)$

λ = vertical distance between successive interparticle equilibrium positions

λ_1 = distance between flow units in the direction of flow

k = Boltzmann's constant

h = Plank's constant

T = the absolute temperature

ΔF = activation energy

R = universal gas constant

$\beta = \dfrac{\lambda}{2\nu kT}$

ν = number of contacts per unit area over the plane of shear

f_1' = shear stress in the viscous element

f_y = yield value or yield strength of the contacts, given by the contact resistance due to adhesion and friction

$f_1 = f_1' - f_y$ is the shear stress that causes flow in the viscous element.

Thus the right hand side of the rheologic model represents the effects of the contact stresses that cause flow. When a shear stress τ is applied, if the stresses on the contacts due to this shear stress exceed the yield value f_y of the contacts, viscous flow occurs. As deformation proceeds, the stresses tending to cause flow are transferred to the stronger contacts represented by k_2 until all flow stops, giving rise to a new yield value of the contacts. This new yield value is then given by the increased resistance of the contacts due to the reforming of stronger contacts.

When a shear stress τ is applied, we have

$$\tau = k_2 \gamma + f_1 \tag{20}$$

$$f_1 = k_1 (\gamma - \gamma_1) \tag{21}$$

where γ is the total shear strain.

Combining (19), (20) and (21), the governing differential equation for this model can be shown to be

$$\frac{d}{dt}[(k_1 + k_2)\gamma - \tau] = k_1 \beta \sinh \alpha f_1 \tag{22}$$

For constant strain rate, $\dot{\gamma}$ = constant

we have

$$\frac{df_1}{dt} = k_1 \left(\frac{d\gamma}{dt} - \beta \sinh \alpha f_1\right) \tag{23}$$

Letting

$$\beta' = \frac{\dot{\gamma}}{\beta}$$

we have

$$\frac{d(\alpha f_1)}{d(\alpha\beta k_1 t)} = \beta' - \sinh(\alpha f_1)$$

substituting for $\quad \sinh(\alpha f_1) = \dfrac{e^{\alpha f_1} - e^{-\alpha f_1}}{2}$

we have

$$\frac{d(e^{\alpha f_1})}{1/2 - 1/2e^{2\alpha f_1} + \beta' e^{\alpha f_1}} = d(\alpha\beta k_1 t)$$

Integrating,

$$\frac{2}{\sqrt{1 + \beta'^2}} \times \tanh^{-1}\left(\frac{e^{\alpha f_1} - \beta'}{\sqrt{1 + \beta'^2}}\right) = \alpha\beta k_1 t - C$$

$$f_1 = \frac{1}{\alpha} \log_e \left[\beta' + \sqrt{1 + \beta'^2} \tanh \frac{\sqrt{1 + \beta'^2}}{2} (\alpha\beta k_1 t - C)\right] \tag{24}$$

Applying the Boundary Condition : $t = 0$, $f_1 = 0$.

$$f_1 = \frac{1}{\alpha} \log_e \left[\beta' + \sqrt{1 + \beta'^2} \tanh\left[\frac{\sqrt{1 + \beta'^2}}{2} \alpha\beta k_1 t + \tanh^{-1} \frac{1 - \beta'}{\sqrt{1 + \beta'^2}}\right]\right]$$

or

$$f_1 = \frac{1}{\alpha} \log_e \left[\beta' + \sqrt{1+\beta'^2} \tanh\left[\frac{\sqrt{1 + \beta'^2}}{2} \frac{\alpha k_1}{\beta'} \gamma + \tanh^{-1} \frac{1 - \beta'}{\sqrt{1 + \beta'^2}}\right]\right] \tag{25}$$

For Creep loading, $\dot{\text{[illegible]}} = 0$ **(see Christensen, 1964)**

From (22)
$$\frac{k_1 + k_2}{k_1 k_2} \frac{df_1}{dt} = - \text{[illegible]}' \sinh \text{[illegible]} f_1 \qquad (26)$$

Solving (26) and applying the Boundary condition:

$$t = 0, \ f_1 = \frac{k_1}{k_1 + k_2}$$

we have

$$f_1 = - \frac{1}{\text{[illegible]}} \log_e \tanh \left[1/2 \ \text{[illegible]} \ \frac{k_1 k_2}{k_1 + k_2} t + \tanh^{-1} \exp \left(- \frac{\text{[illegible]} k_1 \text{[illegible]}}{k_1 + k_2} \right) \right] \qquad (27)$$

Equation (25) expresses the variation of the resistance to viscous flow of the clay particle structure or viscous cohesion with respect to shear deformation under the condition of constant strain rate. Equation (27) expresses the variation of the resistance to viscous flow of the clay particle structure or viscous cohesion with respect to time under the condition of constant shear stress or creep. **After** the evaluation of the parameters [illegible], [illegible], k_1 and k_2, equations (25) and (27) can be used to analyze the behavior of the viscous part of cohesion in clays.

CHAPTER 3

EXPERIMENTAL PROGRAM

3.1 Objective

The purpose of the experimental program is to examine if the hypotheses advanced for the mechanism of friction and cohesion in Chapter 2 can adequately simulate the actual behavior of friction and cohesion in clays.

In order to achieve this objective, the experimental behaviors of friction and cohesion are obtained by carrying out a number of CFS and Creep-CFS triaxial tests on five different clays. The CFS-triaxial tests measure the variation of friction and cohesion with respect to axial strain under different strain rates. The Creep-CFS-triaxial tests measure the variation of friction and cohesion with respect to time under creep. Since the predicted values of cohesion require the parameters in the rheologic model of clay particle structure to be known, a number of creep tests are also carried out in order that these parameters can be evaluated.

3.2 Materials Used

The clays used in this study include laboratory consolidated, compacted and remolded clays, undisturbed clays and Grundite, a commercial illite. The majority of the tests are performed on laboratory consolidated, compacted and remolded specimens of a red clay from Sault Ste. Marie, Michigan. Undisturbed samples in the form of thin-walled shelby tubes were obtained from Willow Run and Marine City, Michigan. The index properties of the clays tested are given in Table 1.

3.3 Sample Preparation

3.3.1 Consolidated Sault Clay

Bulk samples of air-dried Sault Ste. Marie clay were soaked in distilled water for a few days before they were thoroughly remolded at water contents slightly above the liquid limit. The thick slurry was then placed in a 6-inch consolidometer and allowed to consolidate. After a standing period of several weeks, consolidation loads were added to the clay in increments until a pressure of 0.36 kg/cm^2 was attained. For the normally-consolidated specimens, the consolidated cake was then extruded, sliced into pieces, sealed in wax and stored. For the over-consolidated specimens, the cake was loaded to a pressure of 9.0 kg/cm^2. The load was then removed. The unloaded cake was allowed to rebound for several weeks before it was extruded.

3.3.2 Compacted Sault Clay

Bulk samples of air-dried clay were thoroughly remolded and mixed with distilled water to a consistency corresponding to a water content of about 40%. The clay

Table 1 Index Properties of Clays Studied

CLAY	L.L. %	P.L. %	P.I. %	Clay Fraction %
Sault Ste. Marie	60.5	23.6	36.2	60
Willow Run	29.5	19.0	10.5	40
Marine City 1	46.8	24.1	23.7	
Marine City 2	41.4	21.7	19.7	68
Grundite	78.0	25.0	53.0	65

was then left in the moist room for at least a week in order to ensure an even water content distribution. A cake was then made out of the remolded clay by placing it in a static compaction mold. Hand kneading was employed during the placement of the clay in order to remove as much air as possible. In general, a pressure of 1 kg/cm^2 was applied to the cake by the loading ram of a hydraulic testing machine. The pressure was maintained for one hour and released. The cake was then sliced, sealed in wax and stored.

3.3.3 Remolded Sault Clay

Bulk samples of air-dried clay were thoroughly remolded and mixed with distilled water to a consistency corresponding to a water content of about 40%. The clay was then placed in a crock and stored in the moist room for future use. It was molded by hand into a cylinder slightly larger than a triaxial specimen and trimmed to the desired size.

3.3.4 Grundite

The Grundite specimens were prepared in the same manner as was outlined for the compacted Sault clay.

3.3.5 Undisturbed Clays

Undisturbed samples were extruded from 3" O.D. thin-walled shelby tubes and trimmed to the desired specimen size of 3 inches in length and 1.4 inches in diameter.

3.4 Triaxial Tests

All specimens are 3 inches in length and 1.4 inches in diameter. In order to accelerate drainage and pore-water pressure response, filter paper side drains and internal wool drains were used on all specimens. Two "Trojan" rubber membranes were used on all specimens. For the long term creep tests on the undisturbed and laboratory clays, silicon grease was applied between the membranes as an attempt to prevent leakage. In some long term creep tests on undisturbed Marine City clay, a mercury jacket (for details see Bishop and Henkel, 1957) was placed around the specimen in order to prevent osmosis through the membranes.

All samples were consolidated under an all-round pressure. Volume changes were measured throughout the consolidation process. Water contents were measured before consolidation and after completion of the triaxial tests. After consolidation, all samples were back-pressured for at least 10 hours to saturate the sample and the system.

Area corrections have been applied in the evaluation of all the test data (see e.g., Bishop and Henkel, 1957). No attempt was made to correct for the effects of membranes, filter strip restraint and internal drains.

Details of the triaxial testing equipments have been reported elsewhere (see Wu, et al., 1962) and are not repeated here.

3.4.1 CFS Test

The objective of this test is to obtain the development of cohesion (c') and friction (ϕ') with strain under constant strain rate by imposing two different stress states on the specimen through pore-water control. Thus in essence, the CFS test is a drained test under controlled effective stresses. The procedure adopted follows the steps outlined by Schmertmann and Osterberg (1960) with some slight modifications. For a detailed description of the testing procedure adopted in the Soil Mechanics Laboratory at Michigan State University, see Holliday (1963).

The variations of c' and ϕ' with respect to axial strain under different strain rates for the clays testes are presented in graphical form in Figs. A-13, A-14, A-15, A-16, A-17, A-18, A-19, and A-20 in Appendix III. Pertinent details of all the tests are summarized in Table 2.

In Table 2, w_i and w_f are the initial and final water contents. σ_c is the consolidation pressure. $\dot{\epsilon}$ is the constant strain rate at which the test was carried out; it ranges from 0.04 %/hr to 6.7 %/hr. The values of ϵ, c' and ϕ' at the peak deviator stress, $(\sigma_1 - \sigma_3)_{max}$ are denoted by the subscript f. All specimens were strained until the effective principal stress ratio, $\bar{\sigma}_1/\bar{\sigma}_3$ approached a constant value. The values of ϵ, c' and ϕ' at this state are denoted by the subscript u. The mode of failure, observed from visual inspection of the specimen after failure is also included in Table 2.

Table 2 Summary of CFS Tests

Spec. Number	Clay Type	w_1	w_f	σ_c	@ peak Stress $(\sigma_1 - \sigma_3)_{max}$			@ $\bar{\sigma}_1/\bar{\sigma}_3$ = constant end of test			$\dot{\epsilon}$	Failure Mode
		%	%	kg/cm^2	ϵ_f %	c'_f kg/cm^2	ϕ'_f deg.	ϵ_u %	c'_u kg/cm^2	ϕ'_u deg.	%/hr	
R-6	Compacted Sault	48.00	34.20	2.0	-	-	-	10.0	0.257	22.50	0.120	Bulge
R-4		42.90	31.30	"	4.50	0.190	21.20	10.0	0.135	23.60	0.125	Brittle
R-A3		42.00	31.60	"	7.00	0.237	24.30	9.0	0.226	24.30	0.156	Brittle
R-A2		42.00	31.80	"	-	-	-	10.0	0.250	20.00	0.360	Bulge
R-A1		42.00	32.05	"	-	-	-	10.0	0.350	14.50	1.200	Bulge
R-5		49.80	33.90	"	-	-	-	11.0	0.506	7.20	5.60	Bulge
R-4W		47.90	32.80	4.0	-	-	-	11.0	0.620	14.40	1.20	Bulge
R-2		48.65	29.40	6.0	-	-	-	12.0	1.350	10.20	1.20	Bulge
SHR-1	Remolded Sault	40.50	29.85	2.0	-	-	-	9.5	0.390	12.70	1.49	Bulge
SHR-5		39.60	30.70	"	-	-	-	11.0	0.640	6.50	5.79	Bulge
HR-1		45.60	30.20	4.0	-	-	-	10.0	0.550	19.00	1.20	Bulge
HR-2		44.50	27.40	6.0	-	-	-	11.0	1.100	14.00	1.20	Bulge
F-1	Consol. Sault	49.80	32.50	2.0	-	-	-	9.0	0.460	14.60	1.20	Bulge
F-2					-	-	-	10.0	0.320	16.40	1.00	Bulge

Table 2(cont'd) Summary of CFS Tests

Spec. Number	Clay Type	w_1	w_f	σ_c	@ peak Stress $(\sigma_1 - \sigma_3)_{max}$			@ $\bar{\sigma}_1/\bar{\sigma}_3$ = constant end of test			$\dot{\epsilon}$	Failure Mode
		%	%	kg/cm^2	ϵ_f %	c'_f kg/cm^2	ϕ'_f deg.	ϵ_u %	c'_u kg/cm^2	ϕ'_u deg.	%/hr	
F-OC-1 F-OC-2 F-OC-3	Over-Consolida. Sault	28.60 28.60 28.15	29.00 28.65 29.30	2.0 " "	2.50 2.75 1.00	0.410 0.220 0.343	16.90 25.40 16.90	8.0 6.5 6.5	0.520 0.100 0.394	20.70 26.00 13.58	1.120 0.122 3.280	Brittle Brittle Brittle
G-2 G-3 G-5 G-6	Grundite	45.90 47.30 46.40 41.90	34.85 33.60 35.80 34.60	2.0 2.0 2.0 2.0	- - - -	- - - -	- - - -	10.0 10.0 9.0 11.0	0.364 0.430 0.450 0.317	9.53 5.44 2.70 8.40	0.057 1.160 4.150 0.234	Bulge Bulge Bulge Bulge
WR-12 WR-13 WR-7 WR-8	Undis. Willow Run	19.00 17.88 23.39 24.94	18.43 18.22 22.10 24.16	2.0 2.0 3.0 1.0	2.50 2.75 3.40 2.80	0.110 0.02 0.590 0.345	33.50 37.50 17.00 17.40	3.0 3.0 9.5 9.0	0.110 0.00 0.308 0.180	33.50 37.80 24.10 20.70	0.04 0.17 1.50 1.50	Brittle Brittle Brittle Brittle
D-2-4-2	Undis. Marine City	25.20	25.00	2.0	5.0	0.318	23.90	7.0	0.332	20.60	1.00	Brittle

For discussions on the validity of the CFS test, the reader is referred to Schmertmann (1962) and Wu (1963).

3.4.2 Creep-CFS Test

This test is, in essence, a two-phase test consisting of a creep test as the first phase and a CFS test as the second phase. The objective of this test is to obtain the values of cohesion (c'_c) and friction (Φ'_c) after various times of creep. To do this, it is necessary to extrapolate the $c'-\epsilon$ and $\Phi'-\epsilon$ curves of the CFS phase to the axial strain at the end of the creep phase. For a detailed account of the method of extrapolation, see Holliday (1963).

Pertinent details of all the test results are summarized in Table 3. In Table 3, w_i and w_f are the initial and final water contents. $\bar{\sigma}_c$ is the consolidation pressure. ϵ_c is the axial strain at the end of the creep phase. $\dot{\epsilon}_c$ is the rate of creep strain evaluated at or near the end of the strain-time curve of the creep phase. $\dot{\epsilon}$ is the constant strain rate at which the CFS phase was carried out. $k = \bar{\sigma}_1/\bar{\sigma}_3$ is the effective principal stress ratio at the end of the creep phase. c'_c and Φ'_c are the values of c' and Φ' at end of creep at various times of creep t_c.

A creep stress of 1.15 kg/cm^2 with creep time varying from 30 to 7200 minutes was used on the consolidated Sault clay. A creep stress of 1.0 kg/cm^2 with creep time varying from 120 to 4320 minutes was used on the compacted Sault clay.

Table 3 Summary of Creep-CFS Tests

Spec. Number	Clay Type	w_1 %	w_f %	$\bar{\sigma}_c$ kg/cm^2	Creep Stress $(\sigma_1 - \sigma_3)$ kg/cm^2	Creep Time t_c min.	Creep Strain ϵ_c %	$\dot{\epsilon}_c$ @ end Creep %/hr	c_c' @ end Creep kg/cm^2	ϕ_c' @ end Creep deg.	av. CFS $\dot{\epsilon}$ %/hr	k $= \bar{\sigma}_1/\bar{\sigma}_3$ at end creep
F-C-5	Consolidated Sault	40.70	32.20	2.0	1.15	30	1.96	.84000	.575	0.00	1.1.	1.96
F-C-4		48.90	32.40	"	"	60	2.14	.43650	.564	0.40	"	2.17
F-C-2		47.90	32.60	"	"	240	2.31	.22000	.420	6.20	"	2.25
F-C-6		40.80	32.50	"	"	240	2.72	.0825	.473	3.75	"	2.14
F-C-9		40.70	32.00	"	"	390	2.56	.0450	.432	5.10	"	2.10
F-C-8		40.50	33.20	"	"	480	2.90	.0300	.350	7.40	"	1.96
F-C-7		40.65	32.40	"	"	720	2.04	.0200	.403	6.20	"	2.085
F-C-3		47.00	33.10	"	"	1440	2.565	.01395	.393	9.00	0.85	2.85
F-C-1		47.00	33.70	"	"	7200	4.010	.00945	.379	12.21	0.85	3.26

Table 3 (cont'd) Summary of Creep-CFS Tests

Spec. Number	Clay Type	w_1 %	w_f %	σ_c kg/cm^2	Creep Stress $(\sigma_1 - \sigma_3)$ kg/cm^2	Creep Time t_c min.	Creep Strain ϵ_c %	$\dot{\epsilon}_c$ @ end Creep %/hr	c_c' @ end Creep kg/cm^2	ϕ_c' @ end Creep deg.	av.CFS $\dot{\epsilon}$ %/hr	k $= \bar{\sigma}_1/\bar{\sigma}_3$ at end creep
R-C-8	Sault	42.30	31.40	2.0	1.00	120	0.866	.12700	.469	1.00	1.00	1.85
R-C-9		41.80	31.10	2.0	"	480	0.712	.05335	.422	2.85	0.90	1.92
R-C-10		42.60	31.50	"	"	960	1.385	.00500	.372	5.00	0.80	2.02
R-C-11		42.90	32.60	"	"	1440	0.861	.00304	.376	6.00	"	2.43
R-C-7		41.20	32.20	"	"	4320	1.417	.00100	.356	7.40	0.90	2.56

A typical Creep-CFS test data in the graphical form is shown in Fig. A-5 in Appendix III.

3.4.3 Creep Test

As mentioned in 3.1, the objective of the creep test is to obtain the time-deformational characteristics of a clay under creep in order to evaluate the parameters in the rheologic model. With the values of the parameters given, the value of c' can be calculated by means of equations (25) and (27).

In this test, upon completion of consolidation and back-pressure, the sample was loaded with dead weights under undrained condition. Both incremental and single creep loads were used. Axial deformations and pore-pressures were measured and recorded at intervals throughout the entire test. Each creep load was maintained until the pore-pressure changes were negligible and the deformation had almost ceased. The accuracy of the deformation and pore-pressure measurement was $\pm$ 0.0001" and $\pm$ 0.01 kg/cm^2 respectively.

A complete listing of the specimens tested is provided in Table 4. Specimen No. C-C-1, C-C-7 and F-C-9 are quoted from Christensen (1964); Specimen No. IC-1, IC-2, and D-2-4-2 are quoted from Christensen and Wu (1964). A summary of the pertinent details on these tests is given in Tables 4, 5(a) and 5(b).

The method of evaluation of the parameters of the rheologic model has been outlined in detail by

Table 4 Summary of Creep Tests

Specimen No.	Clay Type & Origin	Consolida. Pressure kg/cm^2	Stress History	Initial W.C. %	Final W.C. %
C-C-1	Compacted Sault	2.0	N.C.	42.70	29.10
C-C-7	Compacted Sault	2.0	N.C.	43.80	29.80
F-C-9	Consolida. Sault	2.0	N.C.	54.15	31.80
F-C-1	Consolida. Sault	2.0	N.C.	41.00	31.60
F-OC-1	Consolida. Sault	2.0	O.C.	27.60	27.90
IC-1 IC-2	Grundite	2.0	N.C.	44.30 41.50	34.40 33.20
D-2-4-2	Undisturbed Marine City	2.0	O.C.	26.10	26.10

Table 5(a) Summary of Model Parameters(After R.W. Christensen)

Sample No.	Load Incre.	Initial $(\sigma_1-\sigma_3)$ kg/cm^2	Final $(\sigma_1-\sigma_3)$ kg/cm^2	$\Delta(\sigma_1-\sigma_3)$ kg/cm^2	k_1 kg/cm^2	k_2 kg/cm^2	$\frac{k_1}{k_1+k_2}$	α cm^2/kg	β 10^{-7} min-1	ϵ_o %	ϵ_∞ %
C-C-1	1	0.000	0.500	0.500	7660.00	154.00	0.9830	21.50	1.895	0.0000	0.1081
	2	0.500	0.765	0.265	559.00	65.30	0.8950	28.80	1.503	0.1081	0.2440
	3	0.765	0.999	0.234	1093.00	19.15	0.9820	21.30	3.850	0.2440	0.6580
	4	0.999	1.240	0.241	482.00	10.30	0.9790	20.80	13.24	0.6580	1.4300
	5	1.240	1.490	0.250	606.00	7.43	0.9880	13.84	19.48	1.4300	2.5500
	6	1.490	1.708	0.218	283.00	5.70	0.9820	22.50	15.95	2.550	3.850
	7	1.708	1.890	0.182	248.00	1.08	0.9950	50.90	41.60	3.850	9.370
C-C-7	1	0.000	0.9870	0.9870	516.00	23.20	0.9570	13.96	61.50	0.000	1.420
F-C-9	1	0.000	1.103	1.103	46.70	8.47	0.848	22.70	5.980	0.000	4.350

Table 5(b) Summary of Model Parameters from Creep Tests

Sample No.	Load Incre.	Initial $(\sigma_1 - \sigma_3)$ kg/cm^2	Final $(\sigma_1 - \sigma_3)$ kg/cm^2	$\Delta(\sigma_1 - \sigma_3)$ kg/cm^2	k_1 kg/cm^2	k_2 kg/cm^2	$\frac{k_1}{k_1+k_2}$	α cm^2/kg	β 10^{-7} min^{-1}	ϵ_o %	ϵ_∞ %
F-C-1	1	0.0000	0.5000	0.5000	1580.7	29.30	0.975	14.00	5.440	0.0000	0.535
	2	0.4985	0.7415	0.2430	268.9	27.10	0.908	15.50	8.730	0.5350	1.060
	3	0.7415	0.9950	0.2535	167.0	13.00	0.928	14.60	5.680	1.0600	1.660
	4	0.9950	1.2400	0.2450	32.78	8.32	0.7965	67.35	0.214	1.6600	2.660
F-OC-1	2	0.4950	0.7515	0.2565	411.70	104.30	0.798	23.80	2.970	0.0000	0.0822
	3	0.7515	1.0600	0.3085	423.30	37.20	0.920	19.45	1.545	0.0822	0.3580
	4	1.0600	1.2550	0.1950	453.88	2.12	0.995	17.70	41.200	0.3580	0.6650
D-2-4-2	1	0.2700	0.4700	0.2000	305.00	95.00	0.762	65.00	0.900	0.0000	0.0703
	2	0.4700	0.6700	0.2000	355.00	445.00	0.889	12.00	4.700	0.0703	2.203
	3	0.6700	0.8700	0.2000	323.00	77.00	0.806	30.00	1.300	2.2030	3.068
	4	0.8700	1.0700	0.2000	629.00	41.00	0.938	26.00	2.000	3.0680	4.693
IC-1	1	0.000	0.700	0.700	90.70	9.30	0.910	20.70	7.40	0.000	2.51
IC-2	1	0.000	0.500	0.500	117.0	8.30	0.940	14.60	32.00	0.000	2.01
	2	0.500	0.800	0.300	190.0	10.50	0.950	12.20	16.00	2.010	2.93

Christensen (1964) and is not repeated here. A typical sample calculation of the determination of the model parameters is included in Appendix IV.

All relevant data, upon which the determination of the parameters of the rheologic model is based, are presented in Figures A-6, A-7, A-8, A-9, A-10, A-11 and A-12 in Appendix III. In these figures,

u_o is the deformation at zero time

u_f is the ultimate deformation

$\dot{u}$ is the deformation rate

U^* $= (u-u_o)/(u_f-u_o)$ is the dimensionless creep function

$Z(t)$ $= 1/2$ [illegible] $\dfrac{k_1 k_2}{k_1 + k_2}\, t$ in Equation (27)

A $= \tanh^{-1} \exp \left(- \dfrac{[illegible]\, k_1\, [illegible]}{k_1 + k_2}\right)$ in Equation (27)

and D $= \bar{[illegible]}_1 - \bar{[illegible]}_3$ is the creep stress

In Fig. A-12, the deformation is still progressing when the oil in the triaxial cell became depleted. There followed the temporary release of cell pressure and creep load that accompanied the replacement of the oil supply. The second part of the curve was measured after the cell pressure and creep load were resumed.

A summary of the parameters of the rheologic model is given in Tables 5(a) and 5(b). In Tables 5(a) and 5(b), [illegible]$_o$ and [illegible]$_\infty$ are the initial and final axial strain in % for the load increment shown. All the other notations are defined as before in 2.2.

CHAPTER 4

ANALYSIS OF EXPERIMENTAL RESULTS

In this chapter, the experimental results are analyzed in terms of the hypotheses presented in Chapter 2. The behaviors of friction and cohesion are analyzed separately in 4.2 and 4.3.

4.1 Presentation of Test Data

4.1.1 CFS Tests

The variations of Φ' with respect to axial strain under different constant strain rates for the series of tests on each of the clays (compacted Sault, remolded Sault, over-consolidated Sault, Grundite and undistrubed Willow Run) are shown in Figs. 19, 20, 21, 22 and 23 respectively.

The variations of Φ' with respect to strain rate at axial strains of 1%, 2%, 3%, etc. for the series of tests on each of the clays (compacted Sault, overconsolidated Sault, Grundite and undisturbed Willow Run) are shown in Figs. 24(a), 25(a), 26(a) and 27(b) respectively. These values of Φ' were obtained from the Φ'-. curves. They are tabulated in Tables A-11, A-12, A-13 and A-14 in Appendix III.

The variations of Φ' with respect to the time required to reach the axial strains of 1%, 2%, 3%, etc.

under different constant strain rates for the series of tests on each of the clays (compacted Sault, overconsolidated Sault, Grundite, and undisturbed Willow Run) are given in Tables A-11, A-12, A-13 and A-14 in Appendix III. The value of Φ' as a function of elapsed time is plotted in Figs. 24(b), 25(b), 26(b) and 27(a).

The variations of c' with respect to axial strain under different constant strain rates for the series of tests on each of the clays (compacted Sault, remolded Sault, overconsolidated Sault, Grundite and undisturbed Willow Run) are shown in Figs. 32, 33, 34, 35 and 36 respectively.

The variations of c' with respect to strain rate at axial strains of 1%, 2%, 3%, etc. for the series of tests on each of the clays (compacted Sault, Grundite, overconsolidated Sault and undisturbed Willow Run) are shown in Figs. 37, 38, 39 and 40 respectively. These values of c' were obtained from the $c'-\epsilon$ curves. They are tabulated in Tables A-11, A-12, A-13 and A-14 in Appendix III.

Due to insufficient test data, curves are not shown for the consolidated Sault, remolded Sault and undisturbed Marine City clays.

4.1.2 Creep-CFS Tests

Pertinent details of all the test results have been summarized in Table 3.

The variation of Φ'_c with respect to creep strain rate for the consolidated and compacted Sault Clays is shown in Fig. 28(a).

The variation of Φ'_c with respect to creep time for the consolidated and compacted Sault clays is shown in Fig. 28(b).

The variation of c'_c with respect to creep strain rate for the consolidated and compacted Sault clays is shown in Fig. 41(a).

The variation of c'_c with respect to creep time for the consolidated and compacted Sault clays is shown in Fig. 41(b).

4.2 The Behavior of Friction

4.2.1 The Experimental Behavior of Friction

a. CFS Tests

The experimental behavior of friction in the CFS test may be summarized as follows.

For all the clays tested, Φ' increases with decreasing strain rate and approaches an ultimate value at a small value of strain rate below which it remains virtually constant. This can be seen from Figs. 19, 20, 21, 22, 23, 24(a), 25(a), 26(a) and 27(b).

Alternatively, it can be said that Φ' increases with increasing testing time (or decreasing strain rate) and approaches an ultimate value after a certain minimal of time t_{um} beyond which it remains virtually constant. This can also be seen from Table 2, Figs. 24(b), 25(b), 26(b) and 27(a). For the compacted Sault clay, Grundite and Willow Run clay, it appears that Φ'_u would increase appreciably with further reduction in strain rate. The minimal of time required to attain the ultimate value Φ'_{um} varies with the clay structure. For each of the clays tested, the estimated values are given in Table 6.

For all the clays except Grundite, the minimal of axial strain ϵ_{um} required to attain the fully mobilized value Φ'_u (Φ' at $\bar{\sigma}_1/\bar{\sigma}_3$ = constant) decreases with decreasing strain rate. This is in full agreement with the findings above. The value of ϵ_{um} at the various strain rates for each of the clays (compacted Sault, overconsolidated Sault, Grundite and undisturbed Willow Run) is also given in Table 6.

b. Creep-CFS Tests

The experimental behavior of friction in the Creep-CFS test may be summarized as follows.

As shown in Fig. 28(b), Φ'_c increases with increasing creep time and approaches an ultimate value Φ'_k at a certain time t_k beyond which it remains virtually constant. The value of t_k for the consolidated and compacted Sault Clays is given in Table 7.

The findings of the Creep-CFS tests are in full qualitative agreement with that of the CFS tests.

Table 6. Strain and time characteristics of friction-CFS tests.

Clay	ϵ_{um} %	$\dot{\epsilon}$ %/hr	ϕ'_u deg.	t_{um} min.	ϕ'_{um} degrees
Compacted Sault	10.00	5.160	7.20		
	9.40	1.200	14.40	3,000	25.50
	7.40	0.360	20.00		
	6.40	0.156	24.30		
Over-Consolidated Sault	5.00	3.28	13.58		
	4.50	1.120	20.70	2,300	28.80
	4.00	0.122	26.00		
Grundite	5.00	4.150	2.70		
	7.00	1.160	5.40	9,500	9.40
	7.00	0.234	8.40		
	9.00	0.057	9.50		
Undisturbed Willow Run	5.50	1.500	20.70		
	3.00	0.170	37.80	4,500	33.50
	2.25	0.04	33.50		

Table 7. Friction-time characteristics--Creep-CFS test on Sault clay.

Clay	t_k min.	Φ'_k deg.
Consolidated Sault	7,500	12.50
Compacted Sault	5,000	7.50

c. Discussion

It may be concluded from the experimental findings that the behavior of friction is time-dependent. The nature of friction is such that to attain full mobilization at any stress level below failure or at failure, a certain minimal of time is required.

It is of interest to note that a value of the Hvorslev's true angle of friction (Φ_e) as high as 33-44 degrees had been reported on triaxial tests of Mexico clay under an average constant strain rate of some 0.083%-strain per hour by Lo (1962). A value of Φ' as high as 33.5-37.5 degrees has also been obtained on undisturbed Willow Run clay at an average strain rate of 0.105 %-strain per hour. Although the nature of Mexico clay is expected to be different from that of the undisturbed Willow Run clay, the trend that "friction" is time-dependent is significant.

4.2.2 Analysis of the Bhavior of Friction

a. Behavior of Φ' under Constant Strain Rate

The experimental findings summarized in 4.2.1.a are in qualitative agreement with the hypothesis for the behavior of friction under constant strain rate expressed by equation (17) in 2.1.5. This provides an insight into the actual mechanism of friction in clays. It may be stated that the nature of friction is such that while the slip at the contacts appears to be the governing mechanism, the resistance to shear at these contacts are also governed by a time element. This time element may be related to the states of interparticle force fields at the contacts when the contacts are failed and reformed.

b. Behavior of Φ' under Creep

If one accepts the validity of equation (17), the behavior of Φ' under creep (Φ'_c) may be analyzed according to Equation (18) in which

$$\dot{N}_c \leqslant \dot{N}_m , \qquad \Phi'_c = \Phi'_k$$

if

$$\dot{N}_c > \dot{N}_m , \qquad \Phi'_c = \frac{\Phi'_k}{\Phi'_{um}} \times \Phi'_u$$

where the value of Φ'_u corresponds to $\dot{N} = \dot{N}_c$.

To evaluate Φ'_c in (18), the following procedure is used.

Values of Φ'_u (Φ' @ $\bar{\sigma}_1/\bar{\sigma}_3$ = constant) can be obtained from results of the CFS tests under different constant strain rates for the compacted and consolidated Sault clays in Table 2. With ε_u and $\dot{\varepsilon}$ for each test given in Table 2, the time t_u to reach ε_u for each test is obtained as $t_u = \varepsilon_u/\dot{\varepsilon}$. The displacement at failure, N_u can be

obtained from Curve A in Figs. 14 and 16. Since failure has taken place when N_u is reached, N_u is taken as 6.n.e for all the specimens under consideration. Thus, for each CFS test, $\dot{N} = 6.n.e/t_u$. As an example, we calculate $\dot{N}$ for Specimen R-6 of the compacted Sault clay in Table 2. From Table 2, $\epsilon_u = 9\ \%$ $\dot{\epsilon} = 0.12\ \%/hr$

$$t_u = \epsilon_u/\dot{\epsilon} = 9/0.12 = 75 \text{ hours}$$

$$\therefore \quad \dot{N} = 6.n.e/75 = 0.08 \text{ n.e/hr}$$

In the same manner, other values of $\dot{N}$ for the series of CFS tests on the consolidated, remolded, and compacted Sault clays are computed and summarized in Table A-15 in Appendix V. The corresponding values of ϕ'_u for these specimens are also shown in Table A-15 in Appendix V.

The variation of ϕ'_u with respect to $\dot{N}$ for the compacted Sault, remolded Sault and consolidated Sault clays is shown in Fig. 29. It can be seen from Fig. 29 that the ϕ'_u-$\dot{N}$ characteristics of these clays can all be represented by one straight line. Accordingly, Fig. 29 is used for the prediction of ϕ'_c in the Creep-CFS tests of both the consolidated and compacted Sault clays.

For each of the Creep-CFS tests on the consolidated and compacted Sault clays, the value of k at end of creep is given in Table 3. With this value of k, N_c (displacement under creep) can be obtained from Curve A in Figs. 14 or 16. $\dot{N}_c$ is then obtained as N_c/t_c. t_c, the creep time for each test is given in Table 3. As an example, we calculate $\dot{N}_c$ for Specimen F-C-5 of the consolidated Sault clay in Table 3.

From Table 3: $k = 1.96$ $t_c = 0.5$ hour

For $\rho = 0.3$: From Fig. 14, for $k = 1.96$, $N_c = 2.05$ n.e

$$\therefore \quad \dot{N}_c = N_c/t_c = 2.05/0.5 = 4.10 \text{ n.e/hr}$$

For $\rho = 0.5$: From Fig. 16, for $k = 1.96$, $N_c = 0.9$ n.e

$$\dot{N}_c = N_c/t_c = 0.9/0.5 = 1.8 \text{ n.e/hr}$$

In the same manner, other values of $\dot{N}_c$ for the specimens of the consolidated and compacted Sault clays are computed for $\rho = 0.3$ and 0.5. They are summarized in Table A-16 in Appendix V.

From Table 7:

$\Phi'_k = 12.5$ degrees for the consolidated Sault clay

$\Phi'_k = 7.5$ degrees for the compacted Sault clay

Due to insufficient CFS test data on the consolidated Sault clay, a value of Φ'_{um} for this clay is not available. However, since the Φ'_u-$\dot{N}$ characteristic of this clay can be satisfactorily represented by that of the compacted Sault clay, the same value of Φ'_{um} for the compacted Sault clay is assumed.

Thus, according to Table 6, $\Phi'_{um} = 25.5^{\circ}$.

From Figure 29, for $\Phi'_{um} = 25.5^{\circ}$, $\dot{N}_m = 0.05$ n.e/hr

As an example, we calculate the predicted values of Φ'_c for Specimen F-C-5 of the consolidated Sault clay in Table 3.

$\rho = 0.3$: From Table A-16 in Appendix V, $\dot{N}_c = 4.1$ n.e/hr

Since $\dot{N}_m = 0.05$ n.e/hr, $\dot{N}_c > \dot{N}_m$

From (18),

$$\text{predicted } \Phi'_c = \frac{\Phi'_k}{\Phi'_{um}} \times \Phi'_u$$

From Fig. 29, for $\dot{N} = \dot{N}_c = 4.1$ n.e/hr,

$$\Phi'_u = 6.2 \text{ deg.}$$

Substituting in (18),

$$\text{predicted } \Phi'_c = \frac{12.5}{25.5} \times 6.2 = 3.04 \text{ deg.}$$

$\rho = 0.5$: From Table A-16 in Appendix V, $\dot{N}_c = 0.9$ n.e/hr

Since $\dot{N}_c > \dot{N}_m$

From (18),

$$\text{predicted } \Phi'_c = \frac{\Phi'_k}{\Phi'_{um}} \times \Phi'_u$$

From Fig. 29, for $\dot{N} = \dot{N}_c = 0.9$ n.e/hr

$$\Phi'_u = 10.0 \text{ deg.}$$

$$\therefore \quad \text{predicted } \Phi'_c = \frac{12.5}{25.5} \times 10 = 4.9 \text{ deg.}$$

In the same manner, other values of predicted Φ'_c for the specimens of the consolidated and compacted Sault clays are evaluated at the various creep time t_c in Table 3. Results of the computations of the values of predicted Φ'_c for $\rho = 0.3$ and 0.5 are summarized in Table A-16 in Appendix V.

The above calculations do not take into account the resistance due to adhesion. Estimates show that the adhesion resistance is approximately equivalent to a k of 1.3 (2.1.2, p.27). This means that $k < 1.3$, $N = 0$

If this is included in the calculations, the resulting value of N would be smaller and Φ'_c would be larger. The difference in Φ'_c would be around 25%. Since the calculations for Φ'_c are approximate and are made to check the principle of the particle model, it is felt that the additional refinement of calculating the adhesion resistance is not warranted.

The predicted values of ϕ'_c from Table A-16 in Appendix V are plotted against the creep time t_c in Figs. 30 and 31 for the consolidated and compacted Sault clays respectively.

For comparison, the observed values of ϕ'_c are shown in Figs. 30 and 31 for the two clays. It can be seen from these figures, that the shape of the predicted behavior is in agreement with that of the observed behavior. The magnitude between predicted and observed, however, differs.

It should be noted that values of ϕ'_c are measured in the CFS test at a strain rate $\dot{\epsilon}$ = 0.8 - 1.1 %/hr. This strain-rate is in most cases different from the values of $\dot{\epsilon}_c$ at the end of the creep period. This change in strain-rates may be expected to effect the measured value of ϕ'_c as it has already been shown that ϕ' is strain-rate sensitive. Since the $\dot{\epsilon}$ in the CFS phase is greater than $\dot{\epsilon}_c$, the measured values of ϕ'_c cannot be taken as the true values that exist at the end of the creep period. If one applies a correction with the relationship in Fig. 24, the agreement between measured and calculated (Figs. 30 and 31) would be improved somewhat.

Alternatively, we may compare ϕ'_k with the value of ϕ'_m at the same strain ϵ_c in a CFS test. If we take the slowest CFS test for the compacted Sault clay for ϕ'_m, we get 16^{o} (Spec. RA-3, at ϵ = 1.4%, Fig. 19). This is considerably greater than 7.5^{o}. However, the CFS test is run at a strain-rate of about 1 %/hr. Hence the difference may be due to the strain rate effect.

4.2.3 Summary

A particle model is proposed for the mechanism of friction in clays. In this model, the resistance at the contacts of the particles is assumed to consist of a mineral friction and an adhesion. It varies with the orientation of the particle relative to the direction of shear.

The angle of internal friction is the result of the resistance due to mineral friction at the contacts. The resistance due to adhesion is estimated to be small in comparison with that due to friction. When the matrix is under stress, the adhesion resistance is fully mobilized at all the contacts instantaneously. This quantity is independent of the normal stress and is considered to be a non-viscous cohesion.

When the clay mineral network is under a shear stress, contacts with the smallest resistance along the direction of shear slip first. Following these contact failures, particles are displaced from one position to another. As displacements are taking place, contacts are being reformed. As displacements proceed, contacts along the direction of shear are reformed. The resistance of these reformed contacts dependson the positions taken up by the displaced particles and the elapsed time between displacements. At any stress level below failure or at failure, the maximum value of the angle of internal friction is attained only if the elapsed time between displacements is sufficient for the reformed contacts to develop their maximum resistance to shear.

The model is used to explain the behavior of the angle of internal friction under a constant strain rate test. By means of equations (17) and (18), the data from constant strain-rate tests are used to calculate the angle of internal friction in the creep test.

The experimental behaviors of the angle of internal friction under constant strain rate and creep are in qualitative agreement with the model behaviors.

4.3 The Behavior of Cohesion

4.3.1 The Experimental Behavior of Cohesion

a. CFS Tests

The experimental behavior of cohesion in the CFS test may be summarized as follows.

For all the clays tested, c' is strongly dependent on strain rate. It decreases with decreasing strain rate and approaches an ultimate value at a very small value of strain rate beyond which it remains virtually constant. This can be seen from Figs. 32, 33, 34, 35, 36, 37, 38, 39, and 40.

b. Creep-CFS Tests

The experimental behavior of cohesion in the Creep-CFS test may be summarized as follows.

For the consolidated and compacted Sault clays tested, c'_c decreases with decreasing creep strain rate and approaches an ultimate value at a certain value of creep strain rate beyond which it remains virtually constant; it does not approach zero when the strain rate approaches zero. This is readily seen in Fig. 41(a).

Alternatively, as shown in Fig. 41(b), c'_c decreases with increasing creep time and approaches a constant value rather than zero when the creep time approaches a large value.

c. Discussion

The experimental findings on the behavior of cohesion from the CFS tests indicate that cohesion is strongly dependent on strain rate. The trend indicates that c' does not approach zero as the strain rate continues to decrease. The findings from the Creep-CFS tests indicate clearly that cohesion decreases with increasing time and approaches a constant value rather than zero when the time approaches a large value. It may, therefore, be concluded that viscous flow is only partially responsible for the nature of cohesion. It appears that the nature of cohesion is partly viscous and partly non-viscous.

4.3.2 Analysis of the Behavior of Cohesion

a. Behavior of c' under Constant Strain Rate

The behavior of c' is analyzed in terms of the viscous resistance of the clay particle structure expressed by equation (25) in which

$$f_1 = \frac{1}{\alpha} \log_e \left[\beta' + \sqrt{1 + \beta'^2} \tanh \left(\frac{\sqrt{1 + \beta'^2}}{2} \frac{\alpha k_1}{\beta'} \gamma + \tanh^{-1} \frac{1 - \beta'}{\sqrt{1 + \beta'^2}} \right) \right]$$

The hyperbolic tangent approaches unity if

$$\frac{\sqrt{1 + \beta'^2}}{2} \frac{\alpha k_1}{\beta'} \gamma + \tanh^{-1} \frac{1 - \beta'}{\sqrt{1 + \beta'^2}} \geqslant 3$$

It is shown in Appendix V under "Validity of Equation (25')" that the values of k_1, α and β at all stress levels of the clays tested are such that the hyperbolic tangent does approach unity. Equation (25) is then reduced to

$$f_1 = \frac{1}{\alpha} \log_e (\beta' + \sqrt{1 + \beta'^2}) \doteqdot \frac{1}{\alpha} \log_e 2\beta' \qquad (25')$$

since β' is large compared with 1.

To evaluate f_1 for the compacted Sault clay in a CFS test under a constant strain rate $\dot{\varepsilon}$, values of α and β are required. These parameters are not constant for a single test specimen but vary with the stress level. Hence the values of α and β from creep tests on the compacted Sault clay are only valid within the range of stresses and strains from which the parameters are obtained. For example, in Table 5(a), under the first load increment of Specimen C-C-1 (C-C-1-1) of the compacted Sault clay, the values of 21.5 cm^2/kg and 1.895×10^{-7} min^{-1} obtained for α and β respectively are only valid for the stress range of $D = (\sigma_1 - \sigma_3) = 0$ to 0.5 kg/cm^2, and the strain range of $\varepsilon = \varepsilon_o$ to $\varepsilon_\infty = 0$ to 0.1081 %. These values of α and β, in addition, are only valid for the compacted Sault clay. Accordingly, the value of f_1 evaluated at a value of $\dot{\gamma}_{oct}$ that corresponds to a value of $\dot{\varepsilon}$ in a CFS test of the compacted Sault clay is only valid for $\varepsilon = 0$ to 0.1081 %.

Likewise, the limitations on the validity of f_1 apply to other load increments on the compacted Sault clay and on the other clays.

As an example, we calculate the values of f_1 for the CFS test on Specimen R-A3 of the compacted Sault clay. From Table 2, $\dot{\epsilon}$ = 0.156 %/hr = 2.6×10^{-5} min^{-1}. In an undrained triaxial compression test, $\gamma_{oct} = \sqrt{2}\,\epsilon$ in which ϵ is the major principal strain and hence the axial strain and γ_{oct} is the octahedral shear strain

Therefore, $\dot{\gamma}_{oct} = \sqrt{2}\,\dot{\epsilon} = \sqrt{2} \times 2.6 \times 10^{-5}\ min^{-1}$

$= 3.68 \times 10^{-1}\ min^{-1}$

From Table 5(a), under the first load increment of Spec. C-C-1:

$D = (\sigma_1 - \sigma_3) = 0.0$ to $0.5\ kg/cm^2$

$\epsilon = 0$ to 0.1081 %

$\alpha = 21.5\ cm^2/kg$ and

$\lambda = 1.895 \times 10^{-7}\ min^{-1}$

Therefore,

$$B' = \dot{\gamma}_{oct}/\lambda = 3.68 \times 10^{-5}/1.895 \times 10^{-7} = 194.5$$

$$f_1 = \frac{1}{\alpha} \log_e (2B') = \frac{1}{21.5} \times \log_e (2 \times 194.5) = 0.278\ kg/cm^2$$

From Table 5(a), under the second load increment of Spec. C-C-1:

$D = (\sigma_1 - \sigma_3) = 0.5$ to $0.765\ kg/cm^2$

$\epsilon = 0.1081 - 0.244$ %

$\alpha = 28.8\ cm^2/kg$ and

$\lambda = 1.503 \times 10^{-7}\ min^{-1}$

Therefore,

$$\beta' = \dot{\gamma}_{oct}/\beta = 3.68 \times 10^{-5}/1.503 \times 10^{-7} = 245$$

$$f_1 = \frac{1}{\alpha} \log_e (2\beta') = \frac{1}{28.8} \times \log_e (2 \times 245) = 0.215 \text{ kg/cm}^2.$$

In the same manner, values of f_1 for the CFS tests on compacted Sault, over-consolidated Sault, Grundite, consolidated Sault and undisturbed Marine City clays are computed. Results of the computations are summarized in Tables A-17, A-18, A-19, A-20 and A-21 in Appendix V.

Compacted Sault Clay--The completeness of the data on this clay permits a comparison of the f_1 and c' values in detail.

Results of f_1 values from Table A-17 in Appendix V are plotted against the final axial strain ϵ_∞ obtained from the incremental creep loading tests from which the values of α and β are determined. For example, for Spec. R-A3 in Table A-17:

$f_1 = 0.28$ kg/cm^2 corresponds to $\epsilon = \epsilon_o - \epsilon_\infty = 0.0 - 0.1081$ %

$f_1 = 0.217$ kg/cm^2 corresponds to $\epsilon = \epsilon_o - \epsilon_\infty - 0.1081 - 0.244$ %

$f_1 = 0.249$ kg/cm^2 corresponds to $\epsilon = \epsilon_o - \epsilon_\infty = 0.244 - 0.658$ %

Thus for Spec. R-A3, values of f_1 of 0.28, 0.215 and 0.249 kg/cm^2 are plotted against ϵ_∞ of 0.1081, 0.244 and 0.658 % respectively.

In the same manner, other values of f_1 and the corresponding values of ϵ_∞ are plotted for Spec. R-A3. Figure 42(a) shows the variation of f_1 with respect to the final axial strain ϵ_∞ for the different constant strain rates used in the CFS tests. The value of f_1 for ϵ_∞ of

9.37% in Table A-17 is not plotted in Fig. 42(a). This is because under this load increment, Spec. C-C-1-7 underwent large deformations and the ϵ_{∞} of 9.37% was determined by extrapolation. Hence the parameters may not be very accurate.

For comparison, the observed c'-strain characteristics at different constant strain rates are shown in Fig. 42(b). From Figs. 42(a) and 42(b), it can be seen that the the shape of c' vs ϵ is in good agreement with that of f_1 vs ϵ. At the same strain rate, the predicted values (f_1) are consistently smaller than the observed values (c'). If a value of some 0.125 kg/cm^2 were added to f_1, a quantitative agreement between the predicted and observed values results.

It is noted in 4.3.1.c that the nature of cohesion is partly viscous and partly non-viscous. The theoretical treatment here appears to explain satisfactorily that part of cohesion that is of viscous nature as borne out by the experimental findings on the compacted Sault clay.

<u>Consolidated Sault Clay and Undisturbed Marine City Clay</u>--The f_1 values from Tables A-20 and A-21 in Appendix V are plotted against $\epsilon_o - \epsilon_{\infty}$ in Figs. 43 and 44 for these two clays. For comparison, the c' values are shown in the same figures.

In Fig. 43, with the expection of the f_1 value at ϵ = 1.065 - 1.693 %, the relative values of f_1 and c' are the same as that obtained for the compacted Sault clay--the predicted value (f_1) is consistently smaller than that of the observed value (c'). The theoretical treatment also explains satisfactorily the behavior of the viscous part of cohesion for the consolidated Sault clay.

For the undisturbed Marine City clay in Fig. 44, the shape of c' vs ϵ is in reasonable agreement with that of f_1 vs ϵ.

Over-consolidated Sault Clay and Grundite--Because of the small range of $\epsilon = \epsilon_o - \epsilon_\infty$ in the creep tests from which α and β are determined, the f_1 values from Tables A-18 and A-19 in Appendix V are plotted against the strain rates. Figs. 45(b) and 46(b) show the variation of f_1 with respect to the constant strain rate at different values of $\epsilon = \epsilon_o - \epsilon_\infty$ for the over-consolidated Sault clay and Grundite respectively.

For comparison, the observed c'-strain rate characteristics for these two clays are shown in Figs. 45(a) and 46(a). It can be seen from these figures that the shape of c' vs $\dot{\epsilon}$ is in reasonable agreement with that of f_1 vs $\dot{\epsilon}$ for both clays. It is of interest to note that for both clays, the predicted value (f_1) is again consistently smaller than the observed value (c').

Discussion--It should be noted that the value of c' refers to an α-plane while that of f_1 refers to the octahedral plane. The inclinations of the α-plane and the octahedral plane are respectively at angles of $\alpha = 45^\circ + \frac{\phi'}{2}$

The rate process is represented by a viscous element in a rheologic model. In this model, the angle of internal friction and the non-viscous part of cohesion represent the yield value or yield strength of the contacts. Viscous flow of the particles takes place when this yield value of the contacts is exceeded. The behaviors of the viscous part of cohesion under constant strain rate and creep are expressed by equations (25) and (27).

The experimental findings on the behavior of cohesion show that it is partly non-viscous and partly viscous. The experimental behaviors of the viscous part of cohesion under constant strain rate and creep are in qualitative agreement with the predicted behaviors according to equations (25) and (27).

and 54.7° with the horizontal. Strictly speaking, f_1 should only be compared with c'_{oct} where

$$c'_{oct} = c' \cos(\alpha - 54.7^{\circ}) = c' \cos(\Phi'/2 - 9.7^{\circ})$$

Using an average value of Φ' for the range of strains within which f_1 is valid, the estimated errors are given in Table 8. It can be seen from Table 8 that the error of using c' instead of c'_{oct} is less than 1%. Hence, the errors are negligible.

b. Behavior of c' under Creep (Creep-CFS tests)

The behavior of c'_c is analyzed in terms of the viscous resistance of the clay particle structure under creep expressed by Equation (27) in which

$$f_1 = -\frac{1}{\alpha} \log_e \tanh\left[1/2\,\beta \frac{k_1 k_2}{k_1 + k_2} t + \tanh^{-1} \exp-\left(\frac{\alpha k_1 \beta}{k_1 + k_2}\right)\right]$$

To evaluate f_1 at a time t_c in a Creep-CFS test on the consolidated or compacted Sault Clay, values of k_1, k_2, α and β obtained from single increment creep test are required. Creep tests under $(\sigma_1 - \sigma_3)$ same as that in the Creep-CFS tests have been carried out on the consolidated and compacted Sault clays. Values of k_1, k_2, α and β determined from these creep tests are summarized under Spec. F-C-9 for the consolidated Sault clay and under Spec. C-C-7 for the compacted Sault clay in Table 5(a). With these values of k_1, k_2, α and β, f_1 is evaluated as follows.

Consolidated Sault Clay--From Spec. F-C-9 in Table 5(a),

Table 8. Estimated errors between c' and c'_{oct}.

Clay	Ave. ϕ'	$c'\cos(\frac{\phi'}{2}-9.7^{\circ})$	error % $= \frac{c' - c'_{oct}}{c'_{oct}}$
Compact. Sault	8°	0.995 c'	0.502
Consoli. Sault	8°	0.995 c'	0.502
Over-Con. Sault	8°	0.995 c'	0.502
Und. Marine City	18°	0.999 c'	0.010
Grundite	5°	0.992 c'	0.0805

$$\alpha = 22.70 \text{ cm}^2/\text{kg}\ , \quad \beta = 5.98 \times 10^{-7} \text{ min}^{-1}$$

$$\frac{k_1}{k_1 + k_2} = 0.848 \qquad k_2 = 8.47 \text{ kg/cm}^2$$

Therefore,

$$1/2\ \alpha\beta \frac{k_1 k_2}{k_1 + k_2} = 1/2 \times 22.7 \times 5.98 \times 10^{-7} \times 0.848 \times 8.47$$

$$= 4.87 \times 10^{-5} \text{ min}^{-1}$$

In a triaxial compression test,

the octahedral shear stress $\tau_{oct} = \frac{\sqrt{2}}{3} (\sigma_1 - \sigma_3)$

In the Creep-CFS test series on consolidated Sault clay in Table 3,

$$(\sigma_1 - \sigma_3) = 1.15 \text{ kg/cm}^2 \quad \therefore \quad \tau_{oct} = \frac{\sqrt{2}}{3} (1.15) = 0.542 \text{ kg/cm}^2$$

Substituting and using τ_{oct} for τ,

$$\exp\ (- \frac{\alpha k_1 \tau}{k_1 + k_2}) = \exp\ (- 22.7 \times 0.848 \times 0.542) = 4.65 \times 10^{-5}$$

$$\therefore \quad \tanh^{-1} \exp\ (- \frac{\alpha k_1 \tau}{k_1 + k_2}) = 4.65 \times 10^{-5}$$

Substituting in (27) and using t_c for t,

$$f_1 = - \frac{1}{22.7} \log_e \tanh\ (4.87 \times 10^{-5} t_c + 4.65 \times 10^{-5}) \qquad (27a)$$

Using (27a), f_1 can be evaluated at the various creep times t_c of the series of Creep-CFS tests on the consolidated Sault clay in Table 3.

As an example, we calculate f_1 for Spec. F-C-5 in Table 3. From Table 3, t_c = 30 min.

Substituting for t_c = 30 in (27a), we have

$$f_1 = - \frac{1}{22.7} \log_e \tanh(4.87 \times 10^{-5} \times 30 + 4.65 \times 10^{-5})$$

$$= - \frac{1}{22.7} \log_e \tanh 1.5\text{-}5 \times 10^{-3}$$

$$= + \frac{1}{22.7} \times 6.5 = 0.287 \text{ kg/cm}^2$$

In the same manner, values of f_1 at the other values of t_c of the series of Creep-CFS tests on the consolidated Sault clay in Table 3 are computed and summarized in Table A-22 in Appendix V

Compacted Sault Clay--From Spec. C-C-7 in Table 5(a),

[illegible] = 13.96 cm^2/kg, [illegible] = 61.5×10^{-7} min^{-1}

$$\frac{k_1}{k_1 + k_2} = 0.957 \qquad k_2 = 23.20 \text{ kg/cm}^2$$

The value of [illegible] obtained for Spec. C-C-7 is 61.5×10^{-7} and that obtained for the 4th load increment of Spec. C-C-1 is 13.24×10^{-7} in Table 5(a). Since the two tests are approximately at the same stress level, a single creep loading test should give values comparable to that from the incremental loading test. In view of the fact that the values of [illegible] obtained from all the load increments in Spec. C-C-1 are themselves reasonably consistent, a value of 20×10^{-7} min^{-1} for [illegible] has been assumed as a compromise. In fact, the value of f_1 is relatively insensitive to [illegible]. If [illegible] = 61.5×10^{-7} is used in the calculations, the value of f_1 is only about 30% smaller.

Using [illegible] = 20.0×10^{-7} min^{-1}, substituting for the values of [illegible], [illegible], $\frac{k_1}{k_1 + k_2}$ and k_2, we have

$$1/2 \text{ [illegible] } \frac{k_1 k_2}{k_1 + k_2} = 1/2 \times 13.96 \times 20 \times 10^{-7} \times 23.2 \times 0.957$$

$$= 3.11 \times 10^{-4} \text{ min}^{-1}$$

In the Creep-CFS test series on the compacted Sault clay in Table 3, $(\sigma_1 - \sigma_3) = 1.0$ kg/cm^2

the octahedral shear stress $\tau_{oct} = \frac{\sqrt{2}}{3}(1.0) = 0.465$ kg/cm^2

Substituting and using τ_{oct} for τ,

$$\exp\left(- \frac{\alpha k_1}{k_1 + k_2}\right) = \exp(- 13.96 \times 0.957 \times 0.465) = 0.002$$

$$\therefore \tanh^{-1} \exp\left(- \frac{\alpha k_1}{k_1 + k_2}\right) = 0.002.$$

Substituting in (27) and using t_c for t

$$f_1 = - \frac{1}{\alpha} \log_e \tanh(3.11 \times 10^{-4}\ t + 0.002) \qquad (27b)$$

Using (27b), f_1 can be evaluated at the various creep times t_c of the series of Creep-CFS tests on the compacted Sault clay.

As an example, we calculate f_1 for Spec. R-C-8 in Table 3. From Table 3, $t_c = 120$ min.

Substituting for t_c in (27b), we have

$$f_1 = - \frac{1}{13.96} \log_e \tanh(3.11 \times 10^{-4} \times 120 + 0.002)$$

$$= - \frac{1}{13.96} \log_e \tanh 0.0393 = + \frac{1}{13.96} \times 3.23$$

$$= 0.232 \text{ kg/cm}^2$$

In the same manner, values of f_1 at the other values of t_c of the series of Creep-CFS tests on the compacted Sault clay in Table 3 are computed and summarized in Table A-22 in Appendix V.

Results of the computations on the variation of f_1 with respect to the creep time t_c for the consolidated and compacted Sault clays are plotted in Fig. 47(a). For comparison, the observed behaviors of c'_c for these two clays are shown in Fig. 47(b). From these figures, it can be seen that although there is qualitative agreement between the calculated and measured c', the absolute magnitudes of the two quantities differ by about 0.3 kg/cm^2.

An examination of Table 3 reveals that the strain rates at the end of the creep phase of some of these tests are several hundred times smaller than that of the CFS phase. It appears desirable to estimate the effect of this change in strain rates on the measured c'_c. Assuming that c'_c is solely dependent on the creep strain rate $\dot{\epsilon}_c$, we may obtain values of c' corresponding to the various values of $\dot{\epsilon}_c$ from the c' versus strain rate characteristics. Because of the completeness of CFS test data, the compacted Sault clay is investigated.

For the compacted Sault clay, values of c' corresponding to the values of $\dot{\epsilon}_c$ in the Creep-CFS tests can be obtained from Fig. 37. For example, for $\dot{\epsilon}_c$ = 0.127 %/hr in Spec. R-C-8 (Table 3), the corresponding value of c' obtained from Fig. 37 is 0.18 - 0.26 kg/cm^2.

In the same manner, values of c' corresponding to the other values of $\dot{\epsilon}_c$ in the Creep-CFS test series of the compacted Sault clay are obtained from Fig. 37. For convenience, we designate these values of c' as c'_d. They are compiled in Table A-23 in Appendix V. Fig. 48 shows the comparison of the values of c'_c and c'_d.

It is felt that although this change in strain rates could affect the absolute magnitudes of the measured values of c'_c, the general trend as well as the relative magnitude of c'_c should be valid. In view of this, the measured and calculated values of c'_c are compared by converting them into dimensionless "cohesion" as follows.

For the measured values

the dimensionless "cohesion" $c^* = \dfrac{c'_c - c'_\infty}{c'_o - c'_\infty}$

where

c'_c is the measured value

c'_∞ is the constant value of c'_c when the creep time approaches a large value

and

c'_o is the constant value of c'_c when the creep time approaches zero.

From Fig. 41(b), for both the compacted and consolidated Sault clays, c'_∞ and c'_o are taken as 0.355 kg/cm^2 and 0.575 kg/cm^2 respectively.

For the calculated values

the dimensionless "cohesion" $f^* = \dfrac{f_1 - f_\infty}{f_o = f_\infty}$

where

f_1 is the calculated value in equations (27a) and (27b) for the consolidated and compacted Sault clays respectively

f_∞ and f_o are the calculated values of f_1 at infinity and zero time in equations (27a) and (27b) for the consolidated and compacted Sault clays respectively.

It can be seen from equations (27a) and (27b) that $f_{\infty} = 0$.

Therefore, $f^* = f_1/f_o$

For the consolidated Sault clay, $f_o = -\frac{1}{22.7} \log_e 4.65 \times 10^{-5}$

$= 0.439 \text{ kg/cm}^2$

For the compacted Sault clay, $f_o = \frac{1}{13.96} \log_e \tanh 0.002$

$= 0.445 \text{ kg/cm}^2$

The variations of f^* and c^* with respect to the creep time t_c for the series of Creep-CFS tests on the consolidated Sault and compacted Sault clays are computed and tabulated in Tables A-22 and A-24 in Appendix V.

Fig. 49 shows the comparison of the variations of f^* and c^* with respect to the creep time t_c for the two clays. It can be seen from Fig. 49 that the agreement is reasonably satisfactory. It is noted in 4.3.1.c that the nature of cohesion is partly viscous and partly non-viscous. The theoretical treatment here appears to explain satisfactorily the behavior of the viscous part of cohesion under creep for the consolidated and compacted Sault clays.

4.3.3 Summary

A hypothesis is proposed for the behavior of cohesion in clays. The cohesion is assumed to consist of a non-viscous part and a viscous part. The non-viscous part is the result of the adhesion at the contacts of the particles in the particle model. The behavior of the viscous part follows the flow phenomenon of the clay particle structure as a rate process.

CHAPTER 5

CONCLUSIONS

A particle model is proposed for the behavior of friction and cohesion in clays. In this model, the resistance at the particle contacts is assumed to consist of a mineral friction and an adhesion. It varies with the orientation of the particle relative to the direction of shear.

The angle of internal friction is the result of the resistance due to mineral friction at the contacts. The cohesion consists of a non-viscous part and a viscous part. The non-viscous part of cohesion is the result of the resistance due to adhesion at the contacts. The behavior of the viscous part of cohesion is governed by the flow phenomenon of the clay particle structure and is considered as a rate process.

The model predicts that when a shear stress is imposed on the clay mineral network, contacts with the smallest resistance along the direction of shear slip first. Following these contact failures, particles are displaced from one position to another. The resistance against displacement is due to the viscous part of cohesion whose behavior follows the rate process. As deformation is taking place, stronger contacts are being reformed and the stresses causing flow are transferred to the reformed contacts. The maximum value of the angle of internal

friction at any strain is attained only if the elapsed time between displacements is sufficient for the reformed contacts to develop their maximum resistance to shear.

If the clay mineral network is stressed under a fast strain rate, the rate of contact displacement is fast and the elapsed time between displacements is short. The value of the angle of internal friction attained at any strain or at failure is therefore low. If the strain rate is slow, the rate of contact displacement is slow and the value of the angle of internal friction is high. If the strain rate is such that the elapsed time between displacements is sufficient for the reformed contacts to develop their maximum resistance, a maximum value of the angle of internal friction is attained at any given strain. The viscous part of cohesion decreases with decreasing strain rate.

Under a creep load, the displacements also lead to contacts with greater strengths. After these contacts are reformed, displacements cease. At any creep strain ε_c, to attain a Φ'_c, a displacement N_c must take place. To reach N_c, a time t_c is required. The angle of internal friction Φ'_c therefore increases with the creep time t_c and approaches a maximum value Φ'_k when t_c approaches a large value t_k. The viscous part of cohesion decreases with increasing creep time.

Approximate calculations with the particle model give results that are in reasonable agreement with the experimental data.

BIBLIOGRAPHY

Bishop, A. W. and Henkel, K. J. (1957). The Measurement of Soil Properties in the Triaxial Test. Edward Arnold, London.

Bowden, F. P. and Tabor, D. (1954). Friction and Lubrication of Solids. Clarendon Press, Oxford.

Christensen, R. W. (1964). Analysis of Clay Deformation by Rate Process Theory. Ph.D. thesis, Michigan State University.

Christensen, R. W. and Wu, T. H. (1964). Analysis of Clay Deformation by Rate Process Theory. Journ. Soil Mech. & Found., Proc. ASCE (forthcoming).

Glasstone, S., Laidler, K and Eyring, H. (1941). The theory of Rate Processes. McGraw-Hill, New York.

Holliday, F. J. (1963). Stress Transfer due to Creep in a Saturated Clay. M.S. thesis, Michigan State University.

Horn, H. M. and Deere, D. U. (1962). Frictional Characteristics of Minerals. Geotechnique, Vol. 12, 4 : pp. 319.

Hvorslev, M. J. (1960). Physical Components of the Shear Strength of Saturated Clays, ASCE Research Conference on Shear Strength of Cohesive Soils, pp. 169.

Lambe, T. W. (1960). A Mechanistic Picture of Shear Strength in Clays. ASCE Research Conference on Shear Strength of Cohesive Soils, pp. 555.

Lo, K. Y. (1962). Shear Strength Properties of a Sample of Volcanic Material of the Valley of Mexico. Geotechnique, Vol. 12 : 4 : 303.

Mitchell, J. K. (1956). The Fabrics of Natural Clays and its Relation to Engineering Properties. Proc. HWY. Res. Board, Vol. 35.

Mitchell, J. K. (1964). Shearing Resistance of Soils as a Rate Process. Journ. Soil Mech. & Found., Proc. ASCE, Vol. 90, SM1, pp

Murayama, S. and Shibrata, T. (1961). Rheological Properties of Clays. Proc. 5th Int. Conf. Soil Mech. & Found. Eng., Vol. 1 : 269-273.

Rosenqvist, I. Th. (1959). Mechanical Properties of Soil-Water System. Journ. Soil Mech. & Found., Proc. ASCE, Vol. 85, SM2, pp. 31.

Schmertmann, J. H. and Osterberg, J. O. (1960). An Experimental study of the Development of Cohesion and Friction with Axial Strain in Saturated Cohesive Soils. ASCE Research Conf. on Shear Strength of Cohesive Soils, pp. 643.

Schmertmann, J. H. (1962). Comparison of One and Two-Specimen CFS Tests. Journ. Soil Mech. & Found., Proc. ASCE, Vol. 88, SM6.

Skempton, A. W. (1960). Effective Stress in Soils, Concrete and Rocks. Pore Pressure and Suction in Soils. Butterworths, London.

Tan, T. K. (1957). Discussion, Proc. 4th Int. Conf. Soil Mech. & Found Eng., Vol. 3 : pp. 87-89.

Wu, T. H. Douglas, A. G. and Goughnour, R. D. (1962). Friction and Cohesion of Saturated Clays. Journ. Soil Mech. & Found., Proc. ASCE, Vol. 88, SM3, pp. 1-23.

Wu, T. H. (1963). Discussion on "Comparison of One and Two-Specimen CFS Tests." Journ. Soil Mech. & Found., Proc. ASCE, Vol. 89, SM4, pp. 229.

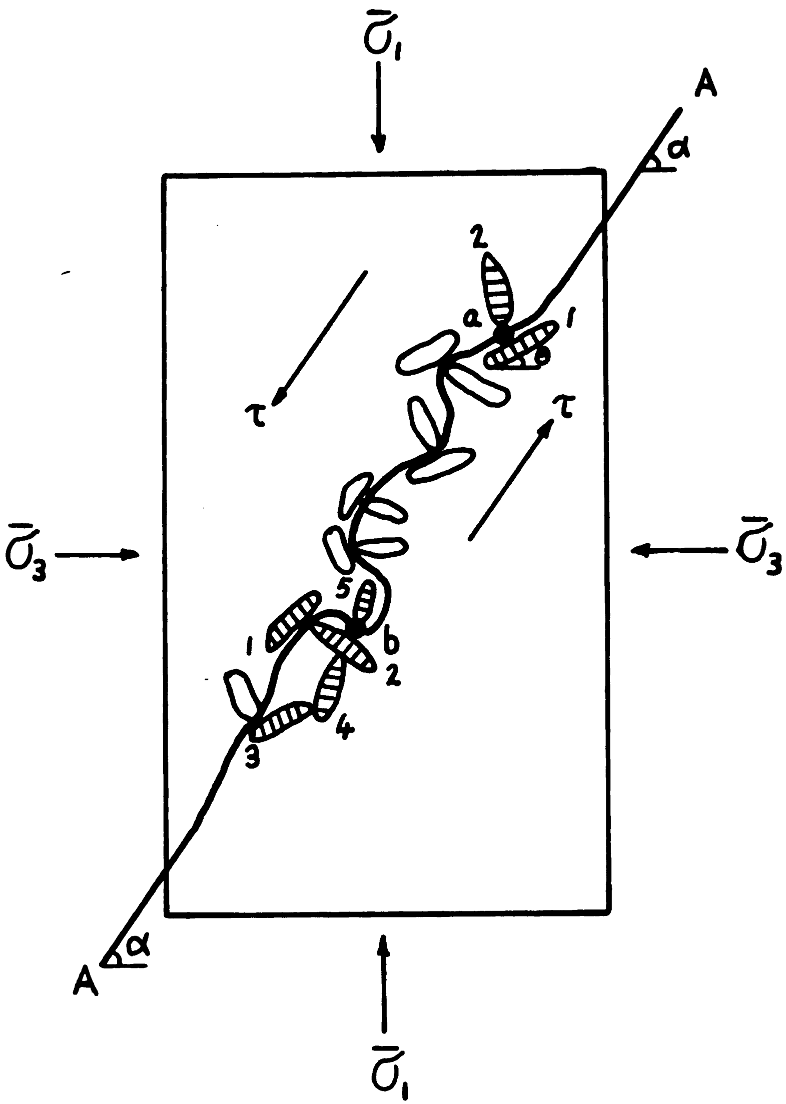

Fig. 1a Section through Particles

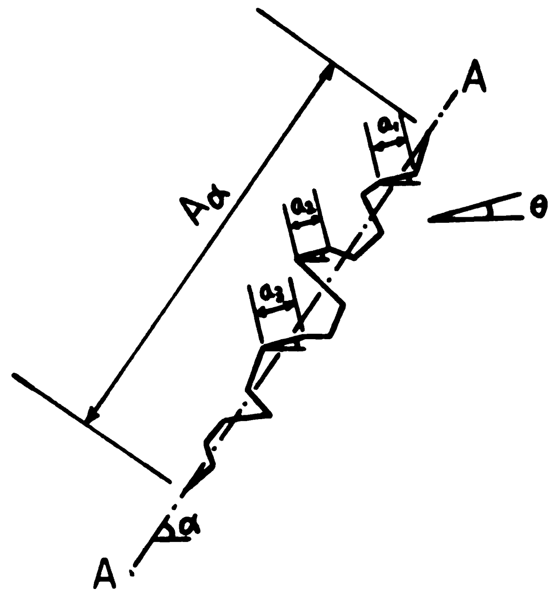

$$A_\theta = a_1 + a_2 + a_3$$

$$A_\alpha = \sum_{\theta=0}^{\theta=\pi} A_\theta \cos(\theta - \alpha)$$

Fig. 1b Definition of A_θ

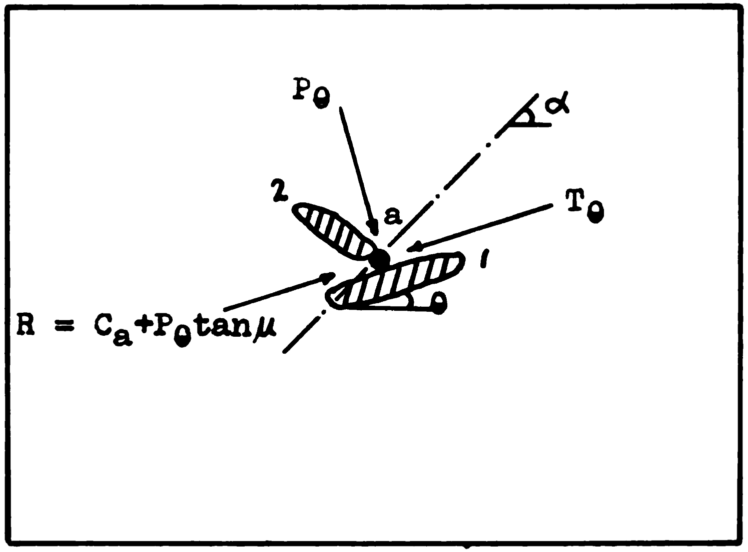

Fig. 2 Sliding Movement and Resistance

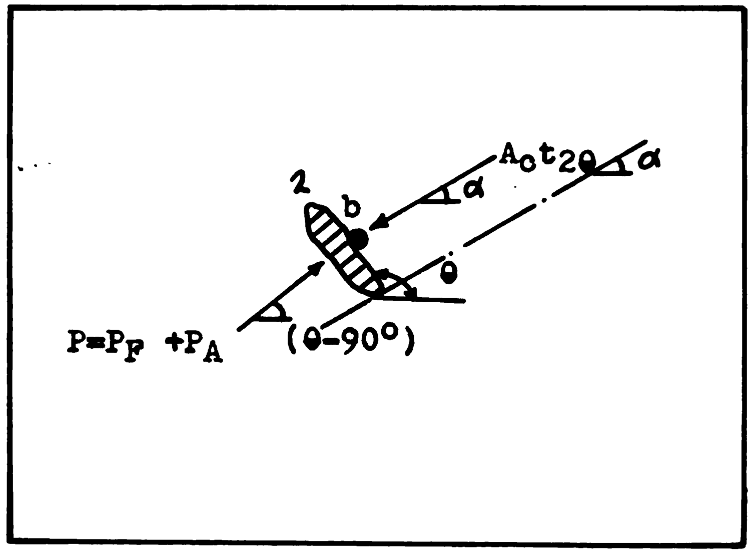

Fig. 3 Displacement Movement and Resistance

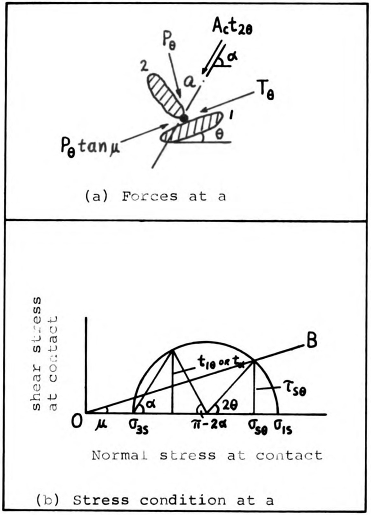

(a) Forces at a

(b) Stress condition at a

Fig. 4. Frictional resistance against sliding.

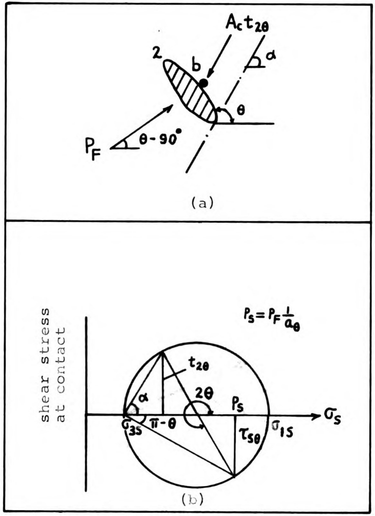

(a)

(b)

Fig. 5. Frictional resistance against displacement.

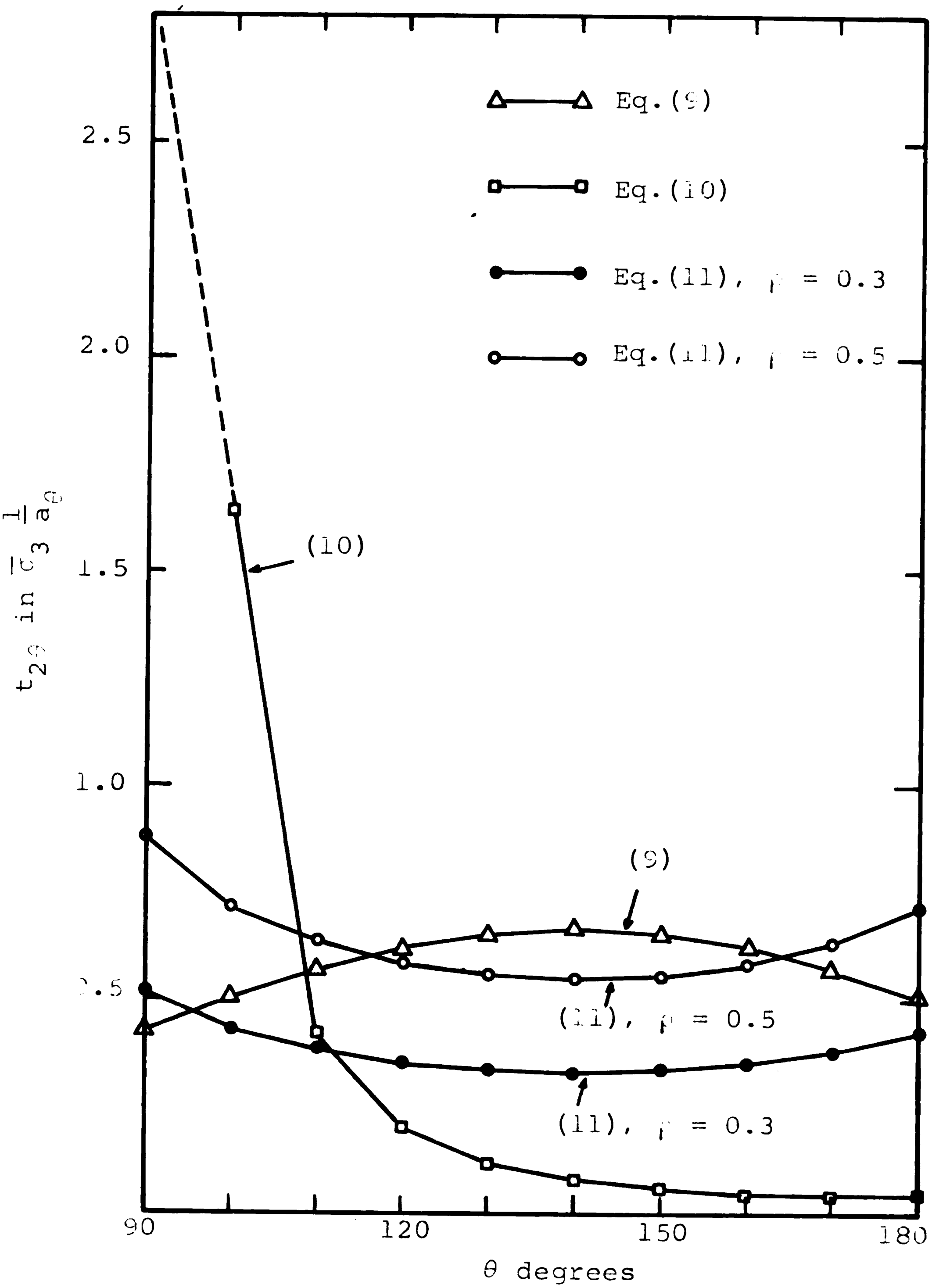

Fig. 5. Comparison of $t_{2\theta}$.

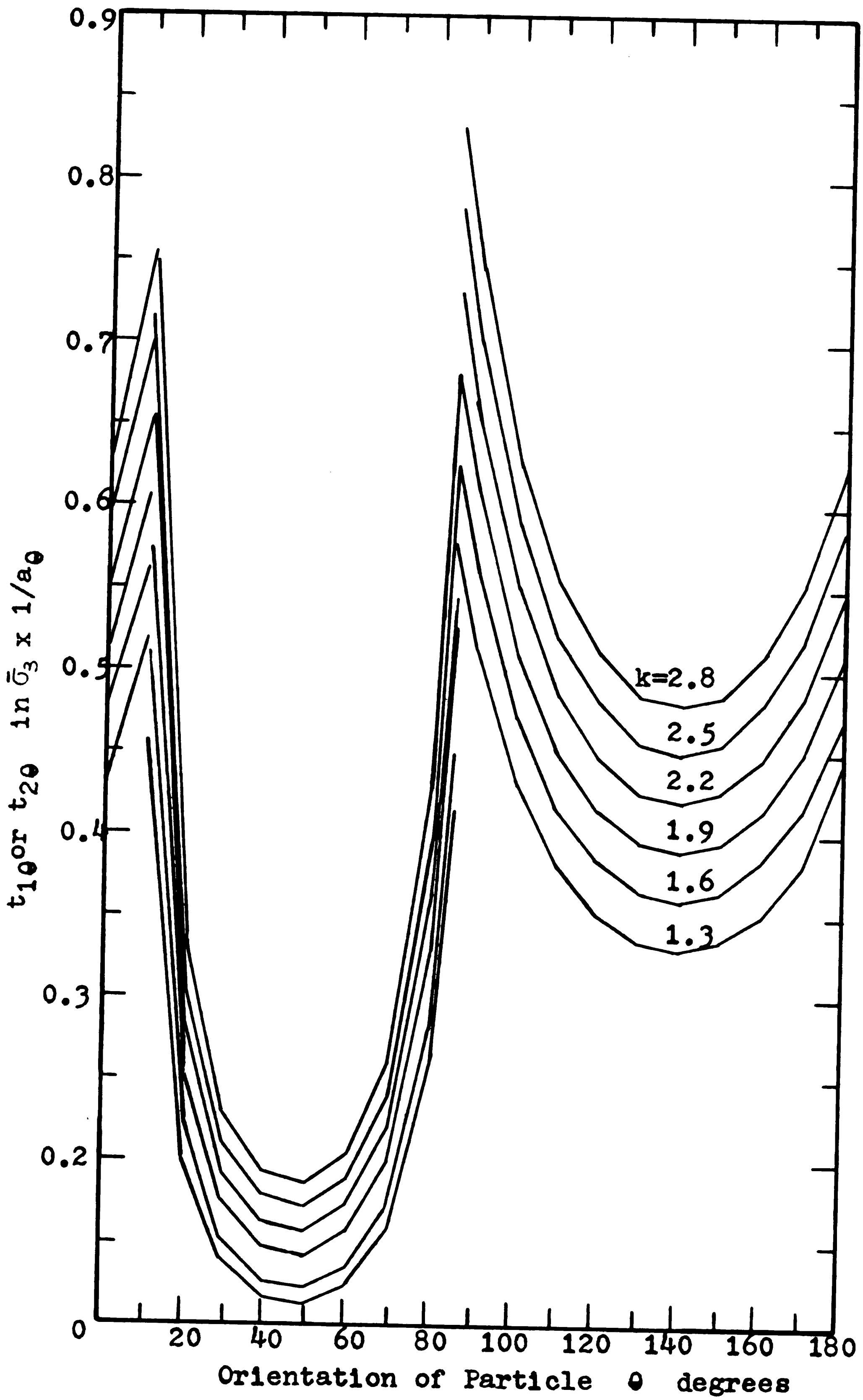

Fig. 7 Spectrum of Friction Resistance--
$\rho = 0.3$

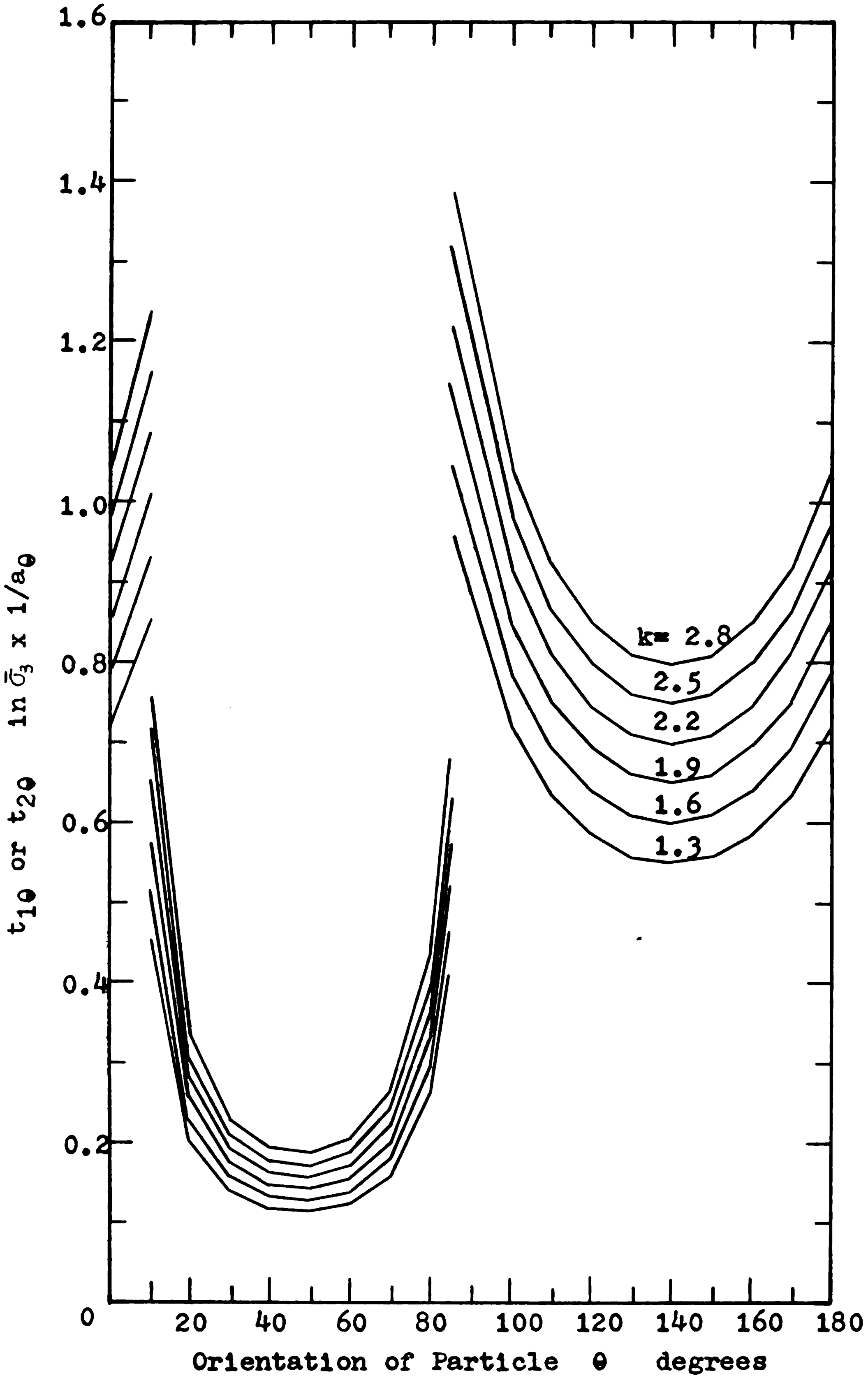

Fig. 8 Spectrum of Friction Resistance-- $\rho = 0.5$

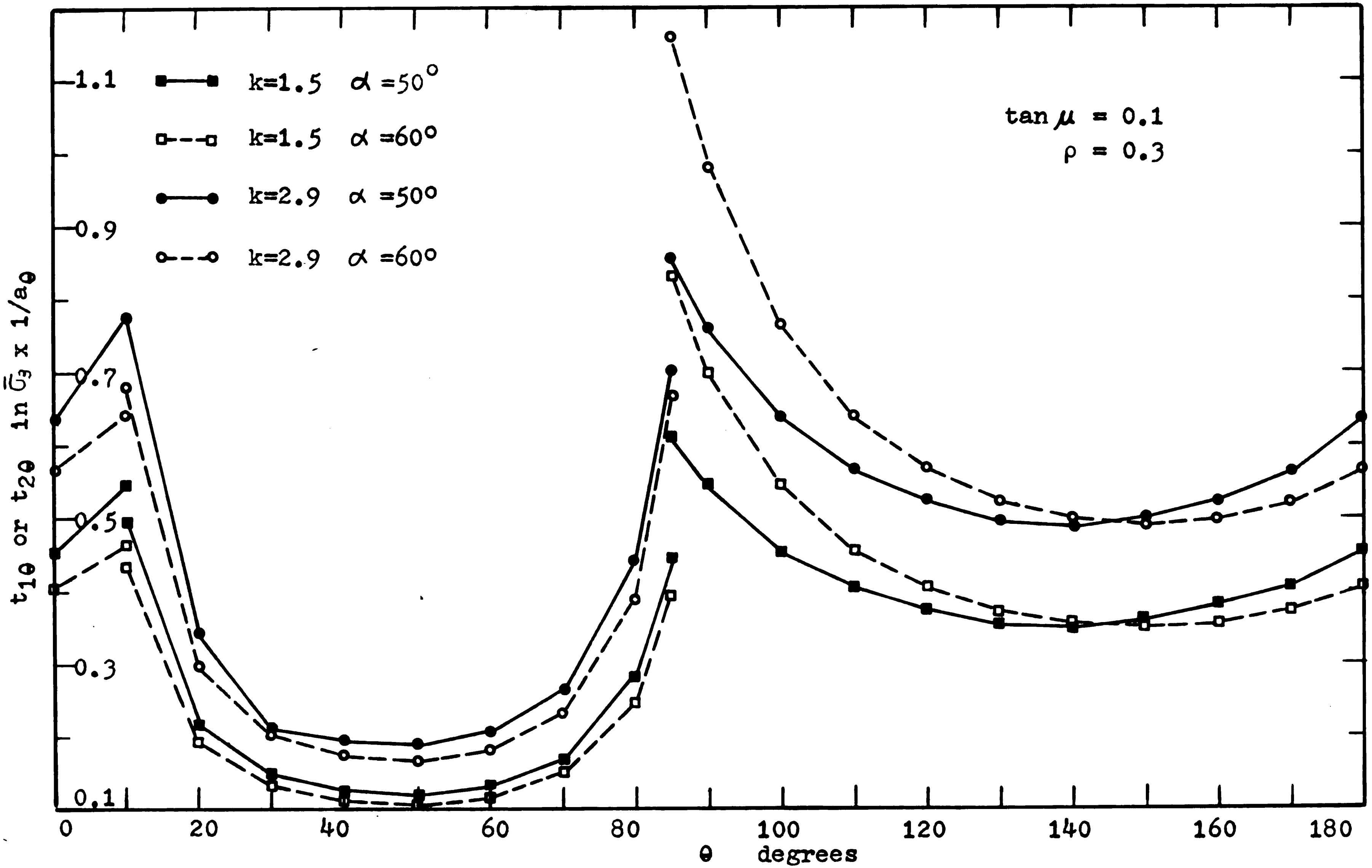

Fig. 9 Comparison of Friction Resistance for α = 50° and 60°

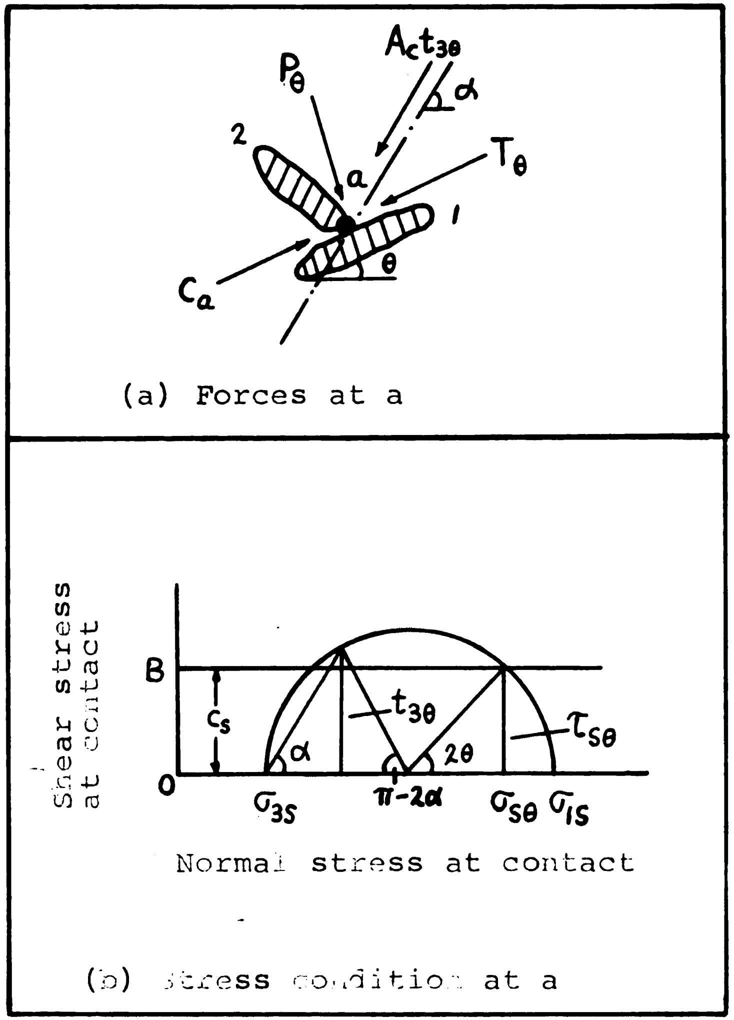

Fig. 10. Adhesional resistance against sliding.

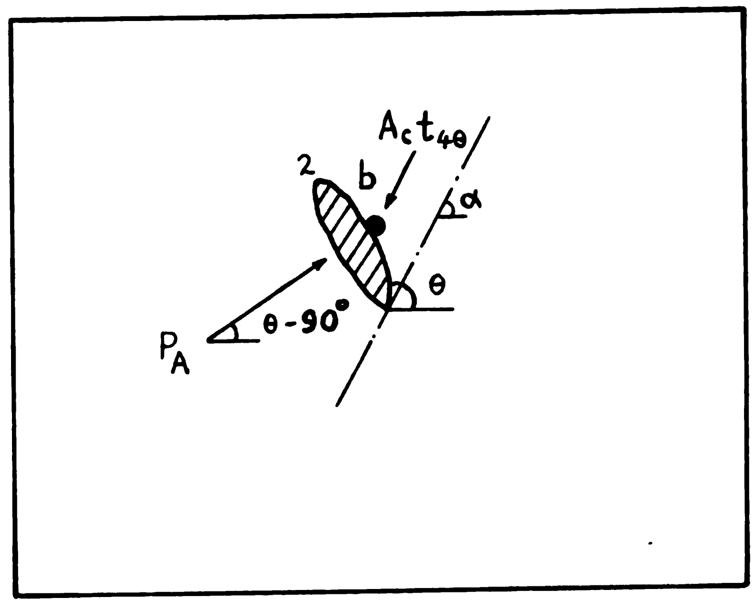

Fig. 11. Adhesional resistance against displacement.

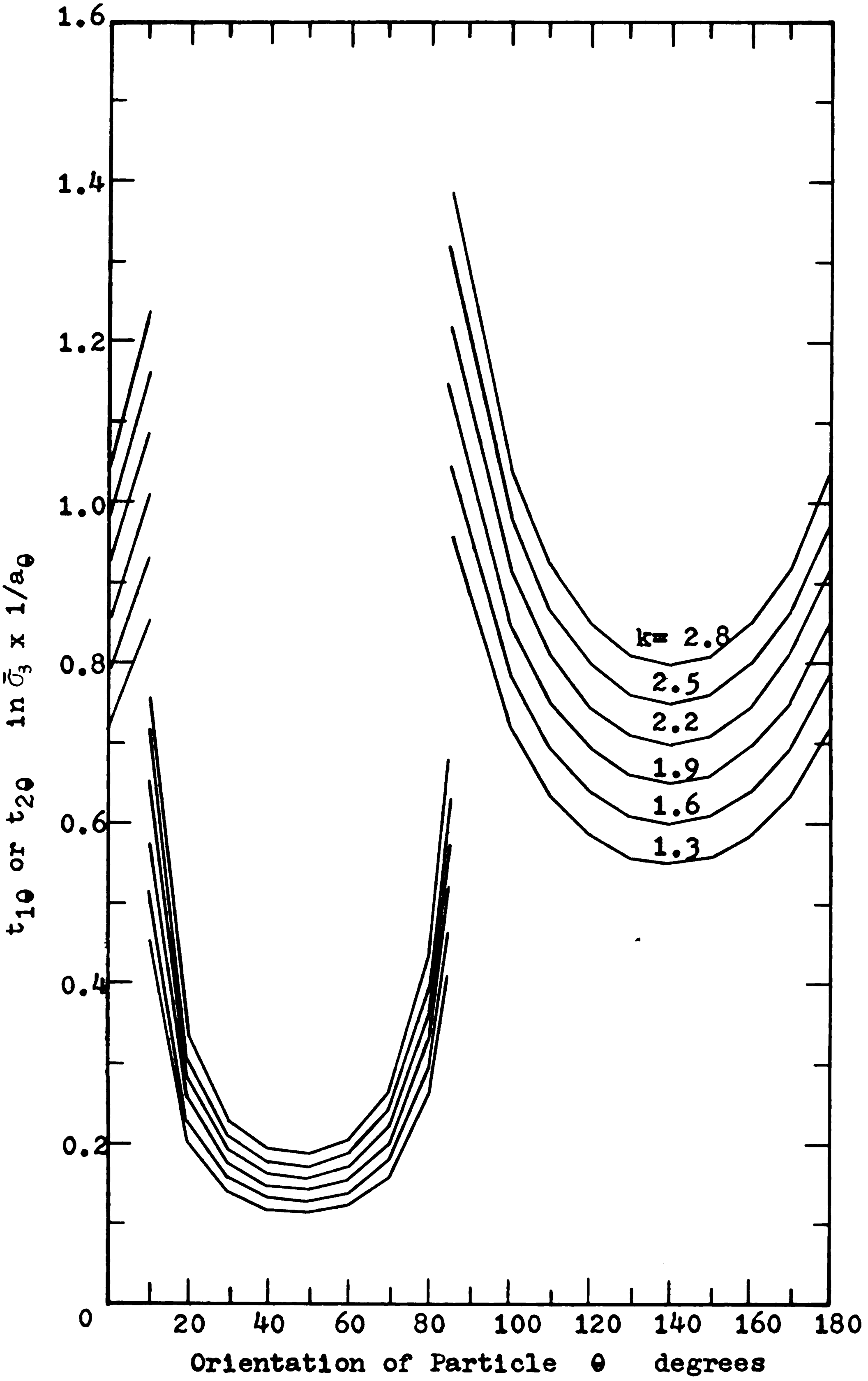

Fig. 8 Spectrum of Friction Resistance--
$\rho = 0.5$

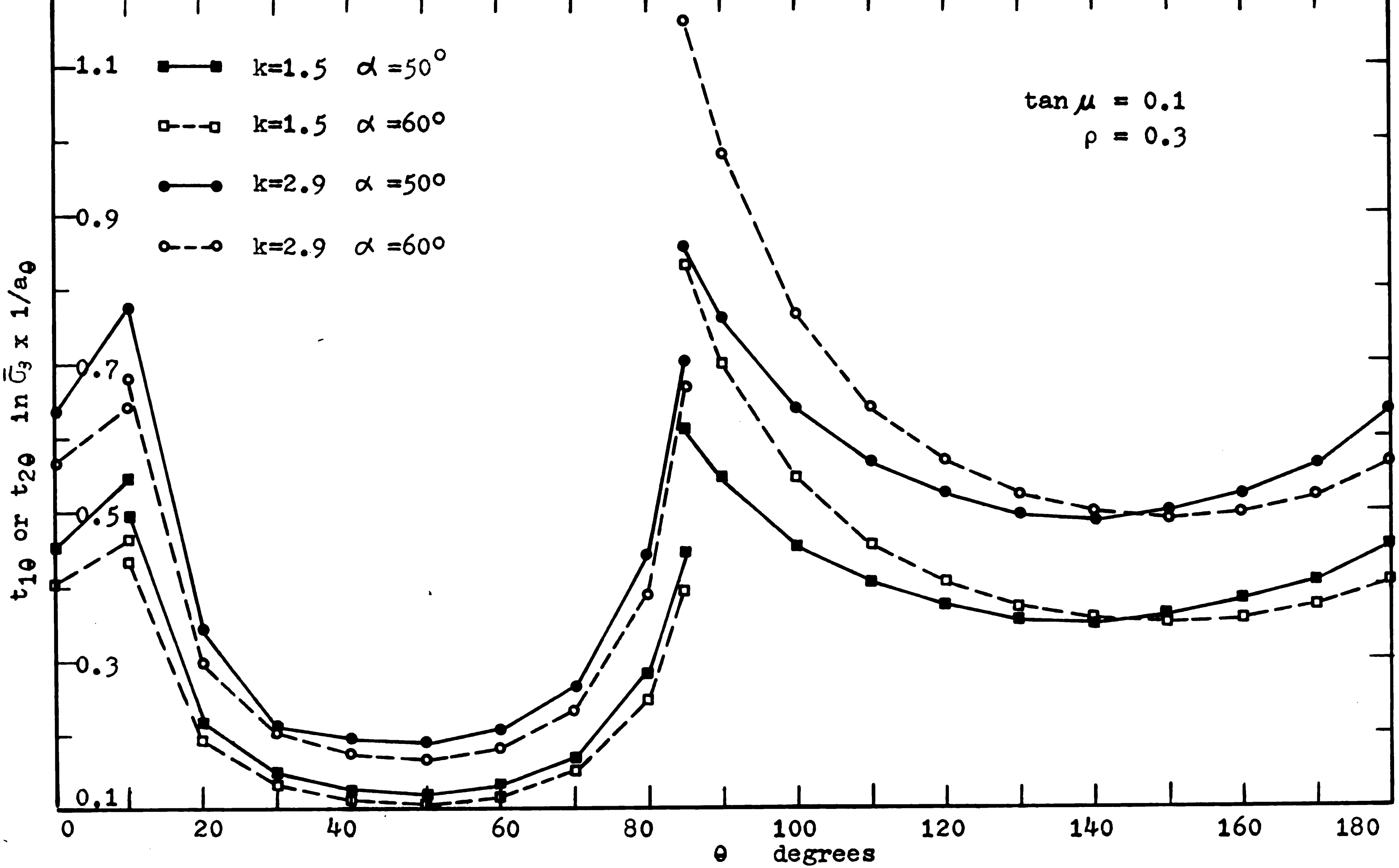

Fig. 9 Comparison of Friction Resistance for α = 50° and 60°

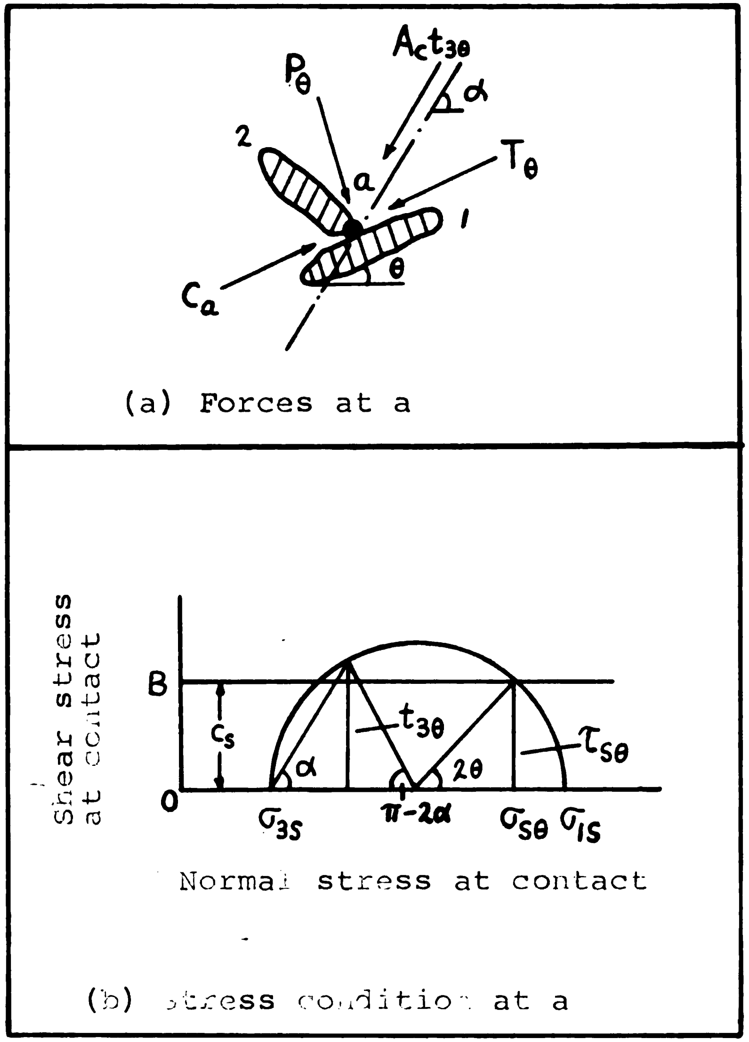

Fig. 10. Adhesional resistance against sliding.

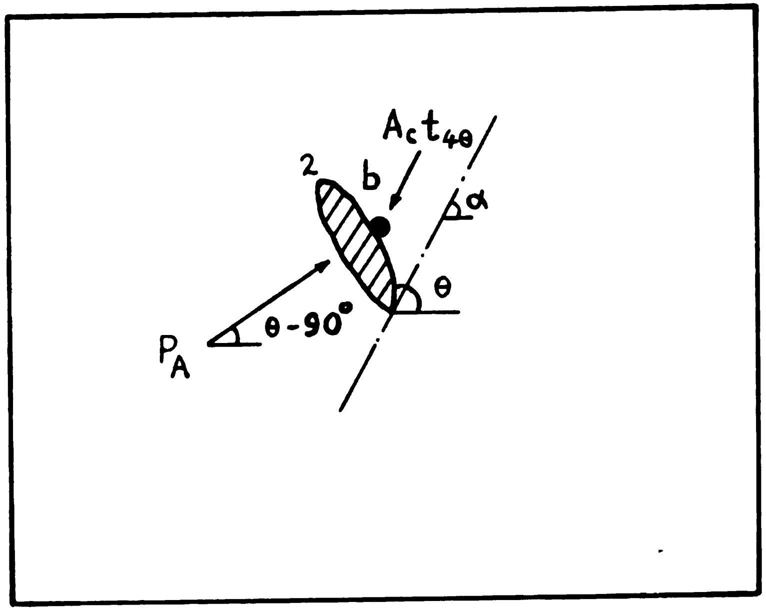

Fig. 11. Adhesional resistance against displacement.

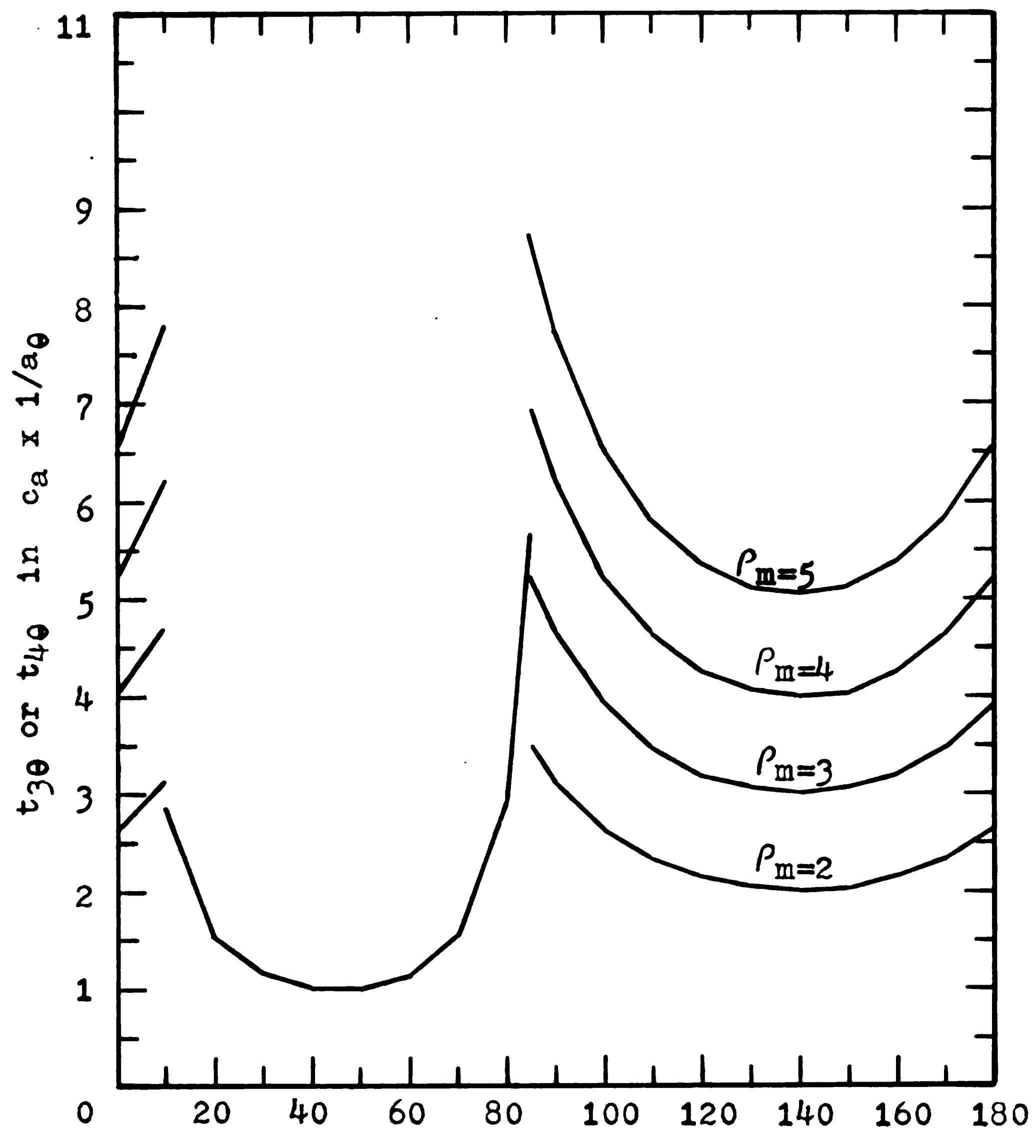

Fig. 12 Spectrum of Adhesion Resistance

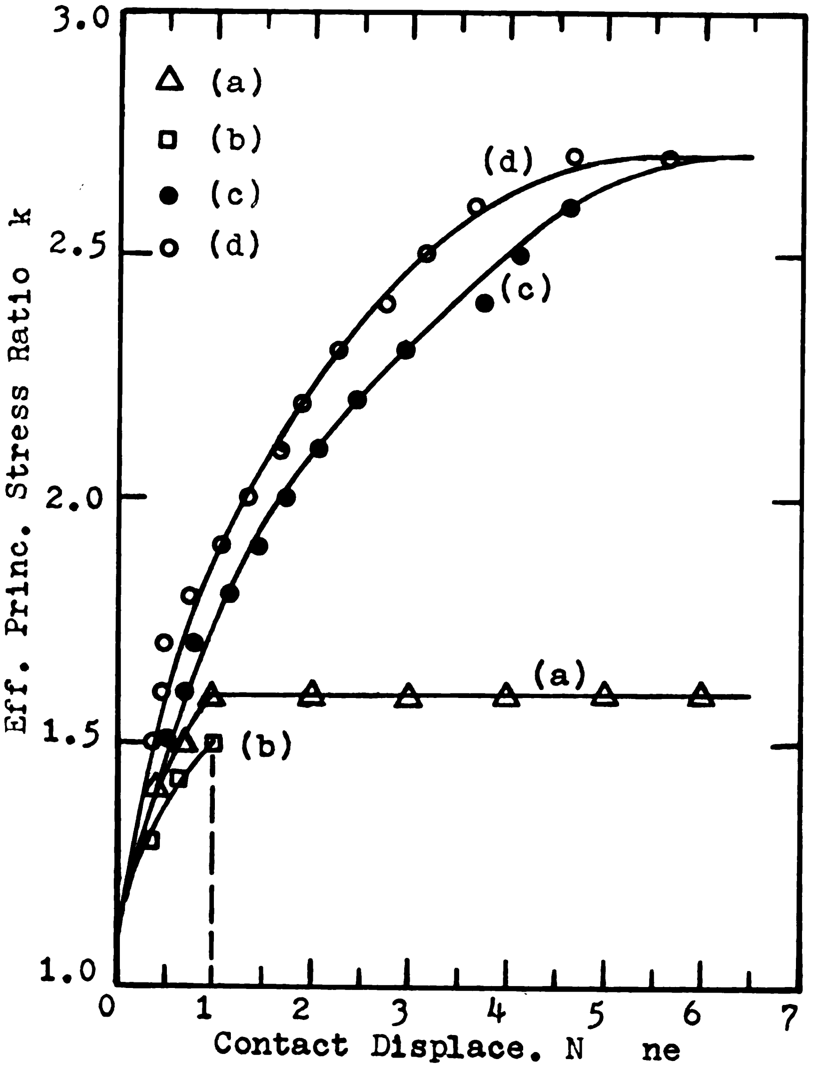

Fig. 13 **Stress-Displacement Curves for $\rho = 0.3$**

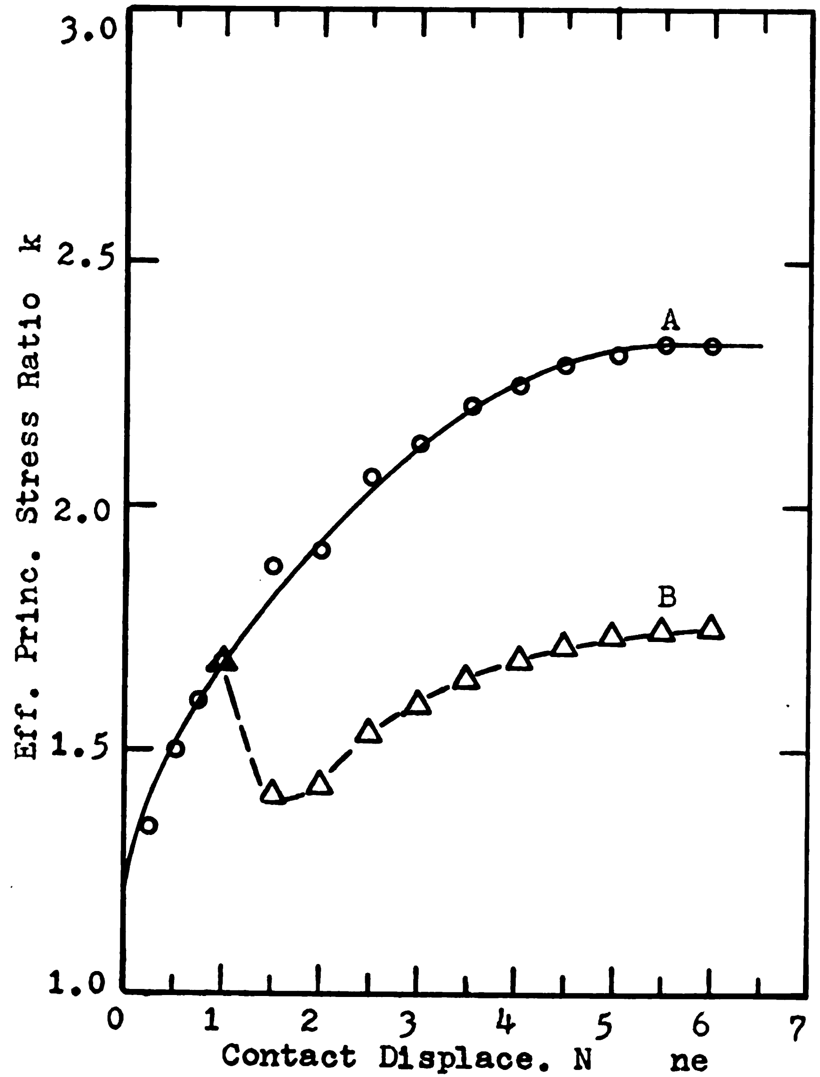

Fig. 14 **Average Stress-Displacement Curves for $\rho = 0.3$**

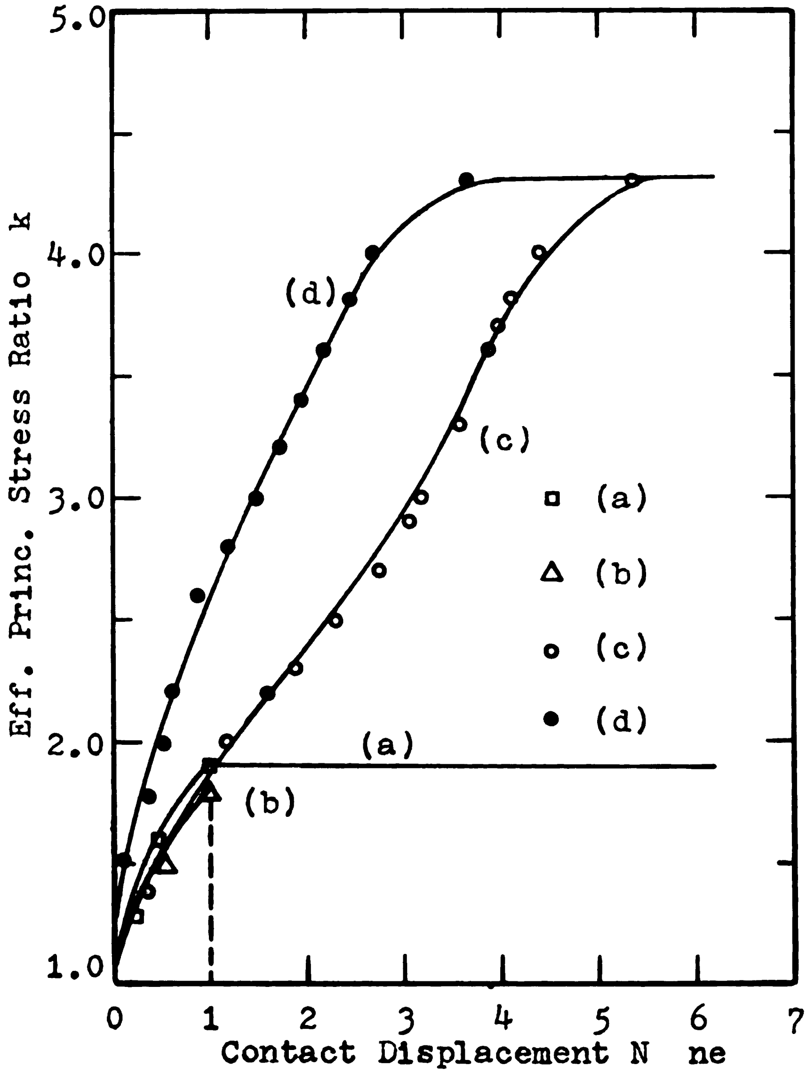

Fig. 15 Stress-Displacement Curves for $\rho = 0.5$

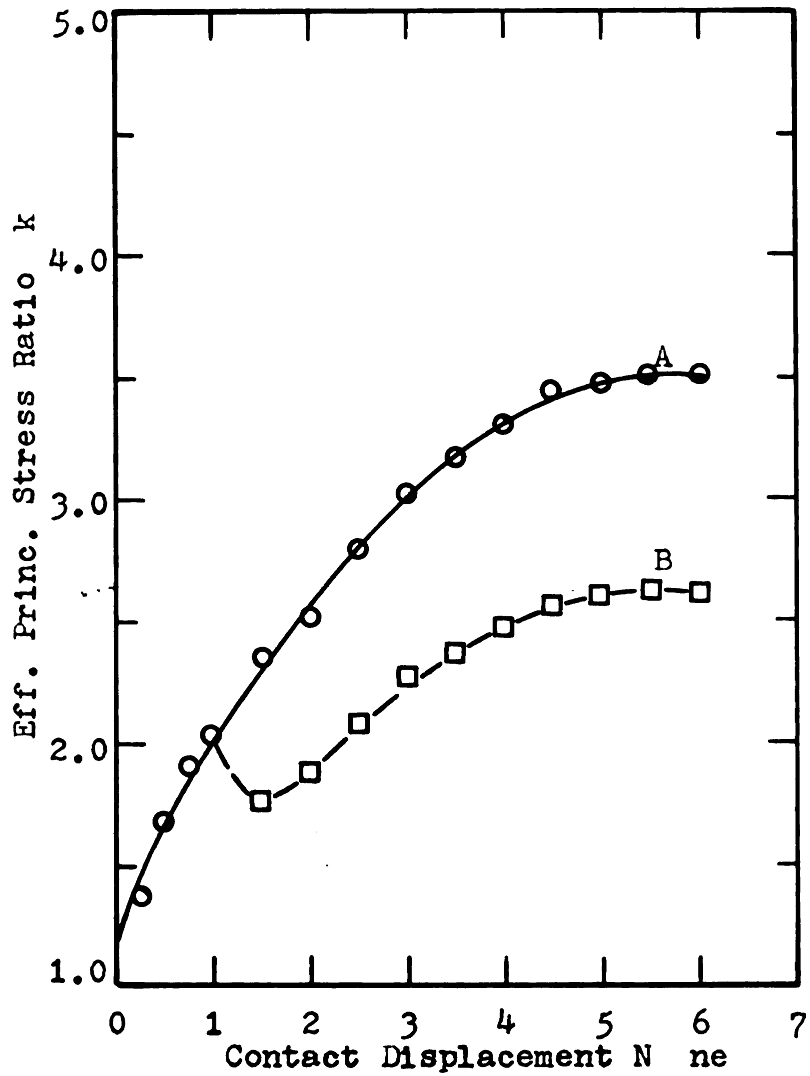

Fig. 16 Average Stress-Displacement Curves for $\rho = 0.5$

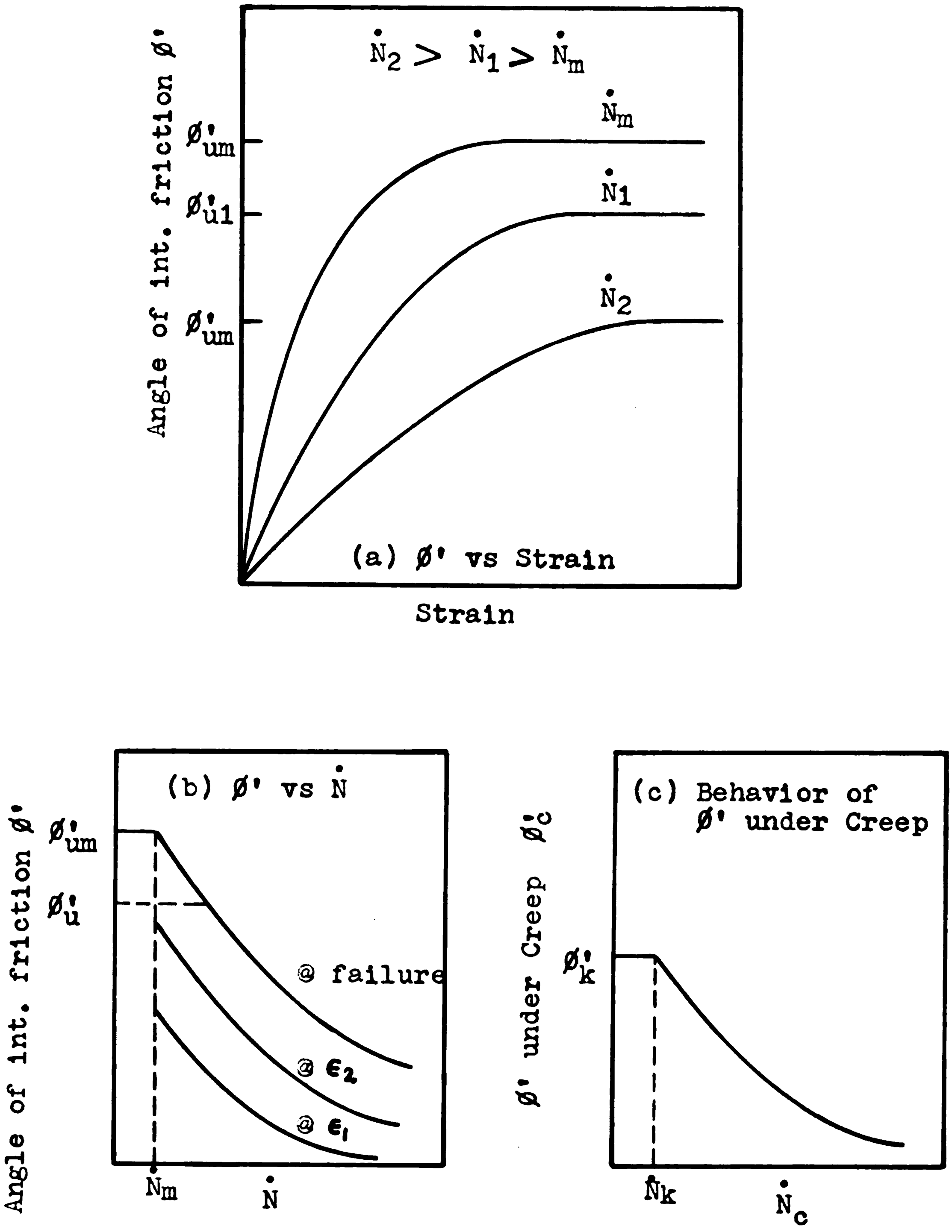

Fig. 17 Behavior of ϕ' according to Particle Model

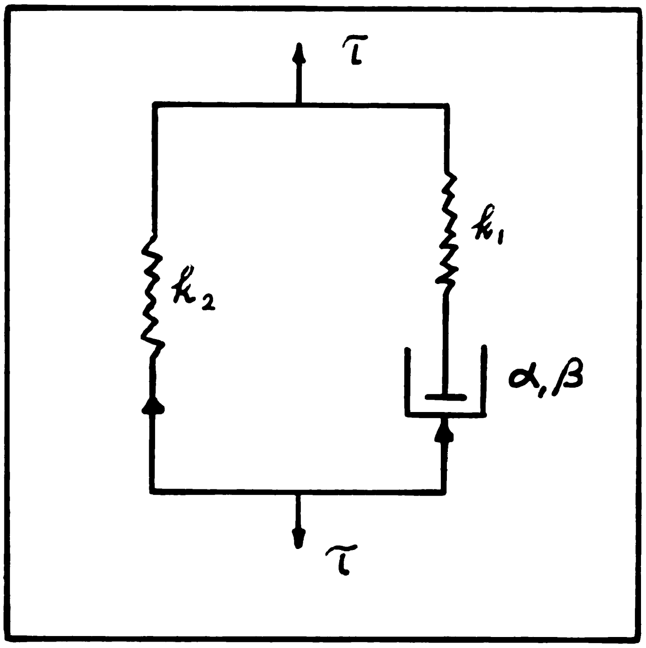

Fig. 18 Rheologic Model for Clay Particle Structure

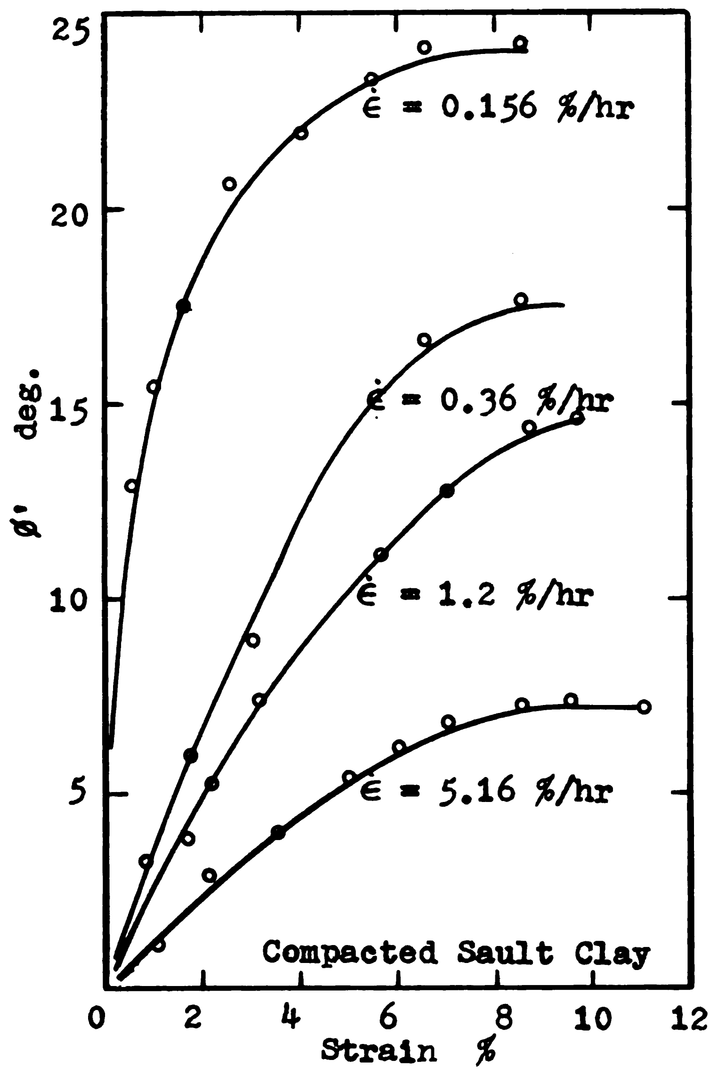

Fig. 19 ø'-Strain Curves--CFS Tests on Compacted Sault Clay

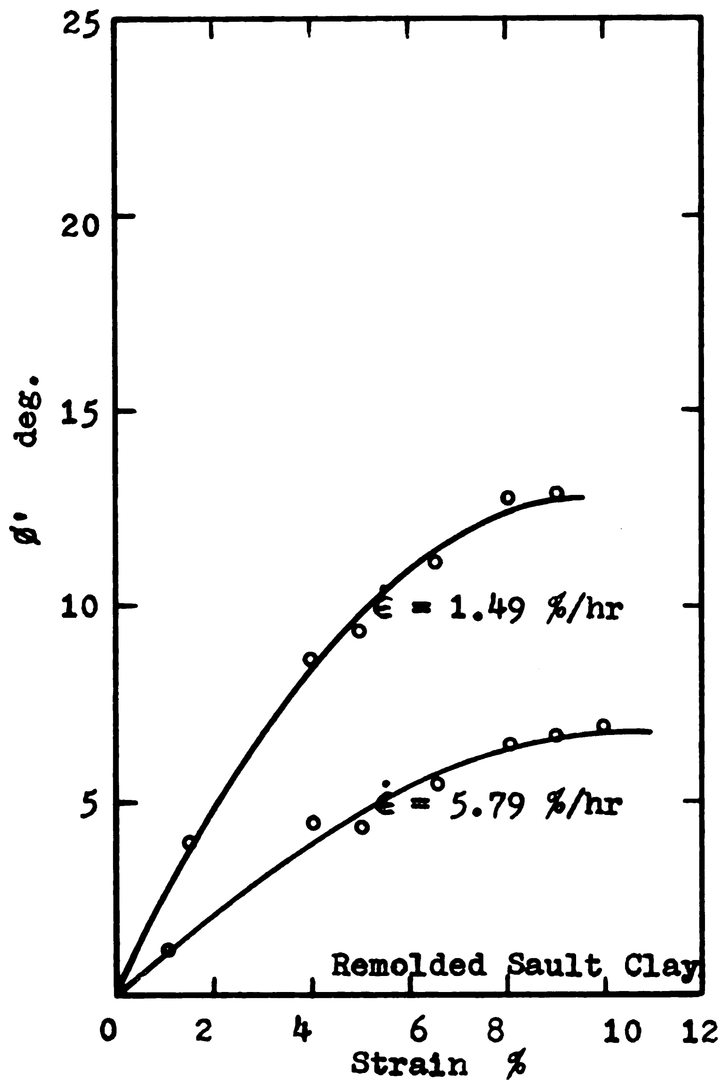

Fig. 20 ø'-Strain Curves--CFS Tests on Remolded Sault Clay

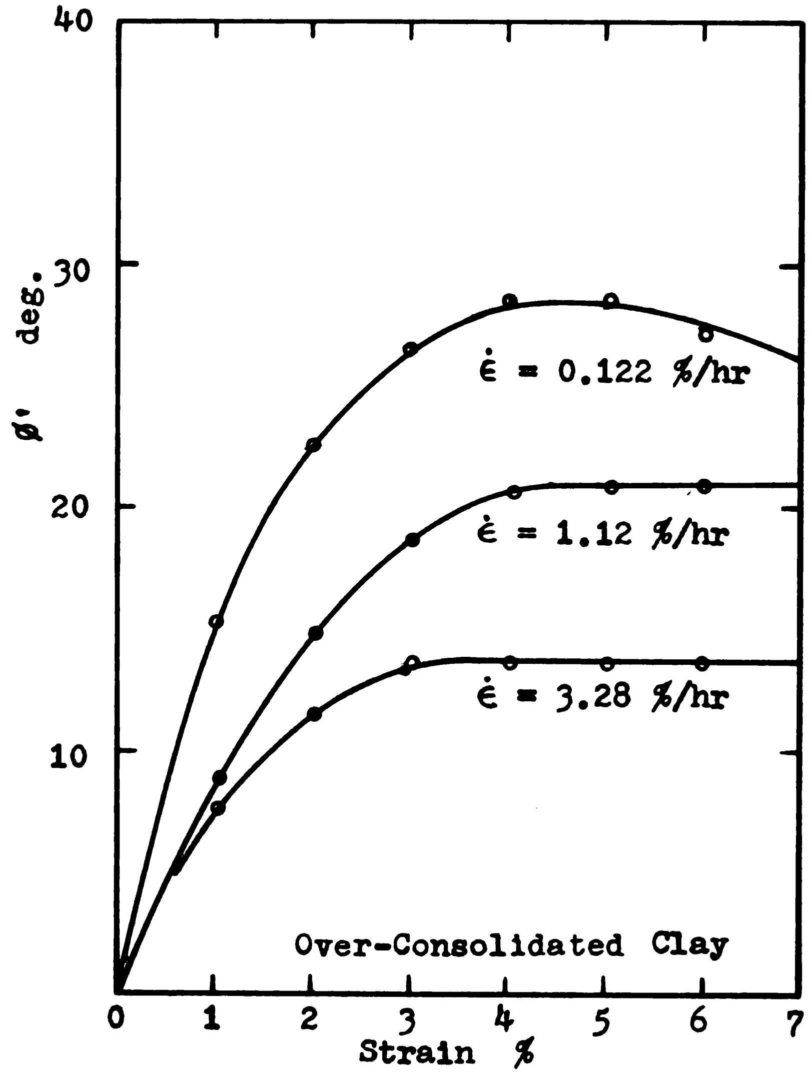

Fig. 21 ø'-Strain Curves--CFS Tests on Over-consolidated Sault Clay

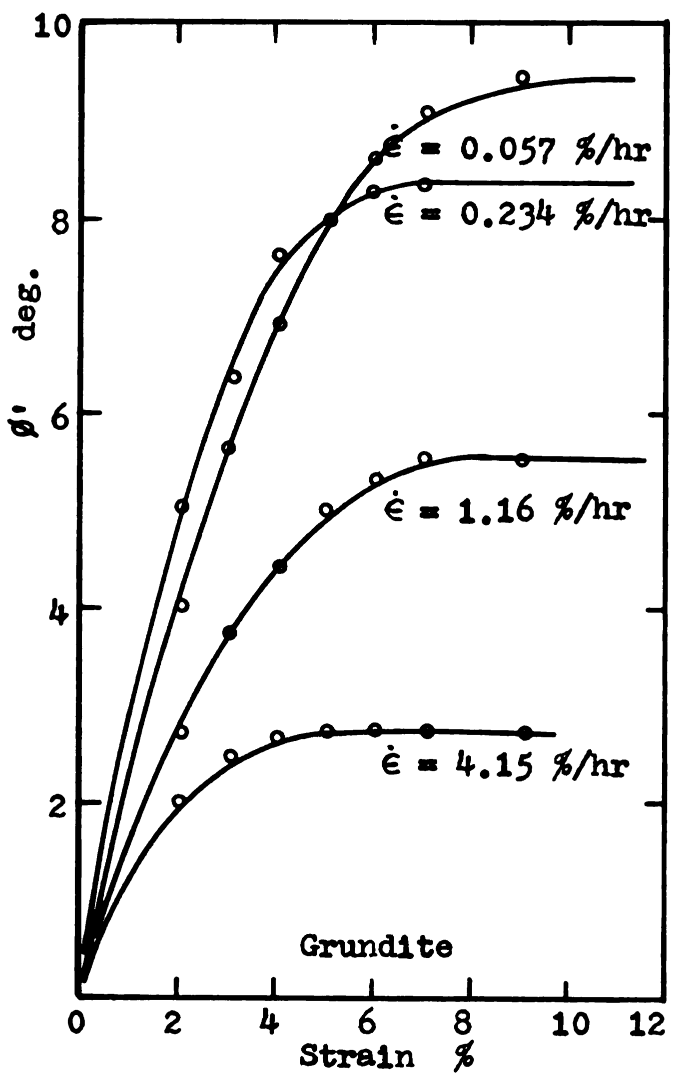

Fig. 22 ø'-Strain Curves--CFS Tests on Grundite

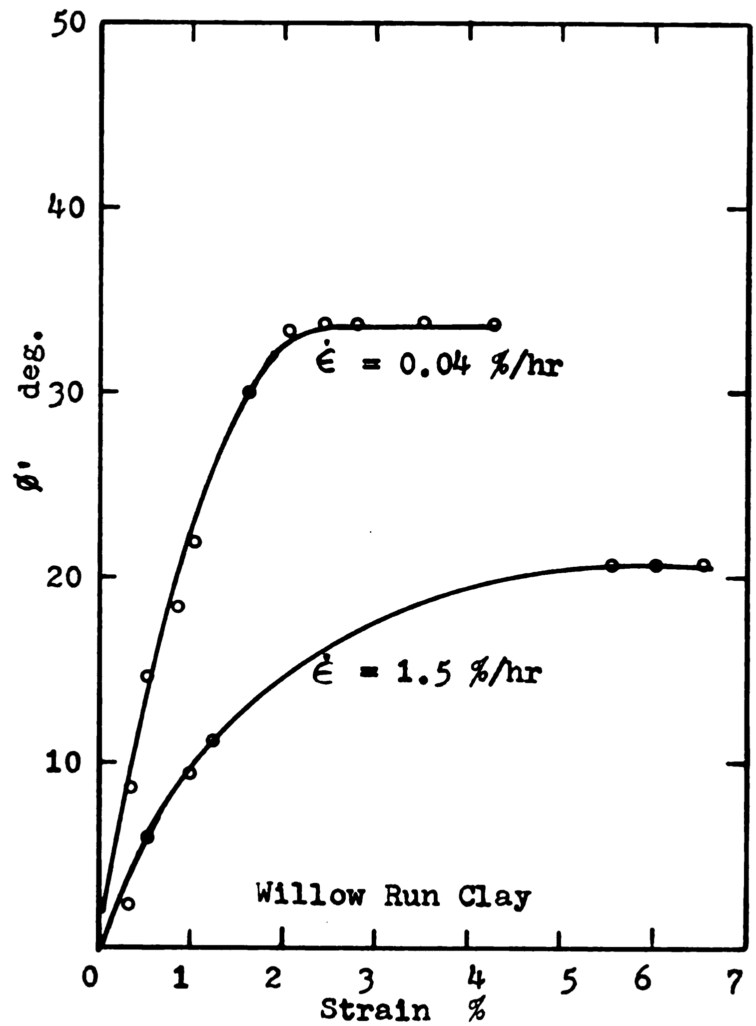

Fig. 23 ø'-Strain Curves--CFS Tests on Undisturbed Willow Run Clay

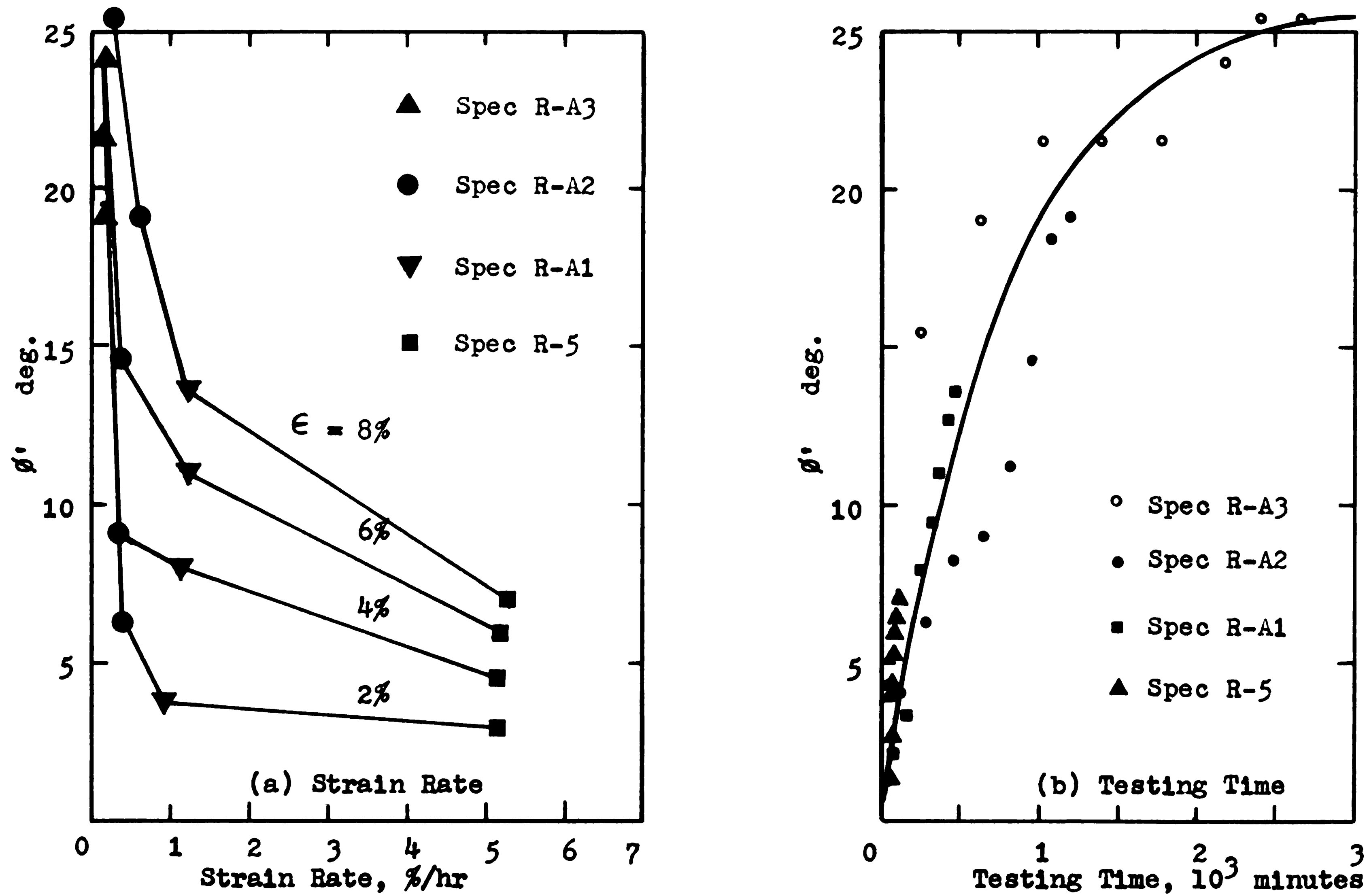

Fig. 24 ø'-Strain Rate and ø'-Time Curves--CFS Tests on Compacted Sault Clay

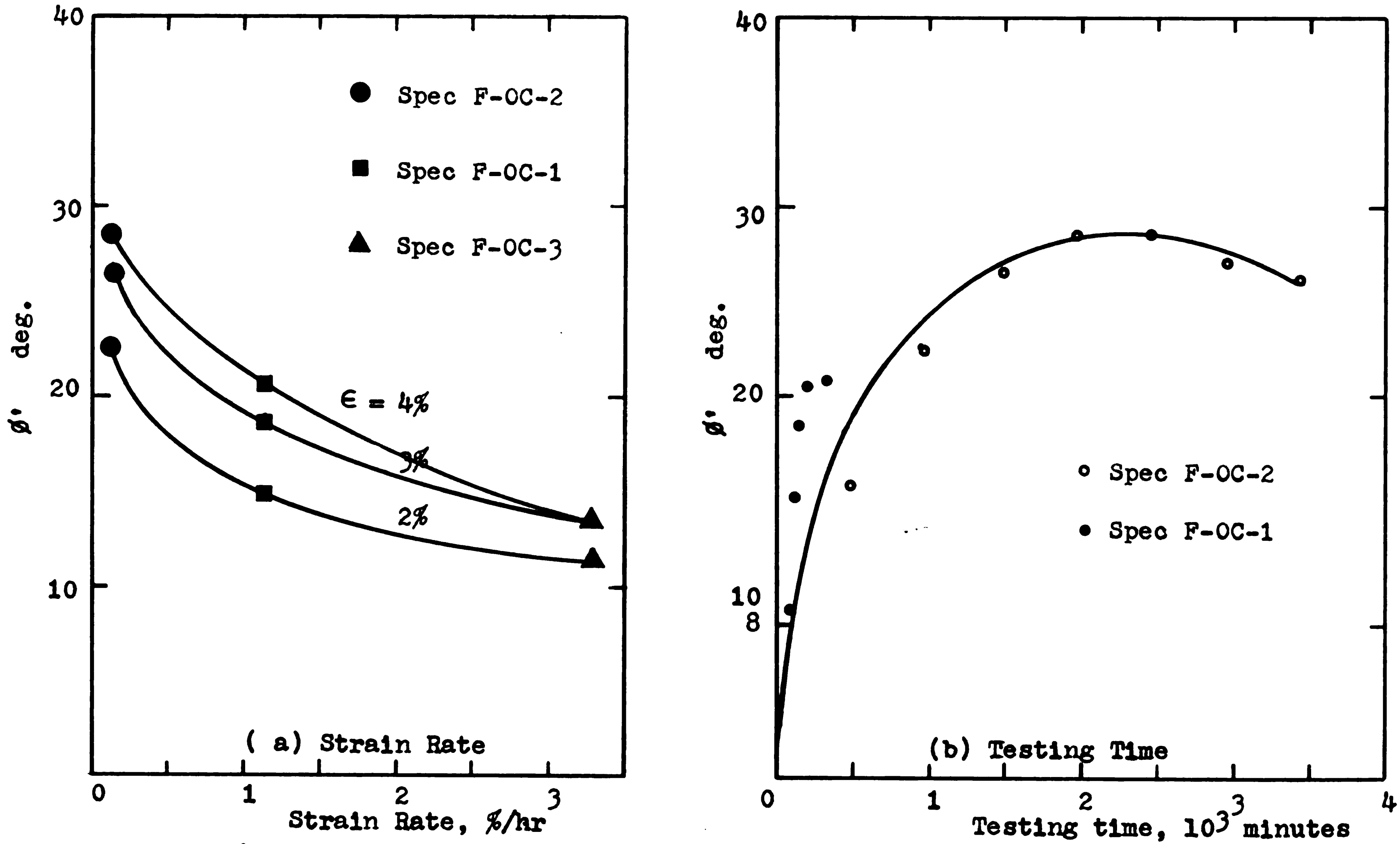

Fig. 25 ø'-Strain Rate and ø'-Time Curves --CFS Tests on Over-consolidated Sault Clay

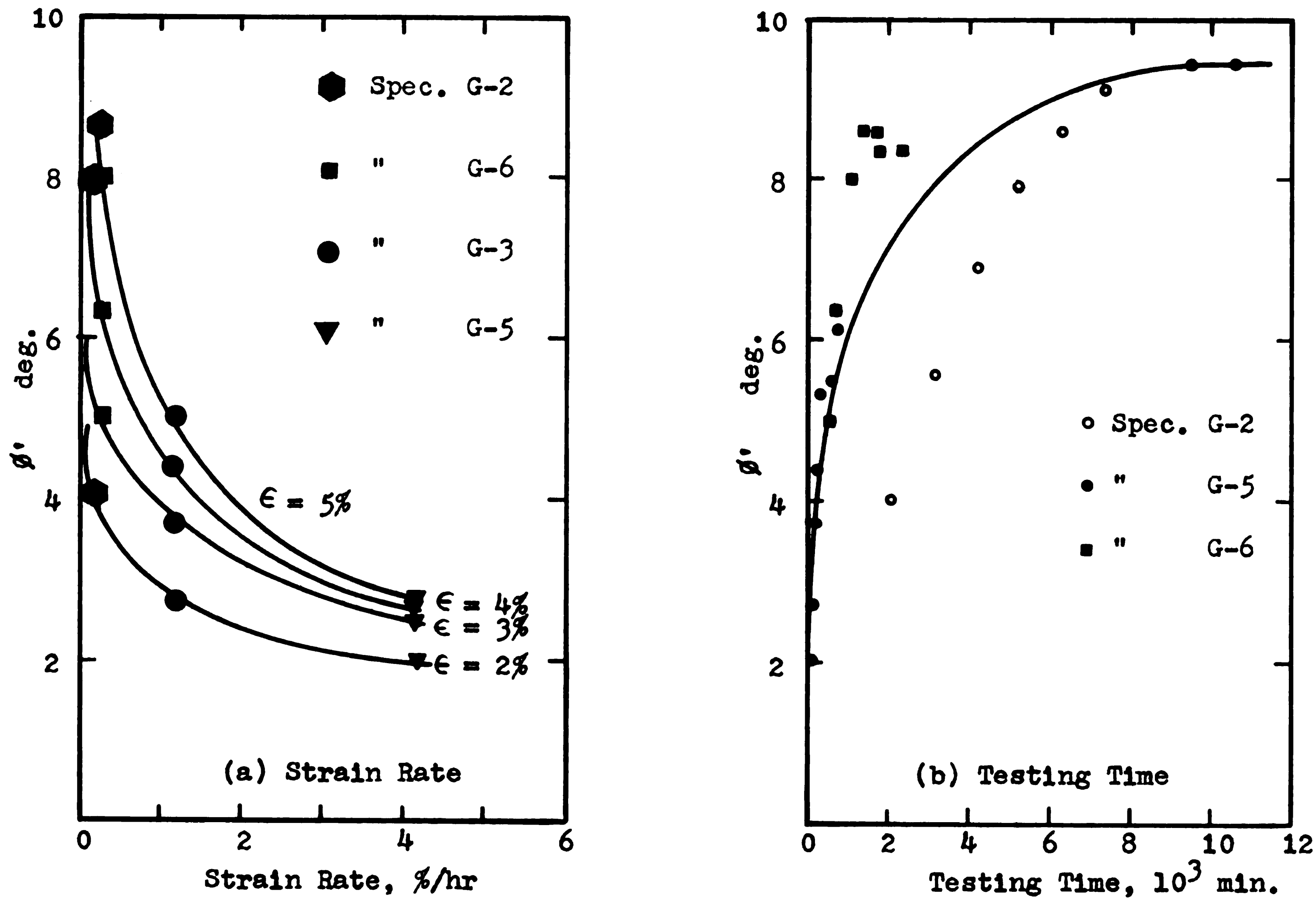

Fig. 26 Ø'-Strain Rate and Ø'-Time Curves--CFS Tests on Grundite

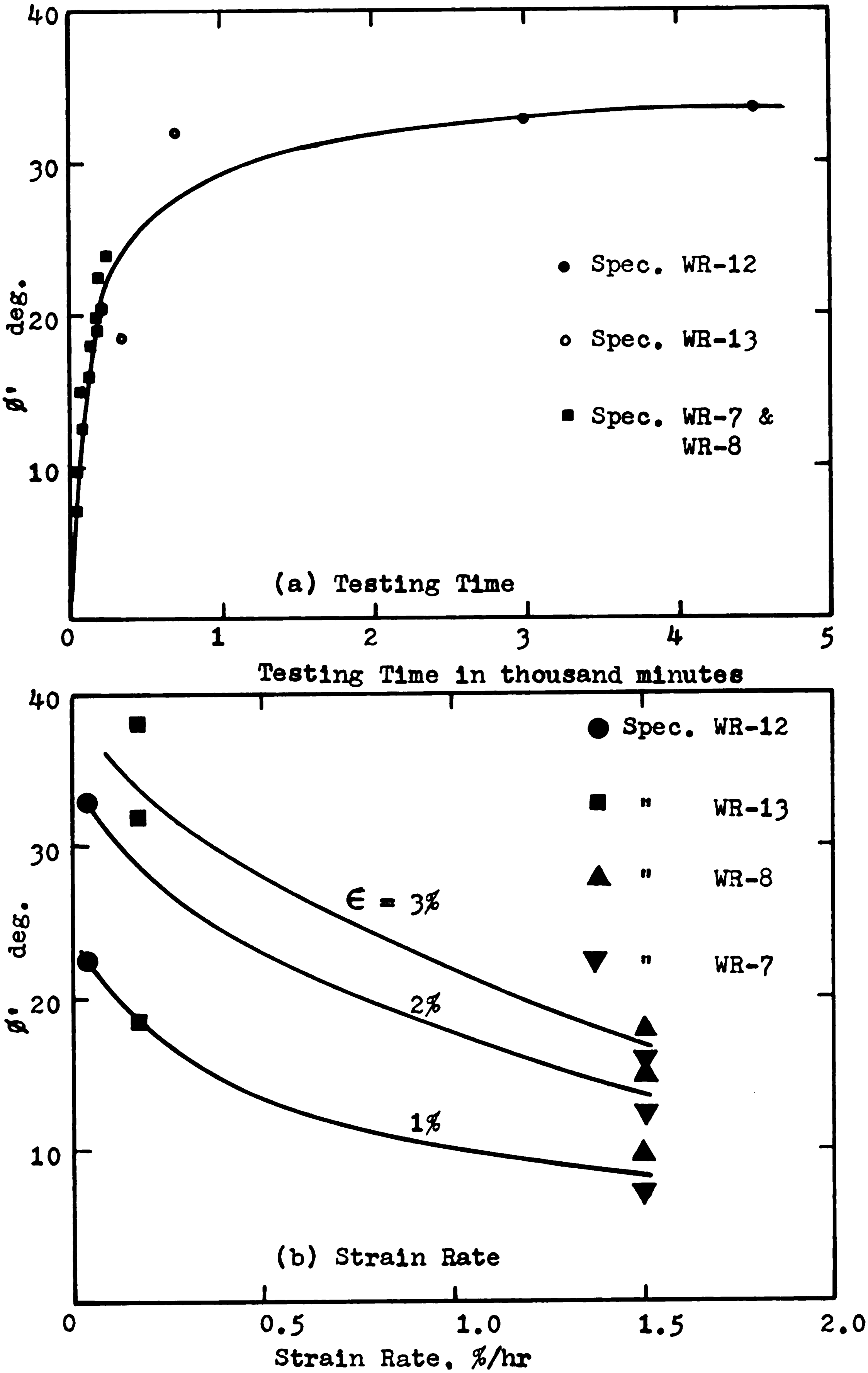

Fig. 27 ø'-Time and ø'-Strain Rate Curves--
CFS Tests on Undisturbed Willow Run Clay

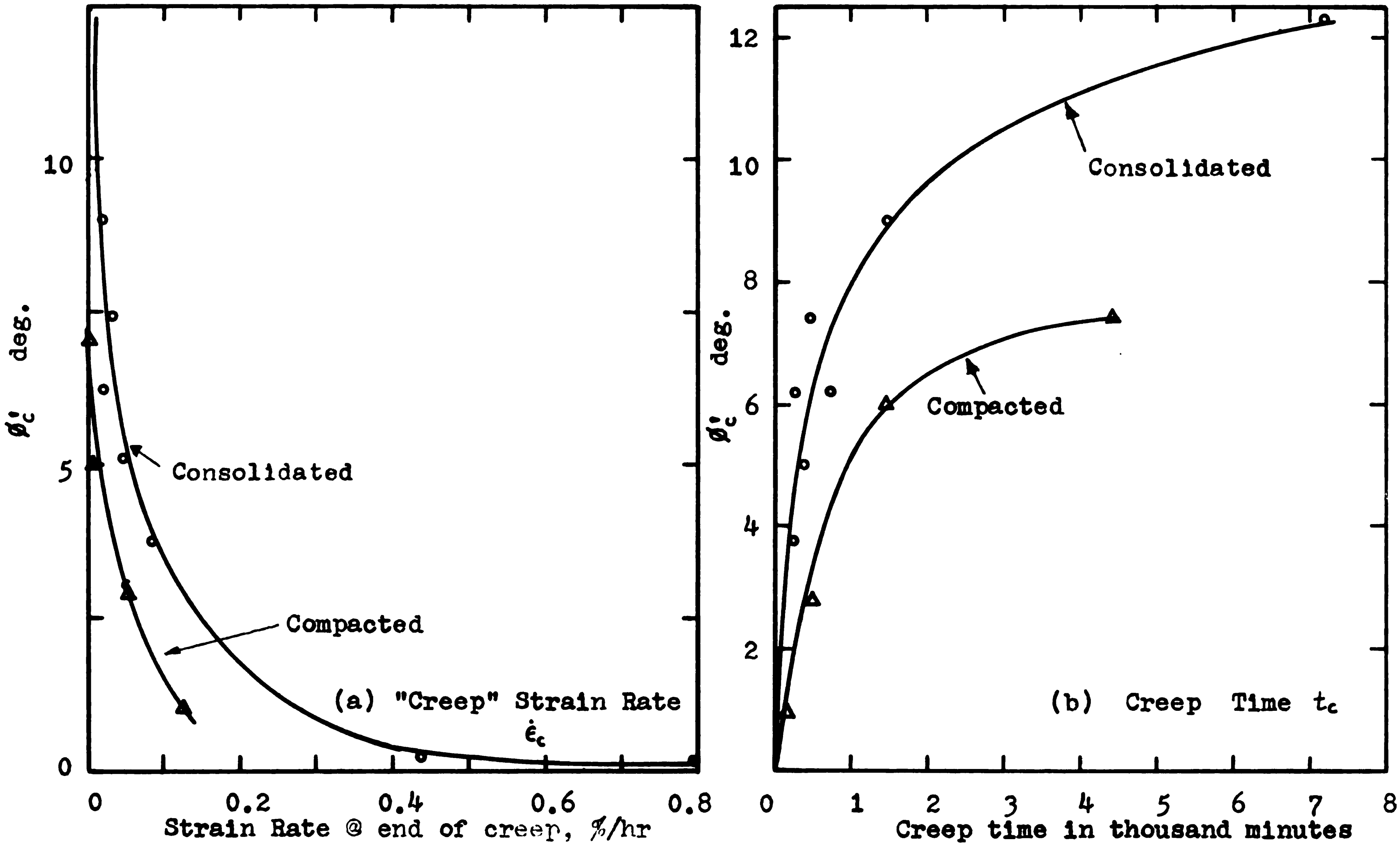

Fig. 28 Behavior of Friction in Creep-CFS Tests on Sault Clay

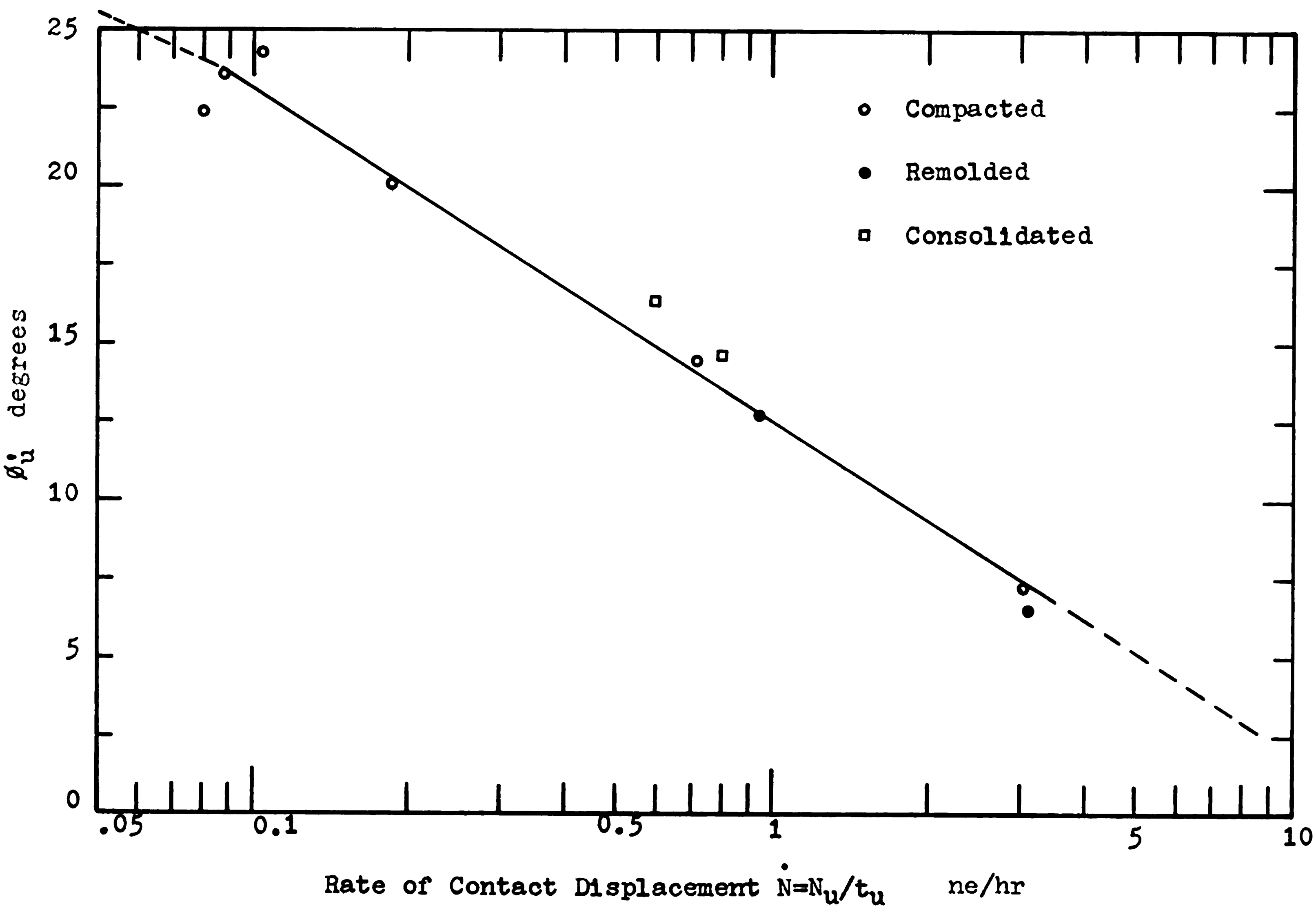

Fig. 29 ϕ'_u-$\dot{N}$ Characteristics--CFS Tests on Sault Clay

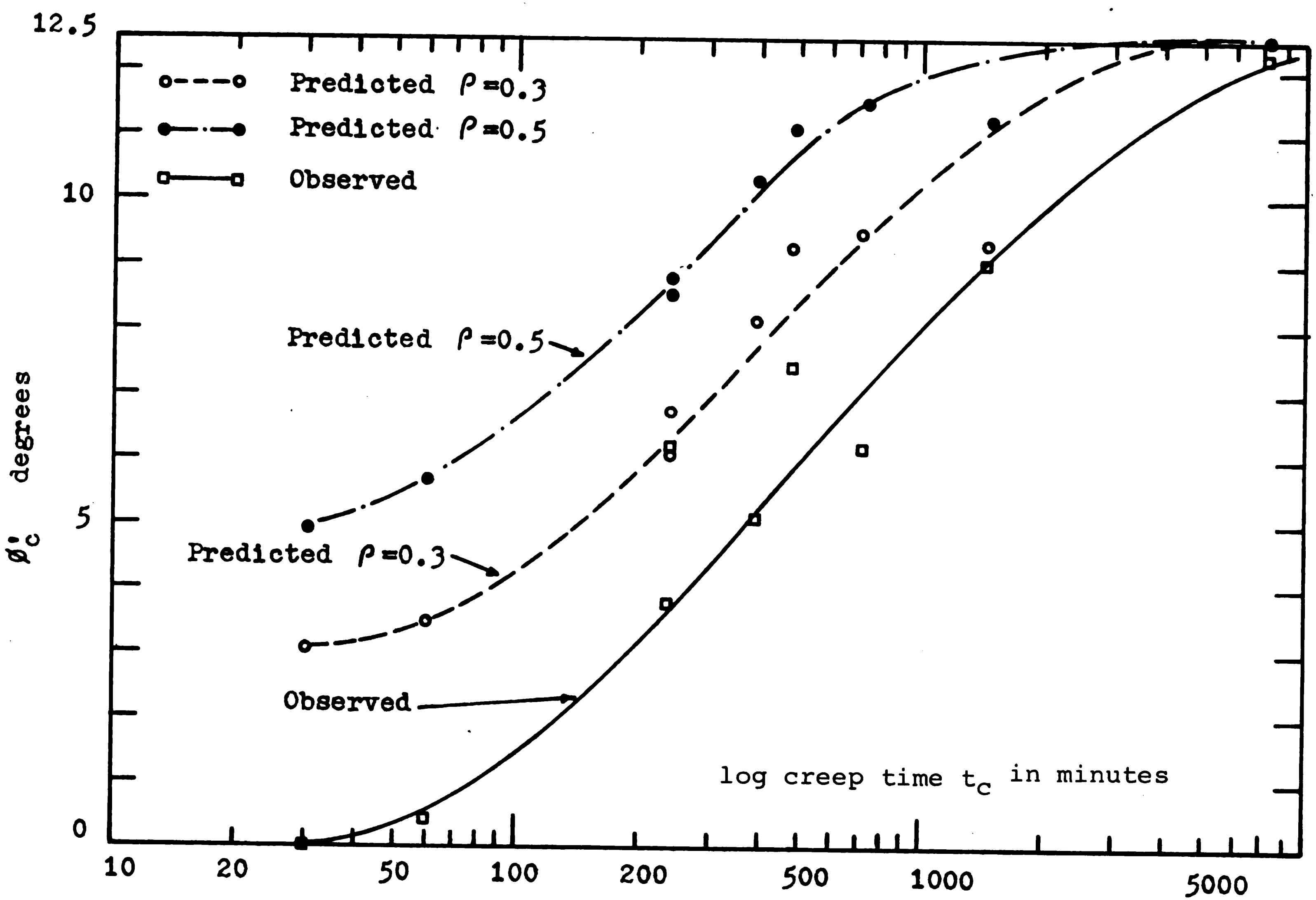

Fig. 30 Comparison of Behaviors of Friction in Creep-CFS Tests on Consolidated Sault Clay

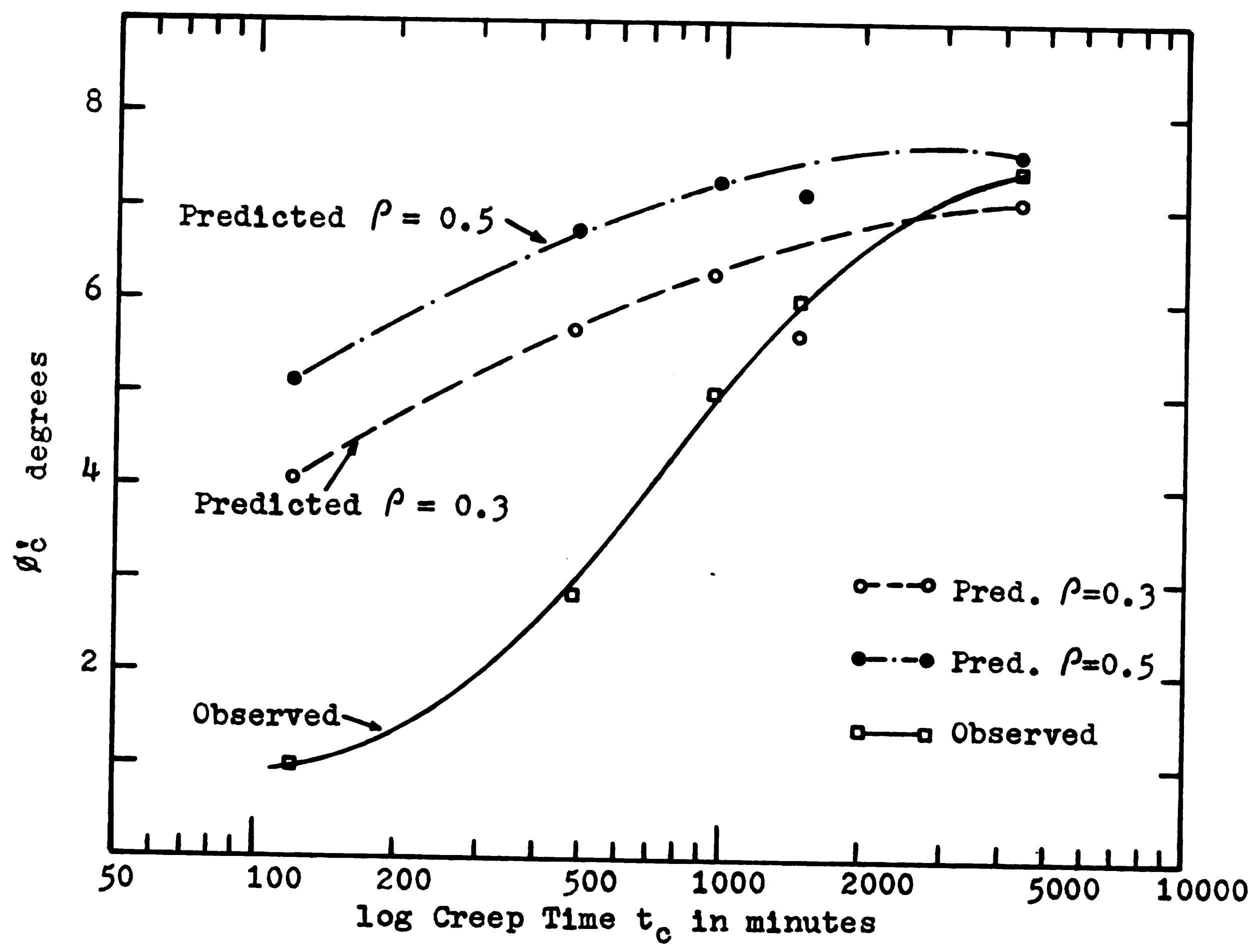

Fig. 31 Comparison of Behaviors of Friction in Creep-CFS Tests on Compacted Sault Clay

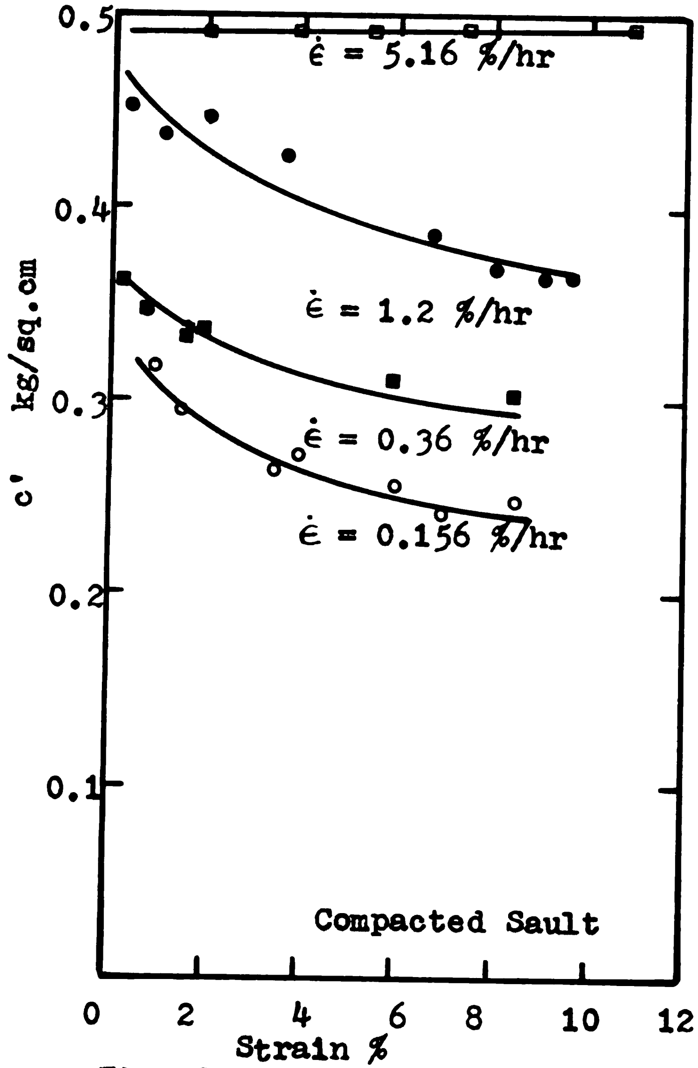

Fig.32 c'-Strain Curves--CFS Tests on Compacted Sault Clay

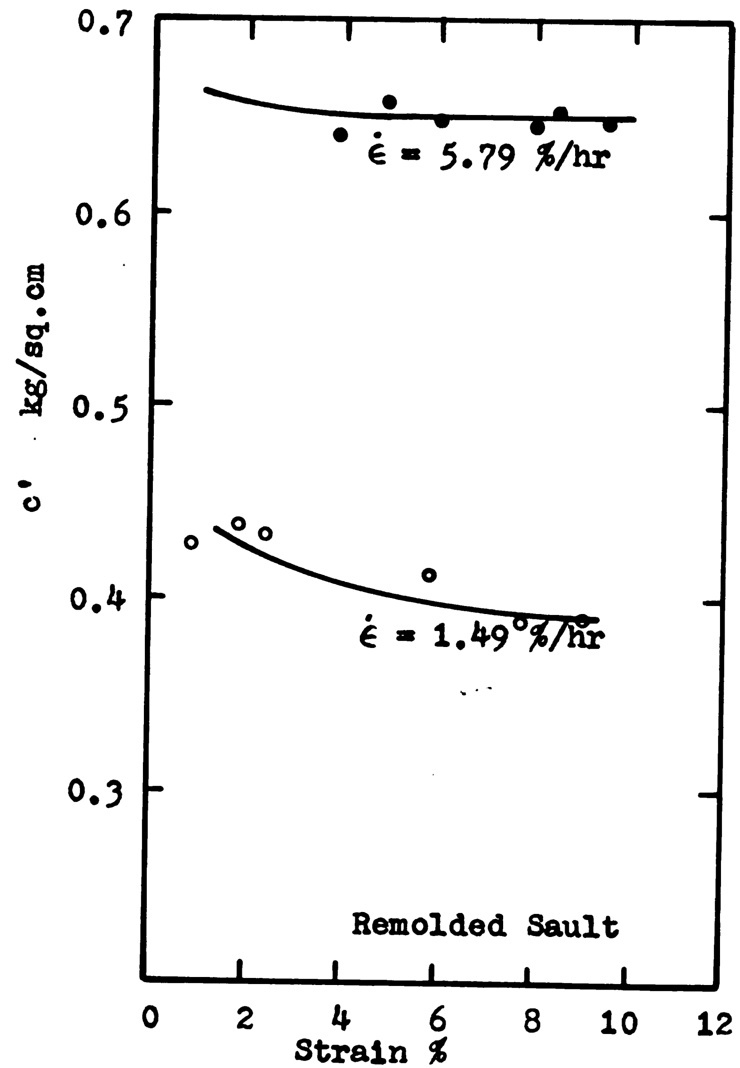

Fig. 33 c'-Strain Curves--CFS Tests on Remolded Sault Clay

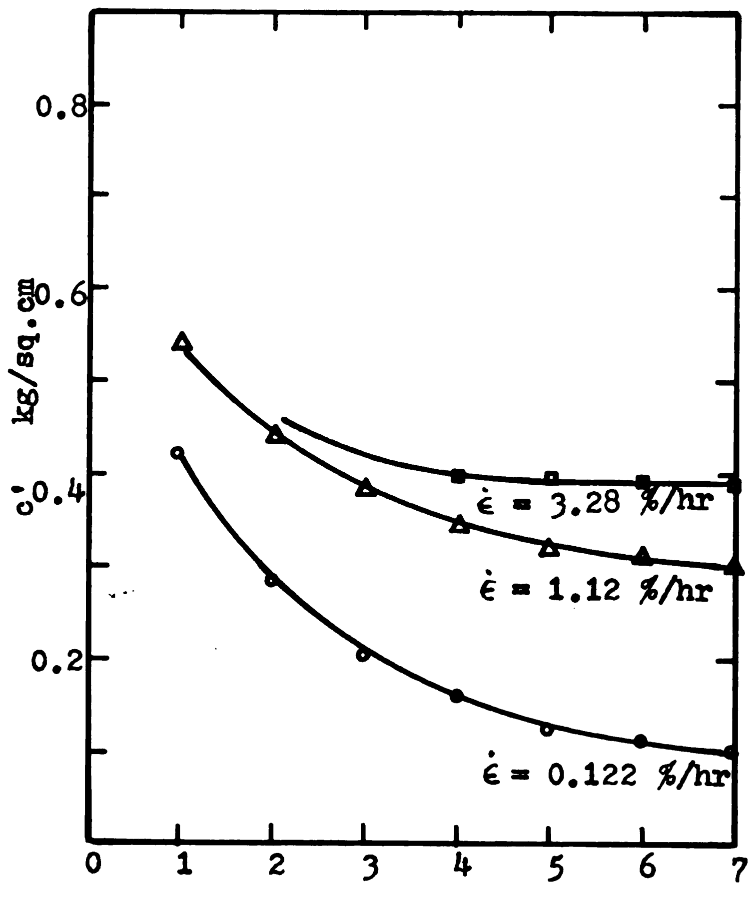

Fig. 34 c'-Strain Curves--CFS Tests on Over-consolidated Sault Clay

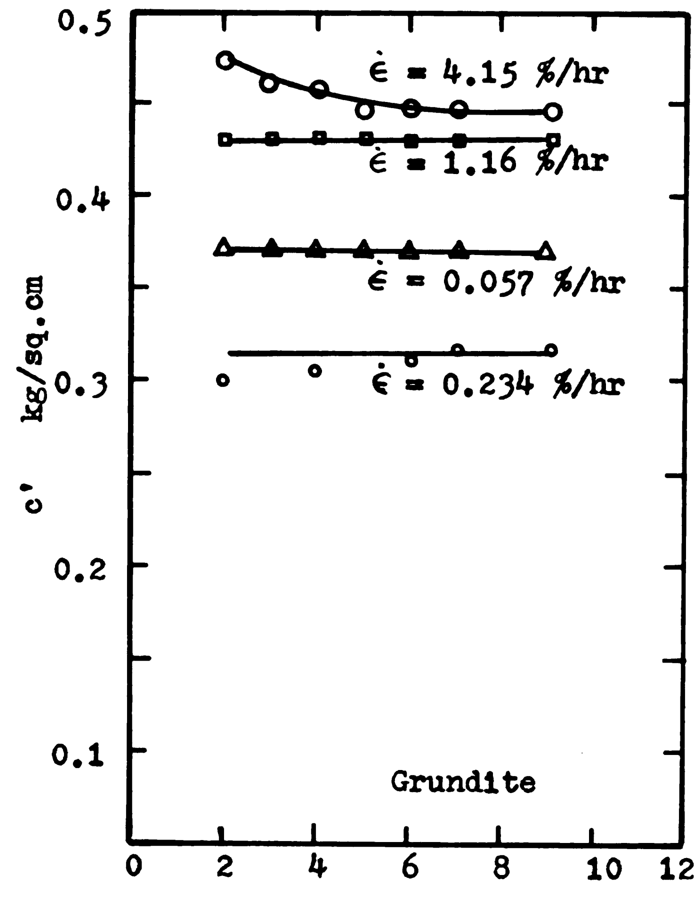

Fig. 35 c'-Strain Curves--CFS Tests on Grundite

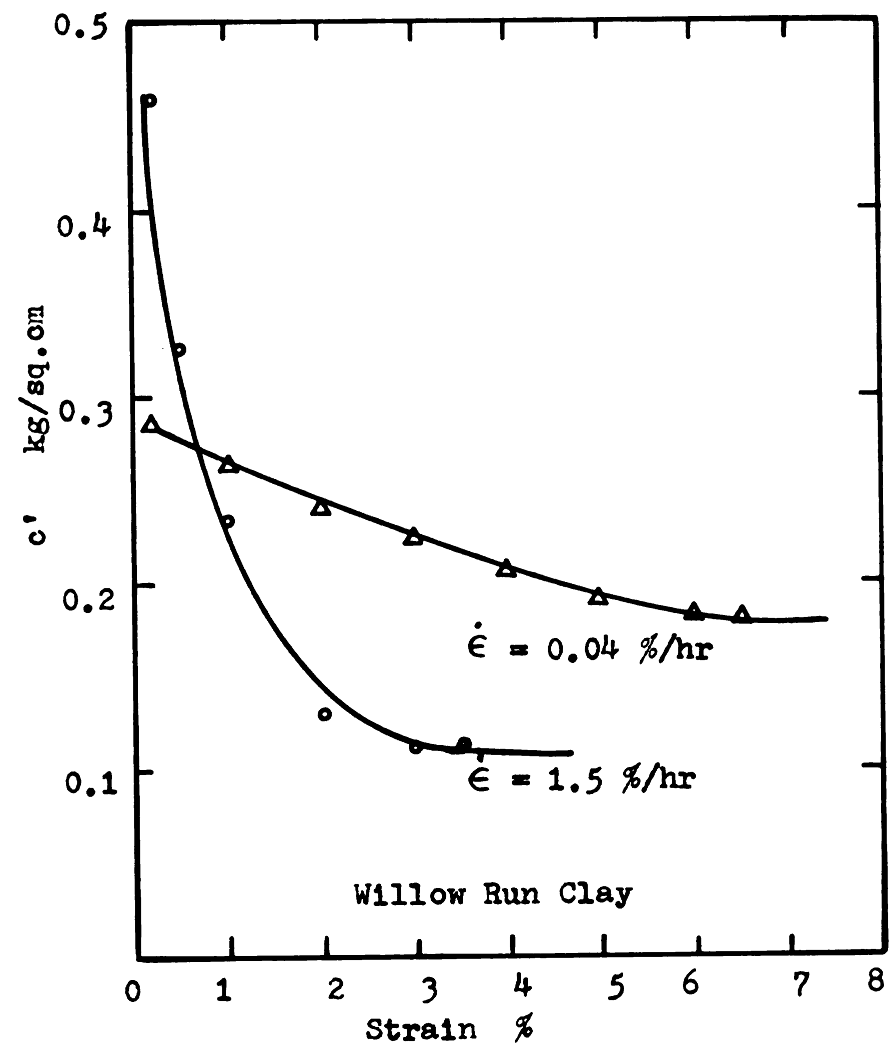

Fig. 36 c'-Strain Curves--CFS Tests on Undisturbed Willow Run Clay

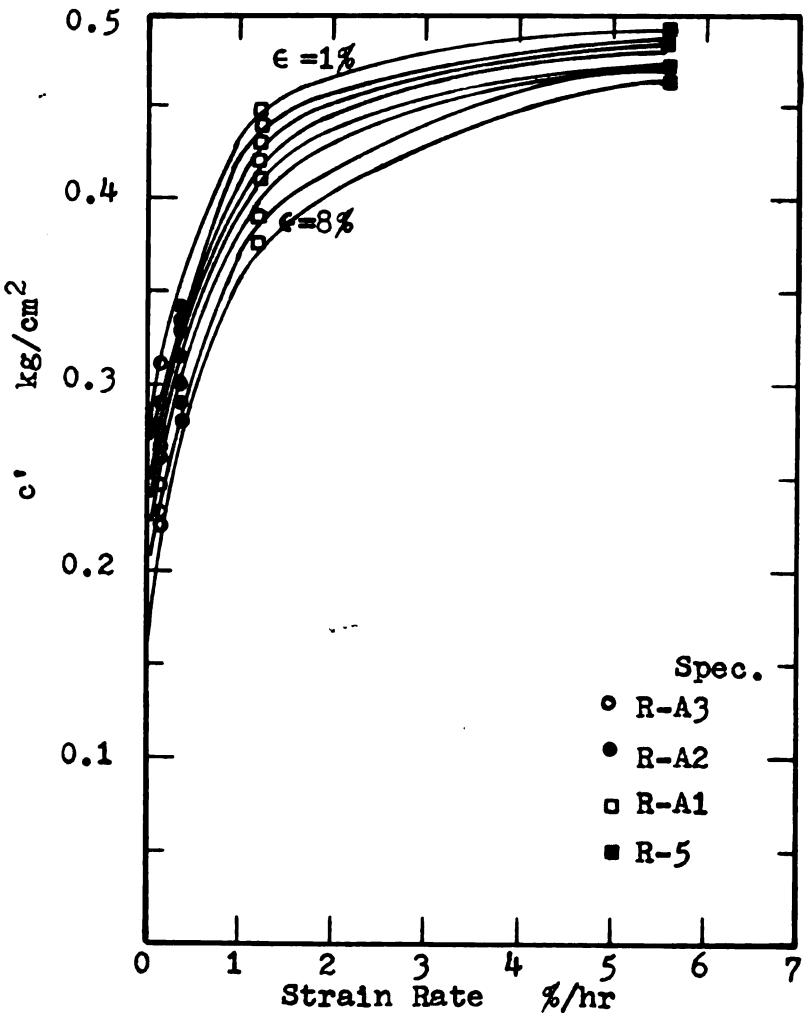

Fig. 37 c'-Strain Rate Curves--CFS Tests on Compacted Sauly Clay

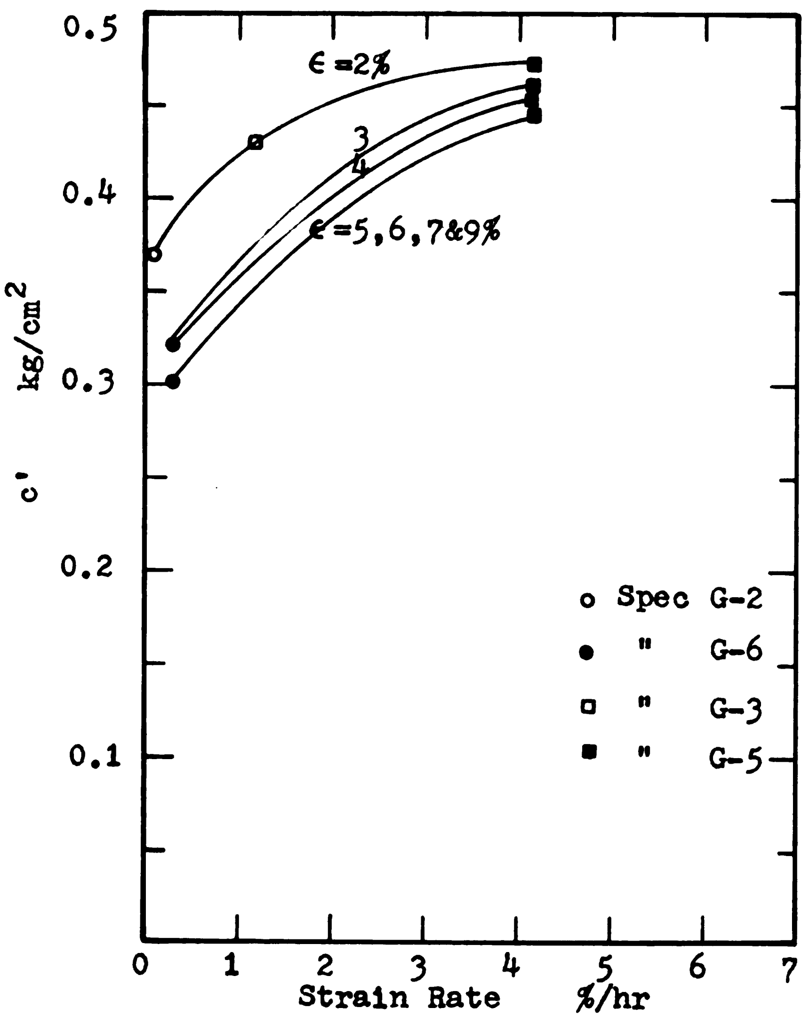

Fig.38 c'-Strain Rate Curves--CFS Tests on Grundite

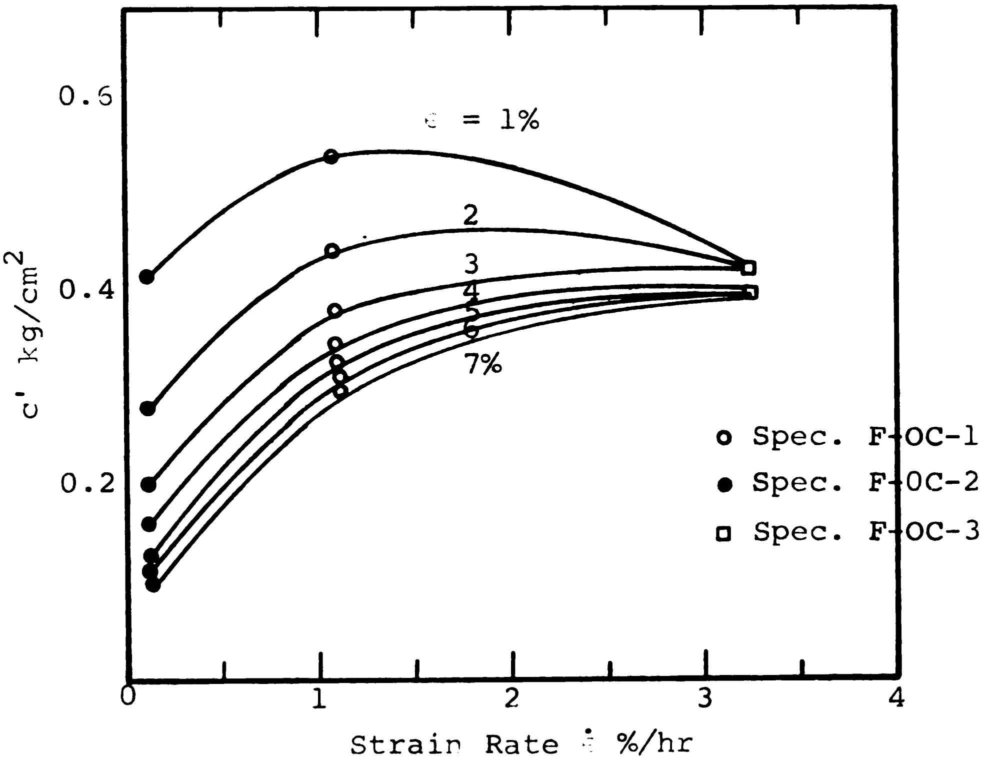

Fig. 39 c'-Strain Rate Curves--CFS Tests on Over-consolidated Sault clay

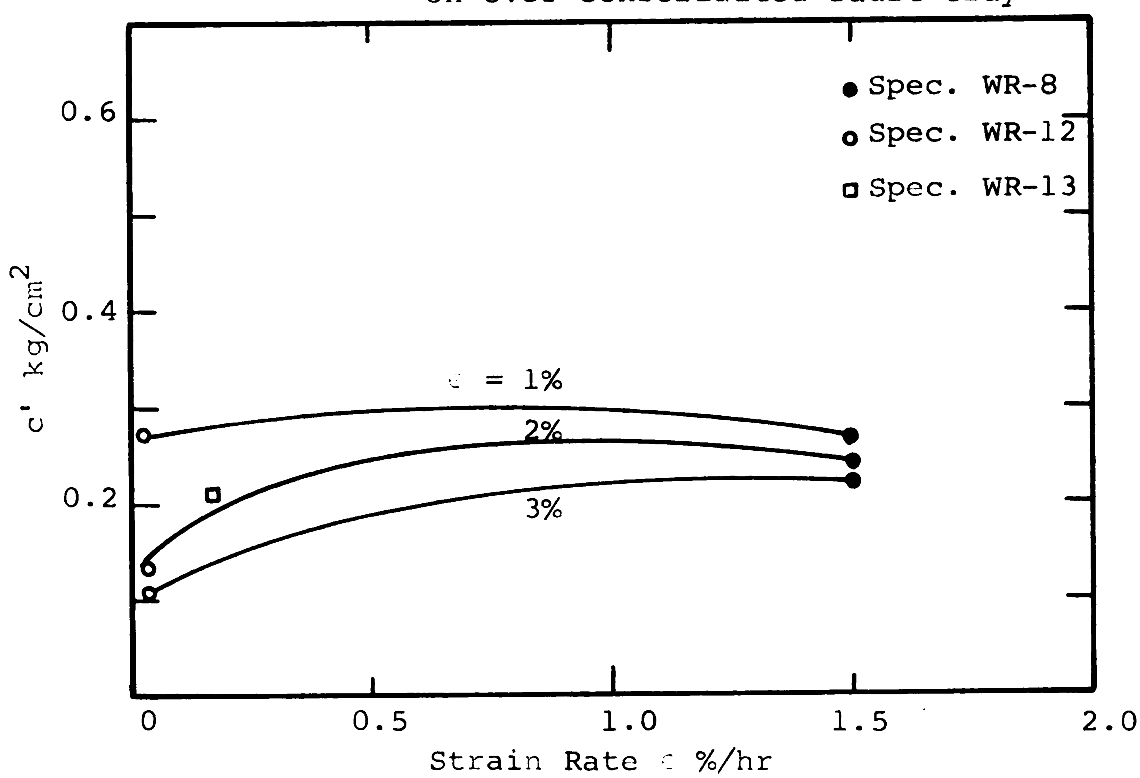

Fig. 40 c'-Strain Rate Curves -- CFS Tests on Undisturbed Willow Run Clay

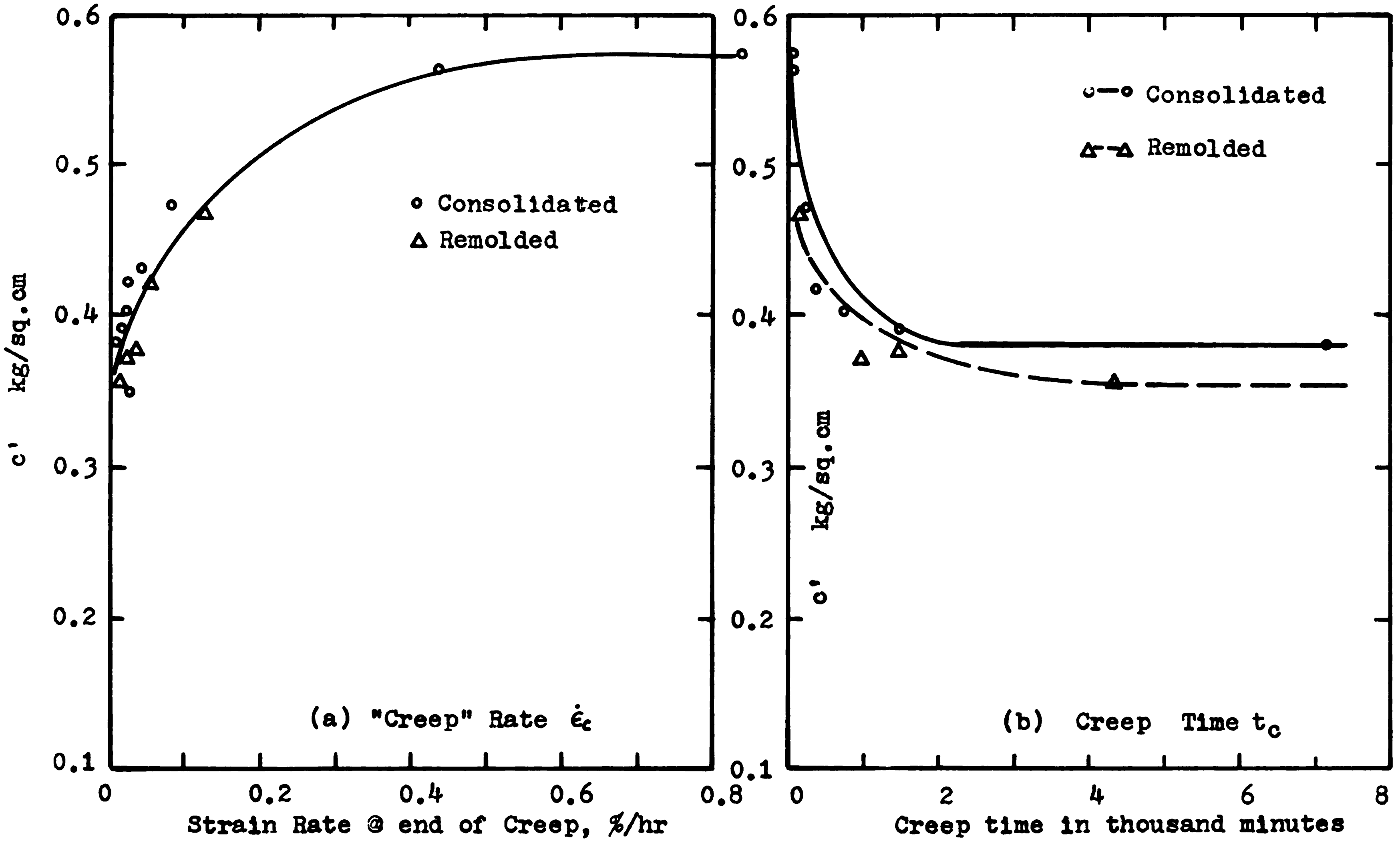

Fig. 41 Behavior of Cohesion in Creep-CFS Tests on Sault Clay

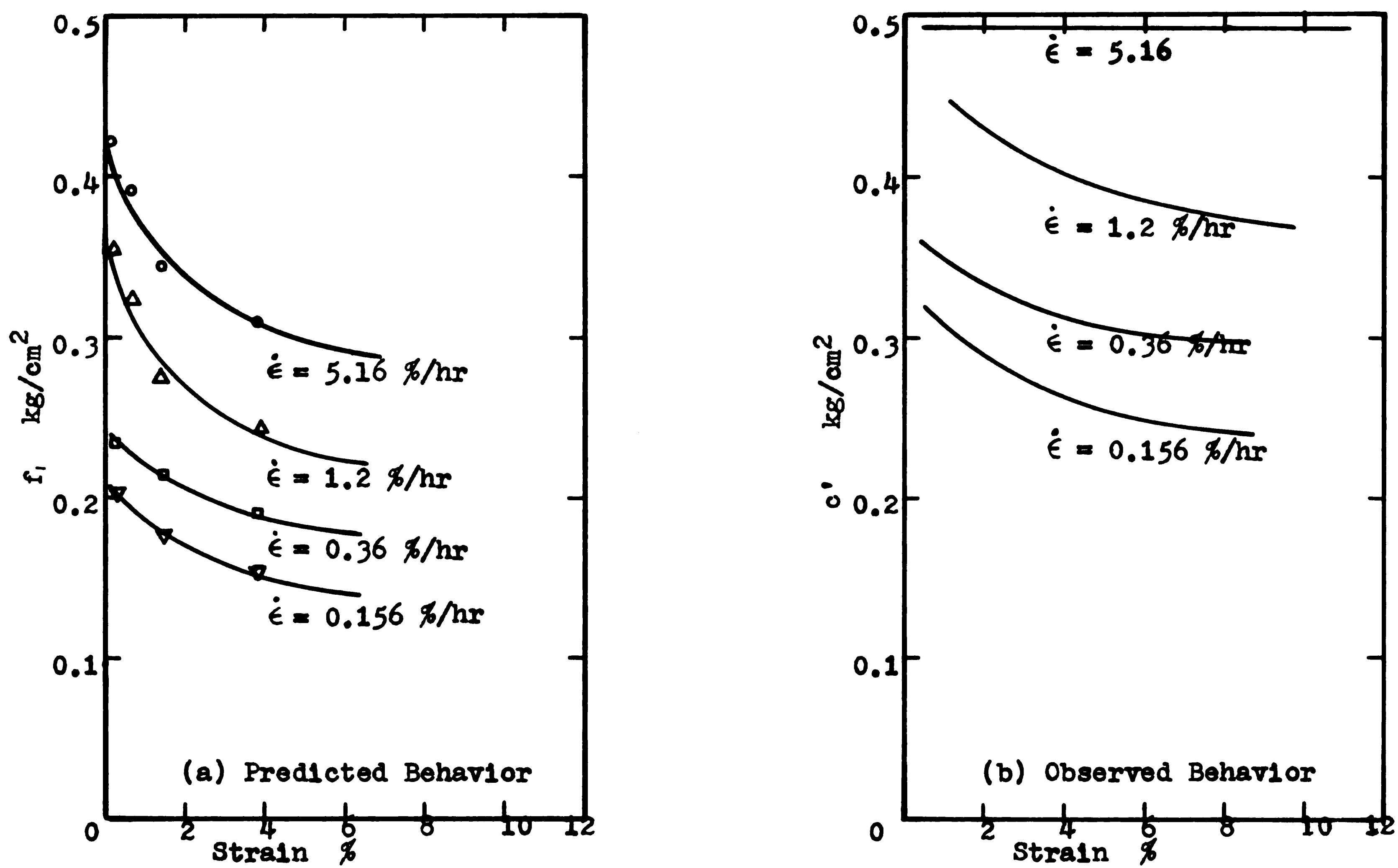

Fig. 42 Comparison of Behaviors of Cohesion : Compacted Sault Clay

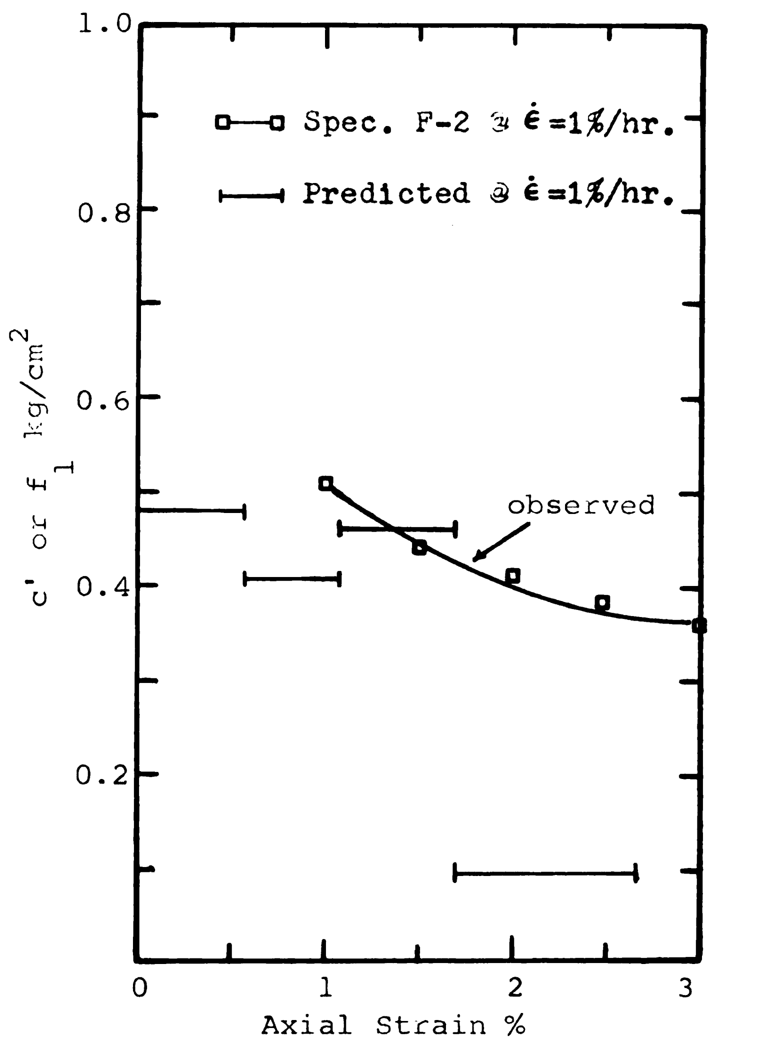

Fig. 43 Comparison of Behavior of Cohesion: Consolidated Sault clay

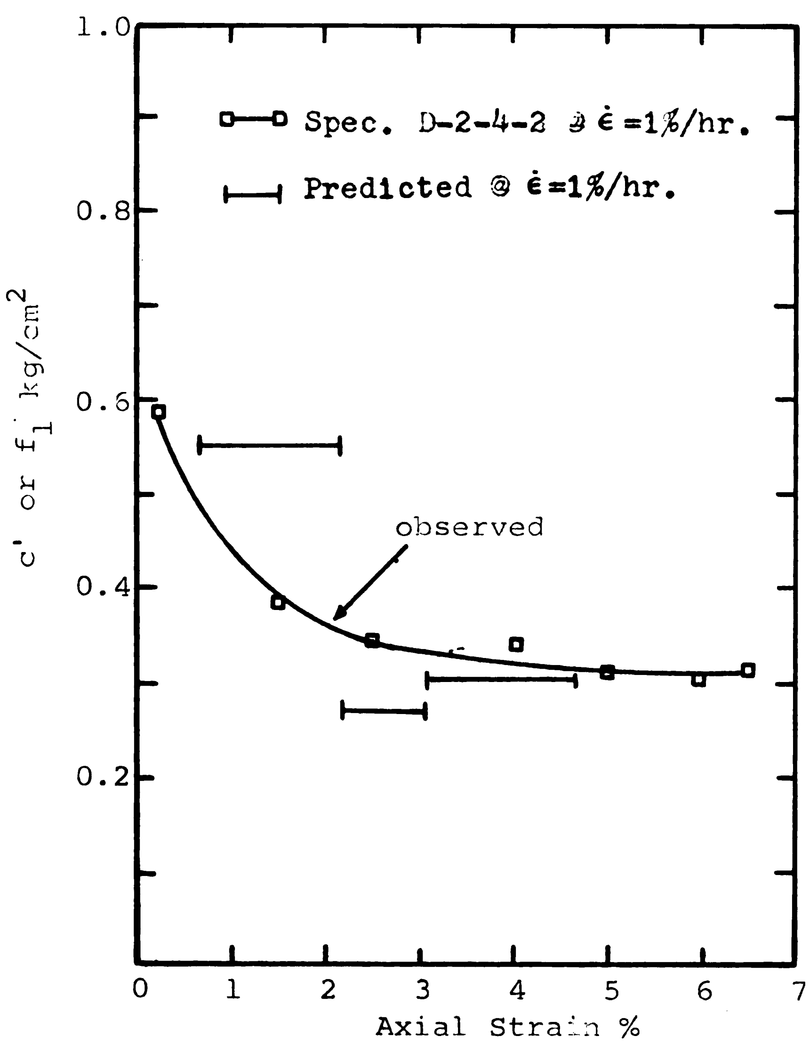

Fig. 44 Comparison of Behavior of Cohesion: Undisturbed Marine City clay

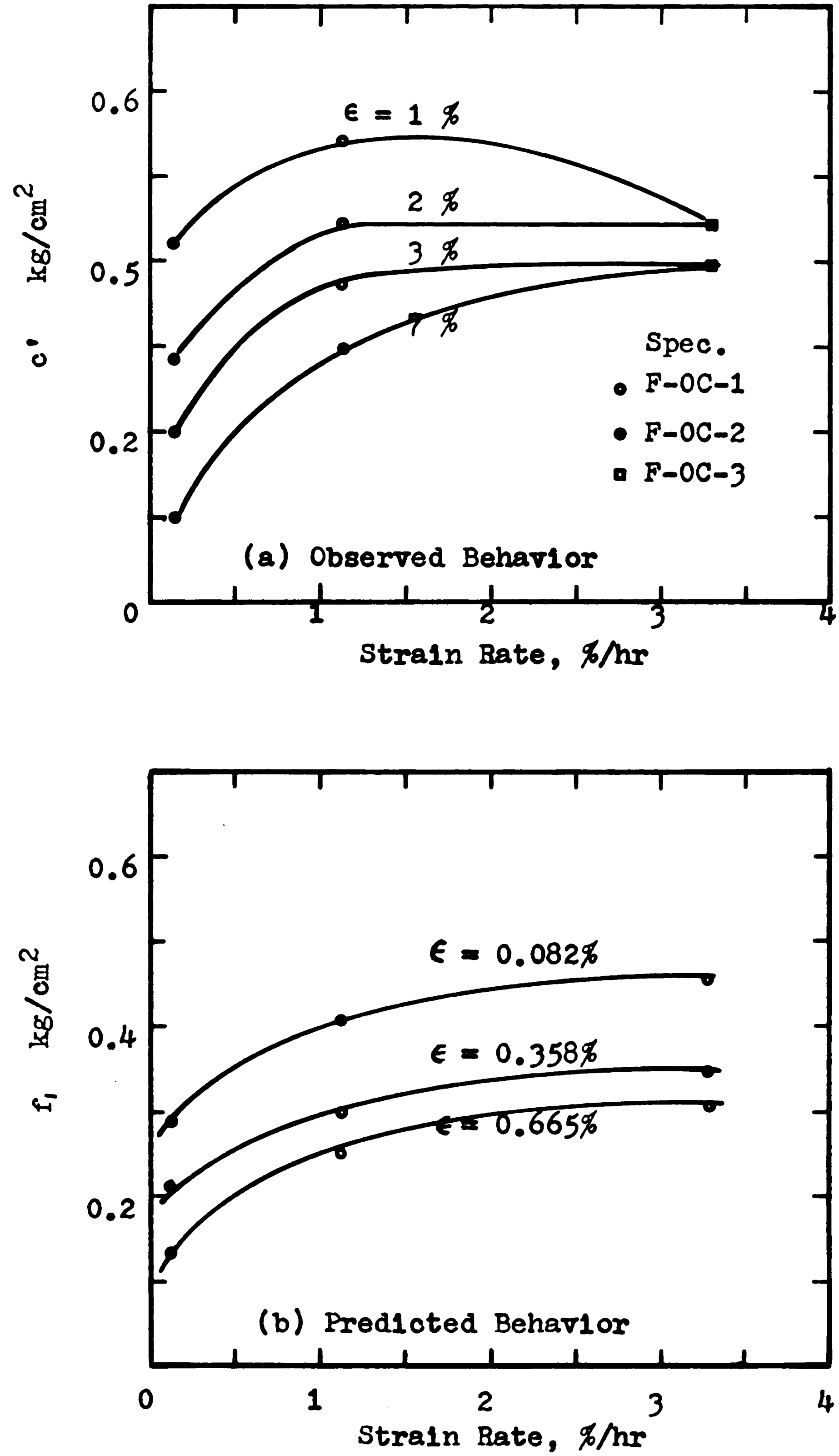

Fig. 45 Comparison of Behaviors of Cohesion : Over-consolidated Sault Clay

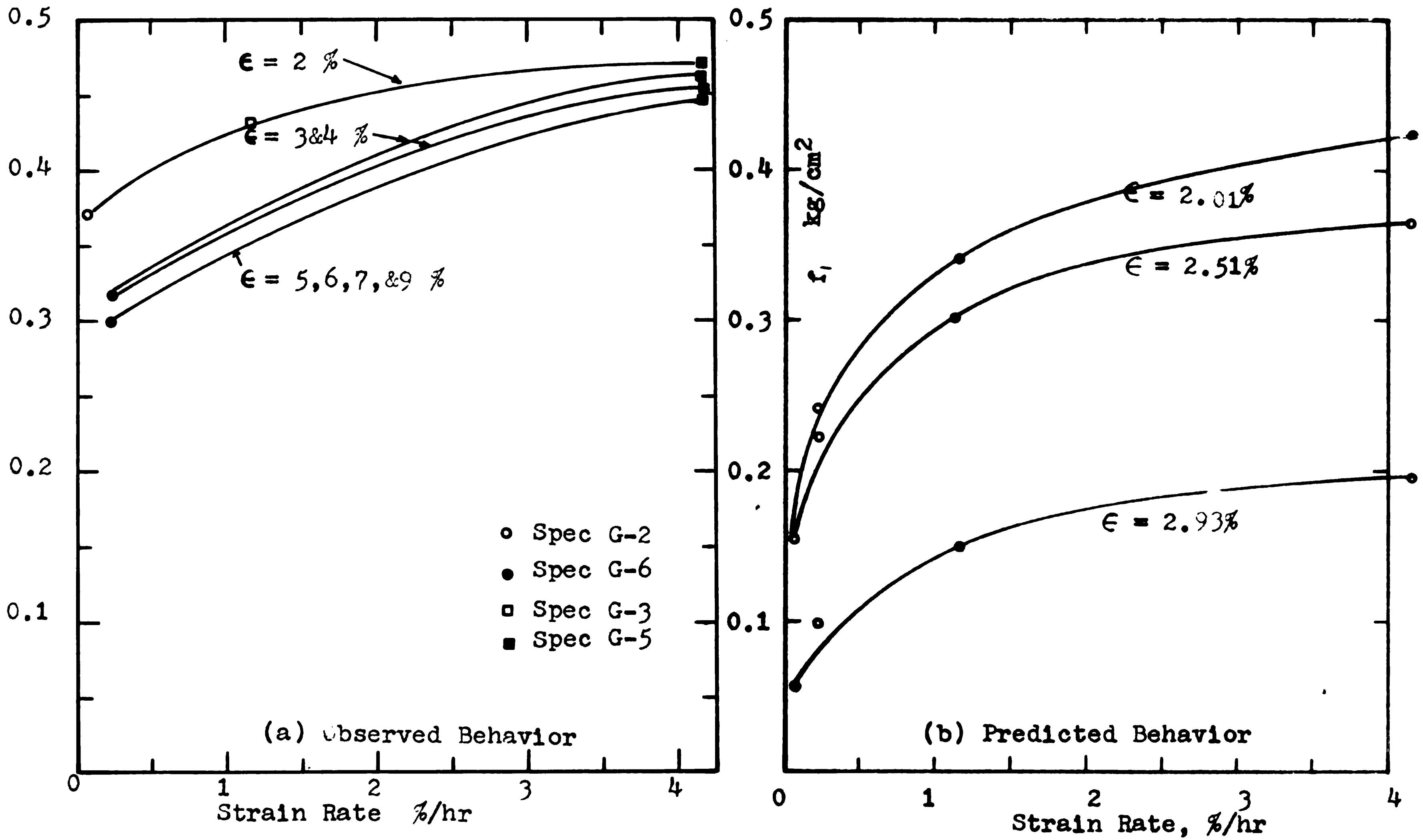

Fig. 46 Comparison of Behaviors of Cohesion : Grundite

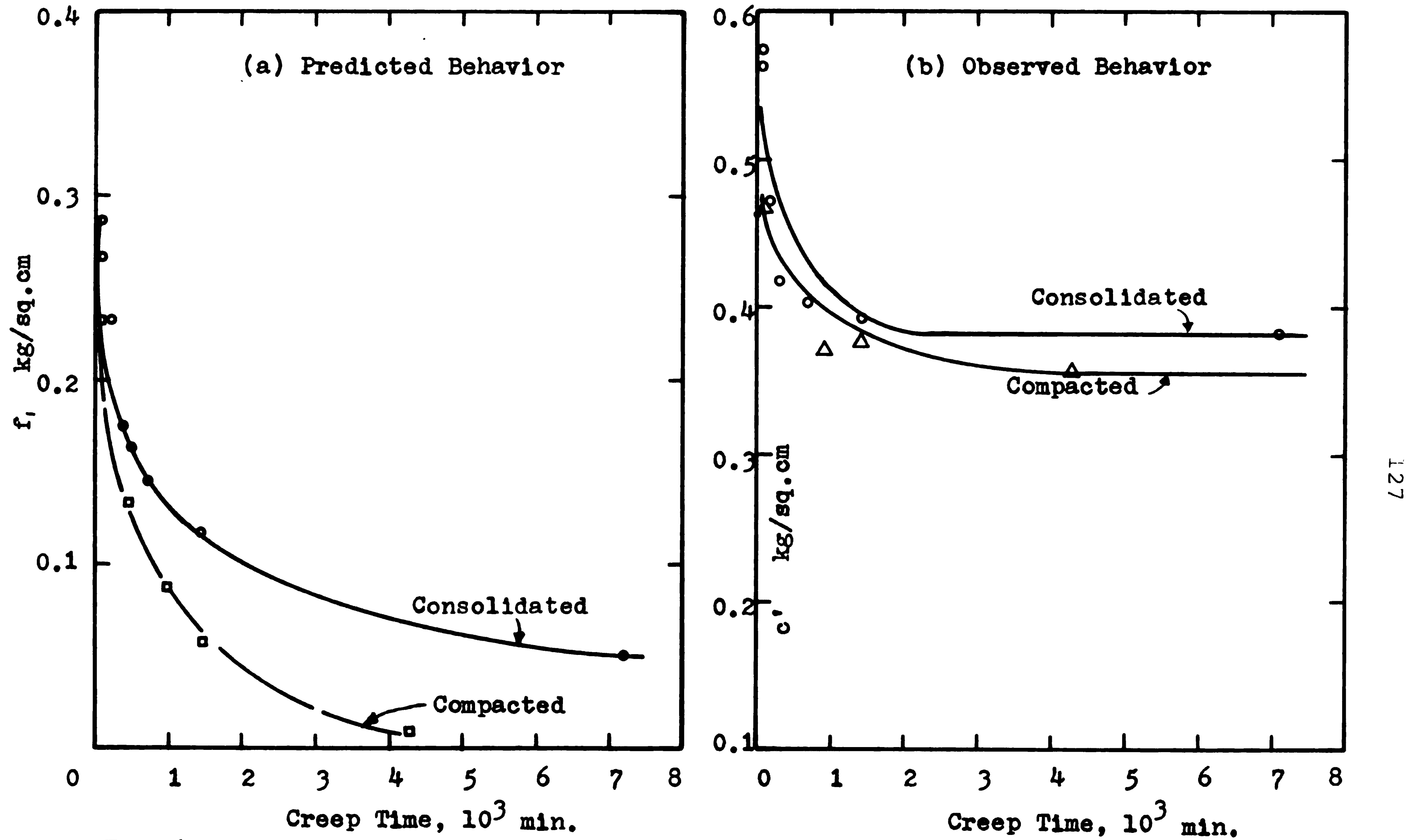

Fig. 47 Comparison of Behaviors of Cohesion in Creep-CFS Tests on Sault Clay

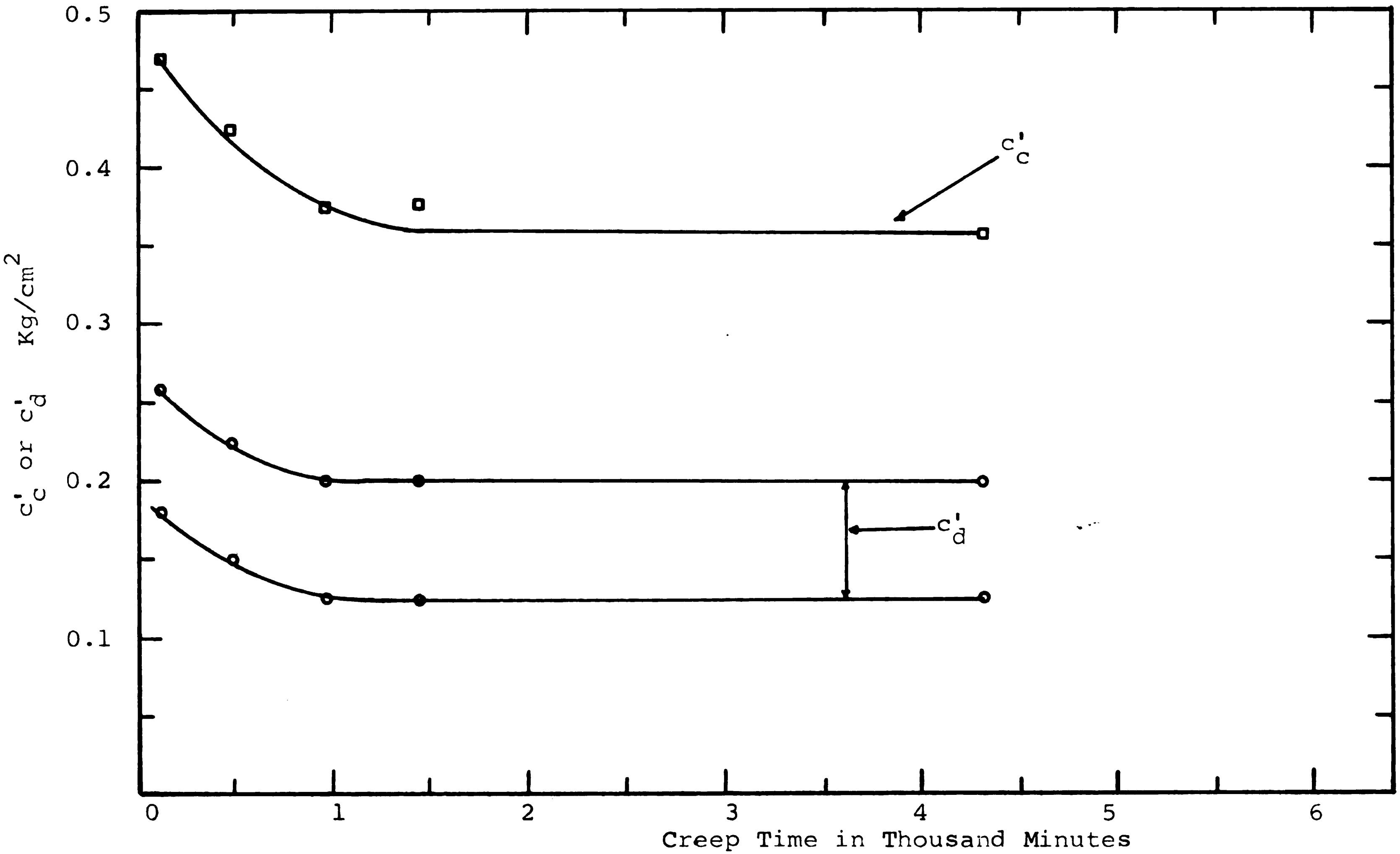

Fig. 48 Comparison of c'_c and c'_d : Creep-CFS Tests on Compacted Sault Clay

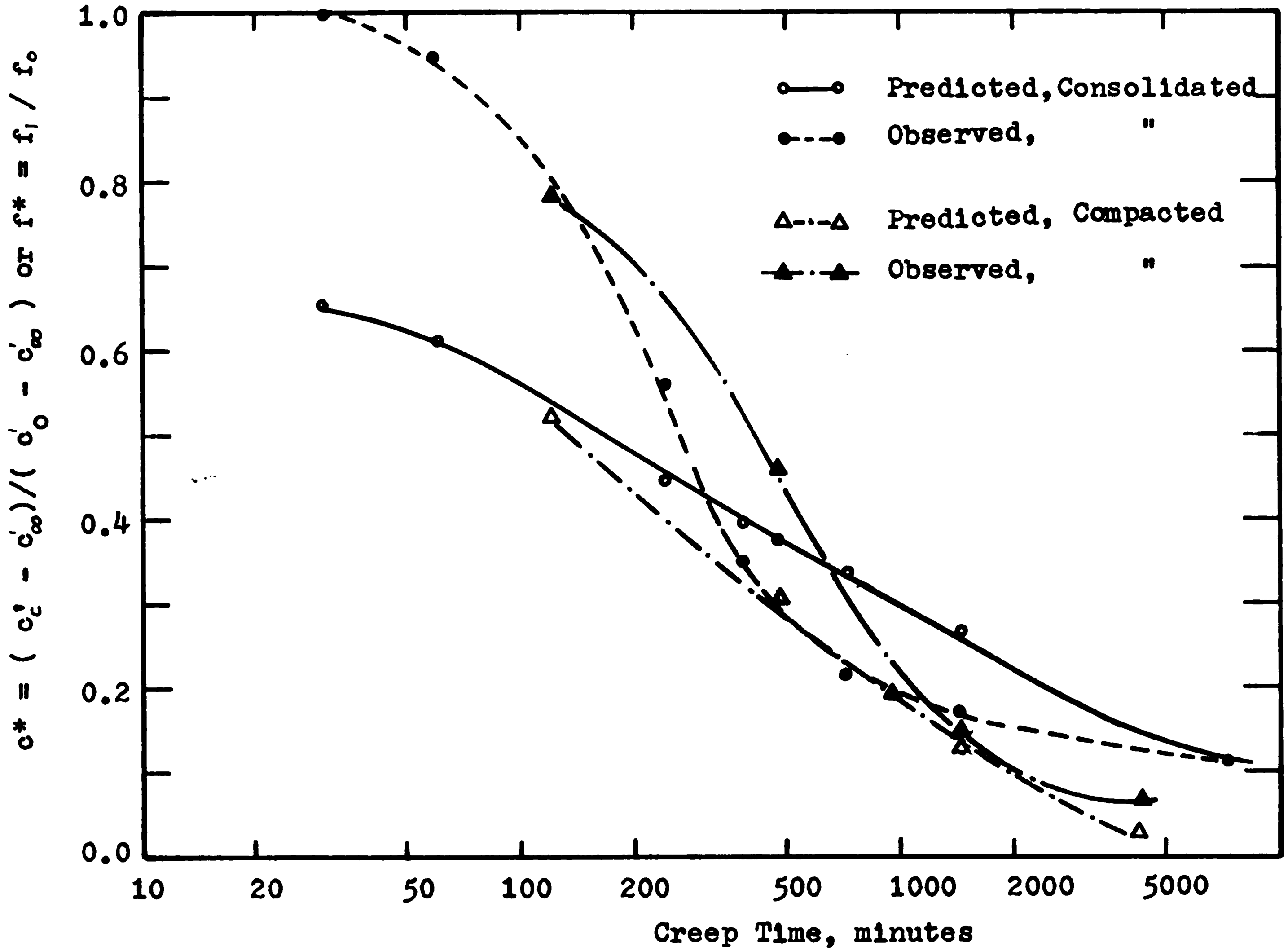

Fig. 49 Comparison of c* and f* : Creep-CFS Tests on Sault Clay

APPENDIX I

COMPUTATIONS OF CONTACT RESISTANCE

Table A-1. Comparison of $t_{2\theta}$

θ deg.	$t_{2\theta}$ in $\bar{\sigma}_3 \frac{1}{a_\theta}$ Equation (9)	Equation (10)	Equation (11) $\rho = 0.3$	Equation (11) $\rho = 0.5$
90	0.423	--	0.513	0.855
100	0.505	1.642	0.430	0.718
110	0.571	0.420	0.381	0.635
120	0.618	0.197	0.351	0.585
130	0.649	0.119	0.336	0.559
140	0.660	0.083	0.330	0.550
150	0.649	0.066	0.336	0.559
160	0.618	0.056	0.351	0.585
170	0.571	0.051	0.381	0.635
180	0.505	0.049	0.430	0.718

Table A-2 Frictional Resistance against Sliding $t_{1\theta}$

θ	F	$t_{1\theta} = \overline{\sigma}_3 (1+k)\frac{1}{2}\sin 2\alpha \times F$ where $F = \dfrac{\tan\mu}{\sin 2\theta - \tan\mu \cos 2\theta} \times \dfrac{1}{a_\theta}$									
deg		k= 1.1	1.2	1.3	1.4	1.5	1.6	1.7	1.8	1.9	2.0
10	.4035	.4170	.4370	.4565	.4760	.4960	.5160	.5360	.5550	.5750	.5950
15	.2420	.2500	.2620	.2740	.2860	.2980	.3100	.3215	.3340	.3460	.3575
20	.1770	.1830	.1920	.2005	.2090	.2180	.2265	.2350	.2440	.2525	.2620
25	.1430	.1480	.1550	.1620	.1690	.1760	.1830	.1900	.1970	.2040	.2110
30	.1225	.1268	.1330	.1390	.1450	.1510	.1570	.1628	.1690	.1750	.1810
35	.1103	.1140	.1195	.1250	.1305	.1360	.1413	.1465	.1520	.1574	.1630
40	.1033	.1070	.1120	.1172	.1222	.1272	.1322	.1372	.1424	.1475	.1525
45	.1000	.1035	.1084	.1133	.1182	.1230	.1280	.1330	.1380	.1430	.1480
50	.0996	.1030	.1080	.1128	.1170	.1225	.1275	.1322	.1372	.1422	.1470
55	.1027	.1060	.1110	.1163	.1214	.1263	.1315	.1363	.1415	.1467	.1517
60	.1090	.1128	.1180	.1234	.1290	.1340	.1395	.1448	.1500	.1556	.1610
65	.1204	.1245	.1305	.1365	.1422	.1480	.1540	.1600	.1660	.1720	.1780
70	.1390	.1438	.1505	.1575	.1642	.1710	.1780	.1845	.1915	.1983	.2050
75	.1700	.1760	.1860	.1925	.2010	.2090	.2180	.2260	.2340	.2425	.2510
80	.2300	.2380	.2520	.2600	.2720	.2830	.2945	.3055	.3170	.3285	.3400
85	.3640	.3760	.4070	.4120	.4300	.4485	.4650	.4835	.5015	.5200	.5380

Table A-2(cont'd) Frictional Resistance against Sliding

θ	F	$t_{1\theta} = \overline{\sigma}_3(1+k)\frac{1}{2}\sin 2\alpha \cdot F$ where $F = \dfrac{\tan\mu}{\sin 2\theta - \tan\mu\cos 2\theta} \times \dfrac{1}{a_\theta}$									
deg		k= 2.1	2.2	2.3	2.4	2.5	2.6	2.7	2.8	2.9	
10	.6150	.6350	.6550	.6750	.6950	.7150	.7150	.7350	.7550	.7750	
15	.2420	.3700	.3815	.3930	.4050	.4170	.4300	.4400	.4525	.4650	
20	.1770	.2700	.2790	.2880	.2960	.3050	.3140	.3220	.3310	.3400	
25	.1430	.2180	.2260	.2320	.2390	.2460	.2535	.2600	.2680	.2745	
30	.1225	.1870	.1930	.1990	.2050	.2110	.2170	.2230	.2290	.2350	
35	.1103	.1680	.1740	.1790	.1845	.1900	.1955	.2010	.2065	.2120	
40	.1033	.1578	.1630	.1680	.1730	.1780	.1830	.1880	.1930	.1985	
45	.1000	.1528	.1575	.1625	.1672	.1720	.1770	.1820	.1870	.1920	
50	.0996	.1520	.1570	.1620	.1665	.1715	.1764	.1812	.1863	.1910	
55	.1027	.1567	.1620	.1670	.1718	.1770	.1820	.1870	.1930	.1970	
60	.1090	.1663	.1718	.1770	.1822	.1800	.1930	.1985	.2040	.2095	
65	.1204	.1840	.1900	.1960	.2015	.2075	.2135	.2190	.2255	.2315	
70	.1390	.2120	.2190	.2260	.2320	.2400	.2460	.2530	.2600	.2670	
75	.1700	.2600	.2680	.2760	.2840	.2930	.3010	.3100	.3180	.3260	
80	.2300	.3510	.3625	.3740	.3850	.3960	.4070	.4190	.4300	.4415	
85	.3640	.5550	.5750	.5915	.6090	.6260	.6450	.6630	.6810	.7000	

Table A-3 Frictional Resistance against Displacement $\rho = 0.2$

θ (deg)	F	$t_{2\theta} = \frac{2+k}{3}\rho\bar{\sigma}_3 \times F$ where $F = 1/\sin(\theta - \alpha) \times \frac{1}{a_\theta}$								
		K= 1.1	1.2	1.3	1.4	1.5	1.6	1.7	1.8	1.9
0	1.305	.2700	.2780	.2870	.2960	.3045	.3130	.3220	.3300	.3390
10	1.555	.3215	.3315	.3420	.3520	.3630	.3730	.3840	.3940	.4050
85	1.740	.3600	.3710	.3830	.3940	.4060	.4180	.4300	.4400	.4530
90	1.555	.3215	.3315	.3420	.3520	.3630	.3730	.3840	.3940	.4050
100	1.305	.2700	.2780	.2870	.2960	.3045	.3130	.3220	.3300	.3390
110	1.155	.2390	.2460	.2540	.2620	.2700	.2770	.2850	.2920	.3000
120	1.065	.2200	.2270	.2340	.2420	.2485	.2560	.2630	.2700	.2770
130	1.050	.2100	.2160	.2235	.2300	.2370	.2440	.2505	.2570	.2670
140	1.000	.2065	.2130	.2200	.2270	.2335	.2400	.2470	.2530	.2600
150	1.015	.2100	.2160	.2235	.2300	.2370	.2440	.2505	.2570	.2640
160	1.065	.2200	.2270	.2340	.2420	.2485	.2560	.2630	.2700	.2770
170	1.155	.2390	.2460	.2540	.2620	.2700	.2770	.2850	.2920	.3000
180	1.305	.2700	.2780	.2870	.2960	.3045	.3130	.3220	.3300	.3390

Table A-3(cont'd) Frictional Resistance against Displacement $\rho = 0.2$

θ deg	F	$t_{2\theta} = \rho \overline{\sigma}_3 \frac{2 + k}{3} \times F$ where $F = 1/\sin(\theta - \alpha) \times \frac{1}{a_\theta}$									
		k= 2.0	2.1	2.2	2.3	2.4	2.5	2.6	2.7	2.8	2.9
0	1.305	.3480	.3570	.3660	.3740	.3820	.2920	.4000	.4100	.4170	.4250
10	1.555	.4150	.4250	.4350	.4450	.4550	.4660	.4770	.4870	.4965	.5070
85	1.740	.4650	.4750	.4880	.5000	.5100	.5200	.5350	.5450	.5555	.5690
90	1.555	.4150	.4250	.4350	.4450	.4550	.4660	.4770	.4870	.4965	.5070
100	1.305	.3480	.3570	.3660	.3740	.3820	.3920	.4000	.4100	.4170	.4250
110	1.155	.3080	.3160	.3240	.3310	.3385	.3460	.3540	.3620	.3690	.3770
120	1.065	.2840	.2910	.2980	.3160	.3120	.3195	.3270	.3340	.3400	.3480
130	1.015	.2710	.2775	.2840	.2910	.2980	.3040	.3115	.3180	.3240	.3320
140	1.000	.2670	.2735	.2800	.2870	.2930	.3000	.3070	.3135	.3200	.3265
150	1.015	.2710	.2775	.2840	.2910	.2980	.3140	.3115	.3180	.3240	.3320
160	1.065	.2840	.2910	.2980	.3060	.3120	.3195	.3270	.3340	.3400	.3480
170	1.155	.3080	.3160	.3240	.3310	.3385	.3460	.3540	.3620	.3690	.3770
180	1.305	.3480	.3570	.3660	.3740	.3820	.3920	.4000	.4100	.4170	.4250

Table A-4 Frictional Resistance against Displacement $t_{2\theta}$ $\rho = 0.3$

θ deg	F	$t_{2\theta} = \rho \bar{\sigma}_3 (2+k)/3 \times F$ where $F = 1/\sin(\theta - \alpha) \times \frac{1}{a_\theta}$ k= 1.1	1.2	1.3	1.4	1.5	1.6	1.7	1.8	1.9	2.0
0	1.305	.4150	.4170	.4300	.4440	.4560	.4700	.4830	.4950	.5090	.5220
10	1.555	.4820	.4970	.5130	.5280	.5450	.5600	.5760	.5910	.6080	.6220
20	2.000	.6200	.6400	.6600	.6800	.6990	.7200	.7400	.7600	.7800	.8000
80	2.000	.6200	.9390	.6600	.6800	.6990	.7200	.7400	.7600	.7800	.8000
85	1.740	.4500	.5560	.5750	.5900	.6100	.6260	.6450	.6600	.6800	.0960
90	1.555	.4820	.4965	.5130	.5280	.5450	.5600	.5750	.5900	.6080	.6220
100	1.305	.4050	.4170	.4300	.4440	.4560	.4700	.4830	.4950	.5090	.5220
110	1.155	.3580	.3690	.3810	.3930	.4050	.4150	.4280	.4380	.4500	.4620
120	1.065	.3300	.3410	.3510	.3630	.3725	.3840	.3940	.4050	.4150	.4260
130	1.015	.3150	.3240	.3355	.3450	.3560	.3660	.3760	.3860	.3960	.4060
140	1.000	.3100	.3200	.3300	.3405	.3500	.3600	.3700	.3800	.3900	.4000
150	1.015	.3150	.3240	.3355	.3450	.3560	.3660	.3760	.3860	.3960	.4060
160	1.065	.3300	.3410	.3510	.3630	.3725	.3840	.3940	.4050	.4150	.4260
170	1.155	.3580	.3690	.3810	.3930	.4050	.4150	.4280	.4380	.4500	.4620
180	1.305	.4050	.4170	.4300	.4440	.4560	.4700	.4830	.4950	.5090	.5220

Table A-4(cont'd)

θ deg	F	$t_{2\theta} = \rho\bar{\sigma}_3(2+k)/3 \times F$ where $F = 1/\sin(\theta - \alpha) \times \frac{1}{a_\theta}$									
		k= 2.1	2.2	2.3	2.4	2.5	2.6	2.7	2.8	2.9	
0	1.305	.5350	.5500	.5610	.5730	.5890	.6000	.6150	.6250	.6380	
10	1.555	.6380	.6530	.6680	.6830	.7000	.7160	.7310	.7450	.7600	
20	2.000	.8200	.8400	.8600	.8800	.9000	.9200	.9400	.9600	.9800	
80	2.000	.8200	.8400	.8600	.8800	.9000	.9200	.9400	.9600	.9800	
85	1.740	.7130	.7310	.7500	.7650	.7830	.8020	.8170	.8330	.8540	
90	1.555	.6370	.6520	.6680	.6820	.7000	.7150	.7300	.7450	.7600	
100	1.305	.5350	.5500	.5610	.5730	.5890	.6000	.6150	.6250	.6380	
110	1.155	.4750	.4850	.4960	.5085	.5200	.5310	.5435	.5540	.5650	
120	1.065	.4360	.4470	.4600	.4680	.4800	.4900	.5010	.5100	.5220	
130	1.015	.4165	.4260	.4360	.4470	.4560	.4670	.4770	.4850	.4980	
140	1.000	.4100	.4200	.4300	.4400	.4500	.4600	.4700	.4800	.4900	
150	1.010	.4165	.4260	.4360	.4470	.4560	.4670	.4770	.4850	.4980	
160	1.065	.4360	.4470	.4600	.4680	.4800	.4900	.5010	.5100	.5220	
170	1.155	.4750	.4850	.4965	.5085	.5200	.5310	.5435	.5540	.5650	
180	1.305	.5350	.5500	.5610	.5730	.5890	.6000	.6150	.6250	.6380	

Table A-5 Frictional Resistance against Displacement $t_{2\theta}$ $\rho = 0.4$

θ deg	F	$t_{2\theta} = \rho \bar{\sigma}_3 (2+k)/3 \times F$ where $F = 1/\sin(\theta - \alpha) \times \frac{1}{a_\theta}$									
		k= 1.1	1.2	1.3	1.4	1.5	1.6	1.7	1.8	1.9	2.0
0	1.305	.5400	.5560	.5740	.5920	.6090	.6260	.6400	.6600	.6780	.6960
10	1.555	.6430	.6630	.6840	.7040	.7260	.7440	.7680	.7980	.8100	.8300
20	2.000	.8280	.8520	.8800	.9080	.9320	.9600	.9860	1.013	1.040	1.068
80	2.000	.8280	.8520	.8800	.9080	.9320	.9600	.9860	1.013	1.040	1.068
85	1.740	.7200	.7420	.7660	.7880	.8120	.8360	.8600	.8800	.9060	.9300
90	1.555	.6430	.6630	.6840	.7040	.7260	.7460	.7680	.7980	.8100	.8300
100	1.305	.5400	.5560	.5740	.5920	.6090	.6260	.6440	.6600	.6780	.6960
110	1.155	.4780	.4520	.5080	.5240	.5400	.5540	.5700	.5840	.6000	.6160
120	1.065	.4400	.4540	.4680	.4840	.4970	.5120	.5260	.5400	.5540	.5680
130	1.015	.4200	.4320	.4470	.4600	.4740	.4880	.5010	.5140	.5280	.5420
140	1.005	.4130	.4260	.4400	.4540	.4670	.4800	.4940	.5060	.5200	.5340
150	1.015	.4200	.4320	.4470	.4600	.4740	.4880	.5010	.5140	.5280	.5420
160	1.065	.4400	.4540	.4680	.4840	.4970	.5120	.5260	.5400	.5540	.5680
170	1.155	.4770	.4930	.5085	.5240	.5390	.5550	.5700	.5850	.6000	.6150
180	1.305	.5400	.5560	.5740	.5920	.6090	.6260	.6440	.6600	.6780	.6960

Table A-5(cont'd)

θ deg	F	$t_{2\theta} = \rho\bar{\sigma}_3(2+k)/3 \times F$ where $F = 1/\sin(\theta - \alpha) \times \frac{1}{a_\theta}$									
		k= 2.1	2.2	2.3	2.4	2.5	2.6	2.7	2.8	2.9	
0	1.305	.7140	.7320	.7480	.7640	.7840	.8000	.8200	.8340	.8500	
10	1.550	.8500	.8700	.8900	.9100	.9320	.9540	.9740	.9930	1.014	
20	2.000	1.094	1.120	1.148	1.174	1.200	1.228	1.254	1.280	1.308	
80	2.000	"	"	"	"	"	"	"	"	"	
85	1.740	.9500	.9760	1.000	1.020	1.040	1.070	1.090	1.110	1.138	
90	1.555	0.85	.8700	.8900	.9100	.9320	.9540	.9740	.9930	1.015	
100	1.305	0.714	.7320	.7480	.7640	.7840	.8000	.8200	.8340	.8500	
110	1.155	.6320	.6480	.6620	.6770	.6920	.7080	.7240	.7380	.7540	
120	1.065	.5830	.5960	.6120	.6240	.6390	.6540	.6680	.6800	.6960	
130	1.015	.5550	.5680	.5820	.5960	.6080	.6230	.6360	.6480	.6640	
140	1.000	.5470	.5600	.5740	.5860	.6000	.6140	.6270	.6400	.6530	
150	1.015	.5550	.5680	.5820	.5960	.6080	.6230	.6360	.6480	.6640	
160	1.065	.5820	.6950	.6120	.62440	.6390	.6540	.6680	.6800	.6960	
170	1.155	.6300	.6460	.6620	.6780	.6930	.7090	.7240	.7400	.7550	
180	1.305	.7140	.7320	.7480	.7640	.7840	.8000	.8200	.8340	.8500	

Table A-6 Frictional Resistance against Displacement $t_{2\theta}$ $\rho = 0.5$

θ deg	F	$t_{2\theta} = \rho \overline{\sigma}_3 (2+k)/3 \times F$ where $F = 1/\sin(\theta - \alpha) \times \frac{1}{a_\theta}$									
		k= 1.1	1.2	1.3	1.4	1.5	1.6	1.7	1.8	1.9	2.0
0	1.305	.6750	.6950	.7180	.7400	.7610	.7840	.8050	.8250	.8470	.8700
10	1.555	.8040	.8290	.8550	.8800	.9075	.9320	.9600	.9850	1.012	1.038
20	2.000	1.035	1.0650	1.1000	1.1350	1.1650	1.2000	1.2300	1.2660	1.3000	1.335
80	2.000	"	"	"	"	"	"	"	"	"	"
85	1.740	.9000	.9280	.9570	.9850	1.0150	1.0450	1.075	1.1000	1.1300	1.162
100	1.305	.6750	.6950	.7180	.7400	.7610	.7840	.8050	.8250	.8470	.8700
110	1.155	.5970	.6150	.6350	.6550	.6750	.6930	.7130	.7300	.7500	.7700
120	1.065	.5500	.5680	.5850	.6050	.6210	.6400	.6580	.6750	.6930	.7100
130	1.015	.5250	.5400	.5590	.5750	.5930	.6100	.6250	.6420	.6600	.6780
140	1.000	.5160	.5320	.5500	.5680	.5840	.6000	.6180	.6320	.6500	.6680
150	1.0150	.5250	.5400	.5590	.5750	.5930	.6100	.6250	.6420	.6600	.6780
160	1.065	.5500	.5680	.5850	.6050	.6210	.6400	.6580	.6750	.6930	.7100
170	1.155	.5970	.6150	.6350	.6550	.6750	.6930	.7130	.7300	.7500	.7700
180	1.305	.6750	.6950	.7180	.7400	.7610	.7840	.8050	.8250	.8470	.8700

Table A-6(cont'd)

θ deg	F	$t_{2\theta} = \rho \overline{\sigma}_3 (2+k)/3 \times F$ where $F = 1/\sin(\theta - \alpha) \times \frac{1}{a_\theta}$									
		k= 2.1	2.2	2.3	2.4	2.5	2.6	2.7	2.8	2.9	
0	1.305	.8920	.9150	.9350	.9550	.9800	1.000	1.025	1.042	1.062	
10	1.555	1.0620	1.0880	1.1120	1.1380	1.1640	1.190	1.218	1.242	1.270	
20	2.000	1.3670	1.400	1.4350	1.470	1.5000	1.5350	1.5700	1.600	1.635	
80	2.000	"	"	"	"	"	"	"	"	"	
85	1.740	1.188	1.220	1.250	1.275	1.305	1.340	1.360	1.388	1.420	
100	1.305	.8920	.9150	.9350	.9550	.9800	1.000	1.025	1.042	1.062	
110	1.155	.7900	.8100	.8280	.8460	.8650	.8850	.9050	.9220	.9430	
120	1.065	.7270	.7450	.7650	.7800	.8000	.8180	.8350	.8500	.8700	
130	1.015	.6940	.7100	.7280	.7450	.7600	.7790	.7950	.8100	.8300	
140	1.000	.6840	.7000	.7180	.7320	.7500	.7680	.7840	.8000	.8160	
150	1.015	.6940	.7100	.7280	.7450	.7600	.7790	.7950	.8100	.8300	
160	1.065	.7270	.7450	.7650	.7800	.8000	.8180	.8350	.8500	.8700	
170	1.155	.7900	.8100	.8280	.8460	.8650	.8850	.9050	.9220	.9430	
180	1.305	.8920	.9150	.9350	.9550	.9800	1.0000	1.0250	1.0420	1.0620	

Table A-6(cont'd)

θ deg	F	$t_{2\theta} = \rho\bar{\sigma}_3(2+k)/3 \times F$ where $F = 1/\sin(\theta - \alpha) \times \frac{1}{a_\theta}$									
		k= 3.0	3.1	3.2	3.3	3.4	3.5	3.6	3.7	3.8	4.0
0	1.305	1.090	1.107	1.130	1.152	1.174	1.198	1.218	1.240	1.260	1.305
10	1.555	1.295	1.320	1.348	1.372	1.400	1.427	1.450	1.475	1.502	1.555
20	2.000	1.667	1.700	1.730	1.768	1.800	1.835	1.867	1.900	1.930	2.000
80	2.000	"	"	"	"	"	"	"	"	"	"
85	1.740	1.450	1.478	1.510	1.540	1.565	1.596	1.623	1.650	1.680	1.740
100	1.305	1.088	1.107	1.130	1.152	1.174	1.198	1.218	1.240	1.260	1.305
110	1.155	.9615	.9800	1.000	1.020	1.040	1.060	1.078	1.095	1.115	1.155
120	1.065	.887	.9050	.9230	.9400	.9580	.9760	.9930	1.010	1.030	1.065
130	1.015	.8450	.8600	.8800	.8950	.9140	.9300	.9450	.9640	.9800	1.015
140	1.000	.8340	.8500	.8660	.8840	.9000	.9170	.9330	.9500	.9660	1.000
150	1.015	.8450	.8600	.8800	.8950	.9140	.9300	.9450	.9640	.9800	1.015
160	1.065	.8870	.9050	.9230	.9400	.9580	.9760	.9930	1.0100	1.030	1.065
170	1.155	.9615	.9800	1.000	1.0200	1.040	1.060	1.0780	1.095	1.115	1.155
180	1.305	1.088	1.107	1.130	1.152	1.174	1.198	1.218	1.240	1.260	1.305

Table A-7(a) Adhesional Resistance against Sliding $t_{3\theta}$

θ(degrees)	sin 2θ	$t_{3\theta}$ in $c_a \times 1/a_\theta$
10	0.342	2.88
20	0.642	1.53
30	0.865	1.14
40	0.985	1.00
50	0.985	1.00
60	0.865	1.14
70	0.642	1.53
80	0.342	2.88
85	0.174	5.66

Table A-7(b) Adhesional Resist. against Displacement $t_{4\theta}$

θ deg.	$1/\sin(\theta - \alpha)$	$t_{4\theta}$ in $c_a \times 1/a_\theta$ ρ_m=2	ρ_m=3	ρ_m=4	ρ_m=5
0	1.305	2.61	3.915	5.22	6.53
10	1.555	3.11	4.665	6.22	7.77
85	1.740	3.48	5.220	6.96	8.70
90	1.555	3.11	4.665	6.22	7.70
100	1.305	2.61	3.915	5.22	6.53
110	1.155	2.31	3.465	4.62	5.77
120	1.065	2.13	3.195	4.26	5.33
130	1.015	2.03	3.045	4.06	5.07
140	1.000	2.00	3.000	4.00	5.00
150	1.015	2.03	3.045	4.06	5.07
160	1.065	?.13	3.195	4.26	5.33
170	1.155	2.31	3.465	4.62	5.77
180	1.305	2.61	3.915	5.22	6.53

APPENDIX II

BEHAVIOR OF THE PARTICLE MODEL

A. Symbols

A. Symbols

Stress	All stresses applied to the matrix are expressed in terms of k, the effective principal stress ratio.
Matrix Failure	That state of stress at which every point on the failure plane satisfies the condition of maximum obliquity.
$\underline{n}$	Number of contacts within a soil area A_α along an α-plane.
M	Range in θ (degrees) in which contact failure occurs under k.
n_m	Number of contact failure in M
τ_α	Applied shear stress along α-plane (failure plane) in force per gross area of soil
stress-factor	A magnification factor on τ_α resulting from redistribution of displaced contacts.

APPENDIX II

BEHAVIOR OF THE PARTICLE MODEL

B. Procedure of Computations of Stress-displacement characteristics according to the modes of:

(a) Partial Remolding

(b) Complete Remolding

(c) Partial Re-orientation

(d) Complete Re-orientation

(a) Partial Remolding.

For simplicity, the distribution of particles is assumed to be uniform throughout the entire range of $\theta = 0^\circ - 180^\circ$ as shown in Fig. A-1-A.

We have accordingly

the distribution function $y = \frac{1}{\pi} \times n = 0.318\ n$

No. of contacts in sliding $= \frac{85-10}{180}\ n = 0.43\ n$

No. of contacts in displacement

$$= \frac{(10-0) + (180-85)}{180}\ n = 0.57\ n$$

All values of τ_α are computed by the expression

$\tau_\alpha \quad = \quad \bar{\sigma}_3 \frac{(k-1)}{2} \sin 2\alpha \times$ stress-factor

$t_\alpha \qquad$ (force per unit contact area) $= \tau_\alpha \quad \times \frac{1}{a_\theta}$

1) k = 1.3

$= 0.1475\ \bar{\ }_3 \qquad t\ = 0.1475\ \bar{\ }_3 \times \frac{1}{a}$

From Fig. A-1-B-1, M = 28-68

$$n_m = \frac{(68-28)}{(85-10)} \times 0.43\ n = 0.235\ n$$

By definition, 0.235 n contacts carry no additional shear stress. Thus, at the end of k = 1.3,

stress-factor = 1/(1-0.235) = 1.31

All the remaining 0.765 n contacts are in the range of

= 10-28 and 68-85 in the sliding group

and = 0-10 and 85-180 in the displacement group

Fig. A-1-B-2 shows the range of contact failure for k = 1.3.

2) k = 1.4

$= 1.31 \times 0.197\ \bar{\ }_3 = 0.258\ \bar{\ }_3 \qquad t\ = 0.258\ \bar{\ }_3 \times \frac{1}{a}$

From Fig. A-1-C-1, M = 16.75-79

$$n_m = \frac{(79-16.75)}{(85-10)} \times 0.43\ n = 0.36\ n$$

Thus, at the end of k = 1.4,

stress-factor = 1/(1-0.36) = 1.56

All the remaining 0.64 n contacts are in the range of

= 10-16.75 and 79-85 in the sliding group

and = 0-10 and 85-180 in the displacement group

Fig. A-1-C-2 shows the range of contact failure for k = 1.4.

3) k = 1.5

$= 1.56 \times 0.246\ \bar{\ }_3 = 0.384\ \bar{\ }_3 \qquad t\ = 0.384\ \bar{\ }_3 \times \frac{1}{a}$

From Fig. A-1-D-1:

In sliding, $M = 12.75\text{-}83$

In displacement $M = 116\text{-}164$

In sliding, $$n_m = \frac{(83-12.75)}{(85-10)} \times 0.43\, n = 0.405n$$

In displacement, $$n_m = \frac{(164-116)}{(10-0) + (180-85)} \times 0.57n = 0.264n$$

Total $n_m = (0.405 + 0.264)\, n = 0.669\, n$

0.699 n contacts carry no additional shear stress. Thus, at the end of k = 1.5,

stress-factor = 1/(1-0.699) = 3.02

All the remaining 0.331 n contacts are in the range of

= 10-12.75 and 83-85 in the sliding group

and = 0-10, 85-116 and 164-180 in the displacement group.

Fig. A-1-D-2 shows the range of contact failure for k = 1.5.

<u>4) k = 1.6</u>

$= 3.02 \times 0.295\, \bar{}_3 = 0.89\, \bar{}_3 \qquad t = 0.89\, \bar{}_3 \times \frac{1}{a}$

From the spectrum of resistance for k = 1.6, M = 0-180. This implies that all contacts have failed and the matrix has reached failure.

<u>(b) Complete Remolding</u>

The initial particle distribution is assumed to follow the same uniform distribution that was used in (a). It is shown in Fig. A-2-A. Accordingly, we have as before:

In Sliding, no. of contacts = 0.43 n, y = 0.328 n

In displacement, no. of contacts = 0.57 n, y = 0.3[illegible] n.

All values of are again computed by the expression

$$= \bar{\sigma}_3 \frac{(k-1)}{2} \times \sin 2 \times \text{stress-factor}$$

$$t = \times \frac{1}{a} \text{ in force per unit contact area.}$$

<u>1) k = 1.3</u>

$$= 0.1475 \, \bar{\sigma}_3 \qquad t = 0.1475 \, \bar{\sigma}_3 \times \frac{1}{a}$$

From Fig. A-2-B-1, M = 28-68

$$n_m = \frac{(68-28)}{(85-10)} \times 0.43 \, n = 0.235 \, n$$

By definition, 0.235 n contacts transfer all of their share of shear stress to the remaining 0.765 n contacts. Thus,

the first stress-factor = 1/(1-0.235) = 1.31.

The first redistribution $t = 1.31 \times 0.1475 \, \bar{\sigma}_3 \times \frac{A}{n \, A_c} = 0.193 \, \bar{\sigma}_3 \times \frac{1}{a}$

From Fig. A-2-B-1, M = 21-75

$$n_m = \frac{(75-21)}{(85-10)} \times 0.43 \, n = 0.315 \, n$$

0.315 n contacts again transfer all of their share of shear stress to the other contacts. Thus,

the second stress-factor = 1/(1-0.315) = 1.46

The second redistribution $t = 1.46 \times 0.1475 \, \bar{\sigma}_3 \times \frac{A}{n \, A_c}$

$$= 0.2155 \, \bar{\sigma}_3 \times \frac{1}{a}$$

From Fig. A-2-B-1 M = 19-76.8

$$n_m = \frac{(76.8-19)}{(85-10)} \times 0.43 \, n = 0.336 \, n$$

The successive transfer of shear stress due to contact failure is continued until the additional stress to be carried by the remaining contacts is negligible.

Thus, at the end of k = 1.3

the final stress-factor = 1/(1-0.344) = 1.52.

All the remaining 0.656 n contacts are in the range of

= 10-13.25 and 77.5-85 in the sliding group

and = 0-10 and 85-180 in the displacement group.

Fig. A-2-B-2 shows the successive range of contact failure for k = 1.3.

2) k = 1.4

$= 1.52 \times 0.197\ \bar{\ }_3 = 0.30\ \bar{\ }_3 \quad t \quad = 0.30\ \bar{\ }_3 \times \frac{1}{a}$

From Fig. A-2-C-1, M = 14.6-81

$$n_m = \frac{(81-14.6)}{(85-10)} \times 0.43\ n = 0.384\ n$$

0.384 n contacts transfer all of their share of shear stress to the remaining 0.616 n contacts. Thus,

the first stress-factor = 1/(1-0.384) = 1.620

The first redistribution $= 1.620 \times 0.197\ \bar{\ }_3 = 0.319\ \bar{\ }_3$

From Fig. A-2-C-1, M = 14-81.5

$$n_m = \frac{(81.5-14)}{(85-10)} \times 0.43\ n = 0.389\ n$$

The final stress-factor = 1/(1-0.389) = 1.635

Thus, at the end of k = 1.4, all the remaining 0.611 n contacts are in the range of = 10-14 and 81.5-85 in the sliding group

and = 0-10 and 85-180 in the displacement group

Fig. A-2-C-2 shows the gross range of contact failure for k = 1.4.

3) k = 1.5

$= 1.635 \times 0.246\ \bar{\ }_3 = 0.4025\ \bar{\ }_3 \quad t \quad = 0.4025\ \bar{\ }_3 \times \frac{1}{a}$

From Fig. A-2-D-1:

In sliding, $M = 12.4\text{-}82.8$

In displacement $M = 111\text{-}170$

In sliding $n_m = \frac{(82.4-12.4)}{(85-10)} \times 0.43\ n = 0.405\ n$

In displacement, $n_m = \frac{(170-111)}{(10-0) + (180-85)} \times 0.57\ n = 0.326\ n$

Total $n_m = (0.405 + 0.326)\ n = 0.731\ n$

0.731 n contacts transfer all of their share of shear stress to the remaining 0.269 n contacts. Thus,

the first stress-factor = 1/(1-0.731) = 3.54

The first redistribution $t_\theta = 3.54 \times 0.246\ \bar{\tau}_3 \times \frac{1}{a}$

$= 0.87\ \bar{\tau}_3 \times \frac{1}{a}$

From Fig. A-2-D-2, contacts in the entire range of M = 0-180 have now failed and the matrix has reached failure.

Fig. A-2-D-2 shows the successive range of contact failure for k = 1.5.

<u>(c) Partial Re-orientation</u>

The initial particle distribution is assumed to follow the same uniform distribution that was used in (a) and (b). It is shown in Fig. A-3-A.

We have, as before:

In sliding, No. of contacts = 0.43 n, y = 0.318 n

In displacement, No. of contacts = 0.57 n, y = 0.318 n

Since the stress-factor is always unity, all values of τ_θ are given by $\bar{\tau}_3 \frac{(k-1)}{2} \sin 2\theta$ without modification.

$t_\theta = \tau_\theta \times \frac{1}{a}$ (in force per contact area)

1) k = 1.3

$$\tau_{m} = 0.1475\ \bar{\sigma}_3 \qquad t_{m} = 0.1475\ \bar{\sigma}_3 \times \frac{1}{a_{m}}$$

From Fig. A-3-B-1, M = 28-68

$$n_m = \frac{(68-28)}{(85-10)} \times 0.43\ n = 0.235\ n$$

By definition, 0.235 n contacts redistribute themselves over the range of θ = 10-28 and 68-85 in the sliding group. Thus at the end of k = 1.3, we have:

0.43 n contacts in θ = 10-28 and 68-85 in the sliding group

0.57 n contacts in θ = 0-10, and 85-180 in the displace. group.

Assuming a uniform redistribution with respect to θ,

$$y \times (28-10 + 85-68) = 75 \times 0.328\ n$$

or $\quad$ y = 0.702 n in θ = 10-28 and 68-85 in sliding

y = 0.311 n in θ = 0-10 and 85-180 in displace.

Fig. A-3-B-2 shows the range of contact failure for k = 1.3.

2) k = 1.4

$$\tau_{m} = 0.197\ \bar{\sigma}_3 \qquad t_{m} = 0.197\ \bar{\sigma}_3 \times \frac{1}{a_{m}}$$

From Fig. A-3-C-1, M = 21.5-28 and 68-74.5

$$n_m = \frac{(28-21.5) + (74.5-68)}{(28-10) + (85-68)} \times 0.43\ n = 0.16\ n$$

Total n_m = (0.235 + 0.16) n = 0.395 n

0.16 n contacts redistribute themselves over the range of θ = 10-21.5 and 74.5-85 in the sliding group.

Thus, at the end of k = 1.4, we have

0.43 n contacts in θ = 10-21.5 and 74.5-85 in the sliding and 0.57 n contacts in θ = 0-10 and 85-180 in the displace.

Assuming a uniform redistribution with respect to θ

$$y \times (21.5-10 + 85-74.5) = 75 \times 0.328\ n$$

or $\quad y = 1.17\ n$ in θ = 10-21.5 and 74.5-85 in sliding

$y = 0.311\ n$ in θ = 0-10 and 85-180 in displacement

Fig. A-3-C-2 shows the range of contact failure for $k = 1.4$.

<u>3) k = 1.9</u>

At the end of $k = 1.8$, we have

0.43 n contacts in θ = 10-13.6 and 82-85 in sliding

and 0.57 n contacts in θ = 0-10 and 85-125 and 154-180 in displacement.

Assuming a uniform redistribution with respect to θ

$$y \times (13.6-10 + 85-82) = 75 \times 0.328\ n$$

or $\quad y = 3.82\ n$ in θ = 10-13.6 and 82-85 in sliding

$$y \times (10-0 + 125-85 + 180-154) = 105 \times 0.311$$

or $\quad y = 0.43\ n$ in θ = 0-10, 85-125 and 154-180 in displacement

Total n_m at the end of $k = 1.8$ is $1.1088\ n$

For $k = 1.9$, $\tau = 0.443\ \bar{\sigma}_3 \quad t = 0.443\ \bar{\sigma}_3 \times \frac{1}{a}$

From Fig. A-3-D-1:

In sliding, $\quad$ M = 13-13.6 and 82-83

In displacement $\quad$ M = 110-125 and 154-169

$$\text{In sliding} \quad n_m = \frac{(13.6-13) + (83-82)}{(13-10) + (85-82)} \times 0.43\ n = 0.1042\ n$$

In displacement,

$$n_m = \frac{(125-110) + (169-154)}{(10-0) + (125-85) + (180-154)} \times 0.57\ n = 0.225\ n$$

Total n_m at $k = 1.9$ equals $(0.1042+0.225)n$ or $0.3293\ n$.

Total n_m = (1.1088 + 0.3293)n = 1.438 n

In the sliding group, 0.1042 n contacts redistribute themselves over the range of = 10-13 and 83-85.

In the displacement group, 0.225 n contacts redistribute themselves over the range of = 0-10, 85-110 and 169-180.

We have, at the end of k = 1.9,

0.43 n contacts in = 10-13 and 83-85 in sliding

and 0.57 n contacts in = 0-10, 85-110 and 169-180 in displace.

Assuming a uniform redistribution with respect to ,

y x (13-10 + 85-83) = 75 x 0.328

or y = 4.91 n in = 10-13 and 83-85 in sliding

y x (10-0 + 110-85 + 180-169) = 105 x 0.311

or y = 0.711 n in = 0-10, 85-110 and 169-180 in displace.

Fig. A-3-D-2 shows the range of contact failure for k = 1.9.

<u>4) k = 2.4</u>

At the end of k = 2.3, we have

0.43 n contacts in = 10.25-10.8 in sliding

0.57 n contacts in = 7-10, 85-93 in displacement

Assuming a uniform redistribution with respect to ,

y x (10.8-10.25) = 75 x 0.328 n

or y = 43.6 n in = 10-10.25 in sliding

y x (10-7 + 193-85) = 105 x 0.311 n

or y = 2.97 n in = 7-10 and 85-93 in displacement.

Total n_m at end of k = 2.3 equals 2.9647 n.

For k = 2.4, $= 0.69\,\bar{\ }_3$ t $= 0.69\,\bar{\ }_3 \times \frac{1}{a}$

From Fig. A-3-E-1:

In sliding, $M = 10.25\text{-}10.8$

In displacement, $M = 7\text{-}10$ and $90\text{-}93$.

In sliding, $n_m = \frac{(10.8-10.25)}{(10.8-10.25)} \times 0.43\ n = 0.43\ n$

In displacement $n_m = \frac{(10-7)\ +\ (93-90)}{(10-7)\ +\ (93-85)} \times 0.57\ n = 0.311\ n$

Total n_m at $k = 2.4$ equals $(0.43 + 0.311)\ n$ or $0.741\ n$

Total $n_m = (2.9647 + 0.741)\ n = 3.7057\ n$

Thus, the entire sliding group is now exhausted.

0.741 n contacts redistribute themselves over the range of = 85-90 in the displacement group. We have, at the end of $k = 2.4$, $1 \times n$ contacts in = 85-90.

Assuming a uniform redistribution with respect to ,

$y \times (90-85) = 180 \times 0.318\ n,$

or $y = 36 \times 0.318\ n$ or $11.45\ n$ in = 85-90

Fig. A-3-E-2 shows the range of contact failure for $k = 2.4$.

<u>5) k = 2.5</u>

$= 0.738\ \overline{}_3 \qquad t \ = 0.738\ \overline{}_3 \times \frac{1}{a}$

From Fig. A-3-F-1, $M = 88\text{-}90$

$$n_m = \frac{(90-88)}{(90-85)} \times n = 0.4\ n$$

0.4 n contacts redistribute themselves over the range of = 85-88. Thus, at the end of $k = 2.5$, we have

$1 \times n$ contacts in = 85-88.

Assuming a uniform redistribution with respect to ,

$y \times (88-85) = 180 \times 0.318\ n$

or $y = 19.1\ n$ in = 85-88.

Fig. A-3-F-1 shows the range of contact failure for $k = 2.5$.

The computations are carried out in the same manner for $k = 2.6$ and 2.7. At $k = 2.7$, all contacts are exhausted and the matrix has reached failure.

(d) Complete Re-orientation

The initial particle distribution is assumed to follow a uniform distribution throughout the entire range of $\theta = 0\text{-}180^{\circ}$ as shown in Fig. A-4-A. We have, accordingly

$$y = \frac{1}{\pi} \times n = 0.318\ n$$

$$\text{Initial no. of contacts in sliding} = \frac{85-10}{180} n = 0.4165\ n$$

$$\text{Initial no. of contacts in displacement} = \frac{(10-0)+(180-85)}{180} \times n$$

$$= 0.5835\ n$$

Since the stress-factor is always unity, all values of τ_θ are given by $\bar{\sigma}_3 \frac{(k-1)}{2} \sin 2\theta$ without modification

$$t_\theta \text{ (in force per unit contact area)} = \tau_\theta \times \frac{1}{a_\theta}$$

1) $k = 1.3$

$$\tau_\theta = 0.1475\ \bar{\sigma}_3 \qquad t_\theta = 0.1475\ \bar{\sigma}_3 \times \frac{1}{a_\theta}$$

From Fig. A-4-B-1, $M = 28\text{-}68$

$$n_m = \frac{68-28}{180} \times n = 0.222\ n$$

By definition, $0.222\ n$ contacts redistribute themselves over the range of $\theta = 0\text{-}28$ and $68\text{-}180$. Thus, at the end of $k = 1.3$, we have $1 \times n$ contacts in $\theta = 0\text{-}28$ and $68\text{-}180$.

Assuming a uniform redistribution with respect to θ,

$y \times (28\text{-}0 + 180\text{-}68) = 180 \times 0.318\ n$

or $y = 0.41\ n$ over the range of θ = 0-28 and 68-180.

Fig. A-4-B-2 shows the range of contact failure for k = 1.3.

<u>2) k = 1.4</u>

$\tau_\theta = 0.197\ \bar{\sigma}_3 \qquad t_\theta = 0.197\ \bar{\sigma}_3 \times \frac{1}{a_\theta}$

From Fig. A-4-C-1, M = 21.5-68 and 68-74.5

$$n_m = \frac{(28-21.5)+(74.5-68)}{(28-0) + (180-68)} \times n = 0.093\ n$$

$$\text{Total} \quad n_m = ().222 + 0.093)\ n = 0.315\ n$$

0.093 n contacts redistribute themselves over the range of θ = 0-21.5 and 74.5-180. Thus, at the end of k = 1.4 we have 1 x n contacts in θ = 0-21.5 and 74.5=180.

Assuming a uniform redistribution with respect to θ,

$y \times (21.5\text{-}0 + 180\text{-}74.5) = 180 \times 0.318\ n$

or $y = 0.451\ n$ over the range of θ = 0-21.5 and 74.5=180

Fig. A-4-C-2 shows the range of contact failure for k = 1.4.

<u>3) k = 1.9</u>

At the end of k = 1.8, we have

1 x n contacts in θ = 0-13.6, 82-125 and 154-180.

Assuming a uniform redistribution with respect to θ,

$y \times (13.6\text{-}0 + 125\text{-}82 + 180\text{-}154) = 180 \times 0.318\ n$

or $y = 0.693\ n$ over θ = 0-13.6, 82-125 and 154-180

Total $n_m = 0.699\ n$

For k = 1.9, $\tau_{\theta} = 0.443\ \bar{\tau}_3$ $\quad t_{\theta} = 0.443\ \bar{\tau}_3 \times \frac{1}{a_{\theta}}$

From Fig. A-4-D-1:

In sliding, M = 13-13.6 and 82-83

In displacement, M = 110-125 and 154-169

$$\text{In sliding, } n_m = \frac{(13.6-13)+(83-82)}{(13.6-0)+(125-82)+(180-154)} \times n = 0.0194n$$

$$\text{In displacement, } n_m = \frac{(125-110)+(169-154)}{(13.6-0)+(125-82)+(180-154)} \times n = 0.363\ n$$

Total n_m at k = 1.9 equals (0.019 + 0.363)n or 0.3824 n

Total n_m = (0.699 + 0.3824) n = 1.08 n

0.3824 n contacts redistribute themselves over the range of θ = 0-13, 83-110 and 169-180. Thus, at the end of k = 1.9, we have 1 x n contacts in θ = 0-13, 83-110 and 169-180.

Assuming a uniform redistribution with respect to θ,

y x (13-0 + 110-83 + 180-169) = 180 x 0.318 n

or y = 1.12 n in θ = 0-13, 83-110 and 169-180.

Fig. A-4-D-2 shows the range of contact failure for k = 1.9.

4) k = 2.4

At the end of k = 2.3, we have

1 x n contacts in θ = 10.25-10.8, 7-10 and 85-93.

Assuming a uniform redistribution with respect to θ,

y x (10.8-10.25 + 10-7 + 93-85) = 180 x 0.318 n

or y = 4.9 n in θ = 10.25-10.8, 7-10 and 85-93

Total n_m = 2.231 n

For k = 2.4, $\tau_{\theta} = 0.69\ \bar{\tau}_3$ $\quad t_{\theta} = 0.69\ \bar{\tau}_3 \times \frac{1}{a_{\theta}}$

From Fig. A-4-E-1:

In sliding, $M = 10.25\text{-}10.8$

In displacement $M = 7\text{-}10$ and $90\text{-}93$

In sliding, $n_m = \dfrac{(10.8-10.25)}{(10.8-10.25)+(10-7)+(93-85)} \times n = 0.048\ n$

In displacement,

$$n_m = \frac{(10-7)+(93-90)}{(10.8-10.25)+(10-7)+(93-85)} \times n = 0.52\ n$$

Total n_m at $k = 2.4$ equals $(0.048+0.52)\ n$ or $0.568\ n$

Total $n_m = (2.231 + 0.568)\ n = 2.799\ n$

0.568 n contacts redistribute themselves over the range of $\theta = 85\text{-}90$. Thus, at the end of $k = 2.4$, we have $1 \times n$ contacts in $\theta = 85\text{-}90$

Assuming a uniform redistribution with respect to θ,

$y \times (90-80) = 180 \times 0.318\ n$

or $y = 36 \times 0.318\ n = 11.45\ n$

Fig. A-4-E-2 shows the range of contact failure for $k = 2.4$.

<u>5) k = 2.5</u>

$\sigma = 0.738\ \bar{\sigma}_3 \qquad t = 0.738\ \bar{\sigma}_3 \times \frac{1}{a}$

From Fig. A-4-F-1, $M = 88\text{-}90$

$$n_m = \frac{(90-88)}{(90-85)} \times n = 0.4\ n$$

$$\text{Total } n_m = (2.799 + 0.4)\ n = 3.199\ n$$

0.4 n contacts redistribute themselves over the range of $\theta = 85\text{-}88$. Thus, at the end of $k = 2.5$, we have $1 \times n$ contacts in $\theta = 85\text{-}88$

Assuming a uniform redistribution with respect to θ,

$$y \times (88-85) = 180 \times 0.318\ n$$

or $$y = 19.1\ n$$

Fig. A-4-F-1 shows the range of contact failure for $k = 2.5$.

The computations are carried out in the same manner for $k = 2.6$ and $k = 2.7$. At $k = 2.7$, the matrix has reached failure.

APPENDIX II

BEHAVIOR OF THE PARTICLE MODEL

C. Illustrations

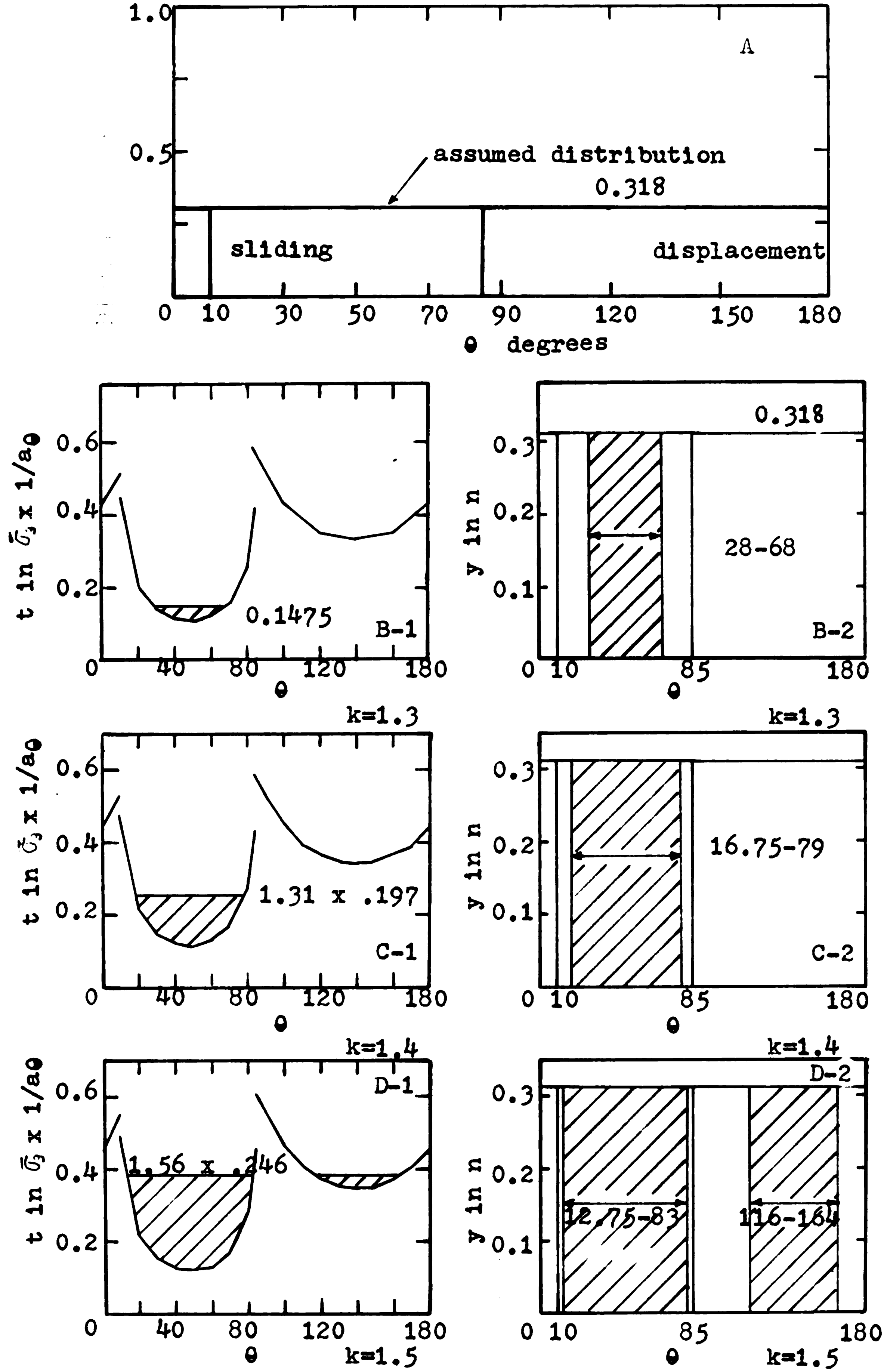

Fig. A-1 Partial Remolding

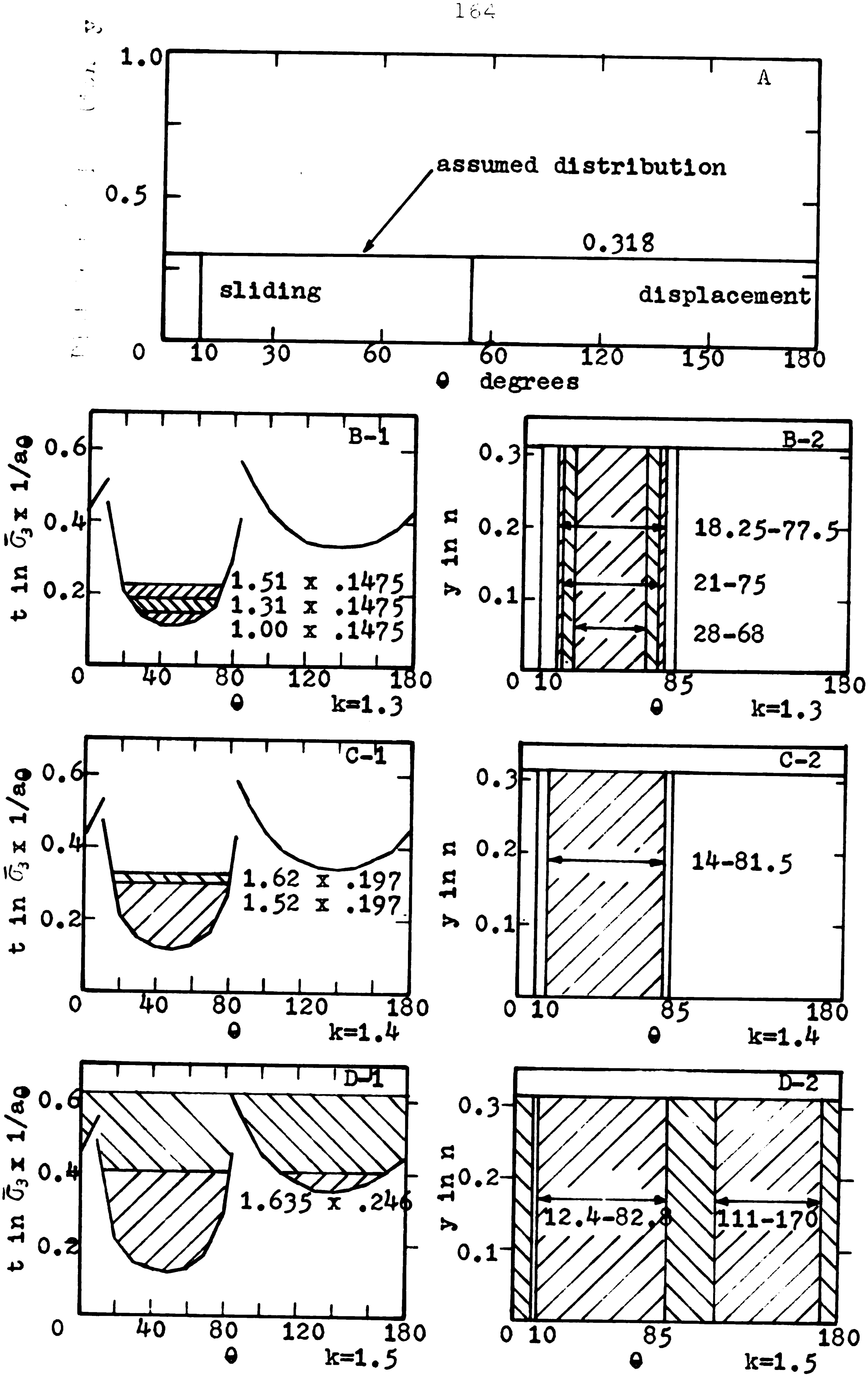

Fig. A-2 (b) Complete Remolding

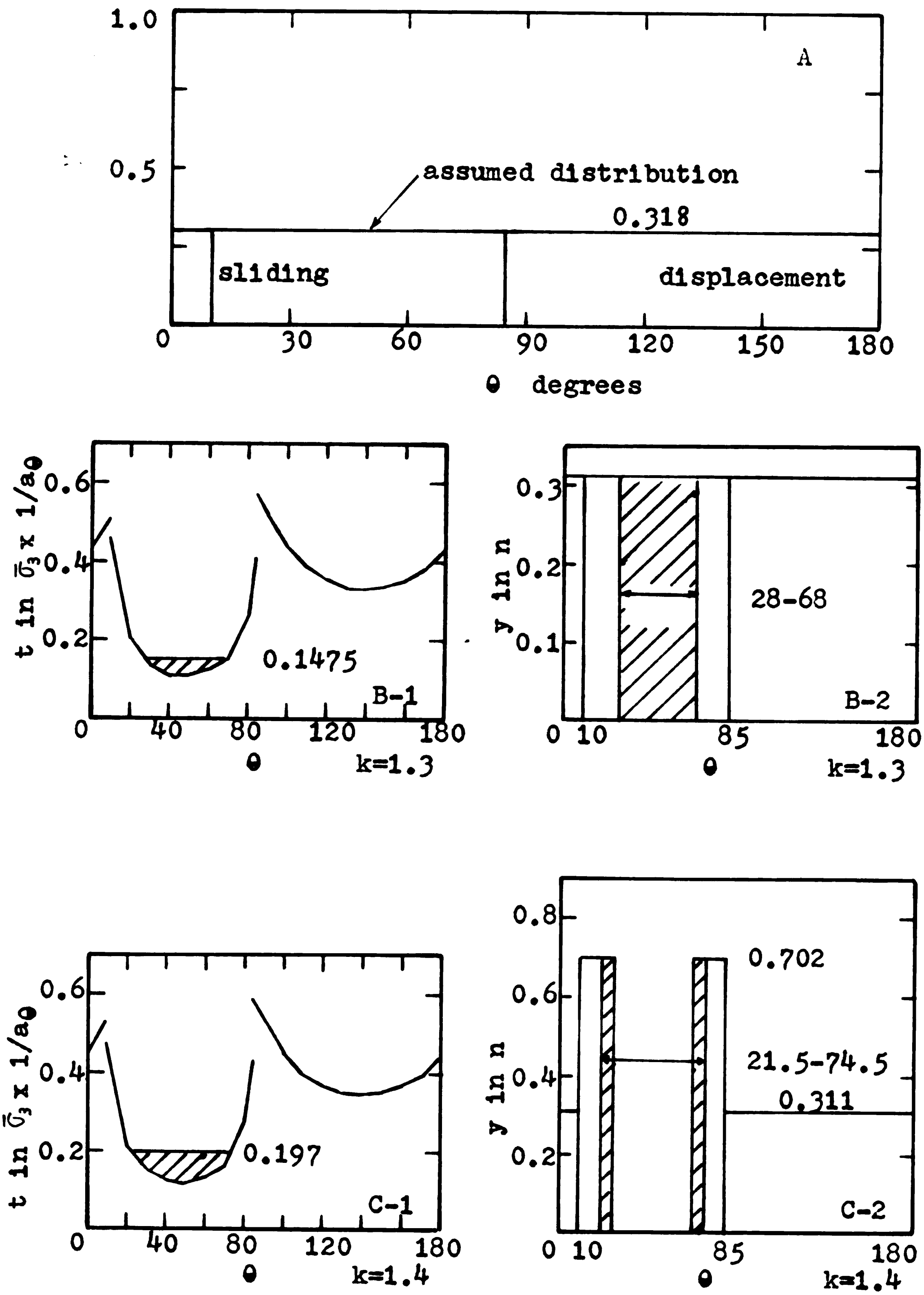

Fig. A-3 (c) Partial Re-orientation

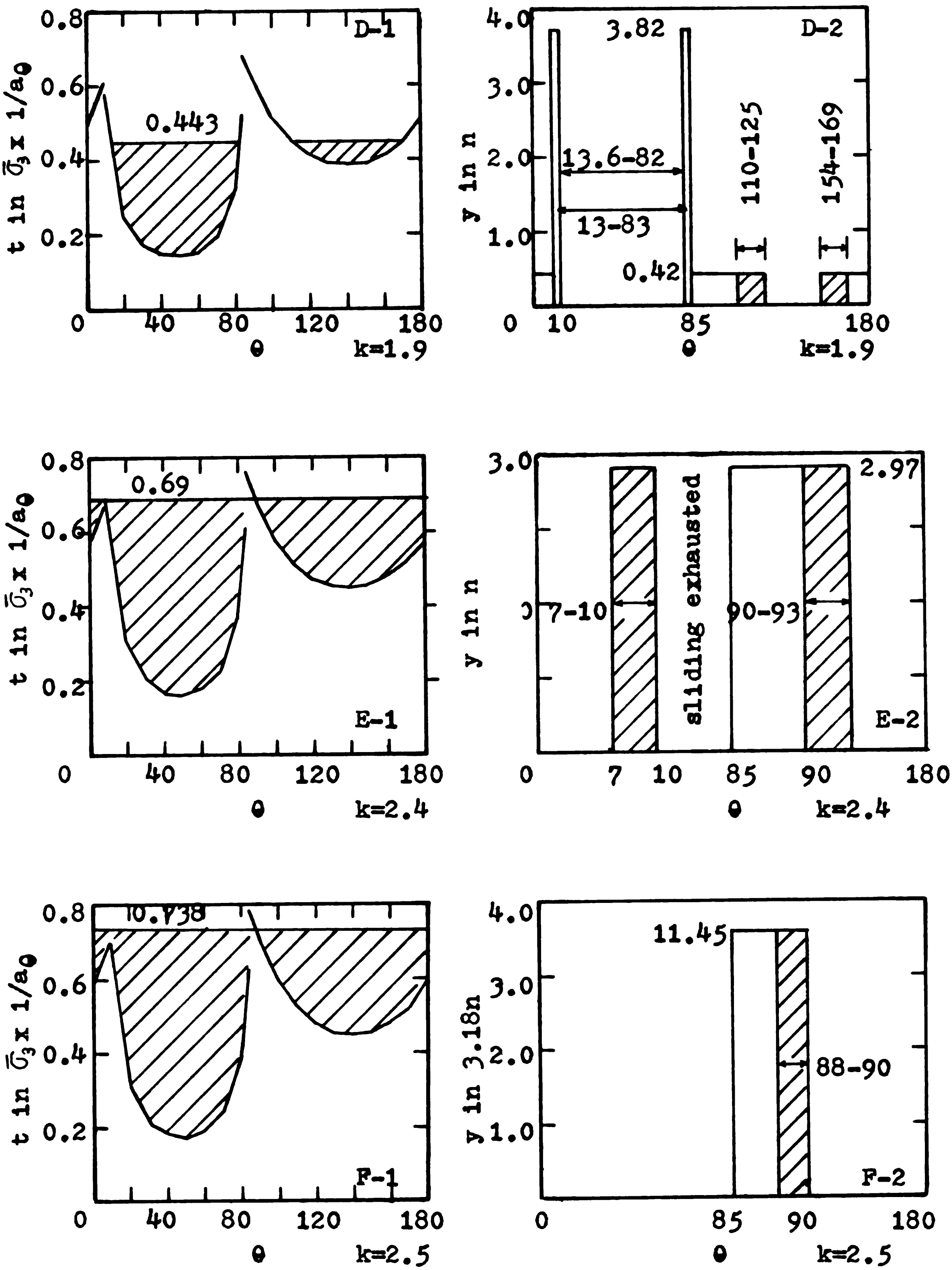
D-1
0.443
t ln $\bar{\sigma}_3$ x 1/a$_\theta$
θ
k=1.9
D-2
3.82
13.6-82
13-83
0.42
110-125
154-169
y ln n
k=1.9
E-1
0.69
k=2.4
E-2
2.97
7-10
sliding exhausted
90-93
k=2.4
F-1
0.738
k=2.5
F-2
11.45
88-90
y ln 3.18n
k=2.5

Fig. A-3(cont'd)

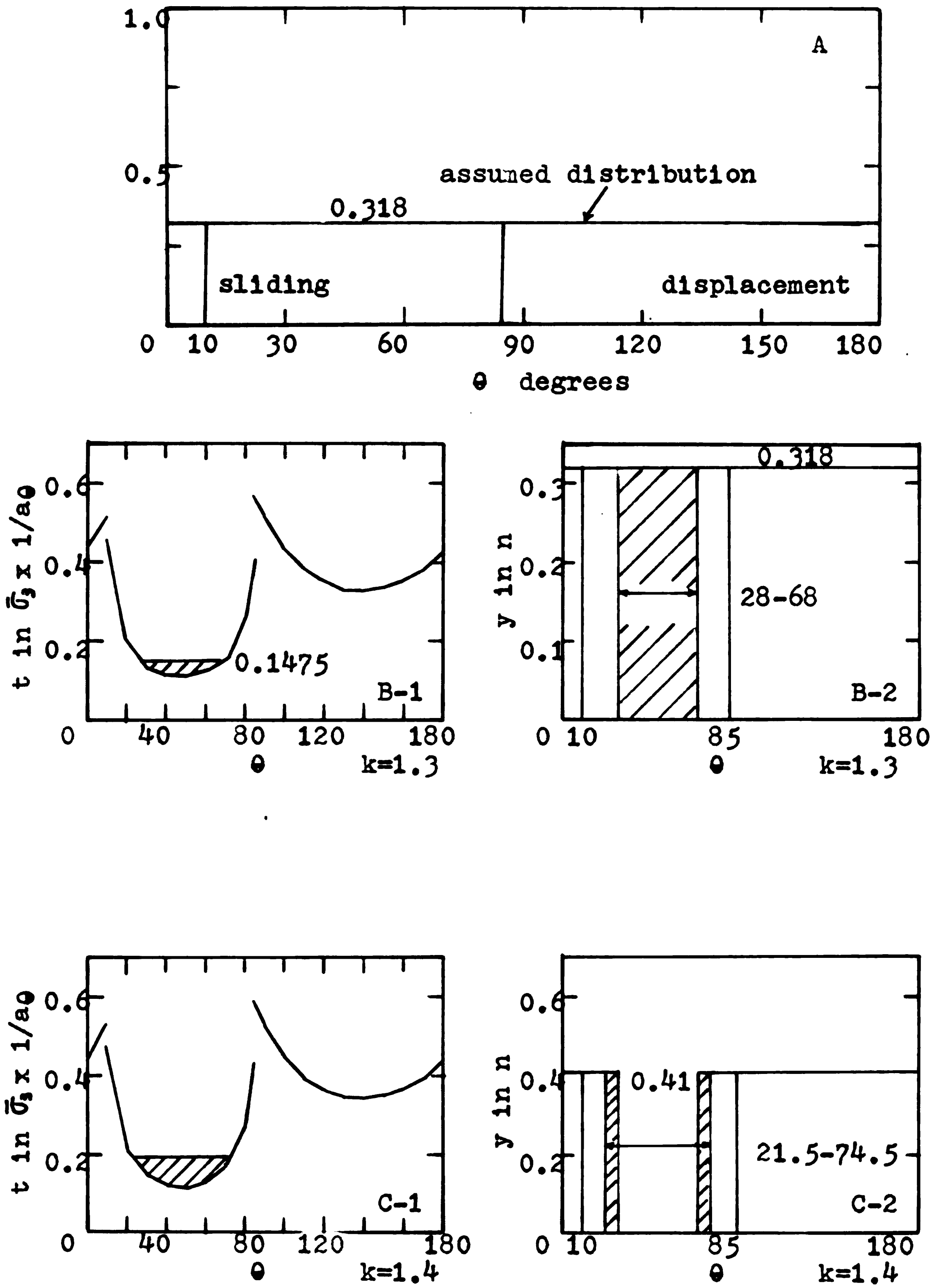

Fig. A-4 (d) Complete Re-orientation

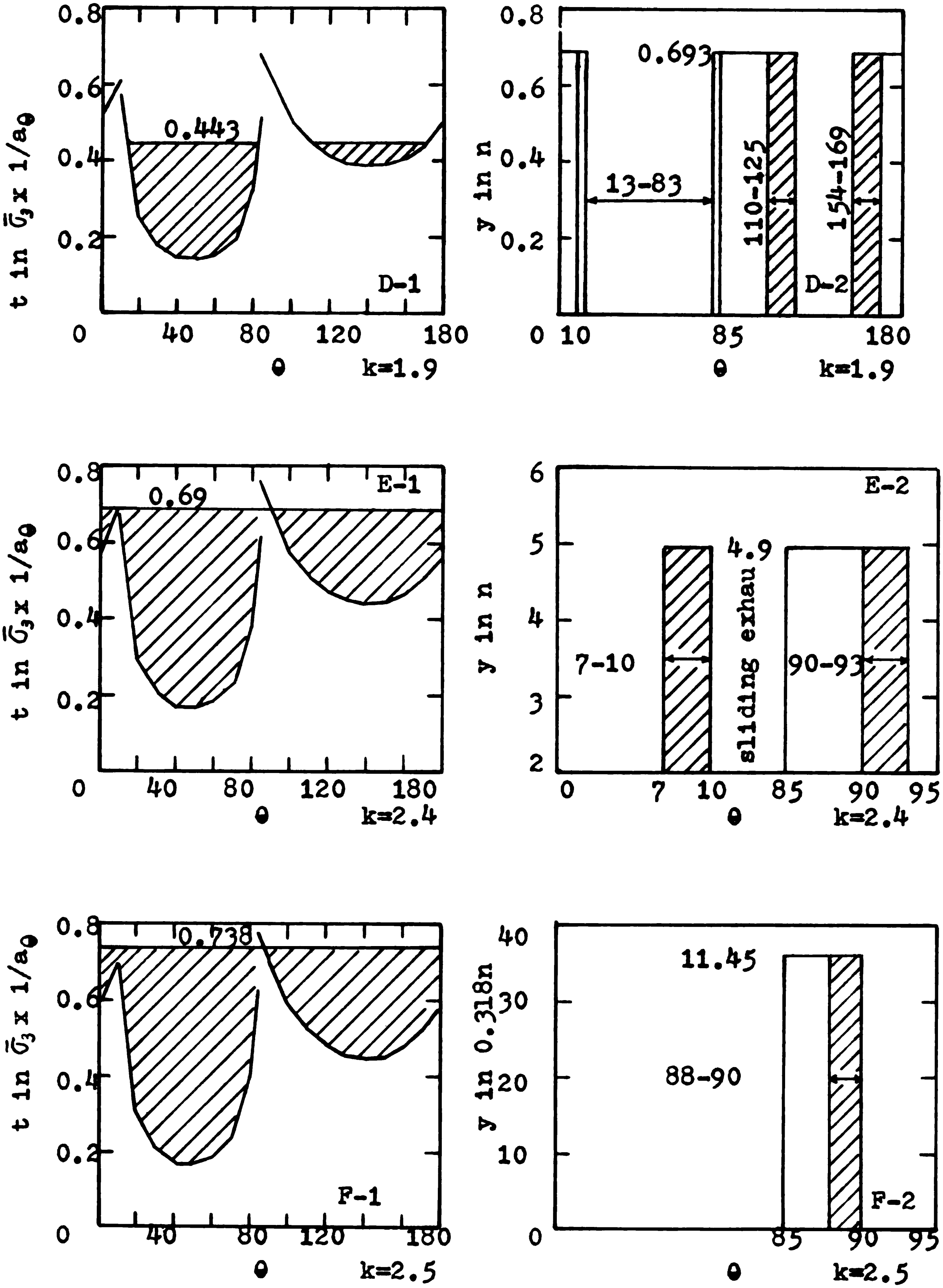
0.8
0.6
0.4
0.2
0
t ln $\bar{\sigma}_3$ x 1/a$_\theta$
0.443
D-1
40
80
120
180
θ
k=1.9
y ln n
0.693
13-83
110-125
154-169
D-2
10
85
180
θ
k=1.9
0.69
E-1
0.2
E-2
6
5
4
3
2
4.9
sliding exhau
7-10
90-93
0
7
10
85
90
95
θ
k=2.4
0.738
F-1
40
30
20
10
y ln 0.318n
11.45
88-90
F-2
θ
k=2.5

Fig. A-4(cont'd)

APPENDIX II

BEHAVIOR OF THE PARTICLE MODEL

D. Results of Computations

Table A-8(a) Behavior of Particle Model

(a) Partial Remolding $\rho = 0.3$

k	$\frac{\tau_\alpha}{\bar{\sigma}_3}$	Sliding $t_{1\theta}$		Displacement $t_{2\theta}$		$\frac{\Sigma n_m}{n}$	Stress-factor
		M deg.	$\frac{n_m}{n}$	M deg.	$\frac{n_m}{n}$		
1.1	0.0493	-	0	-	0	0	1.00
1.2	0.0985	-	0	-	0	0	1.00
1.3	0.1475	28-68	.235	-	0	0.235	1.31
1.4	0.2580	16.75-79	.360	-	0	0.360	1.56
1.5	0.384	12.75-83	.405	116-164	.264	0.669	3.02
1.6	0.890	all	.430	all	.570	1.000	

Table A-8(b) Behavior of Particle Model

(b) Complete Remolding $\rho = 0.3$

k	$\frac{\tau_\alpha}{\bar{\sigma}_a}$	Sliding $t_{1\theta}$ M deg.	Sliding $t_{1\theta}$ $\frac{n_m}{n}$	Displacement $t_{2\theta}$ M deg.	Displacement $t_{2\theta}$ $\frac{n_m}{n}$	$\frac{\Sigma n_m}{n}$	Stress-factor
1.1	0.0493	-	0	-	0	0	1.00
1.2	0.0985	-	0	-	0	0	1.00
1.3	0.1475	28-68	.235	-	0	0.235	1.31
	0.1930	21-75	.315	-	0	0.315	1.46
	0.2155	19-76.8	.336	-	0	0.336	1.49
	0.2200	18.5-77	.339	-	0	0.339	1.51
	0.2230	18.25-77	.334	-	0	0.344	1.52
1.4	0.3000	14.6-81	.384	-	0	0.384	1.62
	0.3190	14.0-81	.389	-	0	0.389	1.64
1.5	0.4025	12.4-82.8	.405	111-170	.326	0.731	5.92
	1.4600	all	.430	all	.570	1.000	

Table A-8(c) Behavior of Particle Model

(c) Partial Re-orientation $\rho = 0.3$

k	$\frac{\tau_\alpha}{\bar{\sigma}_3}$	Sliding $t_{1\theta}$ M deg.	Sliding $t_{1\theta}$ $\frac{n_m}{n}$	Displacement $t_{2\theta}$ M deg.	Displacement $t_{2\theta}$ $\frac{n_m}{n}$	$\frac{\sum n_m}{n}$	Stress-factor
1.2	0.0985	-	0	-	0	0	1.00
1.3	0.1475	28 - 68	.235	-	0	0	1.00
1.4	0.1970	21.5-28 68 - 74.5	.160	-	0	0.395	1.00
1.5	0.2460	18.3-21.5 74.5-77.5	.121	-	0	0.516	1.00
1.6	0.2950	14.8-18.3 77.5-80	.165	-	0	0.681	1.00
1.7	0.3450	14.5-14.8 80 - 81.7	.088	-	0	0.769	1.00
1.8	0.3940	13.6-14.5 81.8-82	.149	125-154	.191	1.109	1.00
1.9	0.4430	13 -13.6 82 - 83	.104	110-125 154-169	.225	1.438	1.00
2.0	0.4925	12.3-13 83-83.4	.129	105-110 169-175	.137	1.704	1.00
2.1	0.5410	11.5-12.3 83.8-84.5	.161	100-105 175-180	.179	2.0435	1.00
2.2	0.5900	10.8-11.5 84.5-85	.258	0-1.0 1.0-4.0 96-100	.166	.4677	1.00
2.3	0.5900	10.3-10.8	.296	4.0-7.0 93- 96	.201	2.9647	1.00
2.4	0.6900	all	.430	7.0-10.0 90-93	.3110	3.7057	1.00
2.5	0.7380		NONE	88-90	.400	4.105	1.00
2.6	0.7870		NONE	86.5-88	.500	4.605	1.00

Table A-8(d) Behavior of Particle Model

(d) Complete Re-orientation $\rho = 0.3$

k	τ_α / $\bar{\sigma}_3$	Sliding t_{10} M deg.	Sliding t_{10} n_m / n	Displacement t_{20} M deg.	Displacement t_{20} n_m / n	$\sum n_m$ / n	Stress-factor
1.3	0.1475	28 - 68	.222	-	-	0.222	1.00
1.4	0.1970	21.5-28 68-74.5	.093	-	-	0.315	1.00
1.5	0.2460	18.3-21.5 74.5-77.5	.0488	-	-	0.3638	1.00
1.6	0.2950	14.75-18 77.5-80	.0501	-	-	0.414	1.00
1.7	0.3450	14.5-14.7 80-81.75	.0174	-	-	0.432	1.00
1.8	0.3940	13.6-14.5 81.75-82	.0102	125-154	0.257	0.699	1.00
1.9	0.4430	13.-13.6 82-82	.0194	110-125 154-169	0.363	1.08	1.00
2.0	0.4925	12.3-13.0 83-83.75	.0294	105-110 169-175	0.216	1.339	1.00
2.1	0.5410	11.5-12.3 83.8-84.5	.0390	0-1 100-105 175-180	0.286	1.662	1.00
2.2	0.5900	10.8-11.5 84.5-85	.0460	1-4 96-100	0.192	1.900	1.00
2.3	0.6400	10.3-10.8	.0278	4-7 93-96	0.303	2.221	1.00
2.4	0.6900	all	.0480	7-10 90-93	0.520	2.799	1.00
2.5	0.7380		NONE	88-90	0.400	3.199	1.00
2.6	0.7870		NONE	86.5-88	0.500	3.699	1.00
2.7	0.836		NONE	all	1.000	4.699	1.00

Table A-9(a) Behavior of Particle Model

(a) Partial Remolding $\rho = 0.5$

k	$\frac{\tau_\alpha}{\bar{\sigma}_3}$	Sliding $t_{1\theta}$		Displacement $t_{2\theta}$		$\frac{\sum n_m}{n}$	Stress-factor
		M deg.	$\frac{n_m}{n}$	M deg.	$\frac{n_m}{n}$		
1.3	0.1475	28 - 68	.235	-	0	.235	1.31
1.4	0.2580	16.8-79	.360	-	0	.360	1.56
1.5	0.384	12.8-83	.405	-	0	.405	1.58
1.6	0.495	11 - 85	.425	-	0	.425	1.74
1.7	0.600	10 - 85	.430	-	0	.430	1.76
1.8	0.691	all	.430	117-163	.254	.684	3.16
1.9	1.400	all	.430	all	.570	1.000	

Table A-9(b) Behavior of Particle Model

(b) Complete Remolding $\rho = 0.5$

k	τ_d / $\bar{\sigma}_a$	Sliding $t_{1\theta}$		Displacement $t_{2\theta}$		$\sum n_m$	Stress-factor
		M deg.	n_m n	M deg.	n_m n	n	
1.3	0.1475	28 - 68	.235	-	0	.235	1.31
	0.1930	21 - 75	.315	-	0	.315	1.46
	0.2155	19-76.8	.336	-	0	.336	1.49
	0.2200	18.5-77	.339	-	0	.339	1.51
	0.2230	18.3-77.5	.344	-	0	.344	1.52
1.4	0.3000	14.6-81	.384	-	0	.384	1.62
	0.3190	14-81.5	.389	-	0	.389	1.64
1.5	0.4120	12.4-82.8	.405	-	0	.425	1.68
	0.413	12-83.8	.411	-	0	.411	1.70
	0.4185	11.9-84	.415	-	0	.415	1.71
1.6	0.5050	10.3-85	.428	-	0	.428	1.75
	0.5160	10 -85	.430	-	0	.430	1.76
1.7	0.6050	all	.430	-	0	.430	1.76
1.8	0.6910	all	.430	117-163	.254	.684	3.16
	1.2450	all	.430	all	.570	1.00	

Table A-9(c) Behavior of Particle Model

(c) Partial Re-orientation $\rho = 0.5$

k	$\frac{\tau_\alpha}{\bar{\sigma}_3}$	Sliding $t_{1\theta}$ M deg.	Sliding $t_{1\theta}$ $\frac{n_m}{n}$	Displacement $t_{2\theta}$ M deg.	Displacement $t_{2\theta}$ $\frac{n_m}{n}$	$\frac{\sum n_m}{n}$	Stress-factor
1.3	0.1475	28 - 68	.235	-	0	.235	1.00
1.4	0.1970	21.5-28 68-74.5	.160	-	0	.395	1.00
1.5	0.2460	18.3-21.5 74.5-75.5	.121	-	0	.516	1.00
1.6	0.2950	14.75-18 77.5-80	.165	-	0	.681	"
1.7	0.3450	14.5-14.7 80-81.8	.088	-	0	.7693	"
1.8	0.3940	13.6-14.5 81.8-82	.149	-	0	.9178	"
1.9	0.4430	13-13.6 82-83	.1042	-	0	1.022	"
2.0	0.4925	12.3-13 83-83.8	.129	-	0	1.151	"
2.1	0.5410	11.5-12.2 83.8-84.5	.161	-	0	1.312	"
2.2	0.5900	10.8-11.5 84.5-85	.258	-	0	1.570	"
2.3	0.6400	10.3-10.8 85	.296	-	0	1.886	"
2.4	0.6900	all	.430	-	0	2.296	"
2.5	0.7380	NONE	NONE	-	0	2..296	"
2.6	0.7870	"	"	-	0	"	"
2.7	0.8360	" "	" "	120-128 152-160	.198	2.723	"
2.8	0.8850	"	"	115-120	.154	2.877	"

Table A-9(c) -- cont'd

k	τ_α / $\bar{\sigma}_3$	Sliding $t_{1\theta}$ M deg.	Sliding $t_{1\theta}$ n_m / n	Displacement $t_{2\theta}$ M deg.	Displacement $t_{2\theta}$ n_m / n	$\sum n_m$ / n	Stress-factor
2.9	0.935	NONE	NONE	111-115	.170	3.047	1.00
3.0	0.985	"	"	108-169 169-172	.128	3.175	"
3.1	1.035	"	"	106-108 172-174	.0975	3.272	"
3.2	1.083	"	"	104-106 174-176.5	.121	3.394	"
3.3	1.132	"	"	101-104 177-179	.154	3.548	"
3.4	1.180	"	"	100-101.5 179-180	.100	3.648	"
3.5	1.231	"	"	0-1.5 98.5-100	.120	2.768	"
3.6	1.280	"	"	1.5-2.5 97.5-98.5	.091	3.859	"
3.7	1.330	"	"	2.5-4.0 97-97.5	.100	3.959	"
3.8	1.380	"	"	4.0-5.0 95.5-97	.139	4.098	"
3.9	1.430	"	"	5.0-6.0 95-95.5	.097	4.195	"
4.0	1.480	"	"	6.0-7.0 94-94	.143	4.338	"

Table A-9(d) Behavior of Particle Model

(d) Complete Re-orientation $\rho = 0.5$

k	$\frac{\tau_\alpha}{\bar{\sigma}_3}$	Sliding $t_{1\theta}$		Displacement $t_{2\theta}$		$\sum n_m$	Stress-factor
		M deg.	$\frac{n_m}{n}$	M deg.	$\frac{n_m}{n}$	n	
1.3	0.1473		.235		.000	0.024	1.0
1.4	0.1970		.093		.000	0.328	"
1.5	0.2460		.049		.000	0.377	"
1.6	0.2950		.050		.000	0.427	"
1.7	0.3450		.017		.000	0.444	"
1.8	0.3940		.010		"	0.455	"
1.9	0.4430		.010		"	0.474	"
2.0	0.4925		.029		"	0.503	"
2.1	0.5410		.039		"	0.542	"
2.2	0.5900		.046		"	0.588	"
2.3	0.6400		.028		"	0.616	"
2.4	0.6900		NONE		"	0.610	"
2.5	0.7380		"		"	0.616	"
2.6	0.7870		"		.2285	0.845	"
2.7	0.8360		"		.1980	1.043	"
2.8	0.8850		"		.154	1.197	"
2.9	0.9350		"		.170	1.367	"
3.0	0.9850		"		.128	1.495	"
3.1	1.035		"		.098	1.592	"
3.2	1.083		"		.1217	1.714	"
3.3	1.132		"		.154	1.868	"
3.4	1.180		"		.100	1.968	"
3.5	1.231		"		.120	2.088	"
3.6	1.280		"		.091	2.179	"
3.7	1.330		"		.100	1.179	"
3.8	1.380		"		.139	2.418	"
3.9	1.430		"		.097	2.515	"
4.0	1.480		"		.143	2.658	"

Table A-10 Calculation of Average Stress-Displacement Curves

Contact Displacem N	$\rho = 0.3$ k						$\rho = 0.5$ k					
n e	(a)	(b)	(c)	(d)	Curve A	Curve B	(a)	(b)	(c)	(d)	Curve A	Curve B
0.25	1.35	1.32	1.30	1.40	1.34	1.34	1.35	1.33	1.30	1.46	1.36	1.36
0.50	1.45	1.42	1.50	1.63	1.50	1.50	1.64	1.56	1.50	2.00	1.675	1.675
0.75	1.53	1.47	1.65	1.77	1.60	1.60	1.81	1.70	1.70	2.34	1.910	1.910
1.00	1.60	1.50	1.76	1.89	1.685	1.685	1.90	1.80	1.87	2.54	2.030	2.03
1.50	1.60	0.00	1.94	2.08	1.875	1.410	1.90	0.00	2.14	3.00	2.350	1.760
2.00	"	"	2.09	2.24	1.910	1.430	"	"	2.16	3.42	2.490	1.870
2.50	"	"	2.21	2.37	2.06	1.545	"	"	2.60	3.86	2.790	2.090
3.00	"	"	2.32	2.48	2.13	1.600	"	"	2.92	4.14	3.02	2.270
3.50	"	"	2.40	2.58	2.20	1.645	"	"	3.30	4.28	3.16	2.370
4.00	"	"	2.50	2.65	2.25	1.690	"	"	3.70	4.30	3.30	2.480
4.50	"	"	2.58	2.69	2.29	1.715	"	"	4.04	"	3.42	2.560
5.00	"	"	2.64	2.70	2.31	1.735	"	"	4.20	"	3.47	2.600
5.50	"	"	2.69	2.70	2.33	1.745	"	"	"	"	3.50	2.625
6.00	"	"	2.70	2.70	2.33	1.750	"	"	"	"	3.50	2.625

Curve A : N = 0 to n e, $k = \frac{(a)+(b)+(c)+(d)}{4}$

N > n e , $k = \frac{(a)+(b)+(c)+(d)}{4}$

Curve B :

$k = \frac{(a)+(b)+(c)+(d)}{4}$

at all values of N

APPENDIX III

TEST DATA

A. Figures

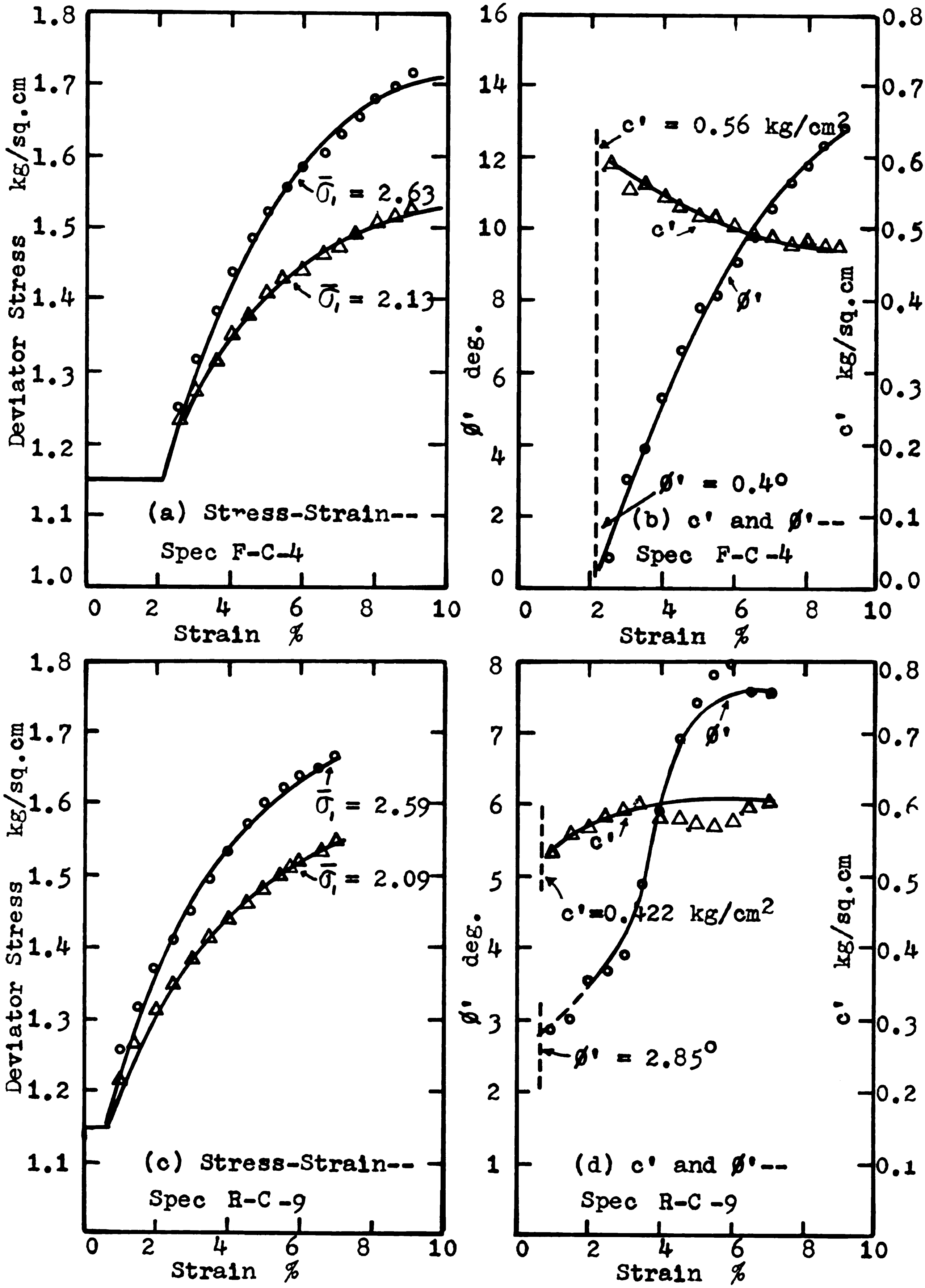

Fig. A-5 Typical Creep-CFS test data for Sault Clay

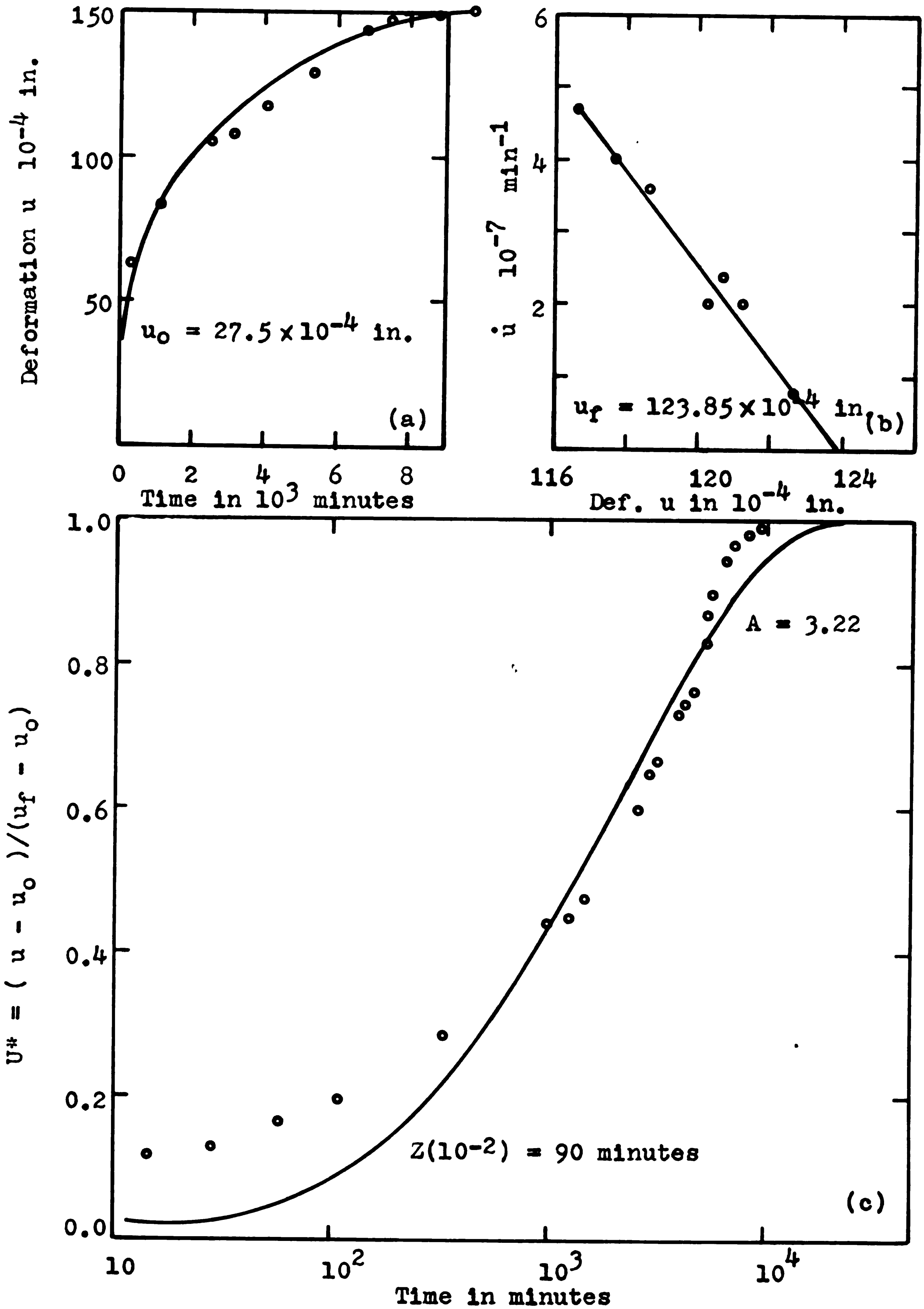

Fig. A-6 Creep Data for F-C-1-1(Spec. No.) : D = 0.0 - 0.5 kg/cm^2

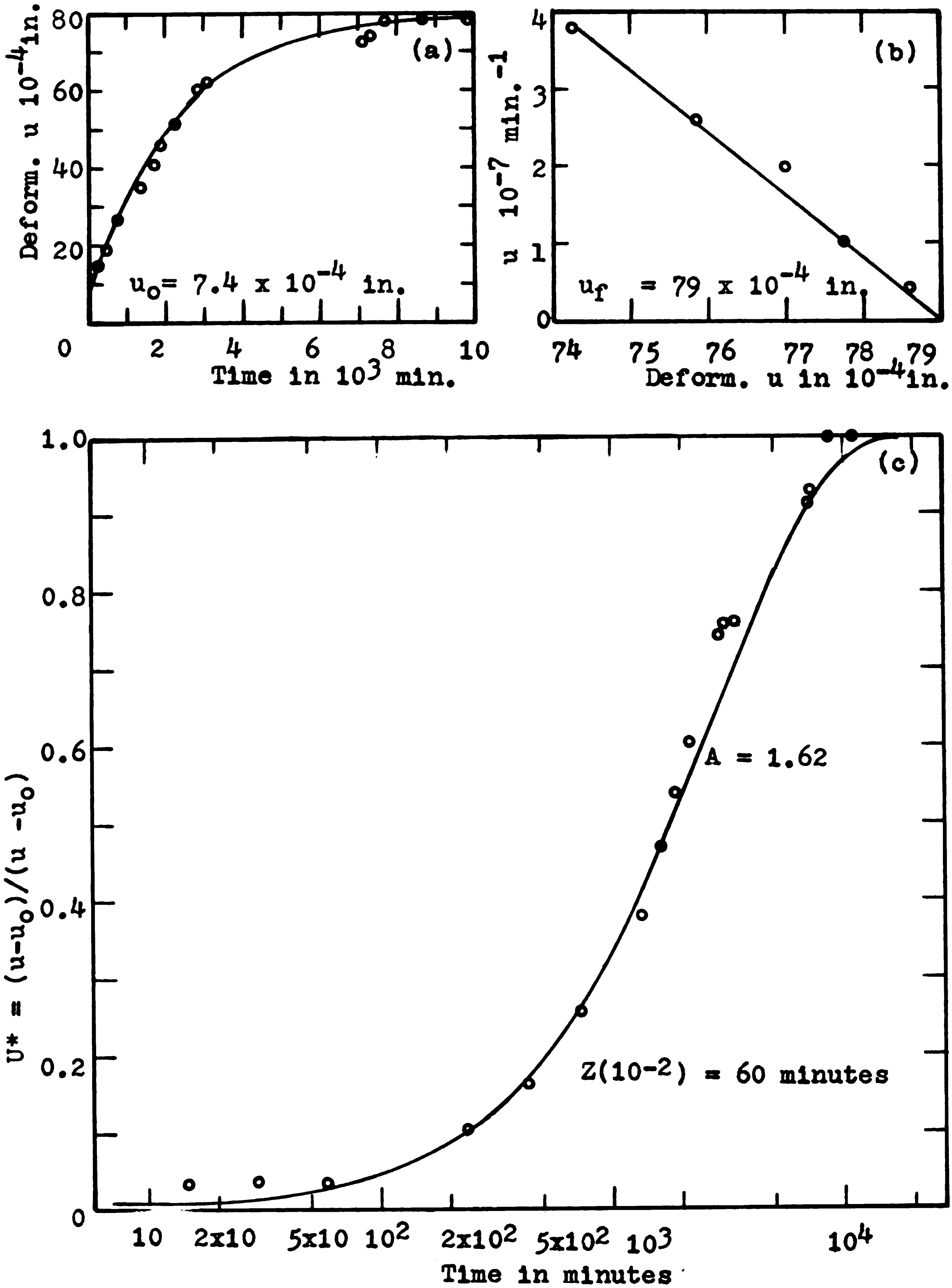

Fig. A-7 Creep Data for F-C-1-2(Spec. No.) :
D = 0.5 - 0.74 kg/cm^2

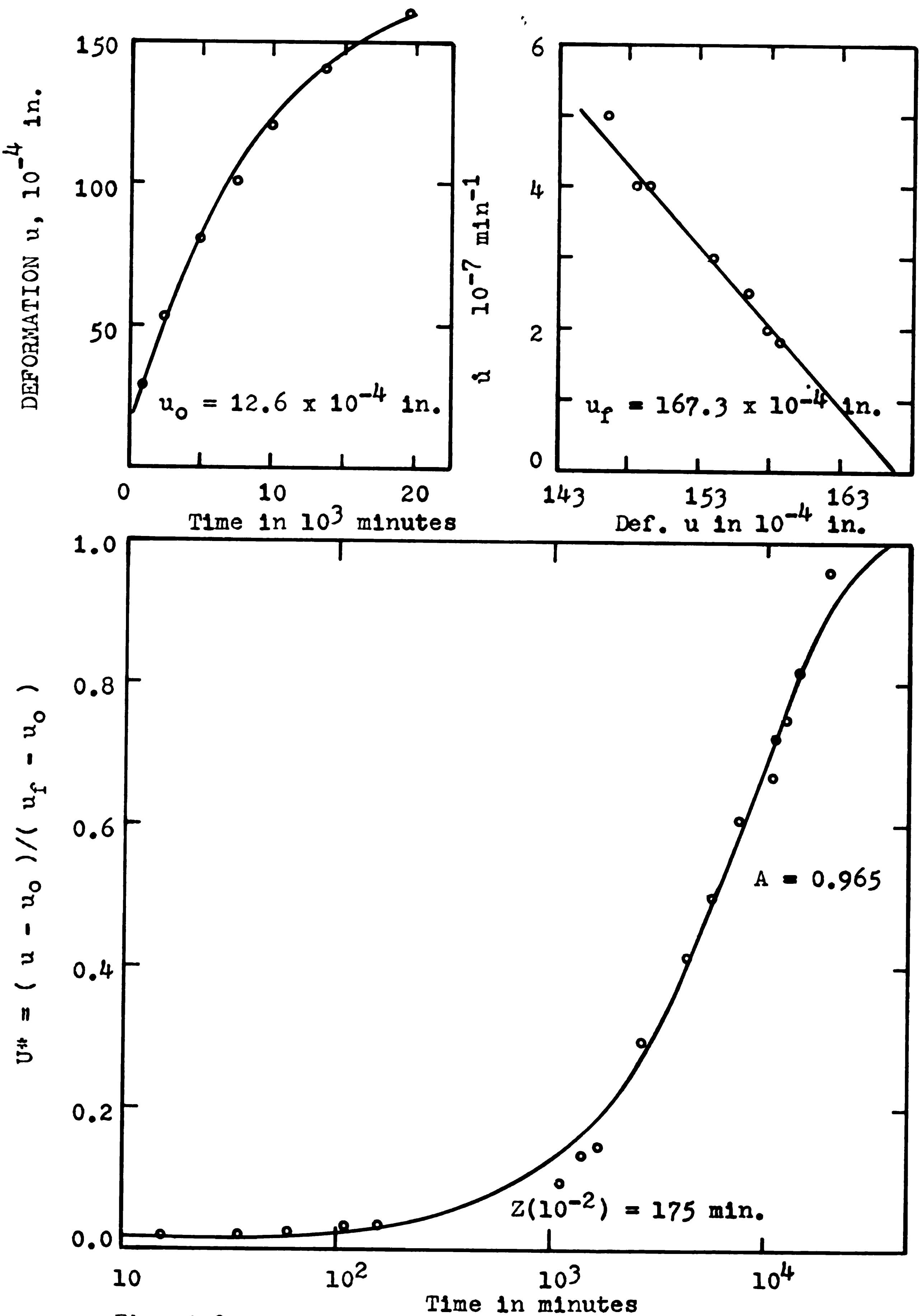

Fig. A-8 Creep Data for F-C-1-3(Spec. No.) :
D = 0.74 - 0.995 kg/cm^2

DEFORMATION u, 10^{-4} in.

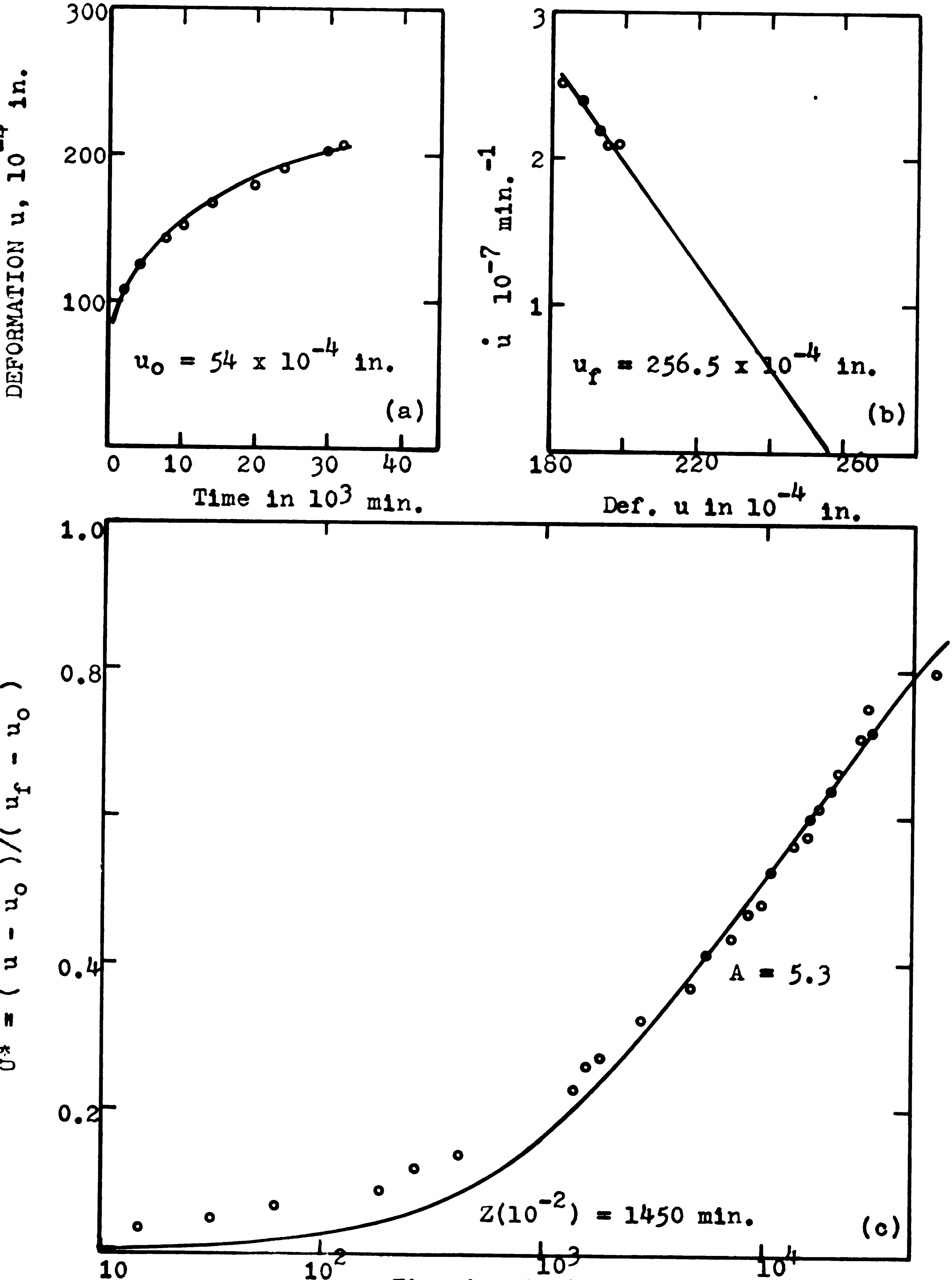

Fig. A-9 Creep Data for F-C-1-4(Spec. No.) :
$D = 0.995 - 1.24$ kg/cm^2

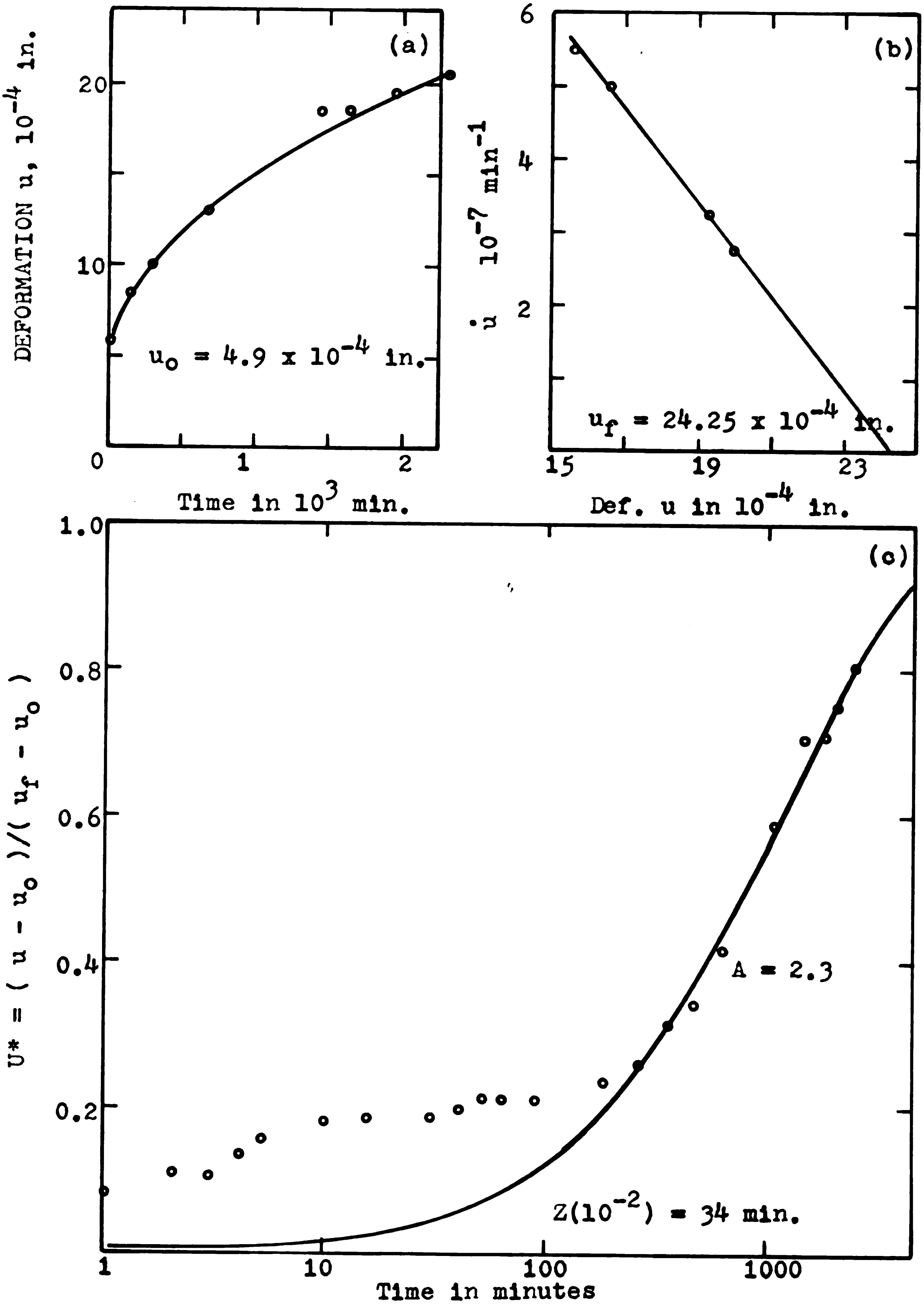

Fig. A-10 Creep data for F-OC-1-2(Spec. No.) : D = 0.495 - 0.75 kg/cm^2

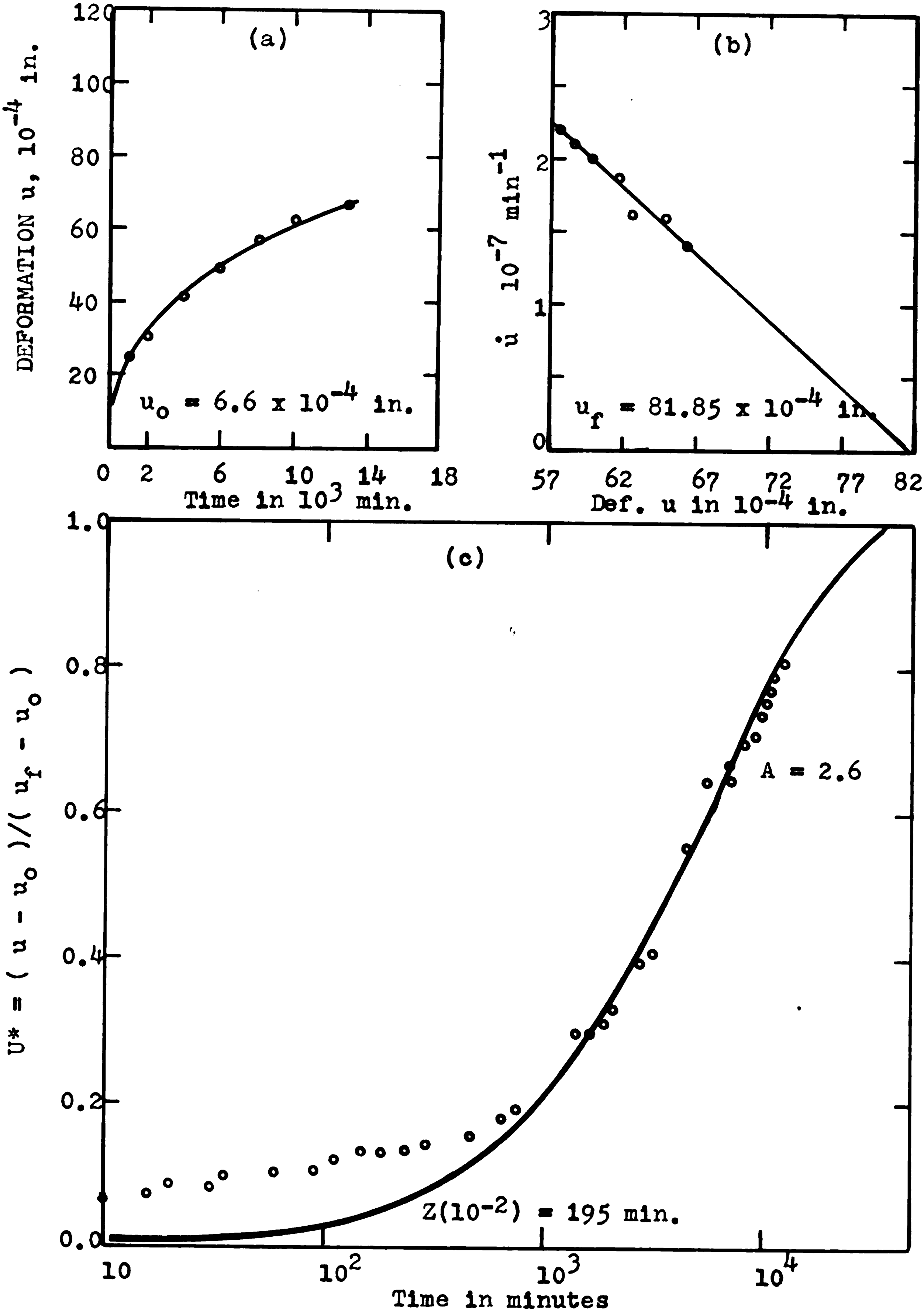

Fig. A-11 Creep Data for F-OC-1-3(Spec. No.) :
D = 0.75 - 1.06 kg/cm²

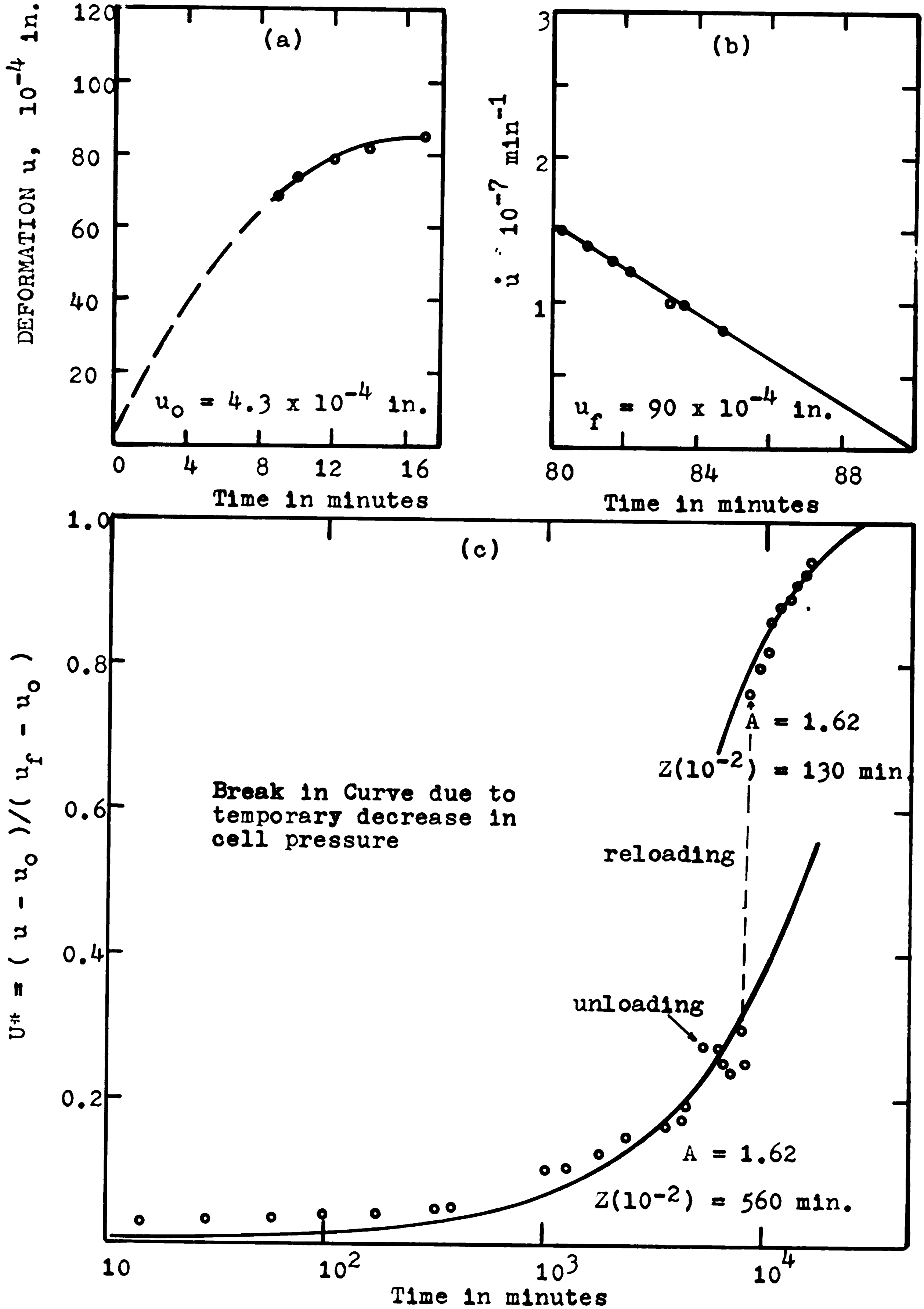

Fig. A-12 Creep Data for F-OC-1-4(Spec. No.) :
D = 1.06 - 1.255 kg/cm^2

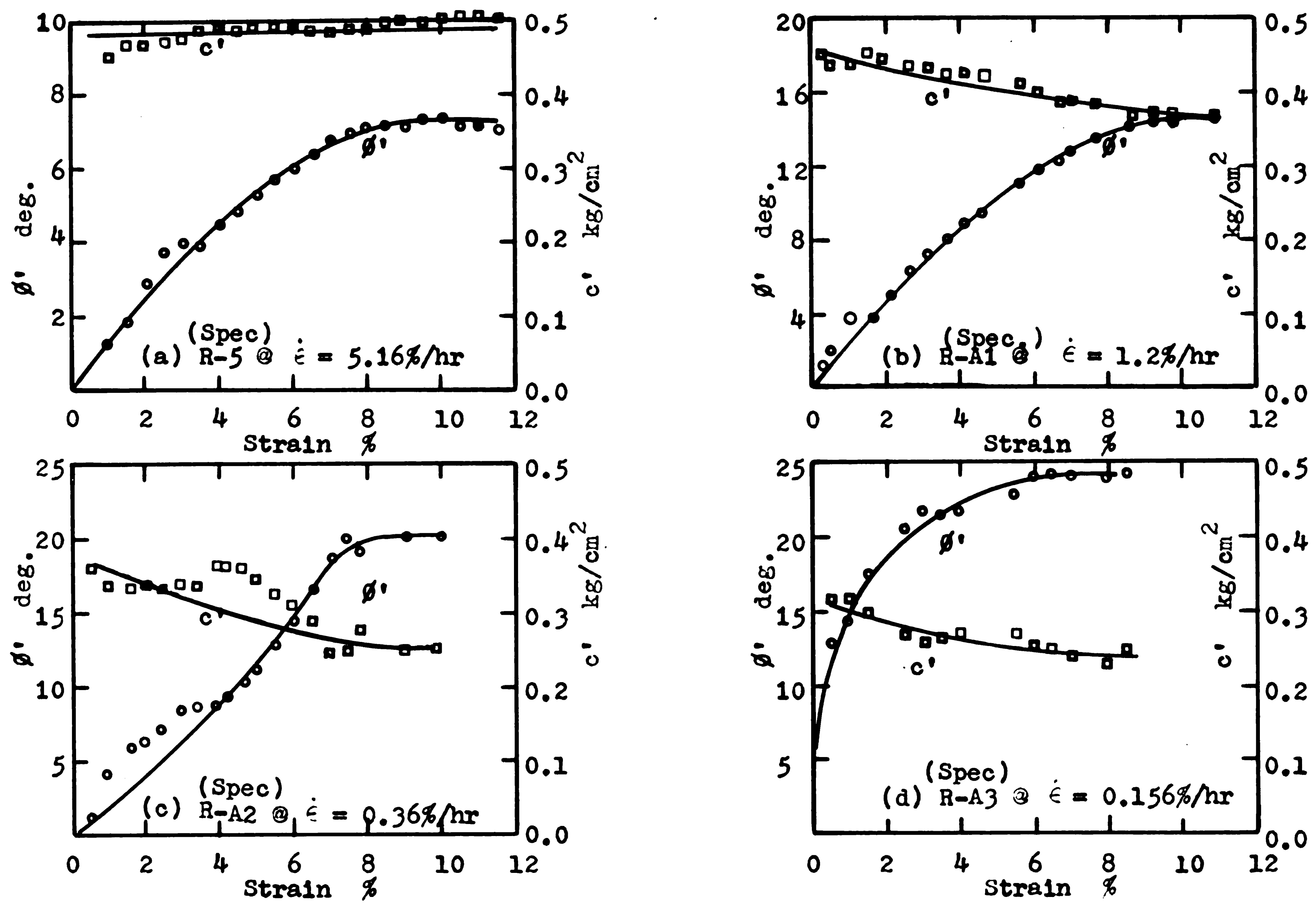

Fig. A-13 Results of c' and ø' for Compacted Sault Clay

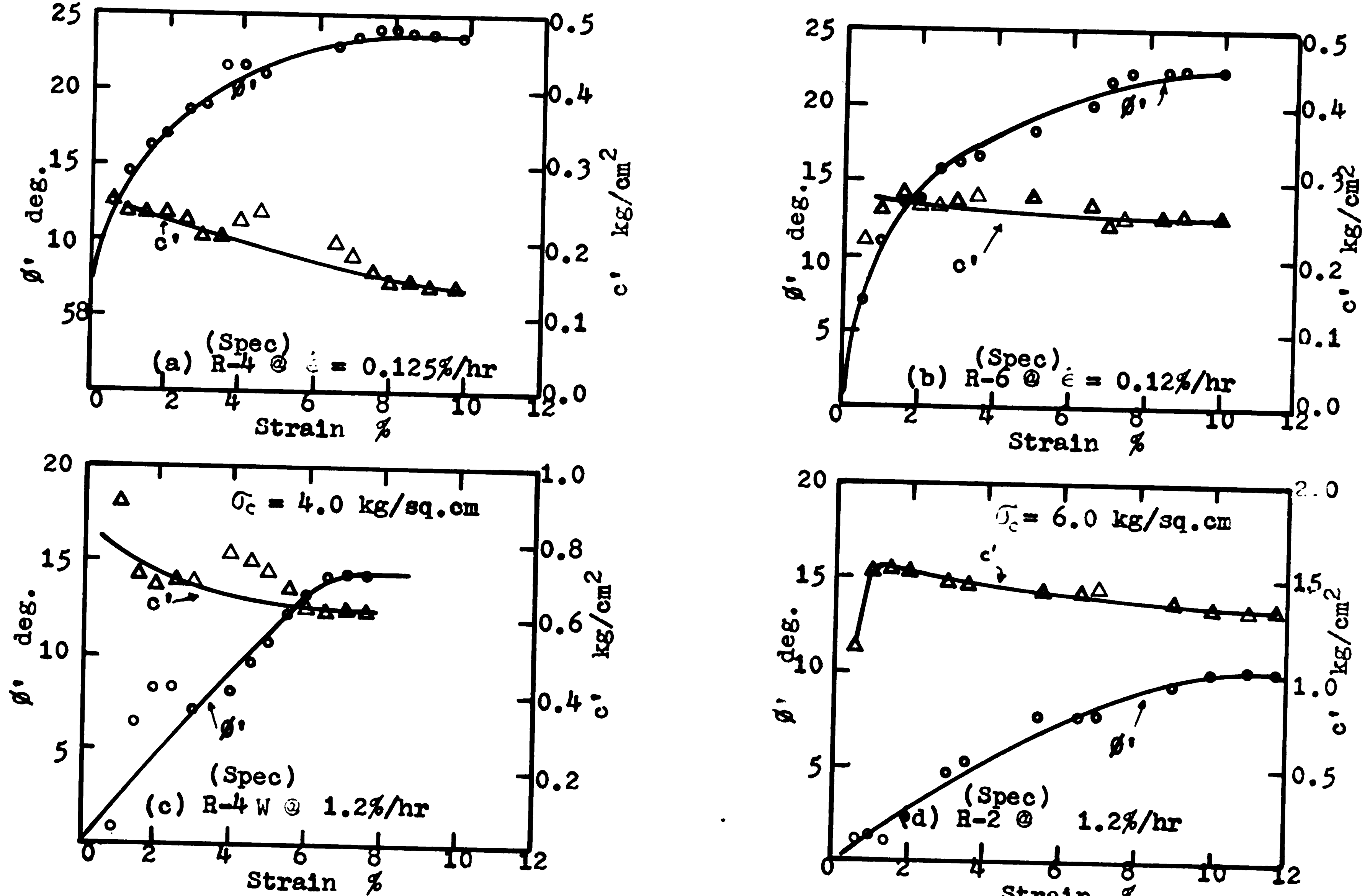

Fig. A-14 Results of c' and ø' for Compacted Sault Clay

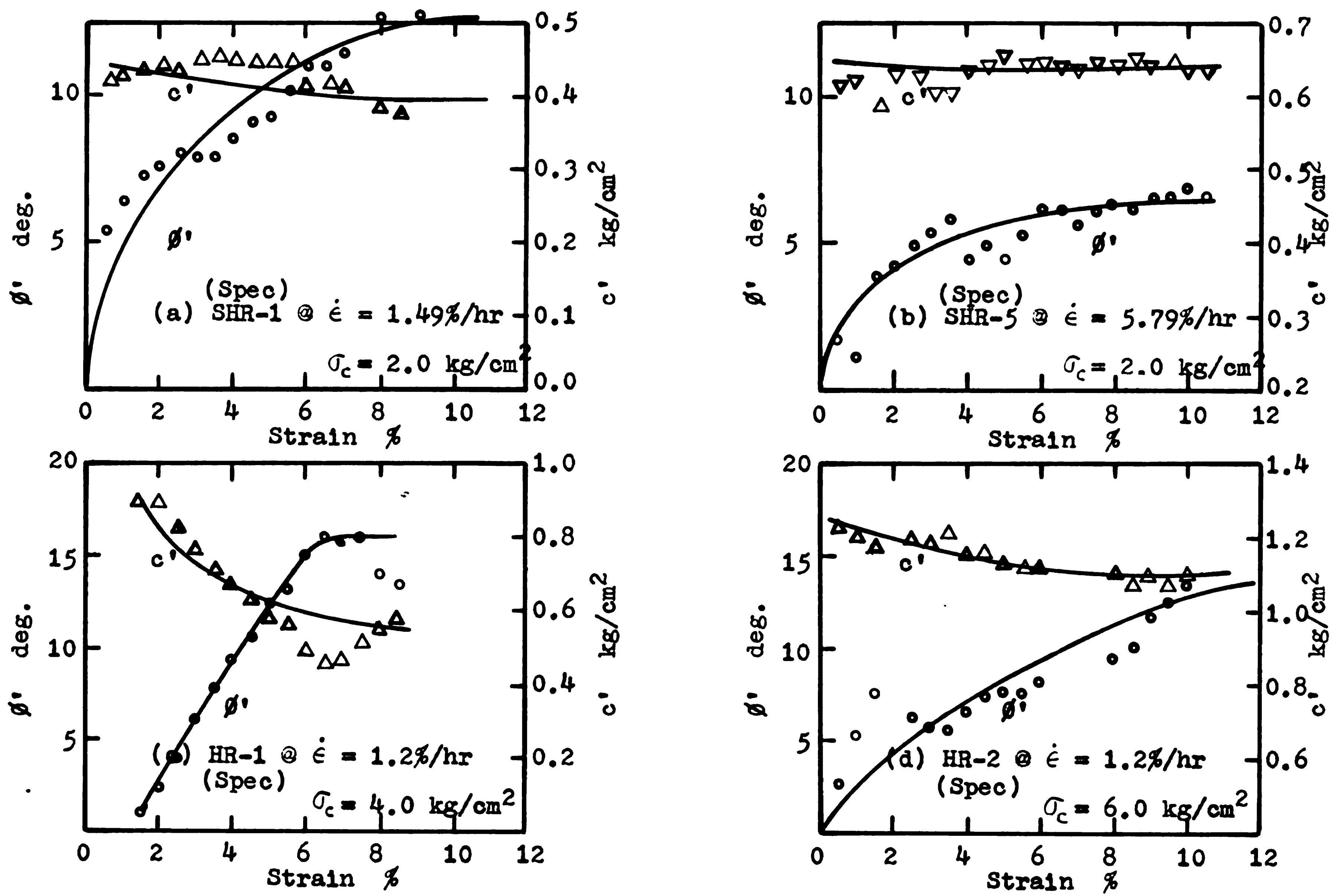

Fig. A-15 Results of c' and ø' for Remolded Sault Clay

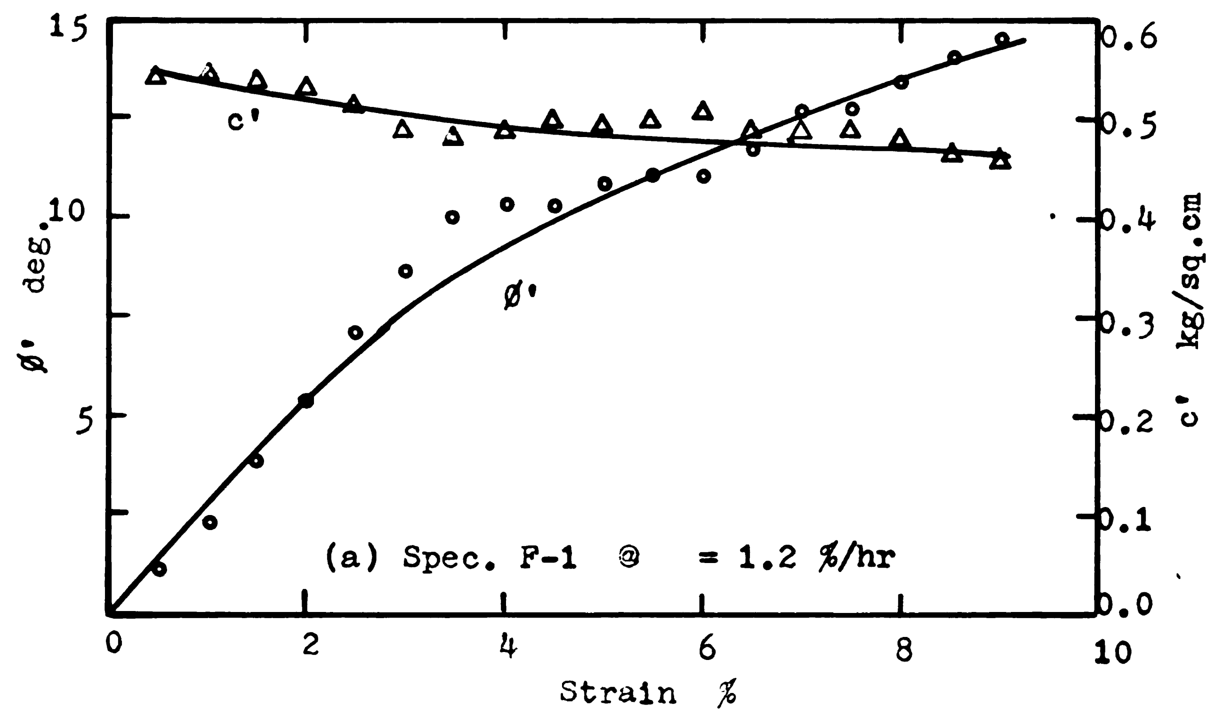

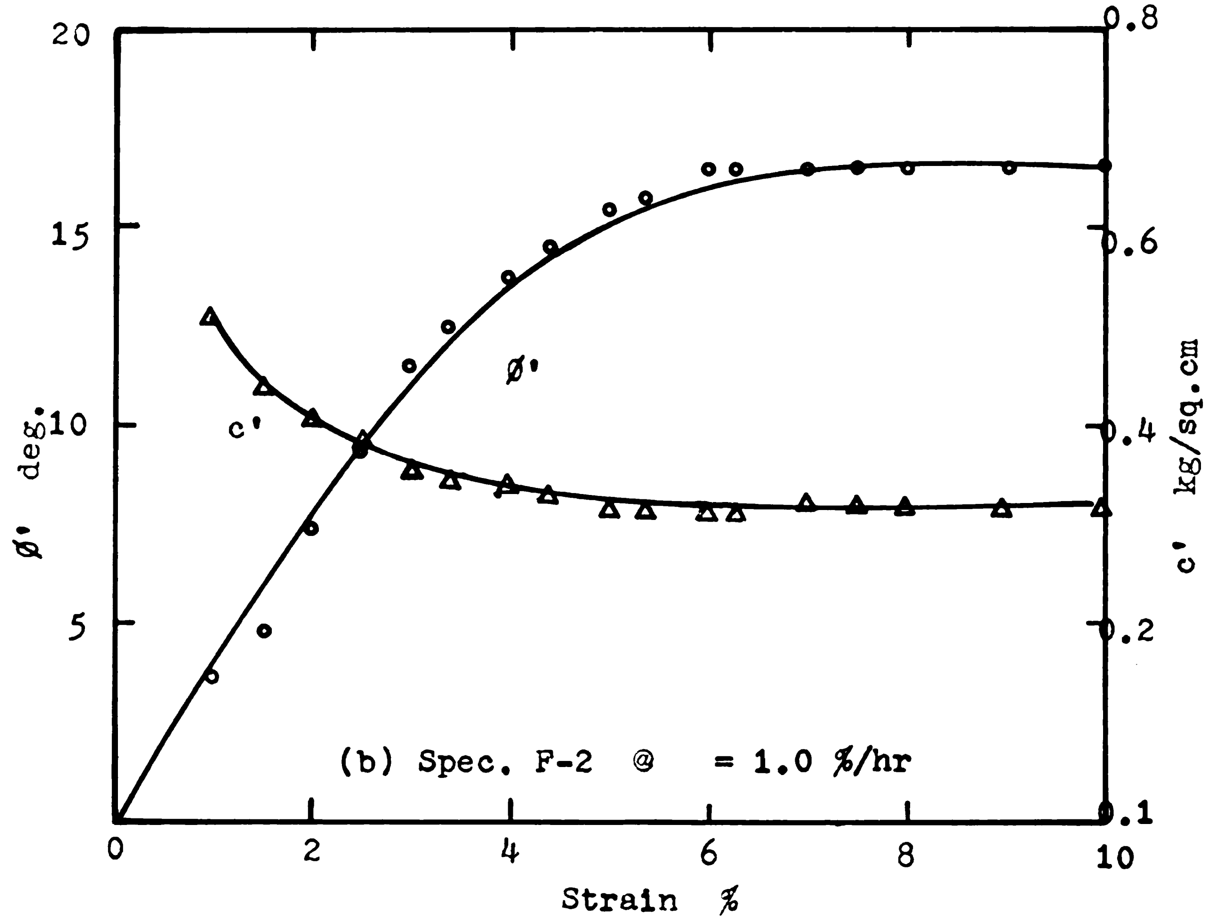

Fig. A-16 Results of c' and Ø' for Consolidated Sault Clay

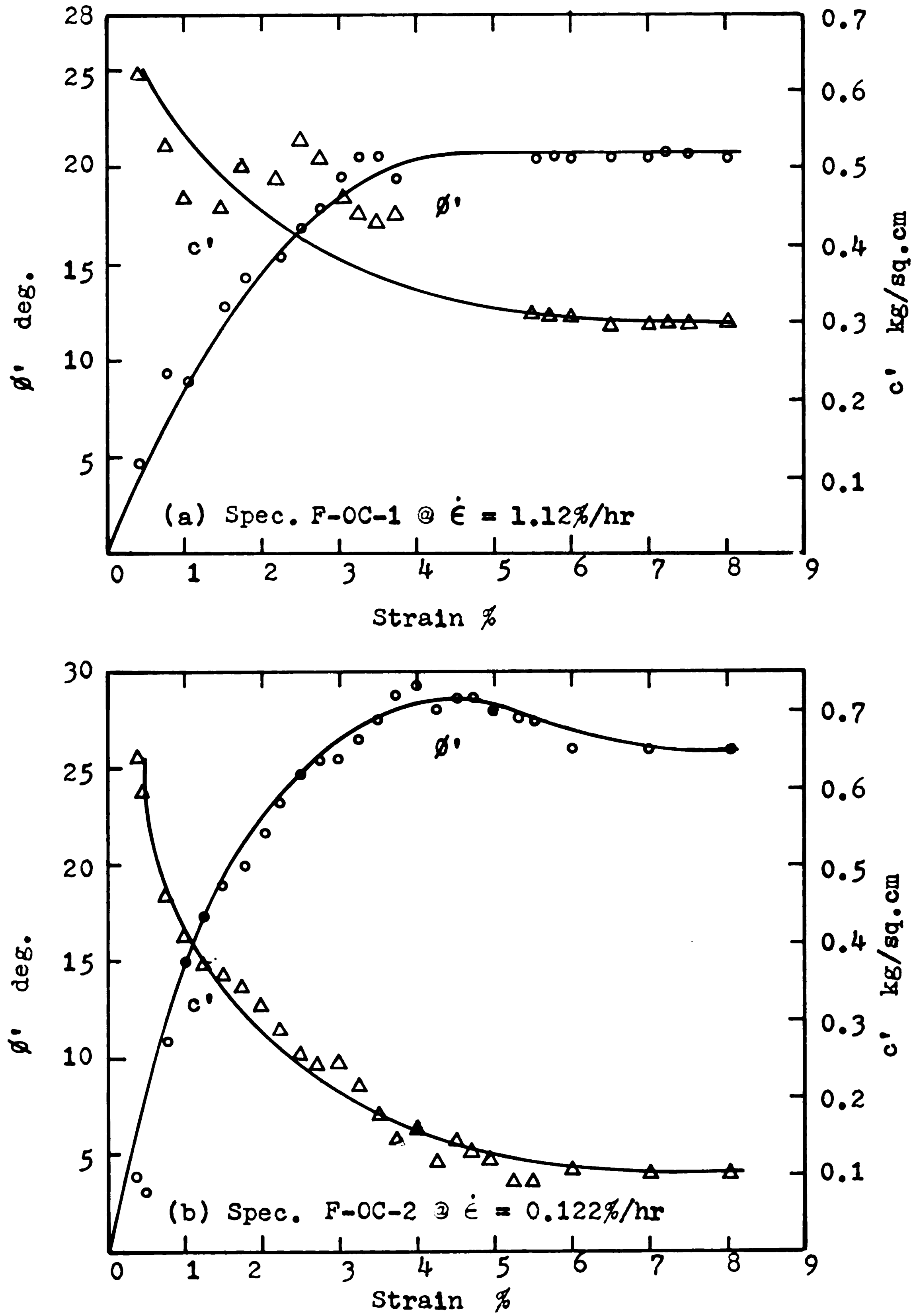

Fig. A-17 Results of c' and ø' for Overconsolidated Sault Clay

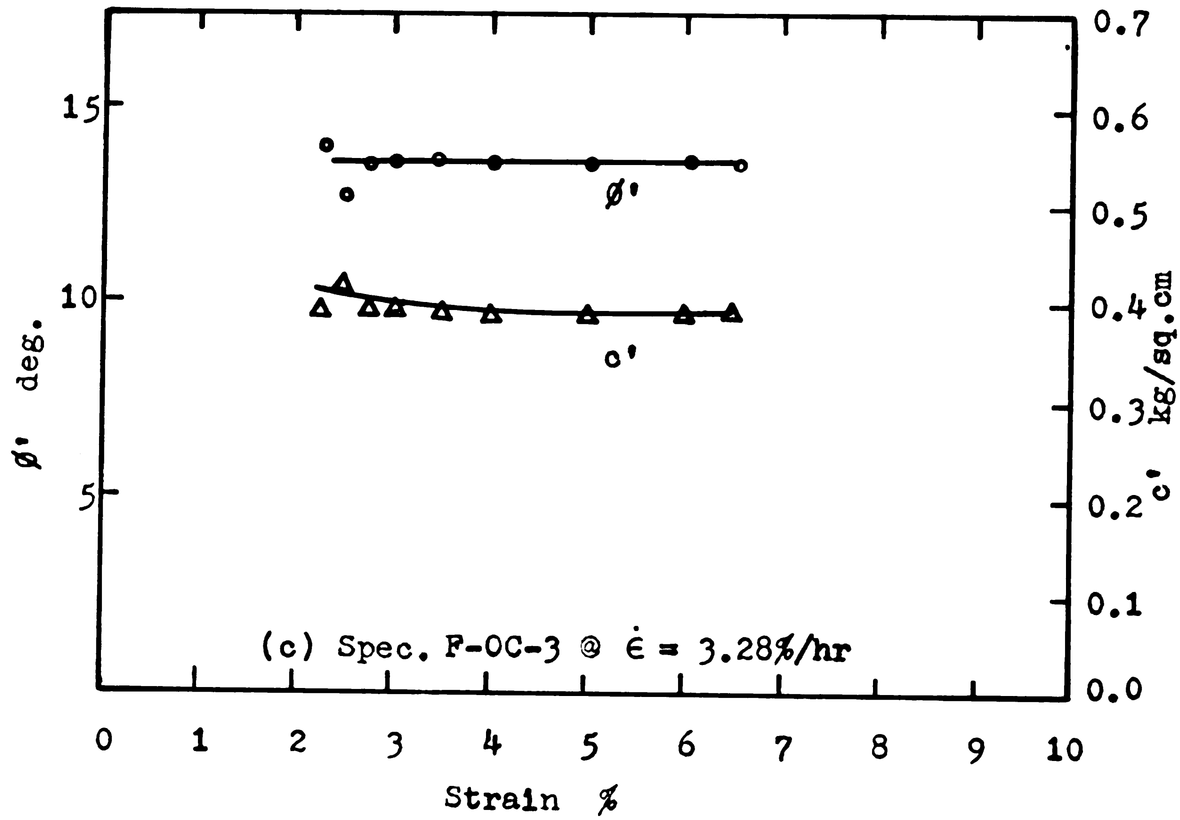

Fig. A-17(cont'd)

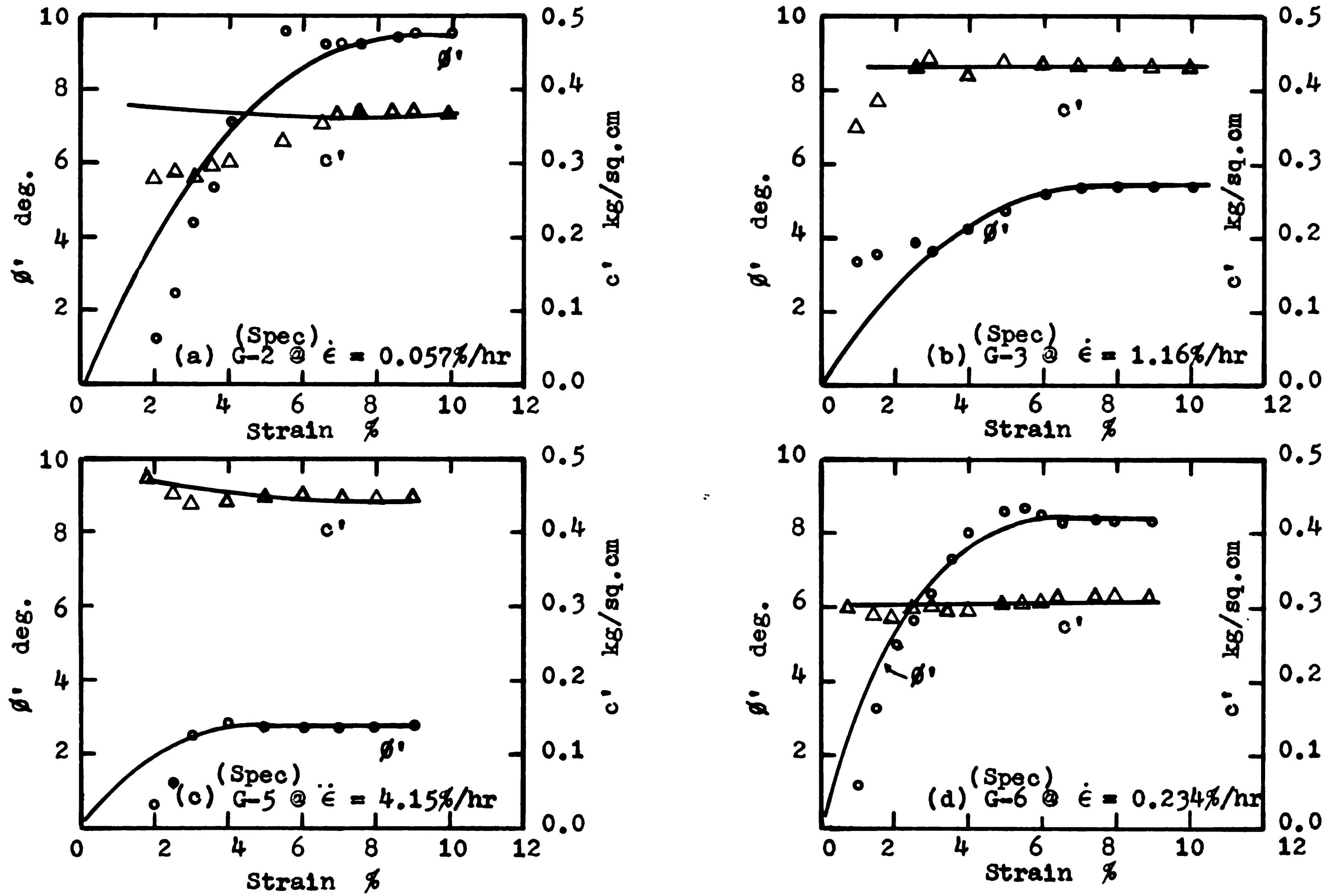

Fig. A-18 Results of c' and ø' for Grundite

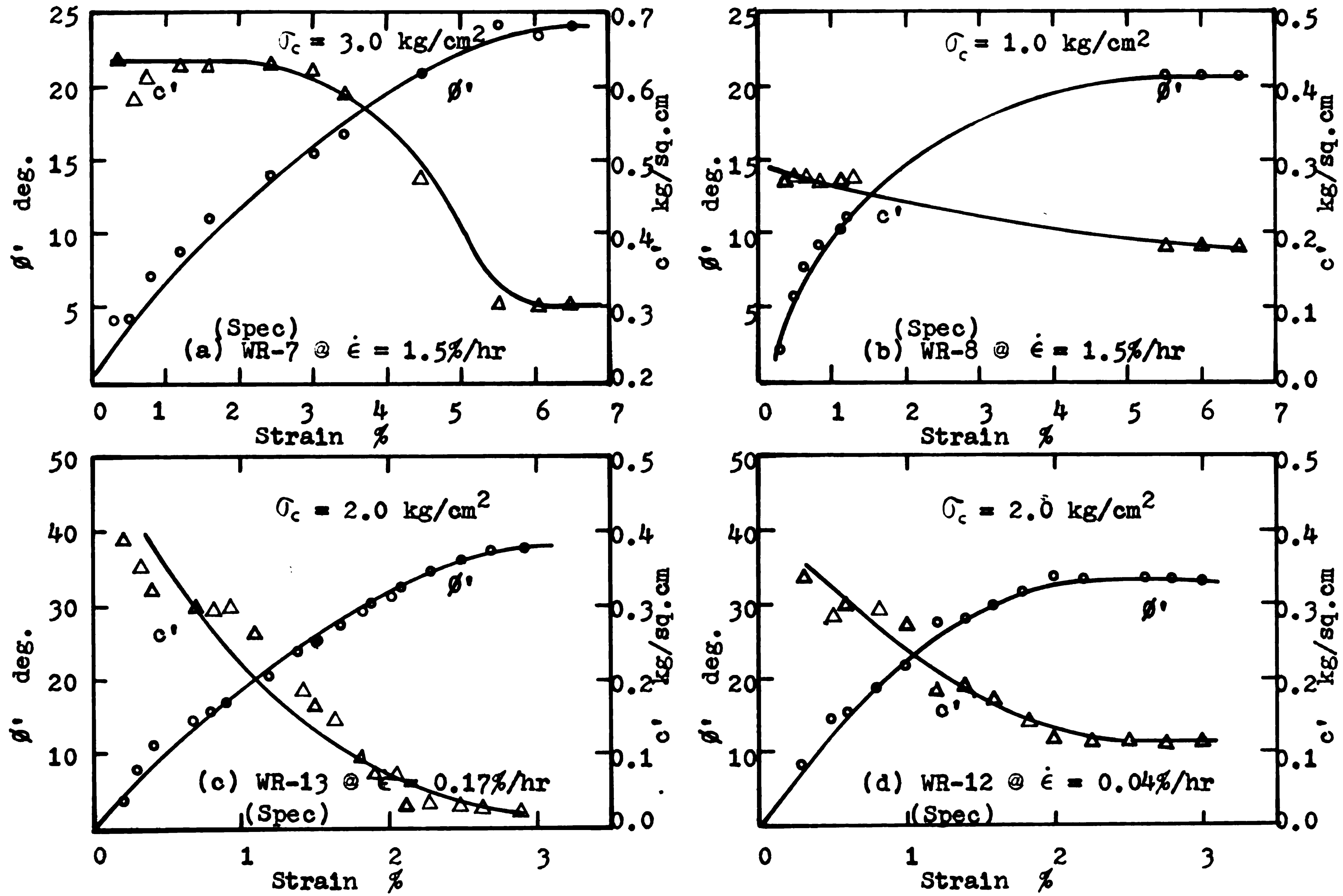

Fig. A-19 Results of c' and ø' for Undisturbed Willow Run Clay

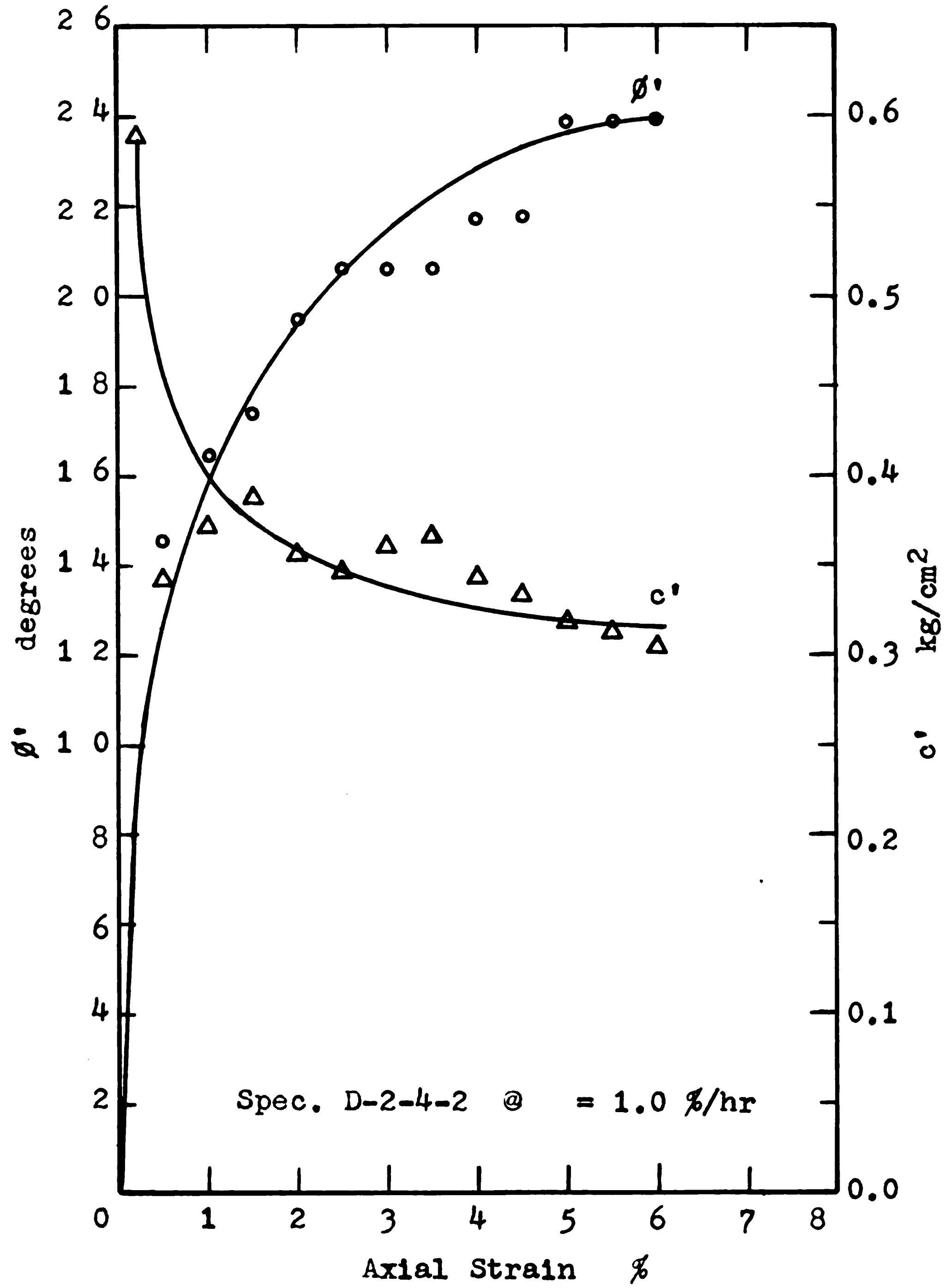

Fig. A-20 Results of c' and Ø' for Undisturbed Marine City Clay

APPENDIX III

TEST DATA

B. Tables

Table A-11 Results of CFS Tests on Compacted Sault Clay

ϵ %		R-A3 (Spec.No)	R-A2 (Spec.No)	R-A1 (Spec.No)	R-5 (Spec.No)
1.0	$\dot{\epsilon}$ %/hr	0.156	0.360	1.200	5.600
	t min.	261.000	116.000	81.600	22.600
	c' kg/cm^2	0.310	0.335	0.447	0.465
	ø' deg.	15.400	4.100	2.200	1.200
2.0	$\dot{\epsilon}$ %/hr	0.156	0.360	1.200	5.600
	t min.	638.000	266.400	148.400	32.200
	c' kg/cm^2	0.290	0.335	0.440	0.465
	ø' deg.	19.000	6.300	3.700	2.800
3.0	$\dot{\epsilon}$ %/hr	0.156	0.360	1.200	5.600
	t min.	1020.000	453.400	201.900	43.900
	c' kg/cm^2	0.275	0.340	0.430	0.470
	ø' deg.	21.600	8.250	6.300	4.000
4.0	$\dot{\epsilon}$ %/hr	0.156	0.360	1.200	5.600
	t min.	1402.000	620.400	255.400	55.600
	c' kg/cm^2	0.265	0.330	0.425	0.485
	ø' deg.	21.600	9.000	8.000	4.600
5.0	$\dot{\epsilon}$ %/hr	0.156	0.360	1.200	5.600
	t min.	1784.000	787.400	308.900	67.300
	c' kg/cm^2	0.260	0.315	0.420	0.490
	ø' deg.	21.600	11.200	9.400	5.300
6.0	$\dot{\epsilon}$ %/hr	0.156	0.360	1.200	5.600
	t min.	2174.000	954.400	358.900	78.900
	c' kg/cm^2	0.245	0.300	0.410	0.490
	ø' deg.	24.000	14.500	11.000	6.000
7.0	$\dot{\epsilon}$ %/hr	0.156	0.360	1.200	5.600
	t min.	2410.000	1089.400	408.900	90.500
	c' kg/cm^2	0.230	0.290	0.390	0.485
	ø' deg.	25.400	18.400	12.600	6.500
8.0	$\dot{\epsilon}$ %/hr	0.156	0.360	1.200	5.600
	t min.	2646.000	1189.400	458.900	101.900
	c' kg/cm^2	0.225	0.280	0.375	0.490
	ø' deg.	25.400	19.000	13.600	7.000

Table A-12 Results of CFS Tests on Over-consolidated Sault Clay

ϵ %		F-OC-1 (Spec.No)	F-OC-2 (Spec.No)	F-OC-3 (Spec.No)	
1.0	$\dot{\epsilon}$ %/hr t min. c' kg/cm^2 ø' deg.	1.120 53.500 0.540 8.800	0.122 491.50C 0.420 15.200	3.280 7.600	
2.0	$\dot{\epsilon}$ %/hr t min. c' kg/cm^2 ø' deg.	1.120 107.000 0.445 14.800	0.122 983.000 0.285 22.400	3.280 0.420 11.400	
3.0	$\dot{\epsilon}$ %/hr t min. c' kg/cm^2 ø' deg.	1.120 160.070 0.385 18.600	0.122 1475.000 0.206 26.500	3.280 0.394 13.580	
4.0	$\dot{\epsilon}$ %/hr t min. c' kg/cm^2 ø' deg.	1.120 214.000 0.345 20.600	0.122 1965.00 0.160 28.500	3.280 0.394 13.580	
5.0	$\dot{\epsilon}$ %/hr t min. c' kg/cm^2 ø' deg.	1.120 268.000 0.320 20.800	0.122 2460.000 0.125 28.500	3.280 0.394 13.58	
6.0	$\dot{\epsilon}$ %/hr t min. c' kg/cm^2 ø' deg.	1.120 321.500 0,310 20.80	0.122 2950.000 0,110 26.90	3.280 0.394 13.580	
7.0	$\dot{\epsilon}$ %/hr t min. c' kg/cm^2 ø' deg.	1.120 375.000 0.300 20.800	0.122 3440.000 0.100 26.000	3.280 0.394 13.580	

Table A-13 Results of CFS Tests on Grundite

ϵ %		G-2 (Spec.No)	G-3 (Spec.No)	G-5 (Spec.No)	G-6 (Spec.No)
2.0	$\dot{\epsilon}$ %/hr	0.057	1.160	4.150	0.234
	t min.	2100.000	103.500	28.900	512.000
	c' kg/cm^2	0.370	0.430	0.470	0.300
	ϕ' deg.	4.000	2.700	2.000	5.000
3.0	$\dot{\epsilon}$ %/hr	0.057	1.160	4.150	0.234
	t min.	3160.000	155.000	43.400	769.000
	c' kg/cm^2	0,3700	0.430	0.460	0.302
	ϕ' deg.	5.600	3.700	2.500	6.370
4.0	$\dot{\epsilon}$ %/hr	0.057	1.160	4.150	0.234
	t min.	4220.000	207.000	57.800	1024.000
	c' kg/cm^2	0.370	0.430	0.455	0.299
	ϕ' deg.	6.900	4.400	2.650	8.000
5.0	$\dot{\epsilon}$ %/hr	0.057	1.160	4.150	0.234
	t min.	5260.000	258.500	72.500	1280.000
	c' kg/cm^2	0.370	0.430	0.445	0.304
	ϕ' deg.	7.900	5.000	2.700	8.600
6.0	$\dot{\epsilon}$ %/hr	0.057	1.160	4.150	0.234
	t min.	6320.000	31 0.000	86.800	1538.000
	c' kg/cm^2	0.370	0.430	0.445	0.310
	ϕ' deg.	8.600	5.300	2.700	8.590
7.0	$\dot{\epsilon}$ %/hr	0.057	1.160	4.150	0.234
	t min.	7380.000	362.000	101.200	1792.000
	c' kg/cm^2	0.370	0.430	0.445	0.317
	ϕ' deg.	9.100	5.500	2.700	8.350
9.0	$\dot{\epsilon}$ %/hr	0.057	1.160	4.150	0.234
	t min.	9480.000	465.000	130.000	2305.000
	c' kg/cm^2	0.370	0.430	0.445	0.317
	ϕ' deg.	9.400	5.500	2.700	8.350

Table A-14 Results of CFS Tests on Undisturbed Willow Run Clay

ϵ %		WR-7 (Spec.No)	WR-8 (Spec.No)	WR-13 (Spec.No)	WR-12 (Spec.No)
1.0	$\dot{\epsilon}$ %/hr t min. c' kg/cm^2 ø' deg.	1.500 40.000 0.635 7.200	1.500 40.000 0.265 9.750	0.170 353.000 0.210 18.500	0.040 1500.000 0.235 22.500
2.0	$\dot{\epsilon}$ %/hr t min. c' kg/cm^2 ø' deg.	1.500 80.000 0.630 12.25	1.500 80.000 0.240 15.000	0.170 706.000 0.065 32.000	0.040 3000.000 0.130 32.800
3.0	$\dot{\epsilon}$ %/hr t min. c' kg/cm^2 ø' deg.	1.500 120.000 0.610 16.000	1.500 120.000 0.225 18.000	0.170 1059.000 0.020 38.000	0.040 4500.000 0.112 33.500
4.0	$\dot{\epsilon}$ %/hr t min. c' kg/cm^2 ø' deg.	1.500 160.000 0.540 19.000	1.500 160.000 0.205 19.800		
5.0	$\dot{\epsilon}$ %/hr t min. c' kg/cm^2 ø' deg.	1.500 200.000 0.410 22.25	1.500 200.000 0.190 20.500		
6.0	$\dot{\epsilon}$ %/hr t min. c' kg/cm^2 ø' deg.	1.500 240.000 0.305 24.000	1.500 240.000 0.180 20.750		

APPENDIX IV

SAMPLE CALCULATION--DETERMINATION OF PARAMETERS IN RHEOLOGIC MODEL

Sample Calculation-Determination of Model Parameters

Spec. No. : F-OC-C-1-2 (Over-Consolidated Sault Clay in Table 5 (b))

$$(\sigma_1-\sigma_3)_i = 0.495 \text{ kg/cm}^2 \qquad \Delta(\sigma_1-\sigma_3) = 0.2565 \text{ kg/cm}^2$$

$$(\sigma_1-\sigma_3)_f = 0.7515 \text{ kg/cm}^2$$

From Fig. A-10 (a) & (b) in Appendix III:

$$u_o = 4.9 \times 10^{-4} \text{ in.}$$

$$u_f = 24.25 \times 10^{-4} \text{ in.}$$

$$(k_1 + k_2) = \frac{\Delta(\sigma_1-\sigma_3)}{3u_o} \times l_o$$

$$= \frac{0.2565}{3(4.9 \times 10^{-4})} \times 2.96 = 516 \text{ kg/cm}^2$$

$$k_2 = \frac{\Delta(\sigma_1-\sigma_3)}{3 \times u_f} \times l_o = \frac{0.2565}{3 \times (24.25 \times 10^{-4})} \times 2.96$$

$$= 104.3 \text{ kg/cm}^2$$

$$k_1 = (k_1 + k_2)-k_2 = 516-104.3 = 411.7 \text{ kg/cm}^2$$

$$\frac{k_1}{k_1 + k_2} = \frac{411.7}{516} = 0.798$$

From Fig A-10(c):

$$\text{for } A = 2.30,\ Z(t) = 10^{-2} \qquad t = 34.0 \text{ minutes}$$

$$\alpha = \frac{3}{\sqrt{2}} \times \frac{A}{\Delta(\sigma_1-\sigma_3)} \times \frac{k_1 + k_2}{k_1}$$

$$= \frac{3}{\sqrt{2}} \times \frac{2.30}{0.2565} \times \frac{1}{0.798} = 23.8 \text{ cm}^2/\text{kg}$$

$$\eta = \frac{2Z(t)\ (k_1 + k_2)}{k_1 k_2\ \alpha t} = \frac{2 \times 0.01 \times 516}{411.7 \times 104.3 \times 23.8 \times 34.0}$$

$$= 2.97 \times 10^{-7} \text{ min}^{-1}$$

APPENDIX V

ANALYSIS OF ϕ'_c and c'_c

Table **A-15** **Friction-Displacement** Rate Characteristics at Failure--
CFS Tests on Sault Clay

CLAY	Test No.	$\dot{\epsilon}$ %/hr	ϵ_u %	t_u hr	ϕ'_u deg	$\rho = 0.3$ $\dot{N} = \frac{6\ ne}{t_u}$ ne/hr	$\rho = 0.5$ $\dot{N} = \frac{6\ ne}{t_u}$ ne/hr
Compacted	R-6	0.120	9.0	75.00	22.30	0.0800	0.0800
	R-4	0.125	8.5	68.00	23.60	0.0883	0.0883
	R-A3	0.156	9.0	57.70	24.30	0.1040	0.1040
	R-A2	0.360	10.0	32.20	20.00	0.1862	0.1862
	R-A1	1.200	10.0	8.34	14.50	0.7200	0.7200
	R-5	5.600	11.0	1.97	7.20	3.050	3.050
Remolded	SHR-1	1.490	9.5	6.37	12.70	0.942	0.942
	SHR-5	5.790	11.0	1.90	6.50	3.160	3.160
Consolida.	F-1	1.200	9.0	7.50	14.60	0.800	0.800
	F-2	1.000	10.0	10.00	16.40	0.600	0.600

Table A-16 Predicted ϕ'_c in Creep-CFS Tests on Sault Clay

Clay	Spec No.	k @ end creep	t_c hr	Observed ϕ'_c deg	$\rho = 0.3$: N_c ne	$\rho = 0.3$: $\dot{N}_c$ ne/hr	$\rho = 0.3$: ϕ'_u @ $\dot{N} = \dot{N}_c$ deg	$\rho = 0.3$: Predic ϕ'_c deg	$\rho = 0.5$: N_c ne	$\rho = 0.5$: $\dot{N}_c$ ne/hr	$\rho = 0.5$: ϕ'_u @ $\dot{N} = \dot{N}_c$ ne/hr	$\rho = 0.5$: Predic ϕ'_c deg
Consolidated Sault	FC5	1.96	0.5	0.00	2.05	4.100	6.20	3.04	0.90	1.800	10.0	4.90
	FC4	2.17	1.0	0.40	3.30	3.300	7.00	3.43	1.25	1.25	11.6	5.70
	FC2	2.25	4.0	6.20	4.00	1.000	12.50	6.13	1.40	0.35	17.5	8.58
	FC6	2.14	4.0	3.75	3.15	0.789	13.80	6.75	1.20	0.30	18.1	8.87
	FC9	2.10	6.5	5.10	2.75	0.423	16.60	8.15	1.13	0.1585	21.0	10.30
	FC8	1.96	8.0	7.40	2.05	0.256	18.90	9.25	0.90	0.1125	22.6	11.10
	FC7	2.09	12.0	6.20	2.75	0.229	19.40	9.50	1.10	0.0916	23.5	11.50
	FC3	2.85	24.0	9.00	6.00	0.250	19.00	9.32	2.61	0.1087	22.8	11.20
	FC1	3.26	120.0	12.20	6.00	0.050	25.50	12.50	3.80	0.0316	25.5	12.50
Compacted Sault	RC8	1.85	2.0	1.00	1.60	0.800	13.70	4.03	0.72	0.36	17.4	5.11
	RC9	1.92	8.0	2.85	1.90	0.238	19.30	5.67	0.85	0.106	22.9	6.74
	RC10	2.02	16.0	5.00	2.35	0.147	21.40	6.30	1.00	0.0625	24,9	7.32
	RC11	2.43	24.0	0.003	6.00	0.250	19.0	5.60	1.75	0.073	14.3	7.15
	RC7	2.56	72.0	7.40	6.00	0.084	24.0	7.05	2.00	0.032	25.5	7.50

Validity of Equation (25')

The exponents of the hyperbolic tangent in equation (25) for the following clays are evaluated as follows.

Compacted Sault Clay--For the range of constant strain rates in the CFS tests, from Table 5(a), it can be shown that

$$20\ cm^2/kg \quad ' = \dot{}_{oct}/ \quad 10 \quad k_1 \quad 200\ kg/cm^2$$

$$\tanh^{-1} \frac{1 - '}{\sqrt{1 + '^2}} \doteqdot 3$$

The hyperbolic tangent therefore approaches unity.

Over-consolidated Sault Clay--From Table 5(b),

$$15\ cm^2/kg \quad ' = \dot{}_{oct}/ \quad 7.8 \quad k_1 \quad 30\ kg/cm^2$$

$$A = \tanh^{-1} \frac{1 - '}{\sqrt{1 + '^2}} \quad 0.696$$

For $_{oct} \sqrt{2} \times 0.655\ \% = 0.925\ \% = 0.925 \times 10^{-2}$,

$$B = \frac{\sqrt{1 + '^2}}{2} \times \frac{k_1}{'} \quad 2.25$$

$$A + B \quad 2.946$$

Therefore $\quad \tanh 2.946 \doteqdot 1$

Similarly, it can be shown that for the consolidated Sault clay, Grundite and undisturbed Marine City clay:

$$\tanh^{-1} \frac{1 - '}{\sqrt{1 + '^2}} \doteqdot 3$$

Thus we have shown that Equation (25') can be used to compute the predicted values of cohesion for the series of CFS tests at the different constant strain rates on the compacted Sault, consolidated Sault, overconsolidated Sault, Grundite and undisturbed Marine City clays.

Table A-17 Predicted Values of Cohesion(f_1)-- Compacted Sault Clay

		Spec. R-4	Spec. R-A3	Spec. R-A2	Spec. R-A2	Spec. R-5
Strain Rate	$\dot{\epsilon}$ %/hr	0.125	0.156	0.360	1.20	5.16
	$\dot{\gamma}_{oct}$ 10^{-5}min^{-1}	2.94	3.78	8.50	28.30	122.00
$D = 0 - 0.5$ kg/cm^2 $\epsilon = 0 - 0.1081$ % $\beta = 1.895 \times 10^{-7}$ min^{-1}	$\beta' = \dot{\gamma}_{oct}/\beta$	151.000	194.50	448.000	1490.00	6420.0
$\alpha = 21.3$ cm^2/kg	$f_1 =$	0.268	0.28	0.319	0.37	0.44
$D = 0.5 - 0.765$ kg/cm^2 $\epsilon = 0.1081 - 0.244$ % $\beta = 1.503 \times 10^{-7}$ min^{-1}	$\beta' = \dot{\gamma}_{oct}/\beta$	196.00	245.00	565.00	1890.0	8160.0
$\alpha = 28.8$ cm^2/kg	$f_1 =$	0.209	0.22	0.246	0.228	0.339
$D = 0.765 - 0.999$ kg/cm^2 $\epsilon = 0.244 - 0.658$ % $\beta = 3.85 \times 10^{-7}$ min^{-1}	$\beta' = \dot{\gamma}_{oct}/\beta$	76.50	95.50	221.0	735.0	3145.0
$\alpha = 21.3$ cm^2/kg	$f_1 =$	0.239	0.249	0.289	0.345	0.414
$D = 0.999 - 1.24$ kg/cm^2 $\epsilon = 0.658 - 1.43$ % $\beta = 13.24 \times 10^{-7}$ min^{-1}	$\beta' = \dot{\gamma}_{oct}/\beta$	22.20	27.80	64.00	213.0	920.0
$\alpha = 20.8$ cm^2/kg	$f_1 =$	0.185	0.196	0.236	0.293	0.364
$D = 1.24 - 1.49$ kg/cm^2 $\epsilon = 1.43 - 2.55$ % $\beta = 19.48 \times 10^{-7}$ min^{-1}	$\beta' = \dot{\gamma}_{oct}/\beta$	15.10	18.70	43.50	145.0	625.0
$= 13.48$ cm^2/kg	$f_1 =$	0.250	0.266	0.327	0.415	0.520
$D = 1.49 - 1.708$ kg/cm^2 $\epsilon = 2.55 - 3.85$ % $\beta = 15.95 \times 10^{-7}$ min^{-1}	$\beta' = \dot{\gamma}_{oct}/\beta$	18.50	23.0	53.5	178.0	765.0
$\alpha = 22.5$ cm^2/kg	$f_1 =$	0.163	0.173	0.210	0.263	0.329
$D = 1.708 - 1.89$ kg/cm^2 $\epsilon = 3.85 - 9.37$ % $\beta = 41.6 \times 10^{-7}$ min^{-1}	$\beta' = \dot{\gamma}_{oct}/\beta$	7.07	8.85	20.4	68.2	292.0
$\alpha = 50.9$ cm^2/kg	$f_1 =$	0.053	0.058	0.074	0.0975	0.1268

Table A-18 Predicted Values of Cohesion(f_1) -- Over-consolidated Sault Clay

		Spec. F-OC-2	Spec. F-OC-1	Spec. F-OC-3
Strain Rate	$\dot{\epsilon}$ %/hr	0.122	1.120	3.280
	$\dot{\gamma}_{oct}$ 10^{-5} min^{-1}	2.880	26.400	77.300
$D = 0.495 - 0.7515$ kg/cm^2 $\epsilon = 0.0 - 0.0822$ % $\beta = 2.97 \times 10^{-7}$ min^{-1}	$\beta' = \dot{\gamma}_{oct}/\beta$	102.000	892.000	2600.000
$\alpha = 19.45$ cm^2/kg	$f_1 =$	0.226	0.317	0.362
$D = 0.7515 - 1.06$ kg/cm^2 $\epsilon = 0.082 - 0.358$ % $\beta = 1.545 \times 10^{-7}$ min^{-1}	$\beta' = \dot{\gamma}_{oct}/\beta$	196.000	1710.00	5000.000
$\alpha = 19.45$ cm^2/kg	$f_1 =$	0.310	0.421	0.477
$D = 1.06 - 1.255$ kg/cm^2 $\epsilon = 0.358 - 0.665$ % $\beta = 41.2 \times 10^{-7}$ min^{-1}	$\beta' = \dot{\gamma}_{oct}/\beta$	7.380	64.500	188.000
$\alpha = 17.7$ cm^2/kg	$f_1 =$	0.155	0.278	0.338

Table A-19 Predicted Values of Cohesion(f_1)--Grundite

		Spec. G-2	Spec. G-6	Spec. G-3	Spec. G-5
Strain Rate	$\dot{\epsilon}$ %/hr	0.057	0.234	1.160	4.150
	$\dot{\gamma}_{oct}$ 10^{-5}min^{-1}	1.325	3.50	27.400	97.200
$D = 0.0 - 0.5$ kg/cm^2					
$\epsilon = 0.0 - 2.01$ %					
$\beta = 32 \times 10^{-7}$ min^{-1}					
	$\beta' = \dot{\gamma}_{oct}/\beta$	4.20	17.30	85.50	306.00
$\alpha = 12.2$ cm^2/kg	$f_1 =$	0.326	0.352	0.483	0.587
$D = 0.5 - 0.8$ kg/cm^2					
$\epsilon = 2.01 - 2.93$ %					
	$\beta' = \dot{\gamma}_{oct}/\beta$	8.42	34.50	171.00	610.00
$\beta = 7.4 \times 10^{-7}$ min^{-1}					
$\alpha = 12.2$ cm^2/kg	$f_1 =$	0.236	0.352	0.483	0.587
$D = 0.0 - 0.7$ kg/cm^2					
$\epsilon = 0.0 - 2.52$ %					
$\beta = 7.4 \times 10^{-1}$ min^{-1}					
	$\beta' = \dot{\gamma}_{oct}/\beta$	18.20	74.50	377.0	132.00
$\alpha = 20.7$ cm^2/kg	$f_1 =$	0.299	0.245	0.322	0.384

Table A-20 Predicted Values of Cohesion(f_1)-- Consolidated Sault Clat

		Spec. F-2
Strain	$\dot{\epsilon}$ %/hr	1.000
Rate	$\dot{\gamma}_{oct}$ 10^{-5} min^{-1}	23.500
$D = 0.0 - 0.5$ kg/cm^2 $\epsilon = 0.0 - 0.57$ % $\beta = 5.44 \times 10^{-7}$ min^{-1} $\beta' = \dot{\gamma}_{oct}/\beta$ $\alpha = 14.0$ cm^2/kg $f_1 =$		435.000 0.483
$D = 0.5 - 0.75$ kg/cm^2 $\epsilon = 0.57 - 1.065$ % $\beta = 8.73 \times 10^{-7}$ min^{-1} $\beta' = \dot{\gamma}_{oct}/\beta$ $\alpha = 15.5$ cm^2/kg $f_1 =$		270.000 0.405
$D = 0.75 - 1.00$ kg/cm^2 $\epsilon = 1.065 - 1.693$ % $\beta = 5.68 \times 10^{-7}$ min^{-1} $\beta' = \dot{\gamma}_{oct}/\beta$ $\alpha = 1.46$ cm^2/kg $f_1 =$		415.000 0.460
$D = 1.0 - 1.25$ kg/cm^2 $\epsilon = 1.693 - 2.66$ % $\beta = 0.214 \times 10^{-7}$ min^{-1} $\beta' = \dot{\gamma}_{oct}/\beta$ $\alpha = 67.35$ cm^2/kg $f_1 =$		11000.000 0.149

Table A-21 Predicted Values of Cohesion(f_1)--
Undisturbed Marine City Clay

			Spec. D-2-4-2
Strain	$\dot{\epsilon}$	%/hr	1.000
Rate	$\dot{\gamma}_{oct}$	10^{-5} min^{-1}	24.000
D=0.27 0.47		kg/cm^2	
ϵ= 0.0 - 0.703		%	
β= 0.9 x 10^{-7}		min^{-1}	
	β'=	$\dot{\gamma}_{oct}/\beta$	2660.000
α= 65 cm^2/kg		f_1 =	0.133
D = 0.47 - 0.67		kg/cm^2	
ϵ = 0.703 - 2.204		%	
β = 4.7 x 10^{-7}		min^{-1}	
	β'=	$\dot{\gamma}_{oct}/\beta$	510.000
α = 12 cm^2/kg		f_1 =	0.580
D = 0.67 - 0.87		kg/cm^2	
ϵ = 2.203 - 3.068		%	
β = 1.3 x 10^{-7}		min^{-1}	
	β'=	$\dot{\gamma}_{oct}/\beta$	1840.000
α = 30 cm^2/kg		f_1 =	0.275
D = 0.87 - 1.07		kg/cm^2	
ϵ = 3.068 - 4.693		%	
β = 2.0 x 10^{-7}		min^{-1}	
	β'=	$\dot{\gamma}_{oct}/\beta$	1270.000
α = 26 cm^2/kg		f_1 =	0.303

Table A-22 Predicted Cohesion (f_1) on Sault Clay--Creep-CFS Tests

CLAY	Creep Time min.	$f_1 = \frac{1}{\alpha} \log \tanh [\frac{1}{2} \alpha\beta \frac{k_1 k_2}{k_1 + k_2} t + \tanh^{-1} \exp(- \frac{\alpha k_1 \tau}{k_1 + k_2})]$ kg/cm^2		$f^* = f_1/f_o$
Consolidated	30 60 240 390 480 720 1440 7200	F-C-9 **(Spec. No.)** $(\sigma_1 - \sigma_3) = 1.15$ kg/cm^2 $\beta = 22.7$ cm^2/kg **α = 5.98 x 10-7 min-1** $\frac{1}{2} \alpha\beta \frac{k_1 k_2}{k_1 + k_2} = 4.87 \times 10^{-5}$ min^{-1} $\tau = \sqrt{2/3} \times 1.15 = 0.542$ kg/cm^2 $\exp(- \frac{\alpha k_1 \tau}{k_1 + k_2}) = 4.65 \times 10^{-5}$ $f_0 = 0.439$ kg/cm^2	0.287 0.268 0.196 0.1743 0.1650 0.1475 0.1170 0.0478	0.6540 0.6100 0.4460 0.3970 0.3760 0.3360 0.2665 0.1090
Compacted	120 480 960 1440 4320	C-C-7 **(Spec. No.)** $(\sigma_1 - \sigma_3) = 0.987$ kg/cm^2 $\alpha = 13.96$ cm^2/kg $\beta = 20 \times 10^{-7}$ min^{-1} **(assumed)** $\frac{1}{2} \alpha\beta \frac{k_1 k_2}{k_1 + k_2} = 3.11 \times 10^{-4}$ min^{-1} $\tau = \sqrt{2/3} (\sigma_1 - \sigma_3) = 0.465$ kg/cm^2 $\exp(- \frac{\alpha k_1 \tau}{k_1 + k_2}) = 0.002$ $f_0 = 0.445$ kg/cm^2	0.2320 0.1350 0.0865 0.0573 0.00996	0.5220 0.3040 0.1945 0.1290 0.0224

Table A-23 Influence of $\dot{\epsilon}$ on c_c' -- Creep-CFS Tests

CLAY	Sample No.	Creep Time t_c min	$\dot{\epsilon}_c$ at end creep %/hr	c_d' kg/cm^2	Observed c_c' kg/cm^2
Compacted Sault	R-C-8	120	0.1270	0.180-0.26	0.469
	R-C-9	480	0.0535	0.15-0.225	0.422
	R-C-10	960	0.0050	0.125-0.2	0.372
	R-C-11	1440	0.00304	0.125-0.2	0.376
	R-C-7	4320	0.0010	0.125-0.2	0.356

Table A-24 Values of c* in Creep-CFS Tests on Sault Clay

Clay	Creep Time min.	c' kg/cm^2	c'_∞ kg/cm^2	$c' - c'_\infty$ kg/cm^2	$c'_o - c'_\infty$ kg/cm^2	$c^* = \frac{c' - c'_\infty}{c'_o - c'_\infty}$
Consolidated Sault	30.00	0.5750	0.3550	0.2200	0.2200	1.000
	60.00	0.5640	"	0.2090	"	0.950
	240.00	0.4200	"	0.0650	"	0.296
	240.00	0.4720	"	0.1230	"	0.560
	390.00	0.4320	"	0.0770	"	0.350
	480.00	0.3500	"	0.0050	"	0.0228
	720.00	0.4030	"	0.0480	"	0.2180
	1440.00	0.3930	"	0.0380	"	0.1730
	7200.00	0.3790	"	0.0240	"	0.1090
Compacted Sault	120.00	0.4690	0.3550	0.1140	0.1450	0.7860
	480.00	0.4220	"	0.0670	"	0.4620
	960.00	0.3720	"	0.0170	"	0.1170
	1440.00	0.3760	"	0.0210	"	0.1450
	4320.00	0.3560	"	0.0010	"	0.0690